GRI-95/0454.2

SECONDARY NATURAL GAS RECOVERY: TARGETED APPLICATIONS FOR INFIELD RESERVE GROWTH IN MIDCONTINENT RESERVOIRS, BOONSVILLE FIELD, FORT WORTH BASIN, TEXAS

VOLUME II: APPENDIX
(May 1, 1993–June 30, 1995)

Prepared by

Bob A. Hardage, David L. Carr, and Robert J. Finley
Bureau of Economic Geology
Noel Tyler, Director
The University of Texas at Austin
Austin, Texas 78713-8924

David E. Lancaster
S. A. Holditch & Associates, Inc.

Robert Y. Elphick
Scientific Software–Intercomp

James R. Ballard
Envirocorp Services & Technology, Inc.

for

GAS RESEARCH INSTITUTE
GRI Contract No. 5093-212-2630
Thomas H. Fate, GRI Project Manager

and

U.S. DEPARTMENT OF ENERGY
DOE Contract No. DE-FG21-88MC25031
Charles W. Byrer, DOE Project Manager

October 1995

GRI-95/0454.2

SECONDARY NATURAL GAS RECOVERY: TARGETED APPLICATIONS FOR INFIELD RESERVE GROWTH IN MIDCONTINENT RESERVOIRS, BOONSVILLE FIELD, FORT WORTH BASIN, TEXAS

VOLUME II: APPENDIX
(May 1, 1993–June 30, 1995)

Prepared by

Bob A. Hardage, David L. Carr, and Robert J. Finley
Bureau of Economic Geology
Noel Tyler, Director
The University of Texas at Austin
Austin, Texas 78713-8924

David E. Lancaster
S. A. Holditch & Associates, Inc.

Robert Y. Elphick
Scientific Software–Intercomp

James R. Ballard
Envirocorp Services & Technology, Inc.

for

GAS RESEARCH INSTITUTE
GRI Contract No. 5093-212-2630
Thomas H. Fate, GRI Project Manager

and

U.S. DEPARTMENT OF ENERGY
DOE Contract No. DE-FG21-88MC25031
Charles W. Byrer, DOE Project Manager

October 1995

DISCLAIMER

LEGAL NOTICE This work was prepared by the Bureau of Economic Geology as an account of work sponsored by the Gas Research Institute (GRI). GRI, nor members of GRI, nor any person acting on behalf of either:

a. Makes any warranty or representation, expressed or implied, with respect to the accuracy, completeness, or usefulness of the information contained in this report, or that the use of any apparatus, method, or process disclosed in this report may not infringe privately owned rights; or

b. Assumes any liability with respect to the use of, or for damages resulting from the use of, any information, apparatus, method, or process disclosed in this report.

50272-101

REPORT DOCUMENTATION PAGE	1. REPORT NO. GRI-95/0454.2	2.	3. Recipient's Accession No.

4. Title and Subtitle
Secondary Natural Gas Recovery: Targeted Technology Applications for Infield Reserve Growth, Boonsville Field, Fort Worth Basin, Texas

5. Report Date
October 1995

6.

7. Author(s)
B. A. Hardage, D. L. Carr, R. J. Finley, D. E. Lancaster, R. Y. Elphick, and J. R. Ballard

8. Performing Organization Rept. No.

9. Performing Organization Name and Address
Bureau of Economic Geology
The University of Texas at Austin
University Station, Box X
Austin, Texas 78713-8924

10. Project/Task/Work Unit No.

11. Contract(C) or Grant(G) No.
(C) 5093-212-2630
(G)

12. Sponsoring Organization Name and Address
Gas Research Institute
8600 West Bryn Mawr Avenue
Chicago, IL 60631
Project Manager: Thomas H. Fate

Department of Energy
Morgantown Energy Technology Center
P.O. Box 880, MS E06
Morgantown, West Virginia 26507-0880

13. Type of Report & Period Covered
Topical Report
5/1/93–6/30/95

14.

15. Supplementary Notes

16. Abstract (Limit: 200 words)

This report documents an assessment of Midcontinent sandstone natural gas reservoirs in Boonsville (Bend Conglomerate Gas) field by integrating four key disciplines: geology, geophysics, reservoir engineering, and petrophysics. Pressure and production data confirm the existence of compartmented or poorly drained gas throughout much of the Bend Conglomerate and suggest that additional gas will be found when well spacing is reduced to 80 acres, although multiple stacked completion opportunities will typically be needed to ensure the economic viability of new infield wells. As part of this analysis, the Lower Atoka Group was divided into 13 third-order genetic sequences, and to our knowledge, this is the first public, comprehensive genetic sequence analysis that relates these Pennsylvanian reservoirs to their seismic response and to gas productivity. A 26-mi^2, 3-D seismic survey was done to test methods for reservoir delineation in thin-bed, hard-rock environments and identified a previously unknown structural component of reservoir compartmentalization in the form of low-displacement faulting commonly associated with karst collapse in deeper carbonate rocks. These karst collapse features extend vertically as much as 2,500 ft and may be a widespread influence on the deposition of younger sediments in the Midcontinent. The ability of the 3-D survey to define stratigraphic entrapments was more variable. Some sequences were imaged quite well, and seismic attribute analyses provided excellent agreement with net reservoir distributions generated from sequence stratigraphic interpretations. In other instances, individual systems tracts and reservoir sandstones that were subsets of genetic sequences proved difficult to trace precisely in the 3-D data, especially when those units were associated with a subtle impedance contrast or were extremely thin.

17. Document Analysis a. Descriptors
3-D seismic, sequence stratigraphy, secondary natural gas recovery, depositional facies, reservoir compartmentalization, Bend Conglomerate Formation, Caddo Formation, Midcontinent, karst collapse

b. Identifiers/Open-Ended Terms
integrated geologic, engineering, petrophysical, and geophysical evaluation of fluvial and fluvio-deltaic reservoirs; identification of secondary natural gas resources

c. COSATI Field/Group

18. Availability Statement	19. Security Class (This Report)	21. No. of Pages
Release unlimited	Unclassified	600
	20. Security Class (This Page)	22. Price
	Unclassified	

(See ANSI–Z39.18) *See Instructions on Reverse*

OPTIONAL FORM 272 (4-77)
(Formerly NTIS–35)
Department of Commerce

RESEARCH SUMMARY

Title	Secondary Natural Gas Recovery: Targeted Technology Applications for Infield Reserve Growth in Midcontinent Reservoirs, Boonsville Field, Fort Worth Basin, Texas
Contractor	Bureau of Economic Geology, The University of Texas at Austin GRI Contract No. 5093-212-2630, "Secondary Natural Gas Recovery—Infield Reserve Growth Joint-Venture: Applications in Midcontinent Sandstones."
Principal Investigators	Robert J. Finley and Bob A. Hardage
Report Period	May 1993–June 1995
Objectives	The objectives of this project are to define undrained or incompletely drained reservoir compartments controlled primarily by depositional heterogeneity in a low-accommodation, cratonic Midcontinent depositional setting, and, afterwards, to develop and transfer to producers strategies for infield reserve growth of natural gas. Integrated geologic, geophysical, reservoir engineering, and petrophysical evaluations are described for complex, difficult-to-characterize, fluvial and deltaic reservoirs in Boonsville (Bend Conglomerate Gas) field, a large, mature gas field located in the Fort Worth Basin of North Texas. The purpose of this project is to demonstrate approaches to overcoming the reservoir complexity and target the gas resource, and to do so by using state-of-the-art technologies that can be applied by a large cross section of Midcontinent operators.
Technical Perspective	Reserve growth resources in the Midcontinent region total as much as 41 Tcf. The region contains the second-largest natural gas reserve growth resource after the Texas Gulf Coast and provides an appropriate resource target for secondary gas recovery (SGR) research following the Gulf Coast project. Secondary or incremental gas may be contained in reservoirs (even those that have conventional porosity and permeability) that are untapped or bypassed or that have incompletely drained areas that are a function of depositional facies, diagenetic, and even structural heterogeneity. The Midcontinent reservoirs selected for this project have more deltaic components than do the dominantly fluvial reservoirs that were the focus of the Gulf Coast SGR project. Further, the Midcontinent reservoirs studied were deposited in a cratonic basin that had relatively low accommodation space and a higher frequency of sea-level fluctuation than did depositional patterns in the Tertiary of the Gulf Coast Basin. Pennsylvanian Midcontinent sandstones are complex, but it is this complexity that creates the opportunity for additional infield gas recovery.
Results	Pressure and production data confirm the existence of compartmented or poorly drained gas reserves throughout much of the Bend Conglomerate, suggesting that additional reserves will be found when well spacing is reduced to 80 acres. Three styles of reservoir compartmentalization were identified in Midcontinent clastic gas reservoirs from the Boonsville analysis: structural, stratigraphic, and a combination of these two styles.

Structural compartments are caused by low-displacement faulting that acts as a partial barrier to gas flow and is commonly associated with karst collapse in deeper carbonate rocks; these features extend vertically as much as 2,500 ft in the project area. This previously unknown karst collapse phenomenon, identified by means of the 3-D seismic survey, may be a widespread influence on the deposition of younger sediments in the Midcontinent.

Stratigraphic compartments may be surface bounded, facies bounded, or cement bounded. Combination-style compartments have both structural and stratigraphic elements and are most commonly surface and fault bounded. The best natural gas reservoirs in Boonsville field occur predominantly as lowstand, valley-fill, conglomeratic sandstones overlying erosional surfaces. Isopach mapping indicates a strong relationship between reservoir distribution and structurally low areas on the pre-Atoka seismic time structure surface, suggesting that subtle elevation differences at the pre-Atoka stratigraphic level controlled the geographical location of incised valleys and the fluvial and fluvio-deltaic axes in which high-energy reservoir facies were concentrated.

Interpretation of these complex reservoirs was aided by a 26-mi^2 3-D seismic survey. Seismic resolution was maximized by using specialized small (10 oz) directional, explosive-source charges; a high data-sampling rate (1 ms); and staggered source and receiver lines that allowed the data to be stacked into high-fold 110- × 100-ft bins for general interpretation or into lower fold 55- × 55-ft bins when interpretations requiring detailed lateral resolution were needed. Precise calibration of thin-bed depths to seismic traveltime was accomplished by recording detailed vertical seismic profile (VSP) data and explosive-source velocity checkshot data at several locations within the 3-D seismic grid.

Whereas the 3-D seismic survey clearly identified the importance of the karst collapse features to reservoir compartmentalization, the ability of the 3-D survey to identify stratigraphic entrapments was more variable. Some sequences, such as the Upper and Lower Caddo, were imaged quite well, once calibrated to well control, and seismic attribute analyses provided excellent agreement with net reservoir distributions generated from sequence stratigraphic interpretations. In other instances, the 3-D data did not always provide conclusive answers. Individual systems tracts and reservoir sandstones that are subsets of genetic sequences were sometimes difficult to trace in the 3-D data, particularly when the acoustic impedance of these units was approximately the same as the acoustic impedance of the bounding beds or if the units were extremely thin.

Judging from the hydrocarbon distribution in the project area, the gas reserves expected in any particular Bend sequence will be approximately 200 MMscf or less, on average, when well spacing is reduced to 80 acres, whereas gas reserves of at least 400 MMscf will typically be required for new wells to be economically attractive. Although individual Bend completions may still encounter gas reserves in excess of 400 MMscf (some recent wells have), it appears that multiple stacked completion opportunities will be needed in new infield wells. Review of the 3-D seismic data suggests that these stacked trapping geometries often exist throughout the Bend interval. Thus, a reasonable approach to

identifying new well locations may be to focus 3-D seismic evaluation on these apparent stacked trapping geometries in areas having the highest likelihood of encountering multiple completion opportunities. An alternate strategy is to use the 3-D data to identify fault-bounded blocks that have no penetrations in subregional or field-scale areas where the pre-Atoka time structure is low and the total Atoka net reservoir isopachs are thick, again increasing the potential for finding multiple vertically stacked completion opportunities.

Technical Approach

This assessment of Midcontinent sandstone natural gas reservoirs in Boonsville field integrated four key disciplines: geology, geophysics, reservoir engineering, and petrophysics. The entire Atoka Group (Lower and Upper) in the project area was divided into 13 third-order genetic stratigraphic sequences. To our knowledge, this is the first public, comprehensive genetic sequence analysis that relates these prolific Pennsylvanian gas reservoirs to their seismic response and to gas productivity. A 26-mi^2 3-D seismic survey was acquired and interpreted to test methods for delineating reservoirs in thin-bed, hard-rock environments. Reservoir facies frameworks, assessed by integrating geological and geophysical approaches, were combined with engineering and petrophysical evaluations of produced gas volumes and reservoir quality.

Project Implications

The compartmentalization of Boonsville field has been demonstrated to have more than one origin. The field, much more complex than originally described, offers a challenge to effective infield drilling. The use of new technologies and the intelligent integration of results of these technologies have shown that fields as complex as Boonsville and their associated problems can be understood and effective production strategies applied. The use of the information gained from this project will have value to other Midcontinent fields and to many basins that have structural and depositional compartmentalization.

CONTENTS—VOLUME I

CONTENTS—VOLUME II

VOLUME I FIGURES AND TABLES

Figures

Tables

VOLUME II FIGURES AND TABLES

Appendix A Figures

Appendix A Tables

Appendix B Figures

Appendix C Figures

Appendix C Tables

Appendix D Figures

Appendix D Table

Appendix E Figures

Appendix F Figures

INTRODUCTION

Contained herein is Volume II of a two-volume report that describes an assessment of Midcontinent sandstone natural gas reservoirs in Boonsville field, a major gas field in the Fort Worth Basin of North-Central Texas. The field demonstration reported in this volume was conducted as part of the Secondary Gas Recovery (SGR) Infield Reserve Growth Joint Venture between the Gas Research Institute (GRI) and the U.S. Department of Energy (DOE), additional support being provided by the State of Texas. Substantial financial contributions were made to this work by OXY USA Inc., Enserch Operating Limited Partnership, and Threshold Development/Arch Petroleum Company, the three field operators who had producing properties inside the 26-mi^2 study area.

Volume I of this report is organized around a series of case studies that evolved from our study of Boonsville field and from the infield wells that were drilled as a result of the project study. The technical details involved in the major disciplines—geology, reservoir engineering, petrophysics, and geophysics—that were integrated in this reservoir characterization have been segregated into this second volume of the report and are presented as a series of appendices.

APPENDIX A

GEOLOGIC EVALUATION OF THE BOONSVILLE PROJECT AREA

Introduction

More than 90 percent of the 2.6 Tcf of natural gas produced at Boonsville field has come from conglomeratic sandstones deposited in the Fort Worth Basin during the Atoka Stage of the Middle Pennsylvanian Period (Fig. A1; Blanchard and others, 1968; Thompson, 1982). The distribution, porosities, and permeabilities of Boonsville sandstones and many other Upper Paleozoic sandstone reservoirs in Midcontinent basins are typically erratic and unpredictable. Previous investigations have concluded that trapping mechanisms are due predominantly to sandstone facies pinch-outs and permeability pinch-outs due to diagenetic cements (Glover, 1982; Lahti and Huber, 1982; Thompson, 1982). Effective characterization and exploitation of these fields are difficult because the sandstone reservoirs, typically thin and discontinuous, represent a variety of complexly intermingled depositional environments and facies and commonly contain pore-occluding diagenetic cements. As compared with other times in geologic history, the fundamental geological controls on reservoir architecture and stacking patterns in marine basins were unique during the Pennsylvanian Era. Specifically the mechanisms that combined to produce complex, compartmentalized reservoirs at the Fort Worth, and many other Midcontinent Basins were:

- Relatively low accommodation setting (i.e., shallow basin)
- High-amplitude, high-frequency sea-level fluctuations
- Tectonic jostling during sedimentation
- Temporal variations in sediment source material
- High rates of sediment supply

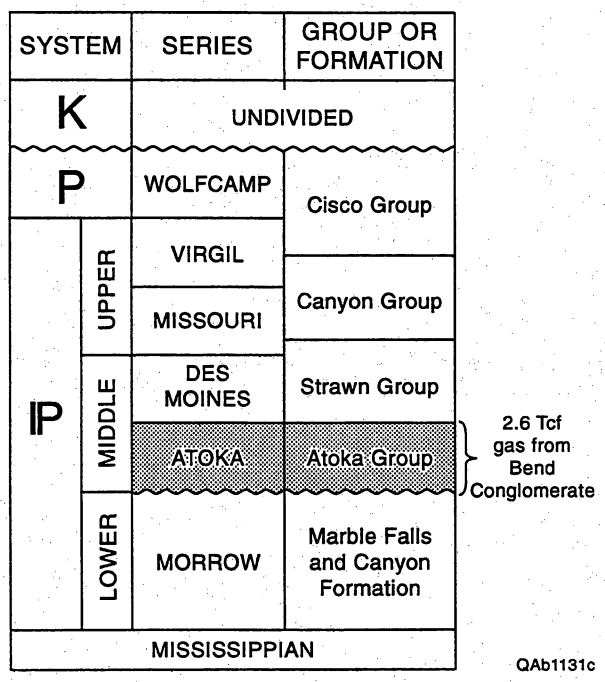

Figure A1. Time-rock stratigraphic column for post-Mississippian strata in the Boonsville Project Area. Modified from Thompson (1982).

- Tropical paleoclimate

The purpose of the geological investigation was to determine how these unique geological circumstances shaped reservoir architecture in this important natural gas province and to outline predictive development strategies that pinpoint optimal infill drilling sites. This appendix describes the geological conditions and concepts, data base, methods of evaluation, and general geological interpretations of the Boonsville Project Area that represent the foundation upon which development strategies were built.

Hydrocarbon Habitat

Gas accumulations in Ouachita foreland basins, including Bend Conglomerate gas in the Fort Worth Basin, occur as large, pervasive, *deep basin accumulations* (Masters, 1979; Meckel and others, 1992). Pennsylvanian gas reservoirs in these basins, typically underpressured, produce little to no water and are relatively tight (typically less than 10 md). They are hydraulically separated from updip/overlying, more permeable, normally pressured water-bearing units (Meckel and others, 1992). The source of the natural gas is probably the abundant humic materials (land-derived, macerated plant material) in shales that encase the sandstone reservoirs (Meckel and others, 1992). Other Ouachita foreland basins having similar habitats, include the Arkoma, Val Verde, and Black Warrior Basins, and possibly the Kerr and Marfa Basins (Fig. 1.3).

Global Stratigraphic Context

Present-day continental margins are comprised of thick, well-preserved Mesozoic and Cenozoic deposits that contain seismically resolvable depositional sequences (Vail and others, 1977; Ross and Ross, 1988). Thick continental margin wedges also formed during the Late Paleozoic; however, individual depositional sequences are much more difficult to identify in the Late Paleozoic wedges because, generally too extensively deformed, they

contain long-ranging, deep-water fossils that are difficult to correlate with shallow-water fossils and many of the wedges have been consumed by subduction zones and no longer exist (Ross and Ross, 1988). Thus, most Late Paleozoic strata preserved today, including those containing hydrocarbon reservoirs, represent the thin, updip stratigraphic remnants of sea-level highstands deposited in stable cratonic areas, such as the U.S. Midcontinent region (Ross and Ross, 1988).

Eustatic Sea Level

The southern supercontinent, Gondwana, drifted through the south-polar region during the Paleozoic, resulting in continental glaciation that controlled ocean water volume and, thus, eustatic (worldwide) sea level (Crowell and Frakes, 1970; Crowell and Frakes, 1975; Crowell, 1982; Caputo and Crowell, 1985). Similar to the more recent Pleistocene ice age, astronomical factors caused glacial ice volume and its reciprocal, ocean-water volume, to vary cyclically with periodicities ranging from about 20,000 to 400,000 yr (Donovan and Jones, 1979; Berger, 1988; Heckel, 1989a, b; Goldhammer and others, 1991; Connolly and Stanton, 1992). The magnitudes of Late Paleozoic sea-level variations are estimated to be on the order of 60 to 200 m (200 to 650 ft) (Heckel, 1977; 1989a, b; Crowley and Baum, 1991), which is a magnitude large enough alternately to expose and drown continental shelves and continental interior seaways.

The high-amplitude, high-frequency signal has been recognized in Late Paleozoic strata worldwide (for example, Heckel, 1977, 1980; Brown and others, 1990; Goldhammer and others, 1991; Youle and others, 1994). Global and regional sea-level histories have been reconstructed from seismic data (Vail and others, 1977) and, in considerably finer detail, from Late Paleozoic rocks (Heckel, 1977, 1986; Ramsbottom, 1979; Saunders and others, 1979; Ross and Ross, 1985; Boardman and Heckel, 1989). Using data from three continents, Ross and Ross (1988) constructed a comprehensive, Atokan eustatic sea-level estimate, which details six major eustatic cycles (Fig. A2).

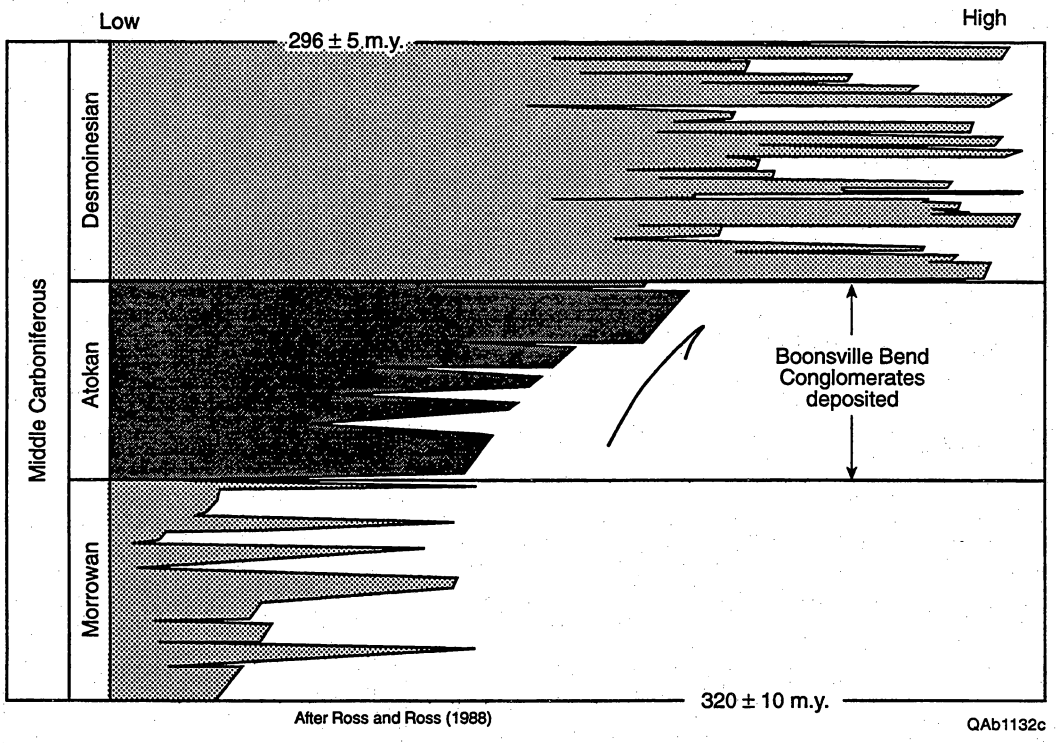

Figure A2. Middle Carboniferous eustatic sea-level changes derived from coastal onlap data.

Late Paleozoic Paleoclimate

During the Pennsylvanian, the U.S. Midcontinent was located in the tropics (Fig. A3), a conclusion supported by both paleomagnetic data (McElhinny, 1973; Morel and Irving, 1978) and paleontological information (Nassichuk and Bamber, 1978; Phillips and Peppers, 1984). The Appalachians lay just south of, and parallel to, the equator, which ran in a line from approximately southern Texas to Maine (Scotese and others, 1979; Heckel, 1980). The Fort Worth Basin and Ouachita Mountains were located in the doldrums, whereas the rest of what is now the central United States straddled the northern trade wind belt (Heckel, 1980). Euramerica remained approximately in this position during the entire Pennsylvanian (Scotese and others, 1979). Phillips and Peppers (1984) analyzed the florae preserved in coals and coal balls from North America and Europe, and, on the basis of palynological changes, were able to document synchronous, global changes in climate. The Early Atokan climate was seasonally dry and wet but became very wet from the Middle Atokan to the Desmoinesian Epoch; the increase in humidity and rainfall parallels, and resulted from, the Atokan global transgression (Fig. A2). The tropical paleoclimate provided optimal conditions for biogenic production of skeletal calcite, which later became an important diagenetic component in sandstone units or formed limestone beds during brief cessations of terrigenous clastic influx.

Fort Worth Foreland Basin: A Mixed Accommodation Basin

The Fort Worth Basin is a Late Paleozoic foreland basin that contains a maximum thickness of approximately 13,000 ft of sedimentary strata, the majority of which are Pennsylvanian in age (Turner, 1957a; Thompson, 1988). In addition to the dominantly Pennsylvanian basin fill, major sequences of Cambrian, Ordovician, Mississippian, and Permian rocks are also present. The Paleozoic units are unconformably overlain and

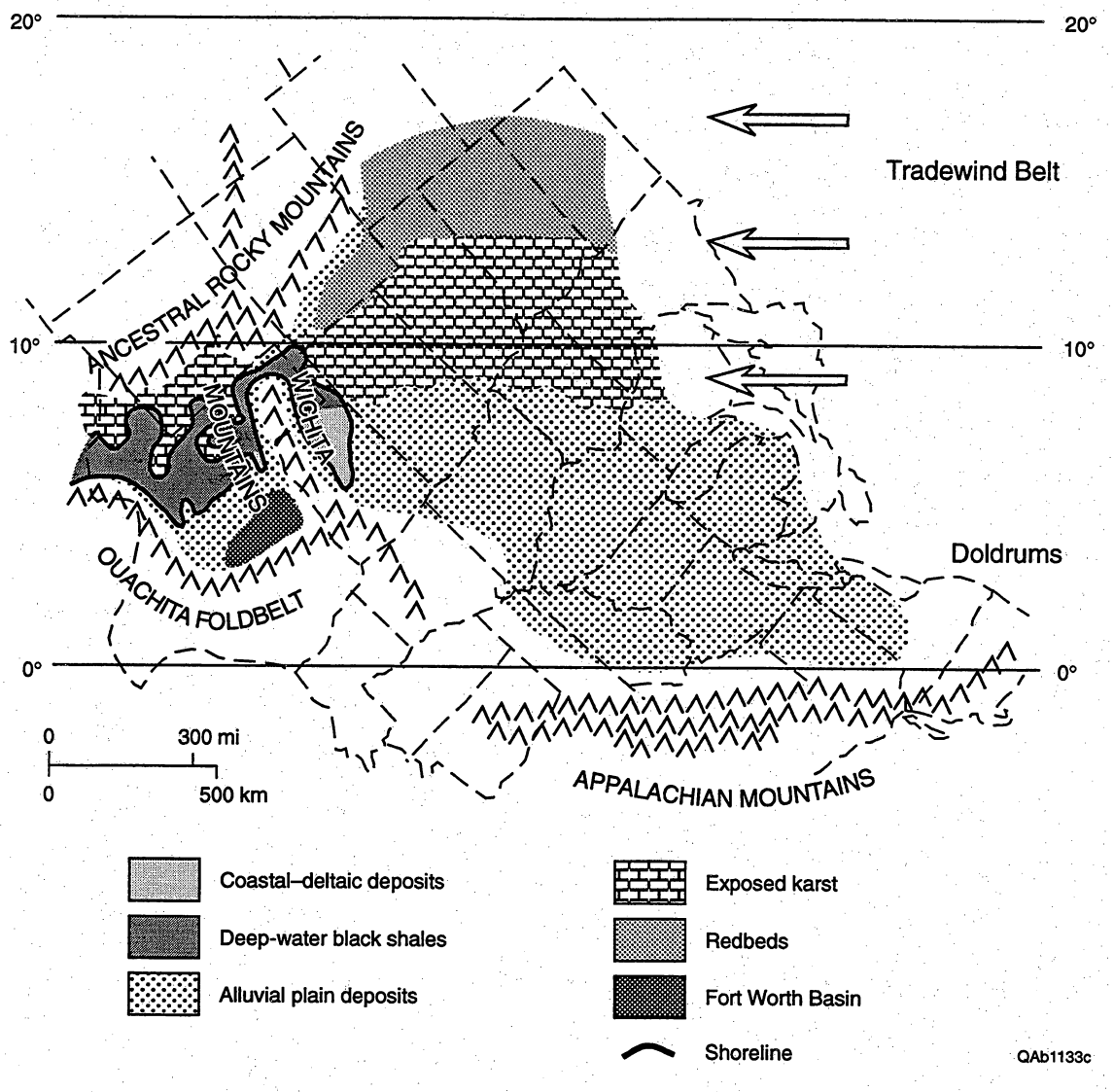

Figure A3. Pennsylvanian paleogeography and lithofacies distribution of the Midcontinent United States during maximum regression (lowstand). After Heckel (1980).

onlapped by Cretaceous strata that occur in the east and southeast parts of the basin (Flawn and others, 1961; Lahti and Huber, 1982; Thompson, 1982, 1988).

In map view, the Fort Worth Basin is an asymmetric, inverted triangle that is approximately 80 mi across and 250 mi long, from apex to base (Fig. A4). Fault-bounded structural uplifts define the eastern (Ouachita Thrust Belt) and northern limits (Muenster Uplift, Red River [=Electra] Uplift) of the basin, but the less distinct western limit is bounded by the Bend Arch, which is a low, north-plunging fold. The Muenster and Red River–Electra Uplifts are both thought to be part of the northwest-trending Amarillo–Wichita Mountain Uplift, which resulted from reactivation of Precambrian boundary faults when Ouachitan compressive stresses were transmitted to the craton (Walper, 1977). A concise synopsis of Fort Worth Basin structural elements can be found in Lahti and Huber (1982).

The Fort Worth Basin is one of several foreland basins formed by, and lying immediately adjacent to, the leading edge of the Ouachita–Appalachian Fold Thrust Belt (Fig. 1.3) (Lahti and Huber, 1982; Thompson, 1982, 1988; Meckel and others, 1992). The Ouachita–Appalachian Fold Thrust Belt is the result of continental collision between the carbonate-dominated, Euramerican (previously fused plates containing parts of North America and Europe) passive margin and the Gondwana supercontinent, which was comprised of parts of present-day Africa, South America, Antarctica, and Australia (Wickham and others, 1976; Meckel and others, 1992). The initial compressional effects began in Early Pennsylvanian time and moved southwestward along the belt in sporadic waves, from the Middle Atlantic region to the southwest Texas–Mexican border area, where it culminated in Early Permian time (Wickham and others, 1976).

Foreland basins are created by subsidence in areas immediately adjacent to complexly folded and faulted overthrust belts (Fig. A4). Subsidence in the overthrust foreland occurs by incremental loading of the lithosphere as successive thrust sheets are emplaced. The load-induced subsidence creates a deep, asymmetric *flexural moat* next to the belt; the

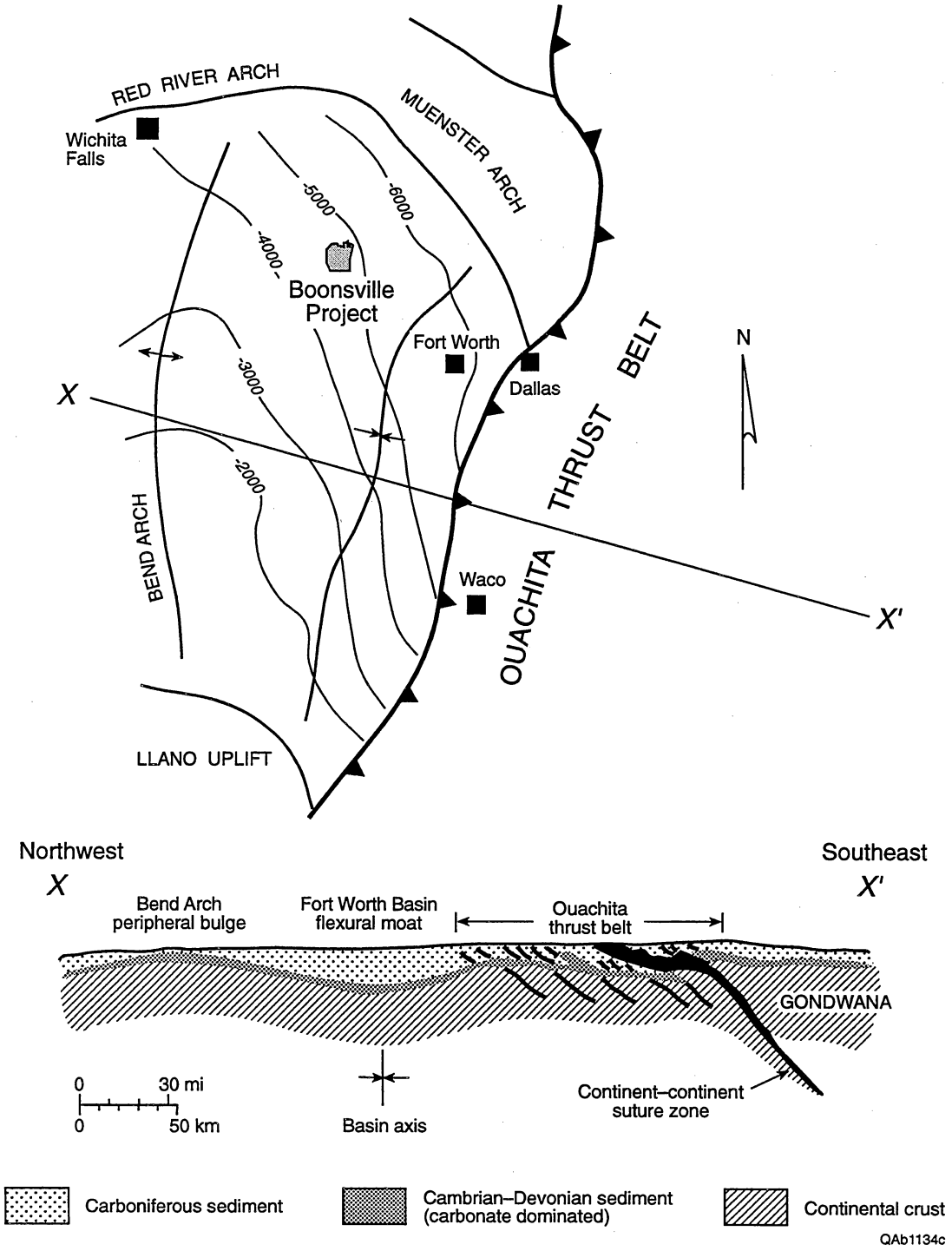

Figure A4. Tectonic and structural framework of the Fort Worth Foreland Basin. Contours represent depth below sea level of the top of the Marble Falls Formation. Structure map after Meckel and others (1992); tectonic cross section after Wickham and others (1976).

flexural moat becomes shallower away from the belt, and, in fact, grades into a slightly positive, upwarped *peripheral bulge* (Quinlan and Beaumont, 1984). The axis of the Fort Worth Basin represents the flexural moat, and the Bend Arch may represent the peripheral bulge that formed in response to Ouachita thrust loading.

Foreland basins are cratonic (or continental) basins that have widely varying amounts of *accommodation*, which is defined as the space below base level (commonly sea level) available for sediment to accumulate (Jervey, 1988). Depending on relative geographic position with respect to the adjacent thrust belt, the flexural moat, or the peripheral bulge, a spectrum of accommodation settings are present, ranging from high in the moat or basin axis, to low near the peripheral bulge. If one considers oceanic, continental margin basins to be *high-accommodation basins*, and at the other extreme, shallow intracratonic basins (for example, Lower Paleozoic U.S.A.) to be *low-accommodation basins*, then foreland basins could be characterized as *mixed-accommodation basins* that, intermediate in total accommodation, nonetheless have wide, intrabasinal variations in local accommodation. The Fort Worth Basin is a mixed-accommodation basin by this definition (Table A1).

Table A1. Accommodation settings of marine sedimentary basins.

Accommodation setting	Structural classification(s)	Generalized stratal architecture	Examples
HIGH	Oceanic continental margins	Vast, thick (tens of thousands of feet and greater); architecture dominated by progradational elements; high preservation potential for diverse facies assemblages: lithology-dominated strata	Gulf of Mexico; other post-Jurassic oceanic basins worldwide
MIXED	Foreland basins, rift basins	Deposits restricted to local–regional areas; varying thicknesses that typically do not exceed thousands of feet; variety of architectural elements that vary through time (vertically in stratigraphic section) and space	Fort Worth Basin, Val Verde Basin, Arkoma Basin, Appalachian Basin, Cretaceous Western Interior Basin
LOW	Shallow cratonic basins	Thin, sand-rich, surface-dominated strata	Lower Paleozoic interior U.S.A.

Reservoir architecture within mixed-accommodation basins is complex. In a mixed setting, small base-level changes result in accommodation changes over short distances that can have a profound impact on depositional environments, facies, and reservoir architecture. These same small changes might not greatly affect sedimentation in a high-accommodation setting. For example, a 100-ft drop in sea level would not change sedimentary environments significantly on a 300-ft deep continental shelf, whereas the same sea-level fall in a 100-ft-deep cratonic shallow seaway would cause a major facies dislocation from shelf mudstones to upper shoreface sandstones or deltaic sediments.

Accommodation Settings and Stratal Architecture

There is a process–response relationship between accommodation, sediment volumes distribution, and the resulting stratal stacking patterns (Gardner and Cross, in preparation). Accommodation is the key variable that determines whether sediment is preserved and is thus intimately related to the relative proportions of time represented by either erosion surfaces or strata.

Sedimentary rocks preserved in thin, intracratonic wedges deposited in mixed-/low-accommodation settings are typically *surface-dominated strata* (Gardner and Cross, in preparation). For a given unit of geologic time, these strata contain many surfaces of erosion or nondeposition. The net time required for the deposition of strata may have been relatively small compared with the erosional–nondepositional breaks in sedimentation (hiatuses or disconformities) represented by the surfaces that separate stratal units. By contrast, in a typical *stratal-dominated* package, such as Mesozoic or Cenozoic continental margin strata, the thick strata themselves represent much greater net time than do the intervening surfaces, which are generally less numerous and less severe in erosional character.

Surface-dominated, terrigenous clastic strata are typically thin and commonly contain sand-prone, lowstand systems tracts that are rarely fully preserved. Once deposited, parts

of the originally complete systems tracts were commonly stripped away by repeated erosional events. Many cycles of erosion and subsequent thin-bed aggradation produce a complex mosaic comprised of the erosional remnants of several or many diachronous (deposited at different times) systems tracts. The overall effect is such that tracing fossil depositional environments is difficult because the rock record in low-accommodation sequences commonly contains only incomplete pieces of individual, time-equivalent strata. It is analogous to reconstructing a jigsaw puzzle after your Irish Setter has chewed up or eaten half the pieces.

The relative amounts of time represented by surfaces or rocks in depositional sequences are controlled by the accommodation history. Fort Worth Basin strata tend to be surface dominated, especially compared with Mesozoic and younger continental margin deposits, such as those in the Gulf of Mexico Basin. Because of their cratonic, mixed- and low-accommodation settings, Midcontinent strata are surface dominated and are typically made up of complex mosaics of thin, incompletely preserved slivers of systems tracts in which sandstone reservoirs occur.

Reservoir Heterogeneity Varies with Accommodation Setting

Facies characteristics within reservoir sandstone bodies vary with accommodation setting (Gardner and Cross, in preparation). In general, preserved assemblages of bedforms are diverse, and greater numbers and volumes of shale interbeds occur in high-accommodation sequences. Because of the ample available space, sediment reworking is minimal and preservation potential for a given depositional event is high. The opposite is true in low-accommodation reservoirs: constant reworking of sediments winnows clays and concentrates framework sand grains in low-accommodation sequences. Crossbed sets in low-accommodation reservoirs are commonly truncated and incomplete and represent *micro*surface-dominated sandstone facies that are, in effect, the small-scale, fractal equivalents of the surface-dominated strata in which they occur. Although systems tracts

tend to be fragmented and sandstone-body geometries hard to predict in low-accommodation, Midcontinent sequences, once found, internal sandstone heterogeneity is generally low in the absence of diagenetic cements, and these units tend to be productive reservoirs.

Well Log Correlation of Surface-Dominated Strata

Log correlations and mapping of depositional environments and facies tracts in surface-dominated strata are especially difficult and prone to error because it is not uncommon for systems tracts and sometimes even entire sequences to be truncated or absent in some of a field's wells. The process of well-log correlation is inherently biased toward lithostratigraphic correlation: the interpreter typically attempts to recognize and relate specific rock units that display a distinctive pattern on the logs. It is easy for the interpreter to string together rock units having a similar log character or units that appear at similar depths, when in reality, time lines, true reservoir compartment geometries, and flow-unit architectures can be vastly different from layer cake lithostratigraphic interpretations. Today's successful geologist must understand and apply chronostratigraphic concepts, which, in subsurface work, means that one must identify and trace the key time lines or chronostratigraphic surfaces that separate rock units in subsurface reservoirs. The process of tracing chronostratigraphic surfaces between wells can be abstract and difficult, requiring the synthesis of cores, logs, and seismic data containing regional information on tectonics, sea-level history, paleoclimates, and sediment supply. However, it is critical to perform the task properly because without an accurate chronostratigraphic framework, subsequent interpretations and mapping of depositional systems and sandstone reservoir geometries are likely to be incorrect.

Stratigraphic Nomenclature

The Railroad Commission of Texas has defined the Bend Conglomerate producing section as "that section found in the interval between the base of the Caddo Lime and the top of the Marble Falls formation." (Fig. 1.5; Railroad Commission of Texas, 1991). For practical purposes, the terms "Bend Conglomerates" and "Atoka Group" are essentially synonymous, and can be used interchangeably. We have retained Thompson's (1982) "Lower Atoka" and "Upper Atoka" division, which splits the Bend Conglomerate interval into geologically distinctive halves. A time-stratigraphic correlation chart for comparing units across the many basins in the Midcontinent U.S.A. appears in Figure 1.4.

Unlike most previous workers, we designate the base of the overlying Strawn to be the top of the Atokan Bend Conglomerates and specifically include the "Caddo Limestone" in the Atoka Group. The base of the overlying Strawn Group is the best practical marker for the top of the Atoka because (1) it represents a major eustatic flooding surface, which can be identified readily on logs even when the Caddo Limestone is not present owing to erosion during the final, major Atokan sea-level lowstand (our Upper Caddo cycle); (2) our work suggests that the "Caddo Limestone" is not a single lithostratigraphic unit but actually a series of offlapping, abandoned delta-platform limestones deposited on prograding, Lower Caddo delta lobes; and (3) the biostratigraphic boundary between the Strawn and the Atoka Groups is poorly defined: Lovick and others (1982) reported that Atokan fusulinids occur in the Caddo Limestone. Also, Cheney and Goss (1952, p. 2254) stated that "the 'Caddo lime' of central Texas is lithologically and structurally more related to the Smithwick and Big Saline [i.e., Atoka] than to the Strawn."

A variety of nomenclatures and zonations have been developed to divide the major zones in the Bend Conglomerates, but the complex stratigraphy, lack of outcrop exposures, and paucity of good index fossils have led to a proliferation of schemes that are not

rigorously correlative to one another (Fig. A5). As a result of the confusion in the published literature, individual operating companies have been forced to develop their own local nomenclatures. Even within the Boonsville Project Area, there were considerable differences in zone definitions, correlations, and names used by our operator-partners. To facilitate communication between the many project participants, and to allow unrestricted geological interpretation of the Bend Conglomerate interval, it was necessary to create a new, more broadly applicable nomenclature system in which the major reservoir zones were divided using the concepts of *sequence stratigraphy* (see later discussion). The type log shown in Figure 1.5 illustrates the stratigraphic framework we used to define the major reservoir zones in the Boonsville Project Area. The zones represent major time-equivalent sequences that were subsequently named for local cultural and geographic features in the project area; the widely utilized terms, Caddo and Davis, were preserved because they fit within our sequence stratigraphic framework.

Sediment Sources

All the Boonsville sequences (Fig. 1.5) that we mapped in the project area, except perhaps for the Davis, were sourced from the north, namely from the Muenster and Red River–Electra elements of the Wichita mountain system. Crossbed dip directions within reservoir sandstones throughout the Atoka section analyzed by means of FMI/FMS borehole imaging tools indicate a north-to-south sediment transport direction (Fig. A6). Petrographic and infrared spectroscopic analyses show increasing percentages of feldspars and igneous–metamorphic rock fragments in sandstones upward through the Atoka section, reflecting the erosional unroofing of the granitic core of the Wichita mountain system (Fig. A7).

There is considerable variation in previous interpretations of Lower Atoka sandstone sediment sources. Brown (1973), Ng (1979), and Thompson (1982, 1988) suggested an eastward Ouachitan source, whereas Lahti and Huber (1982), Lovick and others (1982),

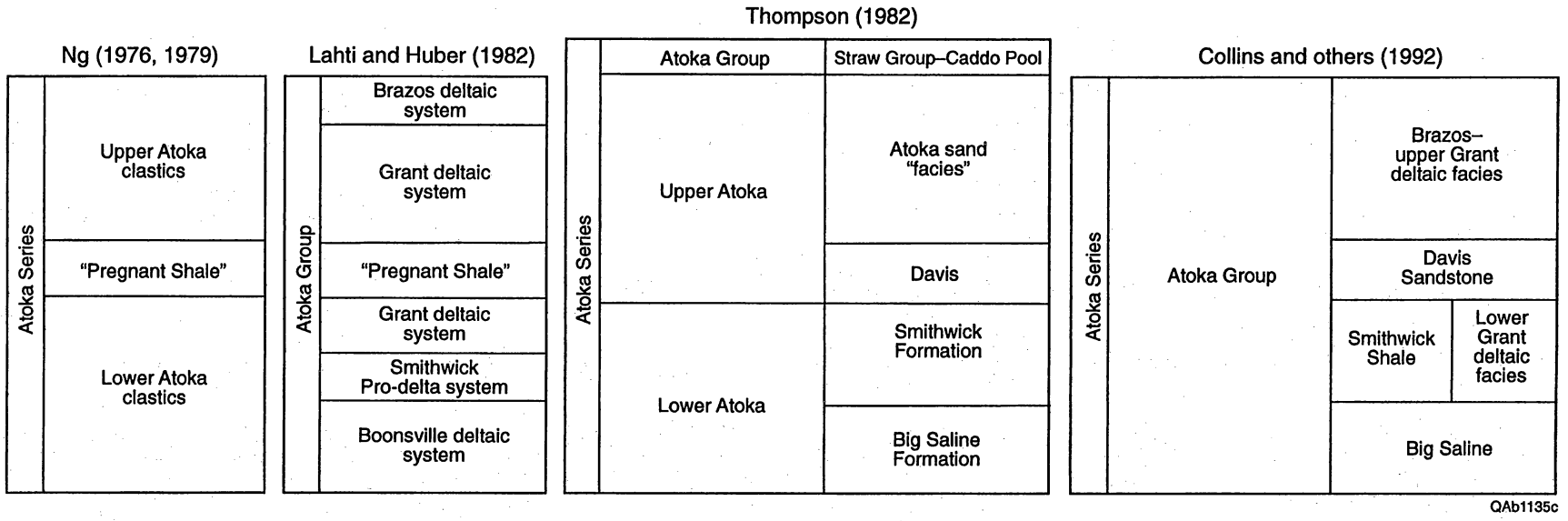

Figure A5. Comparison of stratigraphic nomenclatures for Atokan rocks in the Fort Worth Basin presented by previous workers. The complex geologic relationships have contributed to a proliferation of nomenclatural systems.

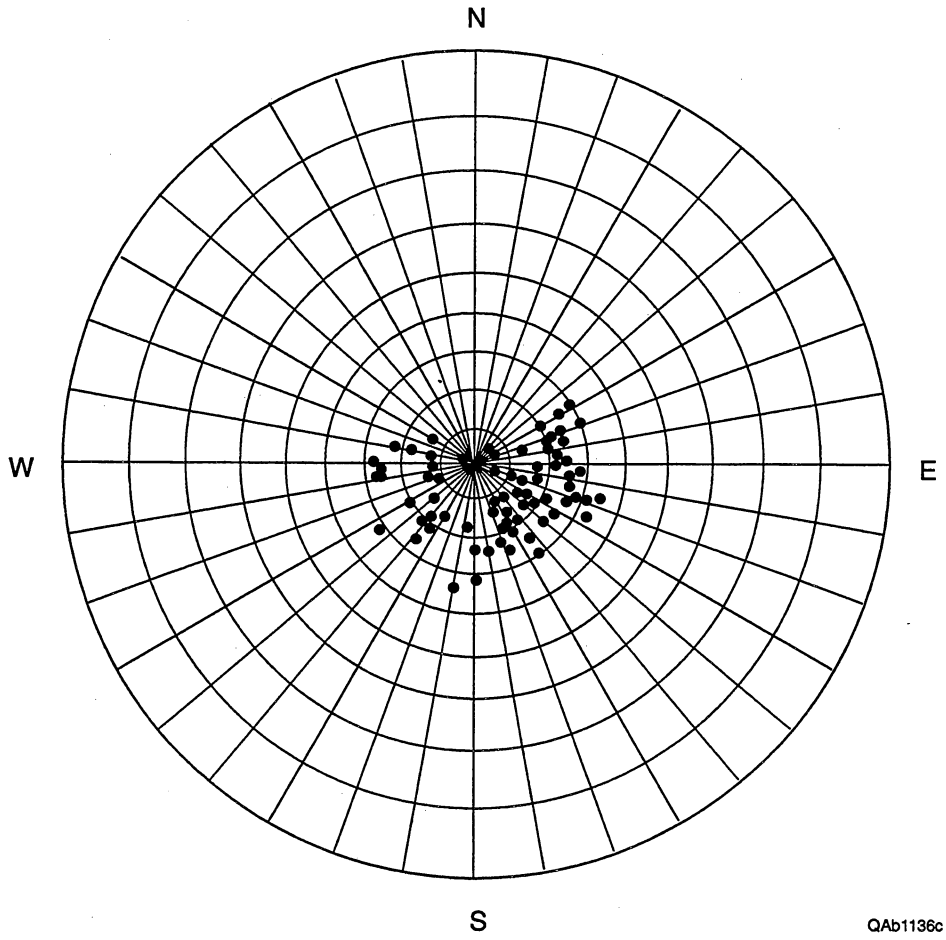

Figure A6. Crossbed dip orientations based on FMI log data from the Lower Atoka, Billie Yates No. 18D.

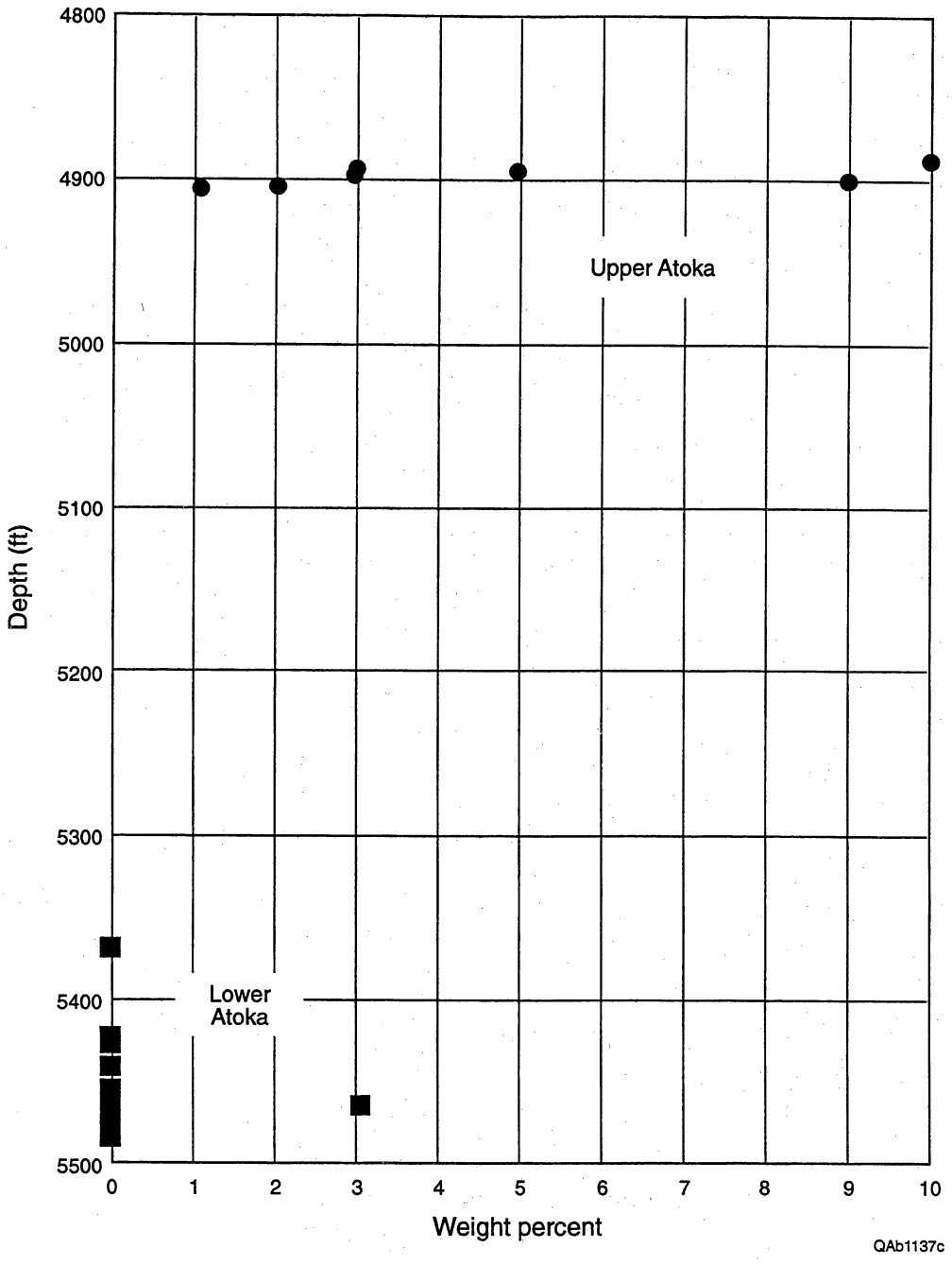

Figure A7. Depth distribution of potassium feldspars determined from infrared spectroscopic analysis of core samples.

Meckel and others (1992), and Ammentorp and Cleaves (1990) agreed with our interpretation for a northern Wichitan source. Review of published literature and communications with Boonsville operators suggests that Thompson's (1982) Ouachitan interpretation may be the most widely applied regional framework in use today, although our data and that of the several others cited above support a northern source.

The Davis sequence (Thompson, 1982; Collins and others, 1992) and the overlying "Grant Deltaic System," which is not present in the SGR Project Area (Lahti and Huber, 1982; also called "Upper Atoka" by Ng, 1979; "Grant Sands" by Lovick and others, 1982; and "Post Davis" by Thompson, 1982), both appear to have been derived predominantly from the Ouachitas. The post-Davis, Upper Atoka in our terminology (Wizard Wells and Caddo sequences; Fig. 1.5), were both sourced from the north; well log and seismic clinoform dip directions, FMI-derived paleocurrents, and petrographic analyses point to a feldspar-rich Wichitan source.

Boonsville Geological Data Set

The data available for evaluating Boonsville Bend Conglomerates in the project area primarily consisted of well log data from 222 wells (Table A2) and some core in and around the 3-D seismic survey. Figure A8 shows the aerial distribution of well log suites and the location of cored wells used in the evaluation.

Table A2. Logging suites from 222 wells available for geological evaluation of Boonsville Project Area.

Suite	Logs typically available	Number of wells	% of total wells
MODERN	Gamma ray; density-neutron, SP; resistivity: dual induction, array induction, phasor induction; microlog; PEF (23 wells); Sonic (15 wells)	105	47.3
IES	SP; resistivity: deep induction, 16" (short) normal; microlog	74	33.3
ES	SP; resistivity: lateral; 64" (long) normal; 16" (short) normal; microlog	43	19.4

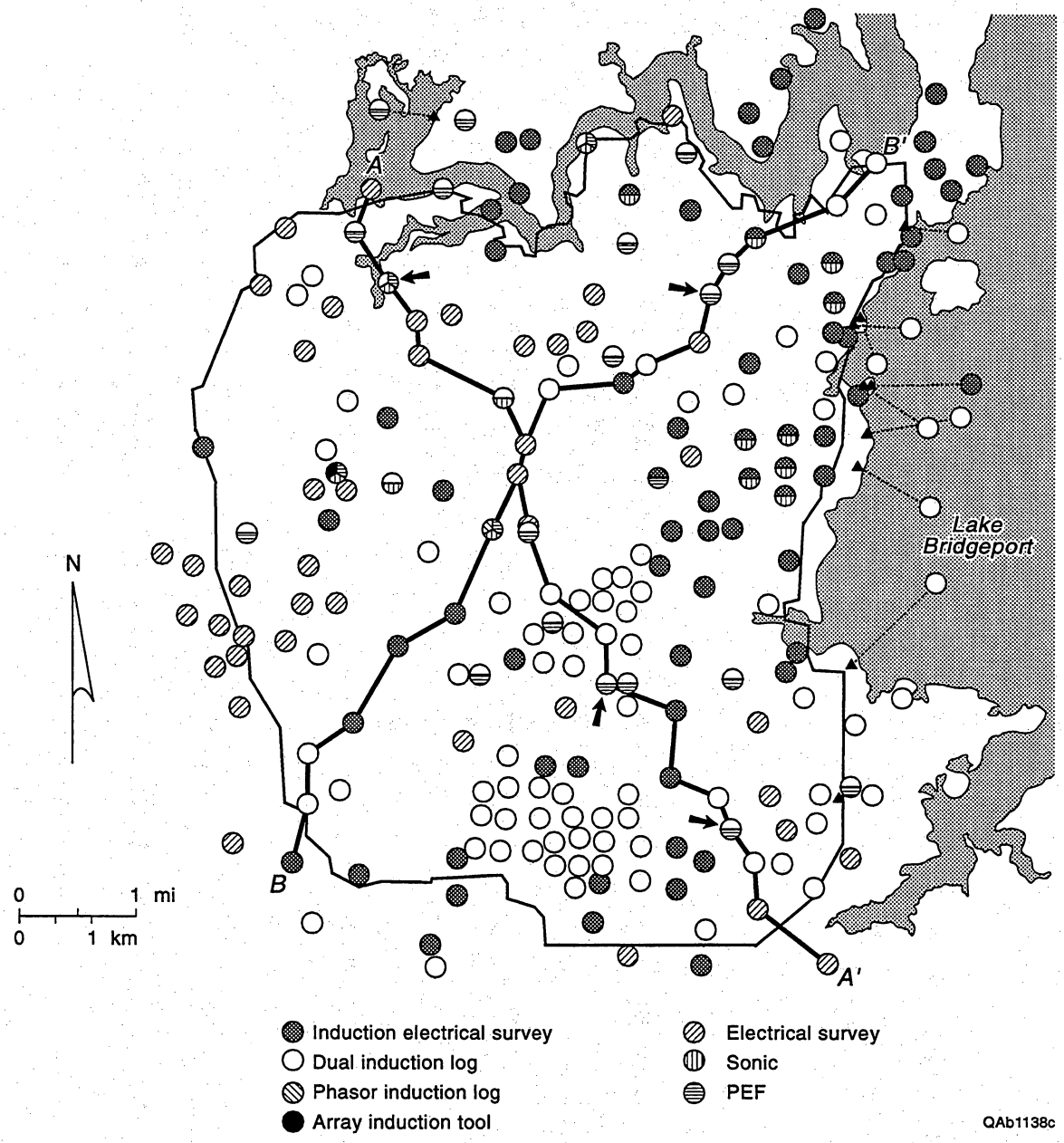

Figure A8. Distribution of well log suites and cores (at arrows) used in the geologic evaluation of the Boonsville Project Area. Boundary represents outline of the 3-D seismic survey.

Methods of Geologic Analysis

OXY U.S.A.'s *Stacked Curves* (*SCPC*) software system was utilized to conduct the geologic evaluation. *Stacked Curves* is a proprietary package developed on a mainframe computer by OXY in the 1980's and recompiled for the IBM-PC platform in the 1990's. It is used extensively throughout the company to determine detailed knowledge of reservoir geometry and associated parameters crucial in infill drilling, field extension, and enhanced recovery projects (Srivistava, 1994). In this project, *SCPC* was used to display, normalize, and perform petrophysical transforms on digital log curves; conduct sequence stratigraphy and correlate reservoir zones; run summations of reservoir parameters; construct reservoir isopach maps; and integrate well data with 3-D seismic data.

OXY also provided a comprehensive digital well data base for the project area and digital well log curves for their acreage. All available log hardcopies from wells within and proximal to Arch-Threshold's and Enserch's properties were digitized and loaded into *SCPC*. Production data for most wells in the project area was also provided by the operator-partners. The SGR reservoir engineering team reviewed production files and constructed an electronic spreadsheet detailing completion zones, dates, and other pertinent data, which were input to the *SCPC* database.

Cores from four wells, totaling 358 ft, were slabbed and described, focusing on lithology, facies and depositional environments, key surfaces, and the impact of each of these parameters on reservoir rock quality. Graphical core descriptions and key symbols are shown in Figures C13 through C17. Three of the four cores were collected cooperatively with each one of the three operator-partners. Fifty thin sections were cut from the cores and analyzed to complement core description observations and to determine porosity types, clast provenance, and diagenetic cements.

A log-calculated facies transform was developed by integrating efforts of the geological and petrophysical teams (detailed in Appendix C). Core-calibrated, log-

calculated facies curves can help identify the complex lithologies in the Bend Conglomerate interval, which include pyrite, ferroan calcite, and dolomite-cemented sandstone facies and marine limestones that are difficult to distinguish from one another in most of the older log data and in many of the modern suites lacking a PEF curve. It is critical to identify the major facies and lithologies accurately, even nonreservoir facies, to make the key surface correlations that define the reservoir architecture.

Application of Sequence Stratigraphy to Boonsville Bend Conglomerates

The concept of *sequence stratigraphy* was instrumental in defining the major time-equivalent or *chronostratigraphic* rock units containing the main reservoir zones in the Boonsville Bend Conglomerates. Sequence stratigraphy is a recent advance representing the synthesis and integration of process sedimentology–depositional systems analysis with seismic stratigraphy research that was created primarily by Exxon Production Research (EPR; for example, Vail and others, 1977). EPR's main premise was that seismic reflections represent *key chronostratigraphic surfaces* that closely approximate time lines, and these surfaces bound genetically related, time-equivalent rock units. Key surface recognition was combined with facies analysis to interpret outcrops, cores, and well logs in the 1980's; refinement and application of sequence stratigraphy continues today (for example, Van Wagoner and others, 1990; Mulholland, 1994). Recognition of key chronostratigraphic surfaces is important in reservoir characterization because these surfaces commonly define sandstone body and internal flow-unit geometries.

Key chronostratigraphic surfaces separate the major types of *depositional systems tracts* that are deposited during distinct phases of a given *base-level cycle*. Base-level cycles (or relative sea-level cycles) result from eustatic sea-level changes, sediment supply, tectonic subsidence, and physiography of the depositional substrate (Cross, 1988; Van Wagoner and others, 1990; Gardner and Cross, in preparation). *Depositional systems* are three-dimensional assemblages of lithofacies, linked by active (modern) or inferred

(ancient) processes and environments (Fisher and McGowen, 1967). A *depositional systems tract* (Brown and Fisher, 1977) is a linked assemblage of contemporaneous depositional systems. The sedimentary deposits of depositional systems tracts are commonly bounded by key surfaces that can manifest themselves as seismic reflections if the combination of bed thickness, acoustic-impedance contrast across surface boundaries, and seismic data-frequency content are favorable.

Boonsville–Atoka Sequences

In the Boonsville Project Area, complexly arranged key chronostratigraphic surfaces are a major control on compartmentalization and architecture of Atokan reservoirs (Fig. 1.6). Key surfaces are widespread physical surfaces that separate younger strata from underlying older strata. Facies offsets, or facies dislocations as they are sometimes called, that interrupt normal Walther's Law facies successions commonly occur at these surfaces. The familiar methods of depositional systems analysis and facies modeling are valid only within time-rock units bounded by key surfaces. After core-calibration, facies, key surfaces, and systems tracts could be inferred from well log responses (Fig. A9), but the degree of reliability varied with data vintage and quality.

Three types of key surfaces were identified, correlated, and used as defining boundaries for Boonsville Bend Conglomerate reservoir zones: flooding surfaces (FS), maximum flooding surfaces (MFS), and erosion surfaces (ES). *Flooding surfaces* are widespread surfaces where evidence of a upward-deepening facies dislocation occurs, such as the contact between rooted, unfossiliferous floodplain mudstones and overlying fossiliferous marine shale. A *ravinement surface* is a type of flooding surface where evidence suggests that transgressive passage of a surf zone has slightly eroded the underlying shallower water facies. Several ravinement-type flooding surfaces occur in

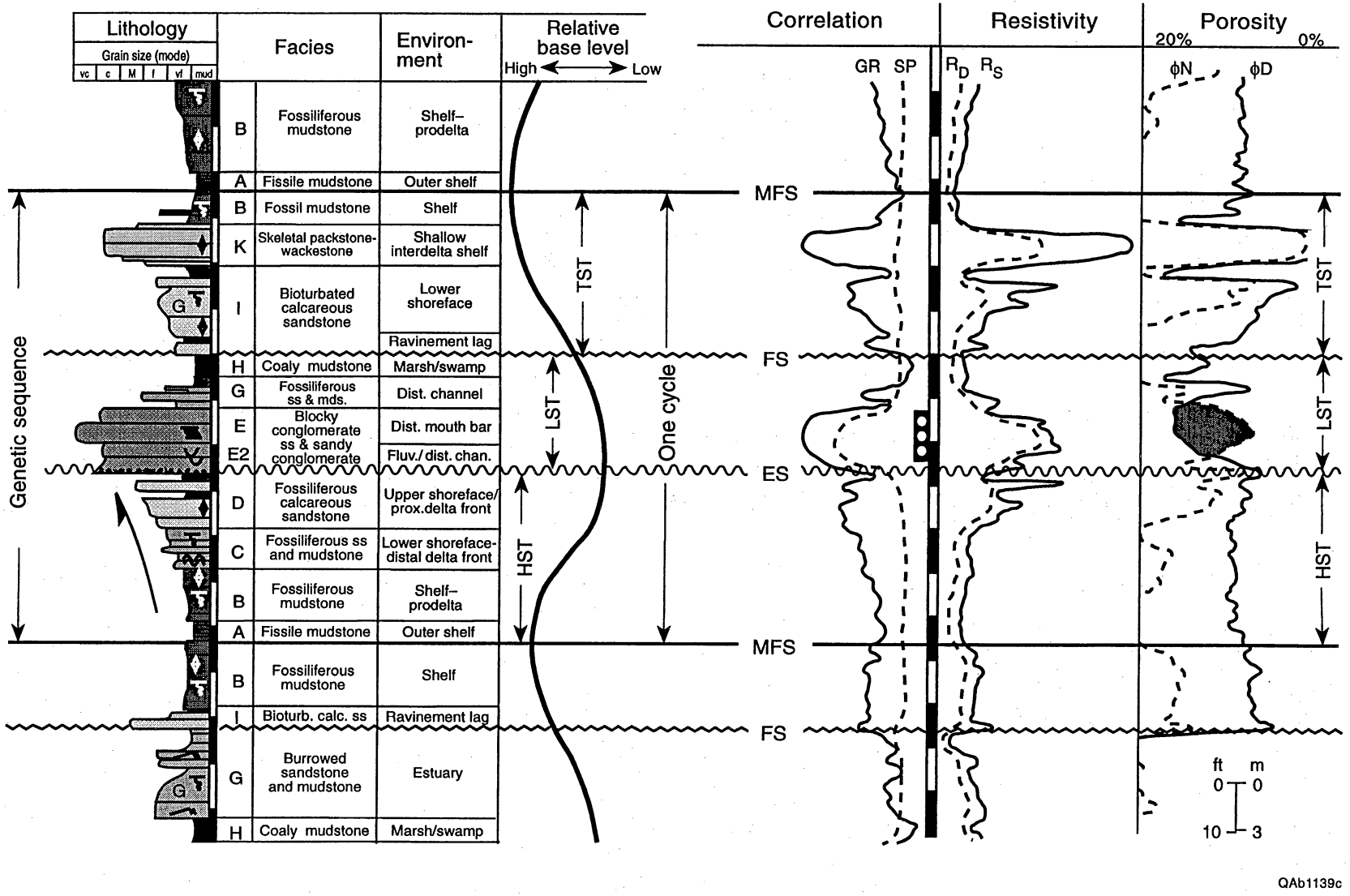

Figure A9. Typical log responses for composite Boonsville Bend Conglomerate genetic sequence.

Bend Conglomerate cores (for example, the lowermost FS illustrated in Figure 1.6), suggesting that these surfaces are a common and typical component of Atokan cyclothems.

Maximum flooding surfaces are widespread, upward-deepening surfaces associated with the inferred, deepest water facies encountered in a succession of strata. The MFS is commonly represented by a thin *condensed section*, typically a black, organic-rich shale having a low-diversity fossil assemblage representing deep-water, sediment-starved conditions. Boonsville Bend Conglomerate maximum flooding shales are slightly bioturbated, sparsely fossiliferous, fissile black shales that typically occur near the base of upward-coarsening facies successions (Fig. 1.6).

The maximum flooding surfaces bound and define the upward-coarsening facies successions and are termed *genetic sequences* (Galloway, 1989; Gardner and Cross, in preparation), which are similar to cycles or cyclothems in other terminology (for example, Wanless and Weller, 1932; Moore and others 1944). At least a dozen genetic sequences averaging approximately 100 ft in thickness have been observed in the Boonsville–Atokan strata of the project area.

One or more *erosion surfaces* occur within the Boonsville–Atokan genetic sequences, where evidence of a facies offset indicating an abrupt decrease in water depth occurs. Many of the erosion surfaces are widespread, and truncation of older strata can be documented on well log cross sections, suggesting that these particular surfaces may be unconformities representing downcutting during periods of subaerial exposure caused by *allocyclic* (extrabasinal) mechanisms, such as eustatic sea-level changes. Other erosion surfaces appear to be local diastems, such as fluvio-deltaic channel avulsion within depositional systems tracts caused by *autocyclic* (intrabasinal) mechanisms. It is difficult to impossible, when working at the field or reservoir scale, to precisely determine the significance and dimension of a particular erosion surface such that an allocyclic or autocyclic distinction can be made. A large-scale, Fort Worth Basin analysis would be required to begin an understanding of the regional context of erosion surfaces encountered in a particular field or

reservoir. However, speculative inferences regarding the relative significance of erosion surfaces were made by comparing the relative ease of ES identification and breadth of occurrence in the project area, sandstone net reservoir isopach map patterns, and depths of truncation. Understanding the regional context of erosion surfaces can help transfer correlation and play concepts to other fields and even other basins where time-equivalent, hydrocarbon-productive strata occur.

Some of the Boonsville–Atokan reservoir units can be more precisely defined by erosion surfaces or a combination of flooding and erosion surfaces. Delineation of depositional sequences that have unconformities or erosion surfaces is a common practice advocated by Exxon Production Research, and in this report, reservoir units defined by erosion surfaces are referred to as Exxon sequences (Fig. A10).

Base-Level Cycles and Systems Tracts

The repetitive pattern of stacked genetic sequences or cyclothems comprising the Bend Conglomerate interval was produced as a result of cyclically fluctuating base level superimposed upon long-term subsidence. Stratigraphic base level is an equilibrium surface, below which sediments can accumulate and above which the processes of erosion are dominant. There are more complex definitions of base level (for example, Shanley and McCabe, 1994; Gardner, 1995a), but for the practical purposes of this field-scale project, base level can be considered to be similar to relative sea level. The term is used herein without specific reference to particular forcing mechanisms, such as eustatic sea level, tectonic movement, sediment supply and sediment loading, and physiography, although global stratigraphic evidence suggests that cyclic stacking of many of the Boonsville–Atokan genetic sequences resulted from glacioeustatically induced base-level changes superimposed upon long-term subsidence of the Fort Worth Foreland Basin.

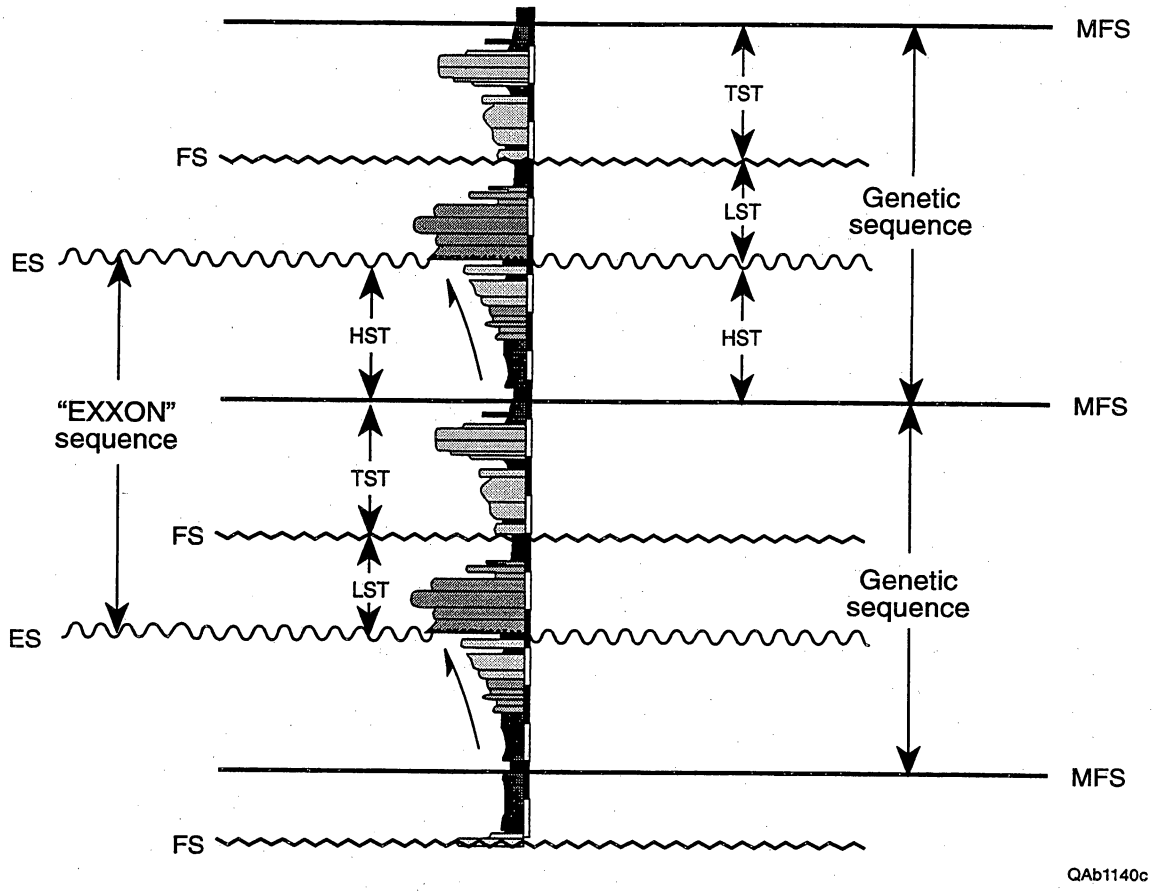

Figure A10. Core graphic illustrating key surface-based sequence terminologies in common use. "Exxon" sequences are defined by erosion surfaces, whereas genetic sequences are defined by flooding or maximum flooding surfaces.

Boonsville–Atokan genetic sequences are made up of three depositional systems tracts associated with highstand, lowstand, and transgressive phases of inferred base level (Fig. 1.6). The deposits of a typical *highstand depositional systems tract* consist of an upward-coarsening facies succession beginning with dark gray, maximum flooding mudstones, and grading upward into highstand calcareous shoreface–delta front sandstones that represent progradational facies that filled accommodation available during base-level maxima and subsequent fall. Highstand tracts are truncated by an erosion surface and overlain by the *lowstand depositional systems tracts* comprising complex, fluvial, and deltaic conglomeratic sandstones, which are capped by estuarine and carbonaceous floodplain mudstones and thin, fine-grained sandstones. *Transgressive depositional systems tracts* consist of bioturbated, calcareous sandstones or shallow-marine limestones that commonly overlie a ravinement surface.

New Interpretation for Bend Conglomerate Reservoirs

We introduce a new interpretation of the Boonsville–Atoka section on the basis of application of sequence stratigraphic concepts: most of the productive, Bend Conglomerate sandstone bodies represent complex mosaics of fluvial and deltaic deposits that formed during base-level lowstands. The sandstone bodies most commonly occur immediately above mappable erosion surfaces, some of which are probably unconformities related to periods of maximum continental (Gondwana) glaciation at the Atokan south pole. The Boonsville Project Area is close to the Fort Worth Basin's peripheral bulge, namely the Bend Arch, which was a shallow area where accommodation was relatively low, such that repeated exposure and incision was followed by inundation and backfilling as base level fell and rose, respectively. These rather severe swings in sedimentary conditions, coupled with high rates of sediment supply and a subtle, complex, structurally controlled physiography resulted in a highly compartmentalized, complex reservoir architecture.

General Geologic Parameters of the Project Area

Gross Stratigraphic Architecture

The Bend Conglomerate interval thins markedly but relatively smoothly from southeast to northwest in the project area, reflecting the onlap of strata onto the Bend Arch, which was the active peripheral bulge of the Fort Worth Foreland Basin during sedimentation. Within the boundaries of the 3-D seismic survey, Atokan strata range from 869 to 1,334 ft, and average 1,078 ft in gross isopach thickness (Figs. A11 through A13). In this report, the Atokan interval is defined by the MFS90, which is the top of the Caddo zone, to MFS10, the base of the Vineyard (Fig. 1.5). Most of the Bend Conglomerate wells in the project area targeted the basal Vineyard zone but stopped short of the Marble Falls to avoid lost circulation of drilling fluids in porous karst zones within the limestone. Because only 13 project area wells penetrated the Marble Falls Limestone, which is the true base of the Atoka interval, the estimate of MFS90 to MFS10 interval made from 117 wells is slightly thinner (91 to 145 ft) but representative of total Atokan–Bend Conglomerate thickness trends.

Total Atoka net reservoir sandstone (Fig. A14) averages 77 ft, but varies considerably within the project area, ranging from 0 to 189 ft, and has strikingly different isopach trends compared with the gross isopach. Net reservoir sandstone values for particular zones were determined for each well by summing the total well log curve footage meeting petrophysical cutoff criteria, namely an SP curve value of less than –30 millivolts and a resistivity of greater than 10 ohm-m. The 75-ft contour in Figure A14 defining two major regions of thin (0 to 75 ft) and thick (75 to 125 ft) net reservoir sandstone roughly corresponds to the west-southwest and east-northeast halves of the project area, respectively. The distribution of net reservoir sandstone indicates that high-energy, fluvio-deltaic systems preferentially occupied the east-northeast half of the area. Structure mapping from both well control and

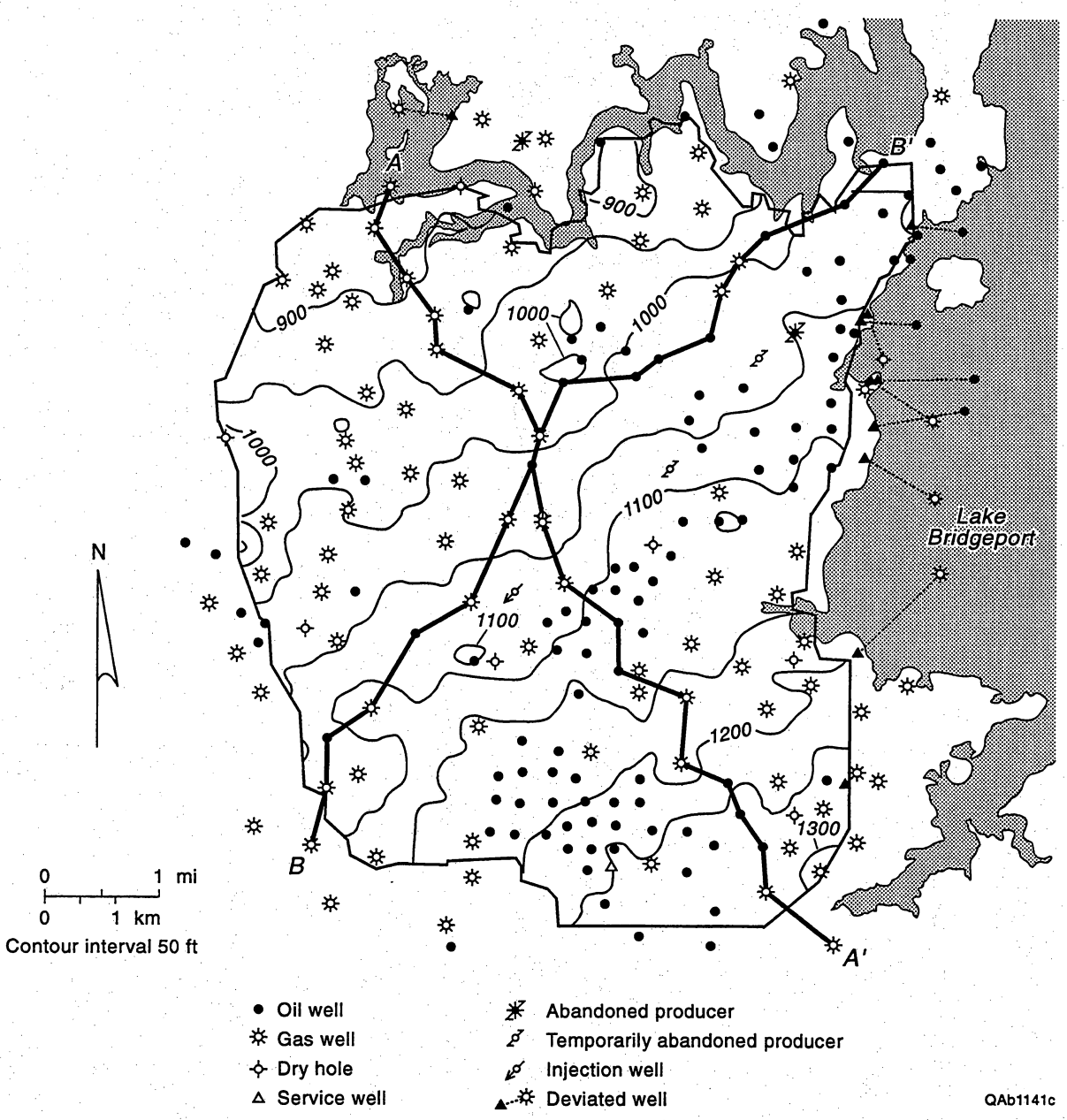

Figure A11. Total Bend Conglomerate (= total Atoka) gross isopach (MFS90–MFS10). Contour interval = 50 ft.

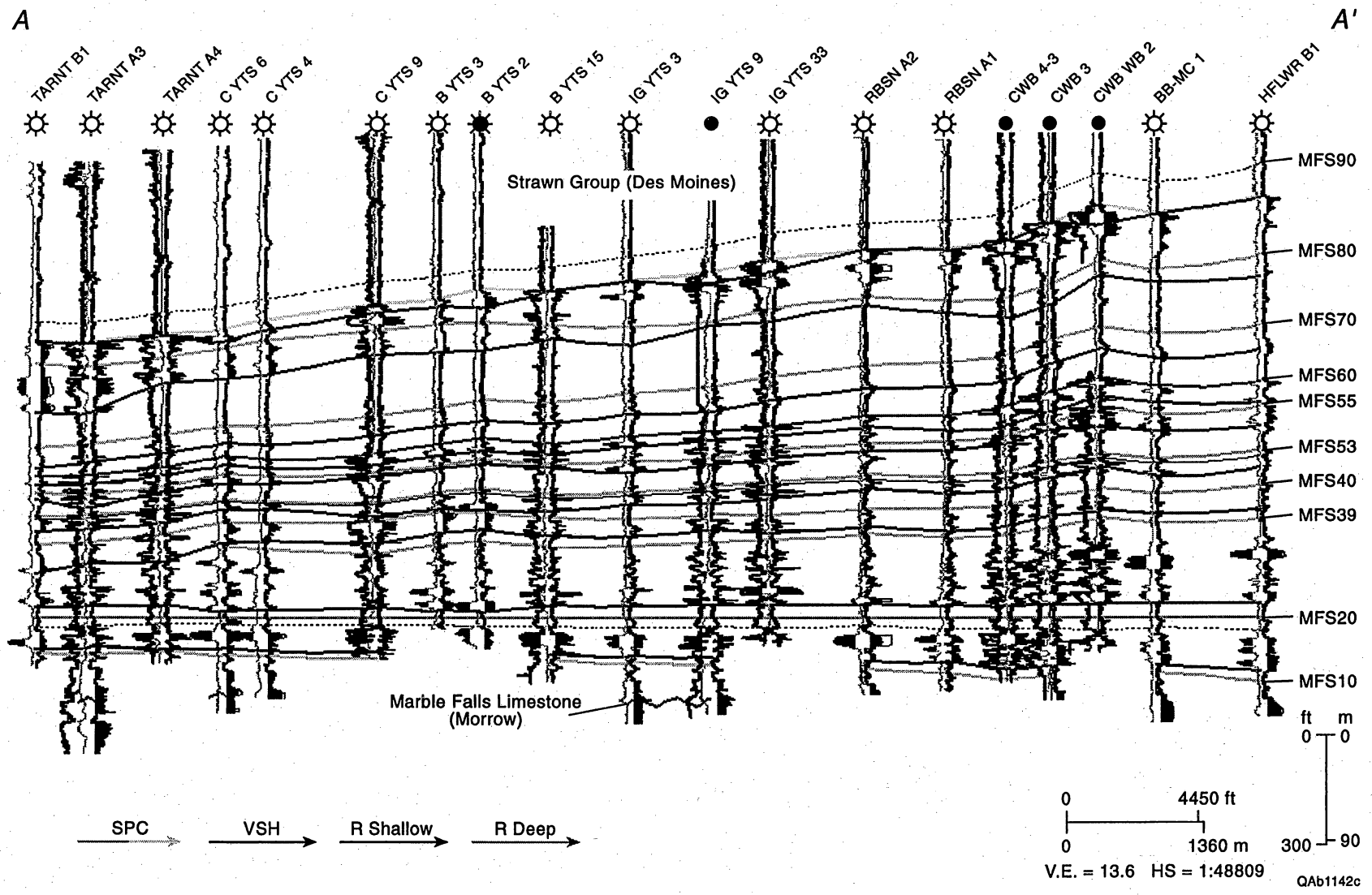

Figure A12. Boonsville stratigraphic cross section A–A′ of Bend Conglomerate using MFS20 (the top of the Vineyard genetic sequence) as a datum.

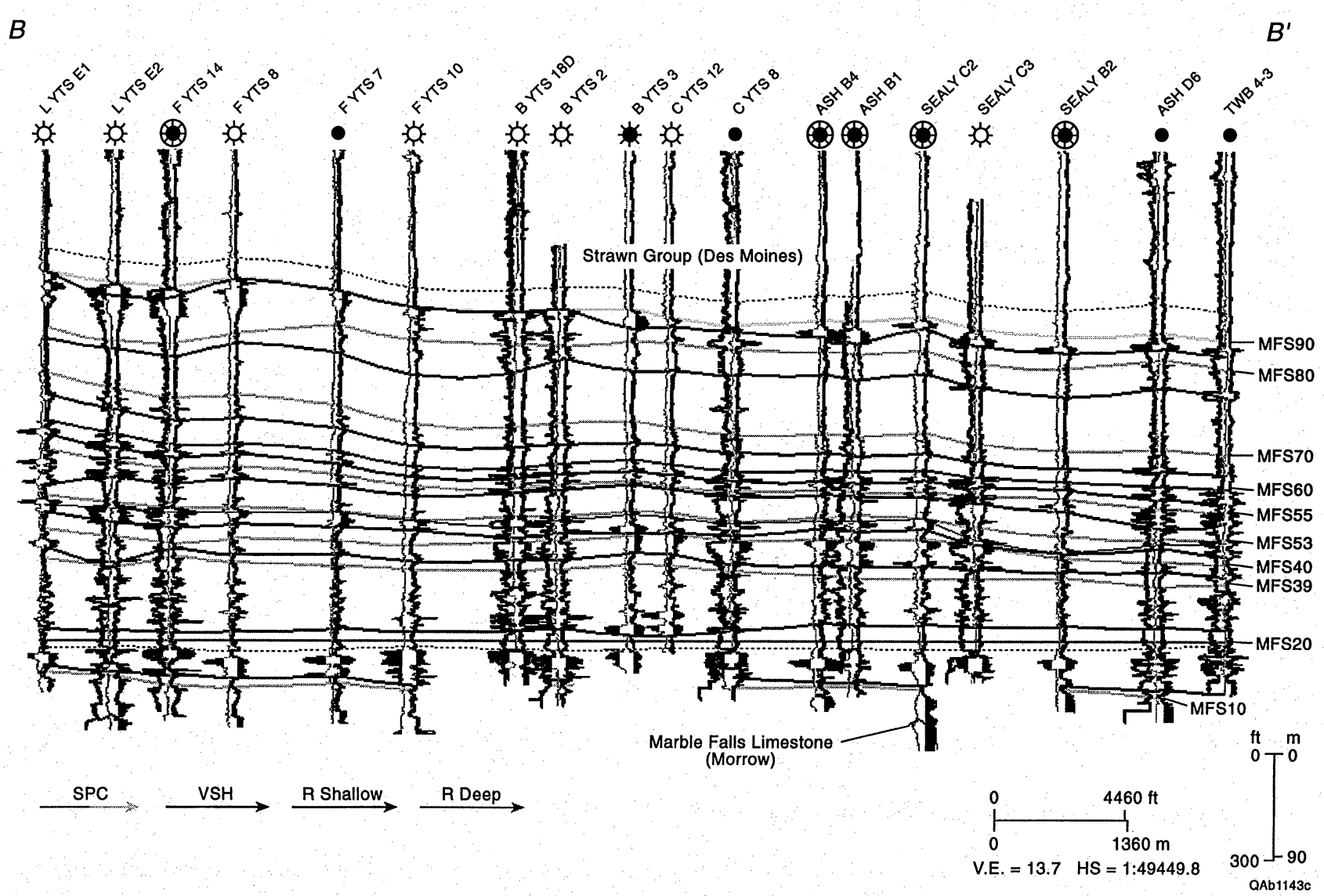

Figure A13. Boonsville stratigraphic cross section B–B′ of Bend Conglomerate using MFS20 (the top of the Vineyard genetic sequence) as a datum.

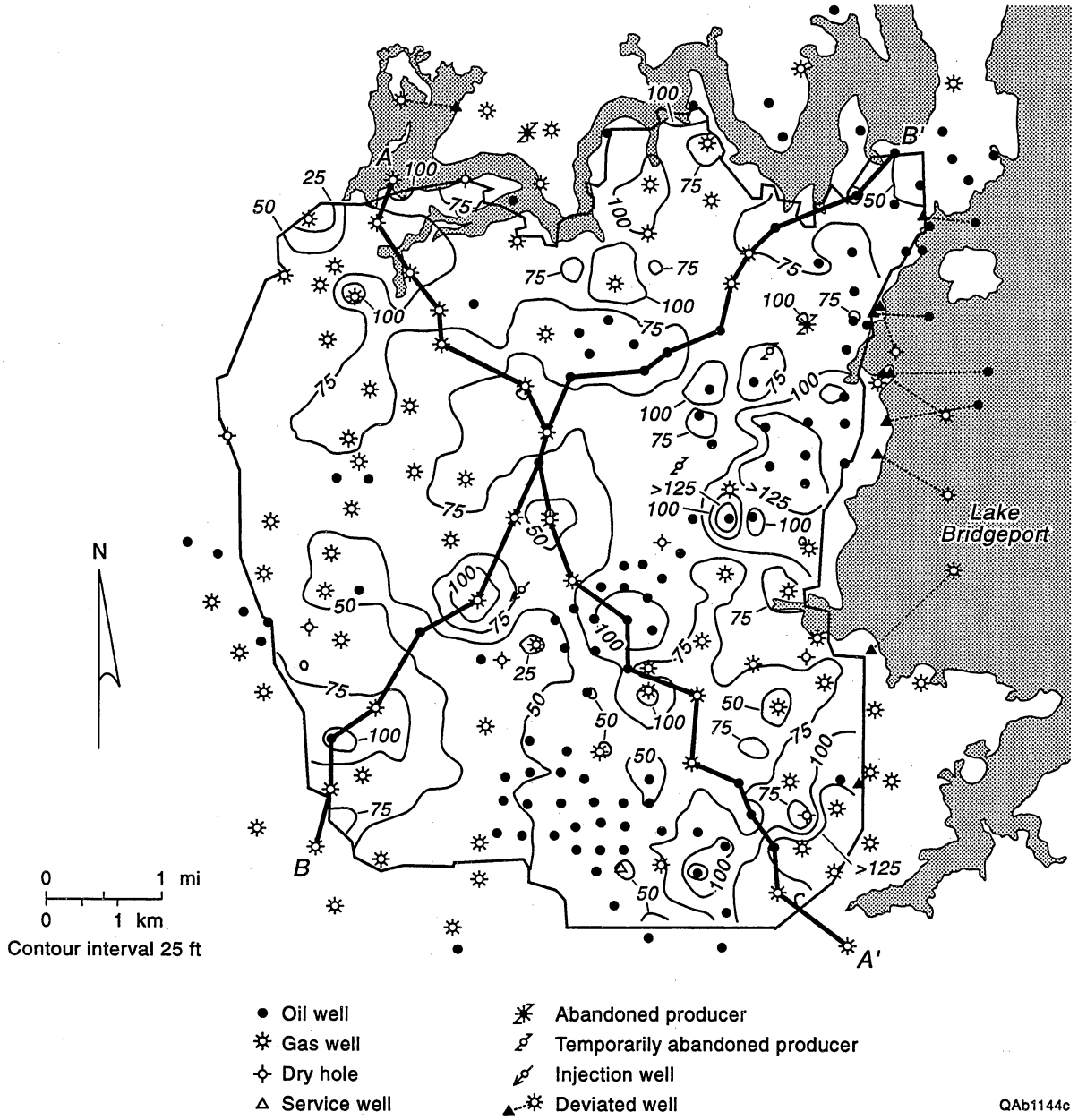

Figure A14. Total Bend Conglomerate net reservoir isopach (MFS90–MFS10). Net reservoir cutoff: SP < –30 mv; Res > 10 ohmm.

3-D seismic suggests a link between basement Paleozoic carbonate structure and thick, multistoried sandstone reservoirs.

Structure

Maps representing structural elevations of well-defined, maximum flooding surfaces that occur near the base, middle, and top of the Bend Conglomerates are presented in Figures A15, A16, and A17, respectively. Structure in the project area is more complex at the base of the Atoka (Fig. A15) and becomes simpler upward through the section, and overall structural dip rotates from east-northeastward to northward upsection. Structure at the MFS20 (or Vineyard) level exhibits a high west side and a southeast-plunging structural nose (referred to as Noles Nose), with lower areas falling off both limbs. Only a small vestige of Noles Nose is apparent at the MFS60 (or Trinity; Fig. A16) level, and the feature is essentially absent at the MFS90 (or Caddo; Fig. A17) level.

Many small-scale, near-vertical fault zones having ovoid time-structure map patterns are present throughout the Bend Conglomerate section and are particularly prevalent in the Lower Atoka and underlying Paleozoic carbonate horizons (Chapter 2). Most of these high-angle, normal and reverse faults have less than 100 ft of displacement and are typically on the order of 20 to 30 ft. The faults rarely penetrate the overlying Strawn Group, indicating that structural movements occurred predominantly during Atoka time. Figures A18 and A19 illustrate the subtle, near-vertical faults, which were added to the well log cross sections after examination of arbitrary 3-D vertical sections coincident with the well control. Although hints of faulting can be detected from well control, confident estimates of vertical displacements and fault-block geometries cannot be determined without 3-D seismic data.

We interpret these features to have resulted from dissolution and subsequent, episodic collapse of karst cavities in the Paleozoic platform carbonate units, namely, the Marble Falls (Pennsylvanian Morrow), Comyn (Mississippian), and Ellenburger (Cambro-Ordovician) Formations underlying the Atoka interval. In map view, the karst collapse

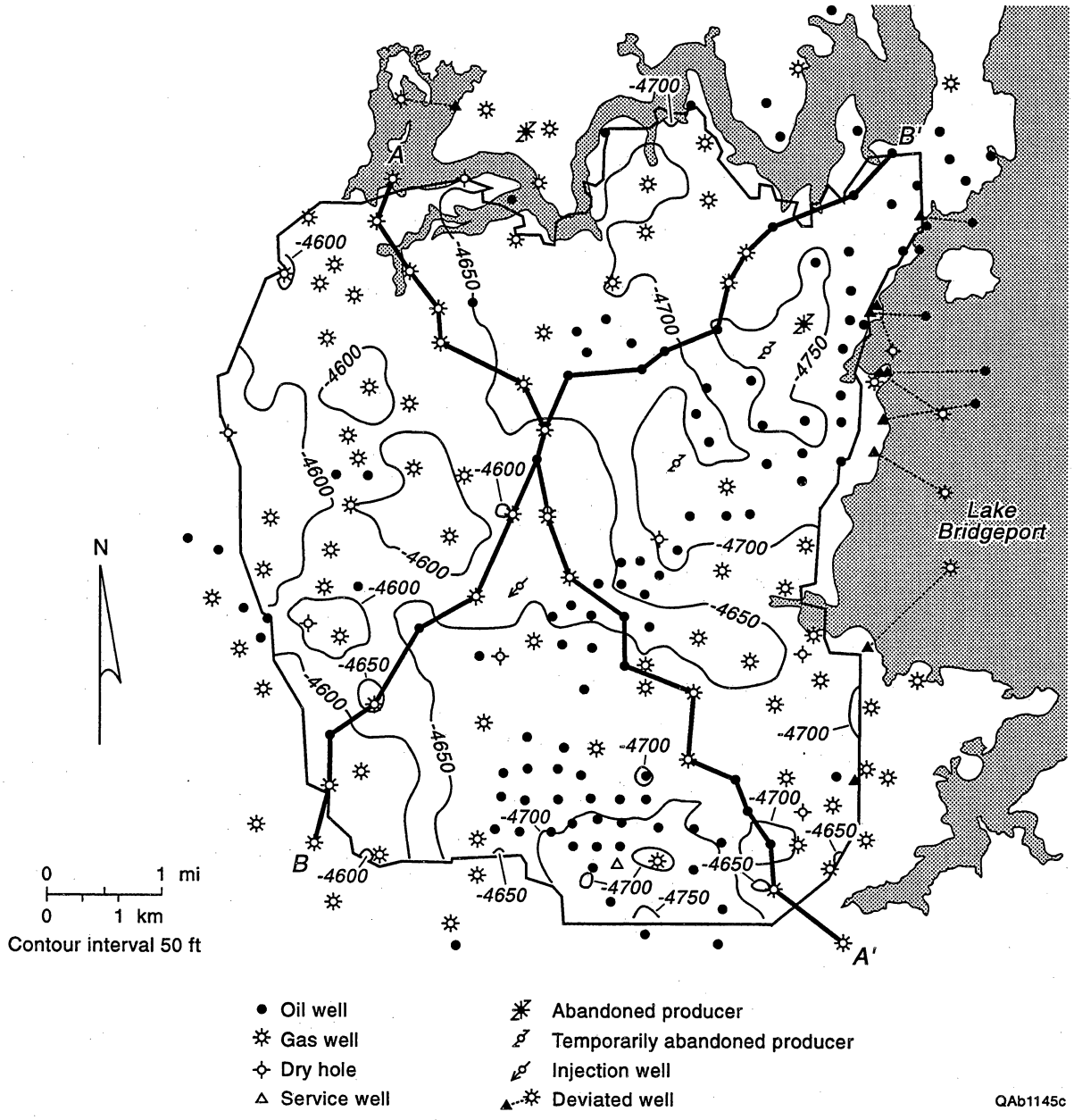

Figure A15. Top of Vineyard genetic sequence (MFS20) measured in depth below sea level. Contour interval = 50 ft.

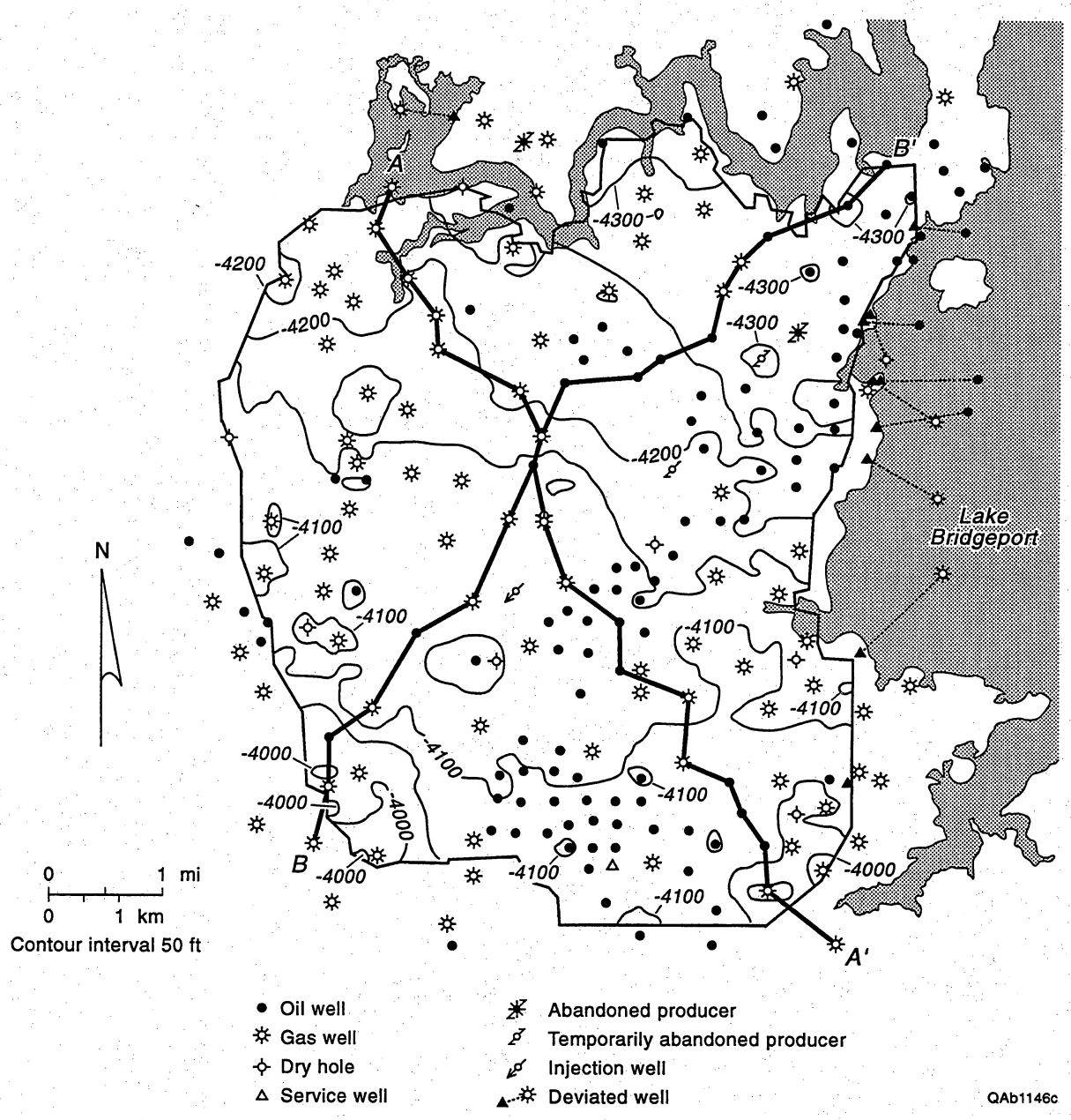

Figure A16. Top of Trinity genetic sequence (MFS60) measured in depth below sea level. Contour interval = 50 ft.

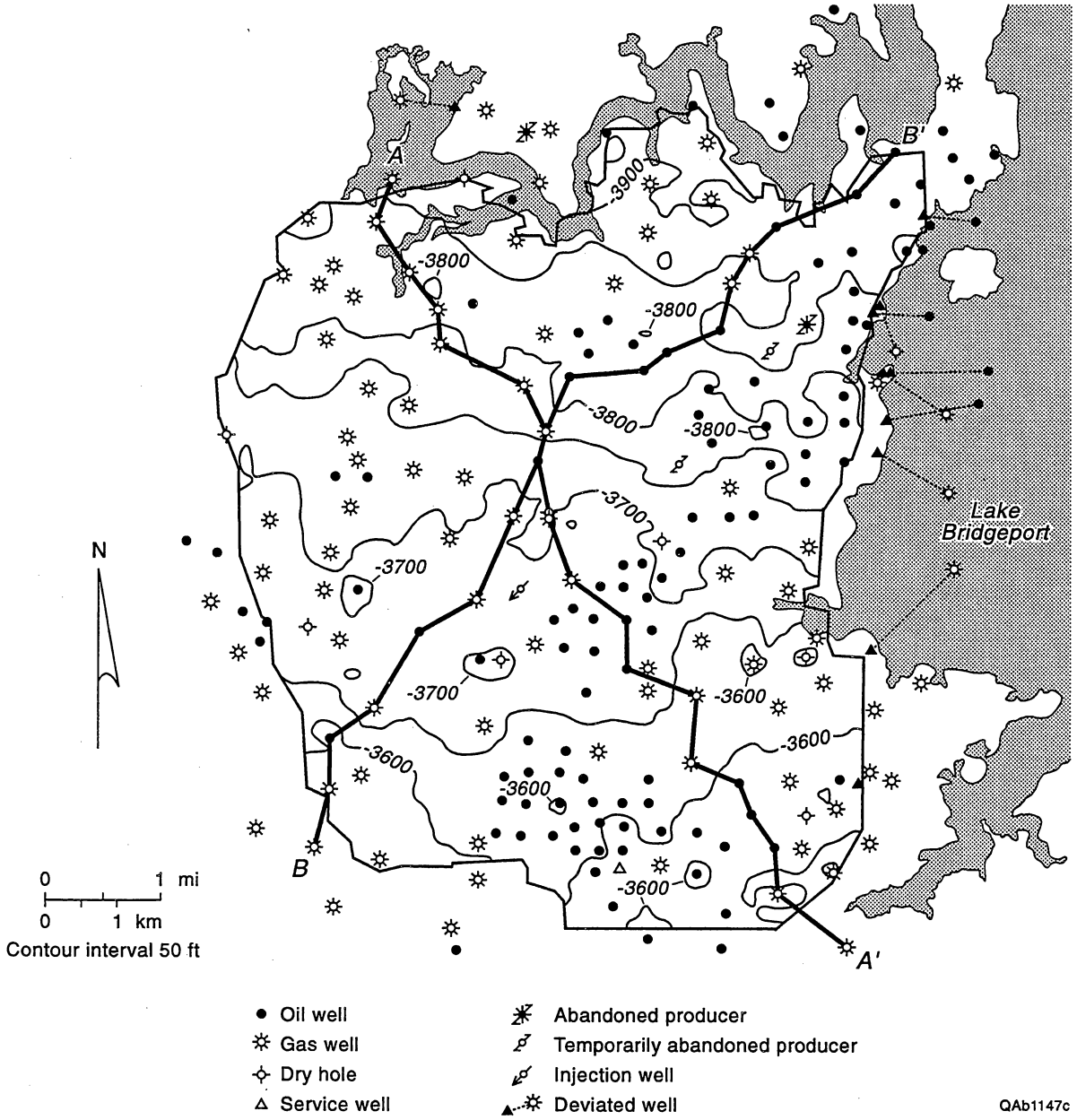

Figure A17. Top of Caddo genetic sequence (MFS90) measured in depth below sea level. Contour interval = 50 ft.

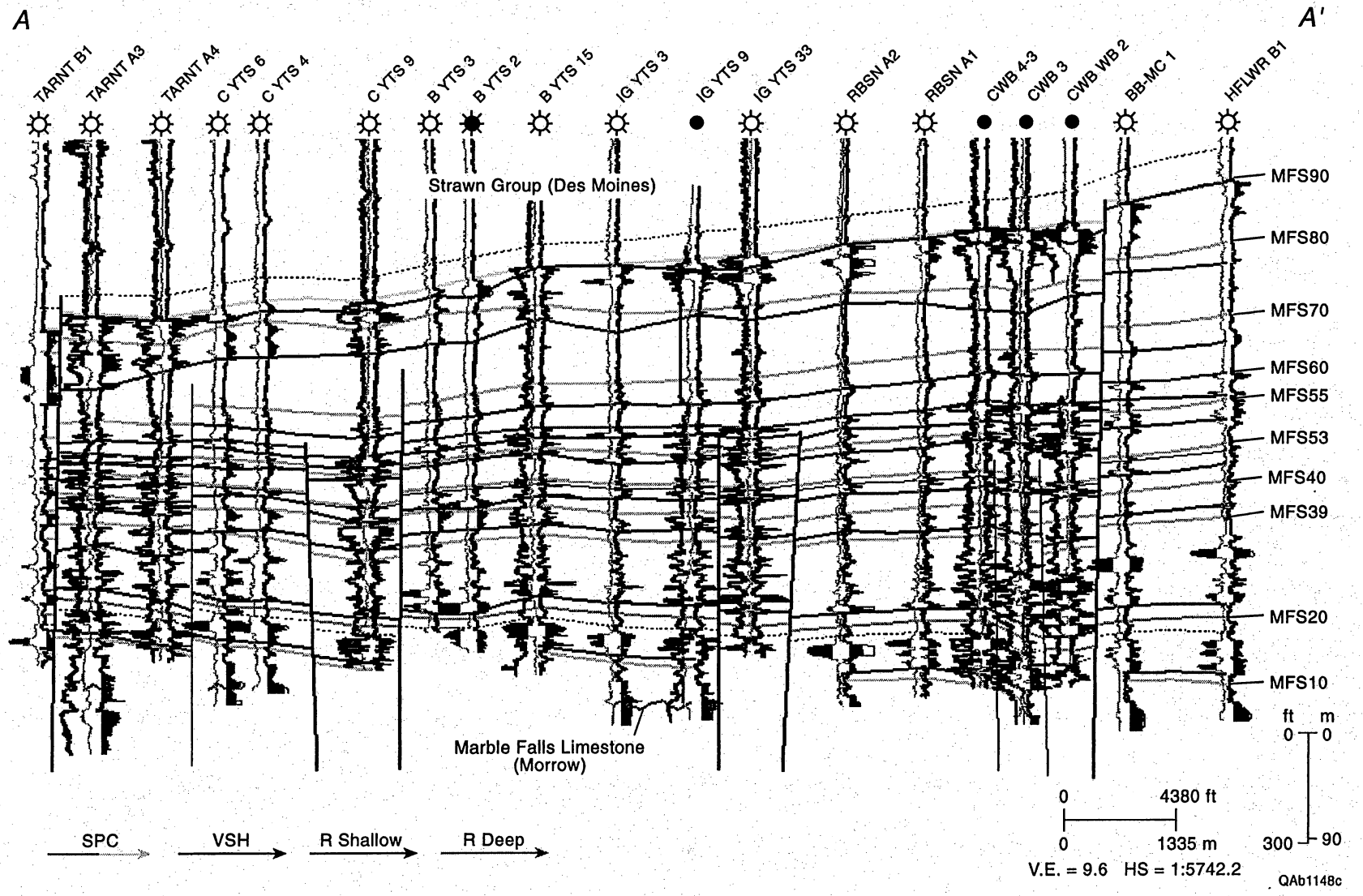

Figure A18. Boonsville structural cross section A–A′ of Bend Conglomerate illustrating faults interpreted from 3-D seismic information. Compare this interpretation with that in Figure A12.

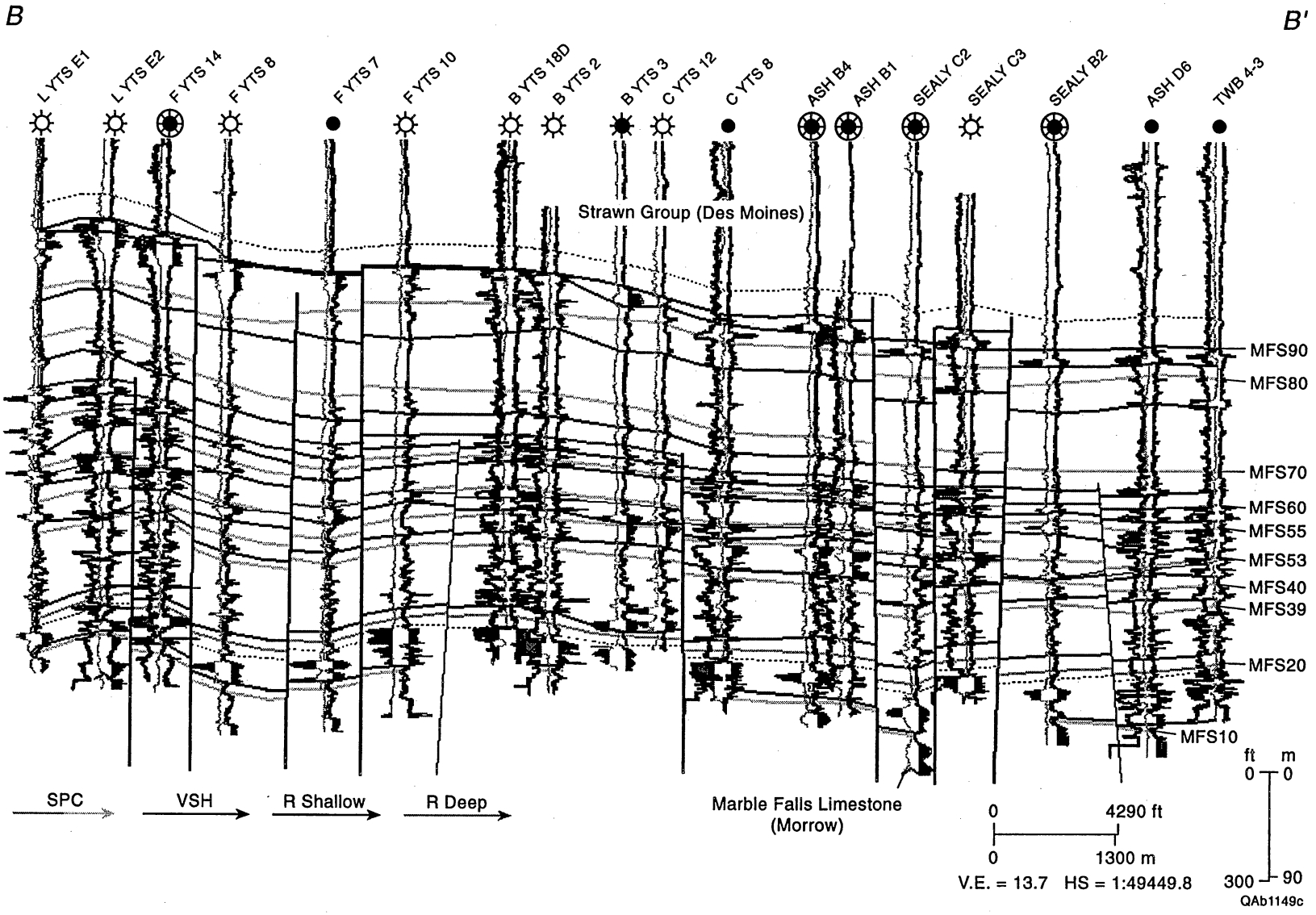

Figure A19. Boonsville structural cross section B–B′ of Bend Conglomerate illustrating faults interpreted from 3-D seismic information. Compare this interpretation with that in Figure A13.

features occur in broadly defined, dominantly north-northwesterly linear groups (Figs. 2.1 and 2.2), suggesting a genetic relationship between karst-dissolution processes and preexisting, subtle basement faulting. The faults are consistently vertical, but horizontally discontinuous, and the extent of vertical displacement at a particular stratigraphic level varies significantly across the project area, suggesting that sites of collapse were anchored in space, but that the collapse events were episodic and localized. The karst collapse features probably represent buried caverns and sinkholes, perhaps similar to those found in Florida, Kentucky, and Central Texas, that were covered by Bend Conglomerate sequences, whose sediment-loading effects most likely triggered collapse.

Structure and Sedimentation

Figure A20 is a near Marble Falls seismic time-structure map that has the total Atokan net reservoir isopach contours of Figure A14 superimposed upon it. A strong relationship exists between structurally low areas on the pre-Atoka surface and areas where thick net reservoir sandstone occurs. The majority of the differences in the two map patterns can be explained by differences in data resolution. The net reservoir isopach map was derived from 117 wells, whereas the time-structure map was constructed from 81,204 data traces: the 3-D seismic map has a nearly 700-fold horizontal resolution advantage over the well-control isopach map.

This positive relationship implies that subtle differences in structural elevation at the pre-Atoka, Paleozoic carbonate stratigraphic level controlled the geographical locations of incised valleys, fluvial and fluvio-deltaic axes in which high-energy reservoir facies were concentrated. Many of the thickest valley-fill sandstone reservoirs occur above or immediately adjacent to vertically faulted karst collapse zones (for example, see Chapter 3). Modern stream and river courses (some now drowned in Lake Bridgeport's waters) also appear to be controlled to a certain extent by the basement structure at the Paleozoic

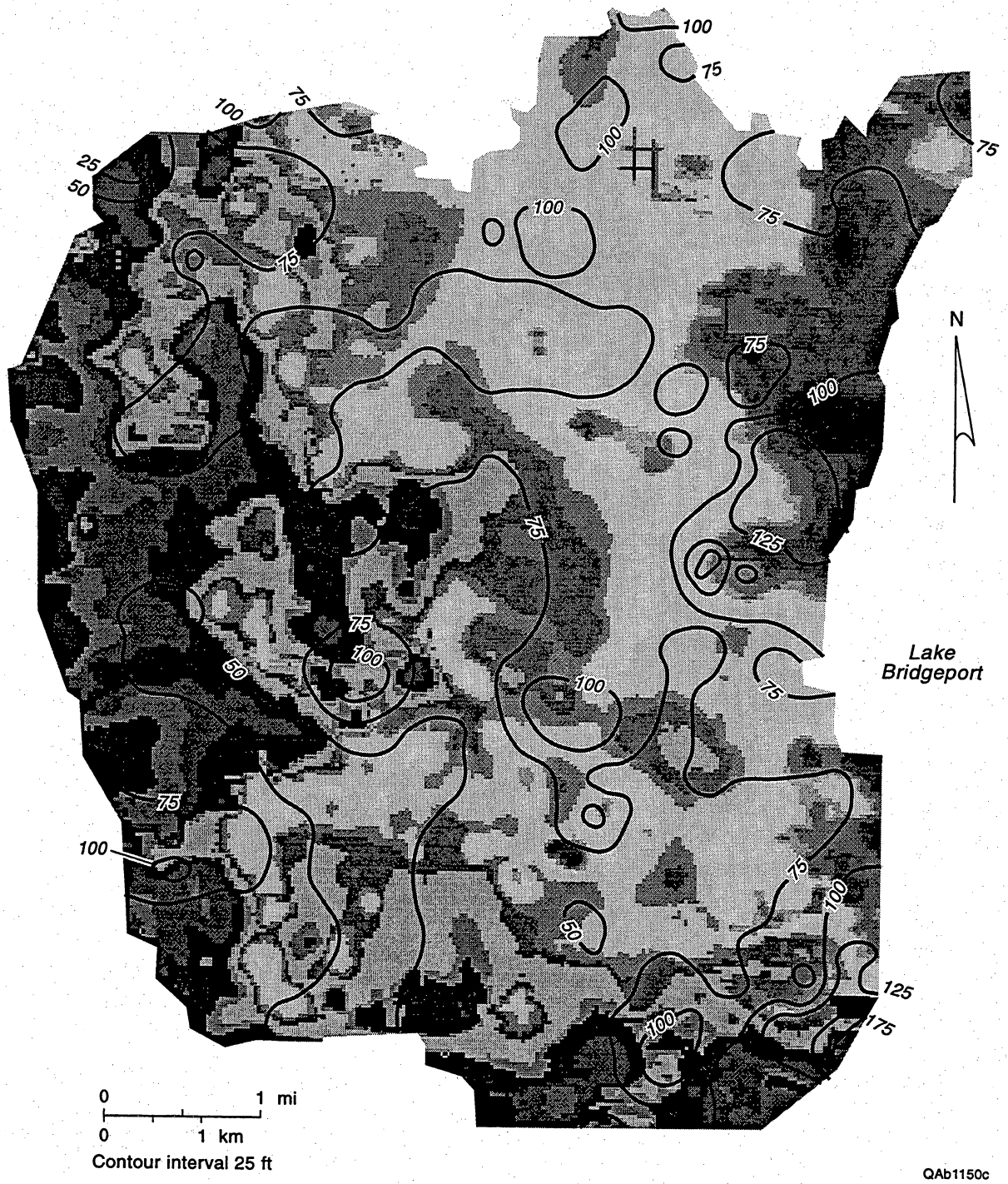

Figure A20. Map of Boonsville Project Area showing the relationship between total Atoka (MFS90–MFS10) net reservoir thickness and deep subsurface structure, as indicated by the top of the Marble Falls Limestone interpreted from 3-D seismic data. Dark shading represents higher elevations of the Marble Falls Limestone; lower elevations in lighter shades.

carbonate level, suggesting that structure has continued to influence the position of depositional systems up to the present time (Fig. A21).

Geologic Controls on Gas Production

Most of the natural gas produced within the Boonsville Project Area has come from the Vineyard zone (Fig. 1.5), which is commonly referred to as the basal conglomerate of the Bend interval. The Vineyard is the most predictable, widespread, and least compartmentalized of the Atoka reservoir sandstones. Although early production data were not available for most wells, productivity estimated from cumulative production data suggests that the best production has occurred where thick Vineyard sandstones are draped over subtle structural highs (Fig. A22).

After more than 30 yr of steady production, the Vineyard zone is widely depleted (Appendix B). It is likely that most future reserve growth will be derived from smaller, more stratigraphically compartmentalized zones overlying the Vineyard.

Reservoir Compartmentalization Styles in Atokan-Bend Conglomerates

The predominant compartmentalization mechanisms observed in the Boonsville Project Area are: *stratigraphic*, comprising surface-bounded, facies-bounded and cement-bounded compartments; *structural*, mainly fault-bounded compartments; and perhaps the most common type encountered at Boonsville is a *combination* of stratigraphic and structural mechanisms.

Stratigraphic Compartmentalization

Surface-bounded compartments result from the juxtaposition of reservoir sandstones and impermeable facies at key chronostratigraphic surfaces. This type of stratigraphic compartmentalization is typically a broad-scale phenomenon because of the widespread

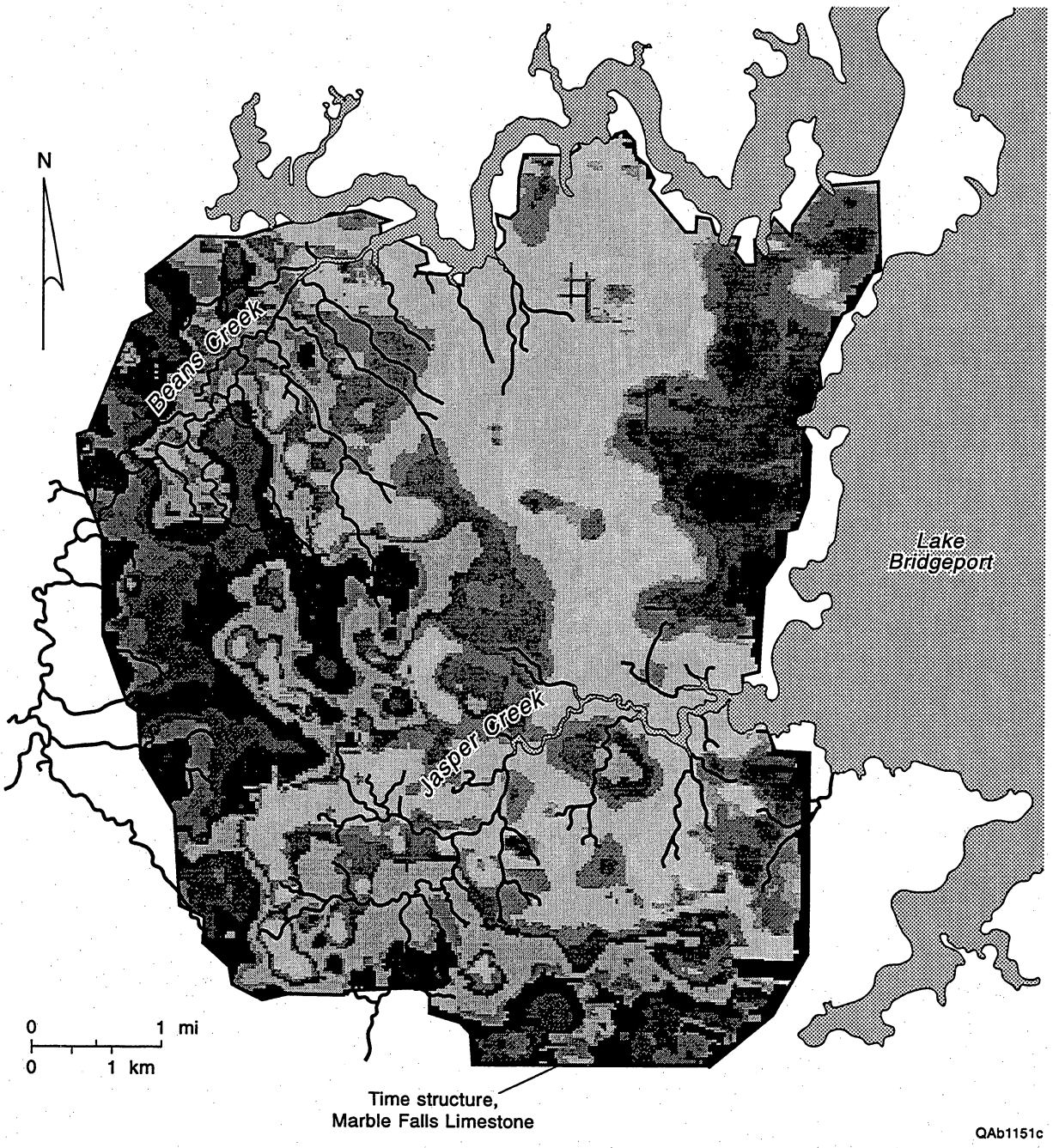

Figure A21. Map of Boonsville Project Area showing the relationship between modern stream drainage and deep subsurface structure, as indicated by the top of the Marble Falls Limestone interpreted from 3-D seismic data. Dark shading represents higher elevations of the Marble Falls Limestone; lower elevations in lighter shades.

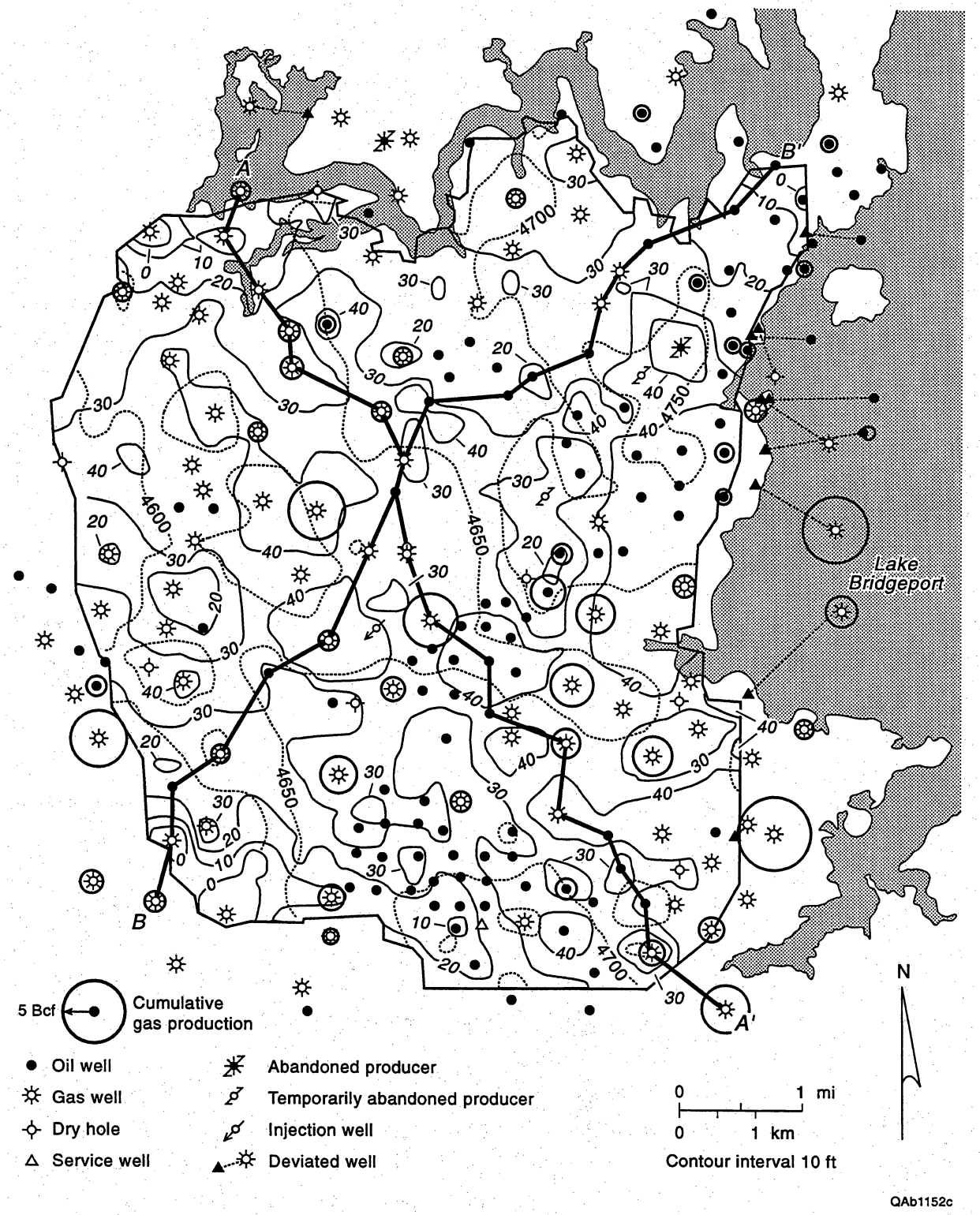

Figure A22. Thick sandstone and subtle structural controls on gas production in the Vineyard sequence. Note that the southeast-northwest-trending line of large cumulative gas production coincides with the thick net reservoir "sweetspot" draped over "Noles' Nose." Color fill = Vineyard net reservoir isopach; bubbles = cumulative gas production. Net reservoir cutoffs: SP < –30 mv; Res > 10 ohmm.

nature of key surfaces. Lowstand valley-fill sandstones common in many Bend Conglomerate sequences are examples of surface-bounded compartments. Most of the stratigraphic compartmentalization in the surface-dominated strata of low–mixed accommodation Midcontinent basins is likely to be of the surface-bounded type.

Facies-bounded compartments result from high-frequency autocyclic processes within the depositional systems tract. For example, mud-drape barriers deposited on point-bar sands during waning flood stages, or, on a larger scale, an abandoned delta lobe can founder and be encased in inner shelf or prodelta mudstones.

Diagenetic cements can occlude porosity in Midcontinent reservoir sandstone units and may be significant intrafacies flow barriers in some instances. Quartz overgrowths, calcite, ferroan calcite, and dolomite are common in project area cores, and secondary porosity is also common, indicating a complex fluid migration history and a high degree of postdepositional redistribution of mineral matter.

Structural Compartmentalization

Several Boonsville wells drilled in small (~ 100 acres), structurally high fault blocks encountered gas at higher than expected pressures in otherwise hydraulically well connected reservoir zones (Caddo, Vineyard), suggesting that the vertical faults observed in the 3-D seismic data can act as partial barriers to fluid flow (see Chapter 2 for details). Because potential fault-bounded compartmentalization can be quickly and easily identified from 3-D seismic, a quick-look infill drilling strategy is to identify fault-bounded blocks having no well penetrations that occur in subregional or field-scale areas where (1) the pre-Atoka time structure is low, (2) total Atoka net reservoir isopachs are thick, and (3) net pay interval maps indicate good potential for finding multiple reservoir zones.

The apparently episodic fault movements, inconsistent vertical displacements, and the general lack of lateral continuity suggest that the sealing properties may be variable as well. Even so, knowledge of fault-block geometries can nonetheless help in identifying areas

having a higher potential for isolating fluid communication between otherwise continuous reservoir zones, and can therefore be used to upgrade locations and reduce risks in development drilling programs.

Combination of Stratigraphic and Structural Compartmentalization

It is likely that a spectrum of compartment types exist between those of purely structural and those of purely stratigraphic origin. In addition, because of the structural influence on sandstone distribution, and because of the limited degree to which stratigraphic compartments can be resolved, it is sometimes difficult to precisely determine the relative impact of structural versus stratigraphic mechanisms.

Detection Resolution of Compartment Types

As mentioned earlier, most types of stratigraphic compartments in Atokan-Bend Conglomerates are difficult to predict using existing technologies. Large-scale, surface-bounded reservoir zones can be differentiated using well control, and the numerous lowstand valley-fill sandstone reservoirs throughout the Atoka section provide many good examples. Surface-bounded compartmentalization can also be detected using seismic attributes analysis, with requirements being that stratigraphically calibrated isochrons (i.e., seismic reflectors) can be readily traced in zones where net reservoir values in sandstone bodies exceed 25 to 30 ft in thickness over large areas (for example, Upper and Lower Caddo, Chapter 3) and the reservoir boundaries are defined by appreciable seismic reflection coefficients. It is difficult to detect surface-bounded compartments by means of seismic attributes analysis in some of the Lower Atoka, thin-bed zones that have significant reserve growth potential because these reservoirs have subtle reflection coefficients, causing thin-bed detection to be problematic.

We were unable to document facies- or cement-bounded compartmentalization definitively using well control or 3-D seismic because they occur within surface-bounded systems tracts and thus operate at a very small scale (tens to hundreds of feet). A large core data base coupled with detailed petrographic analyses would be required to properly assess compartmentalization at scales relevant to lateral changes in facies and cements. However, this type of compartmentalization is probably common in the Bend Conglomerates; several case history examples document closely spaced wells that are hydraulically isolated from one another because of fine-scale barriers likely to be the result of facies changes, cements, or both (for example, I. G. Yates No. 33).

Although nearly impossible to delineate using well control, structural, fault-bounded compartments can be quickly and easily identified in the 3-D seismic data. Very fine scale fault displacements of less than 20 ft, and fault-block geometries can be mapped with confidence from the 3-D seismic data. The seismic data do not, however, provide information regarding the sealing qualities of the faults nor estimates of reservoir pressures: these must be inferred from well log geology and engineering assessments of pressure regimes in the targeted reservoir zones.

Relationship between Compartment Size and Relative Accommodation

Although the Fort Worth Basin accommodation setting was low to intermediate during the Atoka, accommodation varied through Atoka time such that each of the Bend Conglomerate sequences (Fig. 1.5) was deposited under unique conditions that affected their respective reservoir properties. Accommodation is the amount of space that was available below base level, the level below which the sediment of a particular sequence could accumulate, and this dimension cannot be determined precisely. However, geological parameters such as gross thickness, average net reservoir sandstone thickness, average net:gross ratio, and number of individual sandstone beds per zone can help provide a

comparative estimate of the relative amount space available during deposition of each reservoir-bearing sequence at Boonsville (Table A3).

Table A3. Semiquantitative relationship between relative accommodation and typical compartment size.

Relative accommodation setting	Estimate of typical compartment sizes	Geologic description
HIGH	?<100 MMcf ?<50 acres	High gross (G); low net/gross; small, relatively tight facies-bounded compartments: for example, downlapping deltaic lobes separated by shale barriers
INTERMEDIATE	100–250 MMcf 10–75 acres	Intermediate gross; variable net/gross; commonly surface bounded compartments; variable permeability: for example, multistoried channel-fill or valley-fill deposits
LOW	200 MMcf to >1 Bcf 50 to > 160 acres	Low-intermediate gross; high net/gross; hydraulically well connected; variable permeability: for example, relatively sheetlike, continuous sandstone with multiple, internal erosion surfaces; best potential for structural compartmentalization

Figure A23 illustrates the semiquantitative relationship between estimated relative accommodation and typical reservoir compartment-size estimates (in MMcf reserves), which were calculated in the engineering analysis (Appendix B). Most of the lower accommodation settings (for example, Vineyard, Trinity) occurred during deposition of the bottom half of the Atoka section, whereas the highest accommodation settings (for example, Davis, Wizard Wells) are younger, upper Atoka sequences. Three specific examples of Boonsville sequences are presented below to illustrate the characteristics of reservoirs deposited in high, intermediate, and low relative accommodation settings.

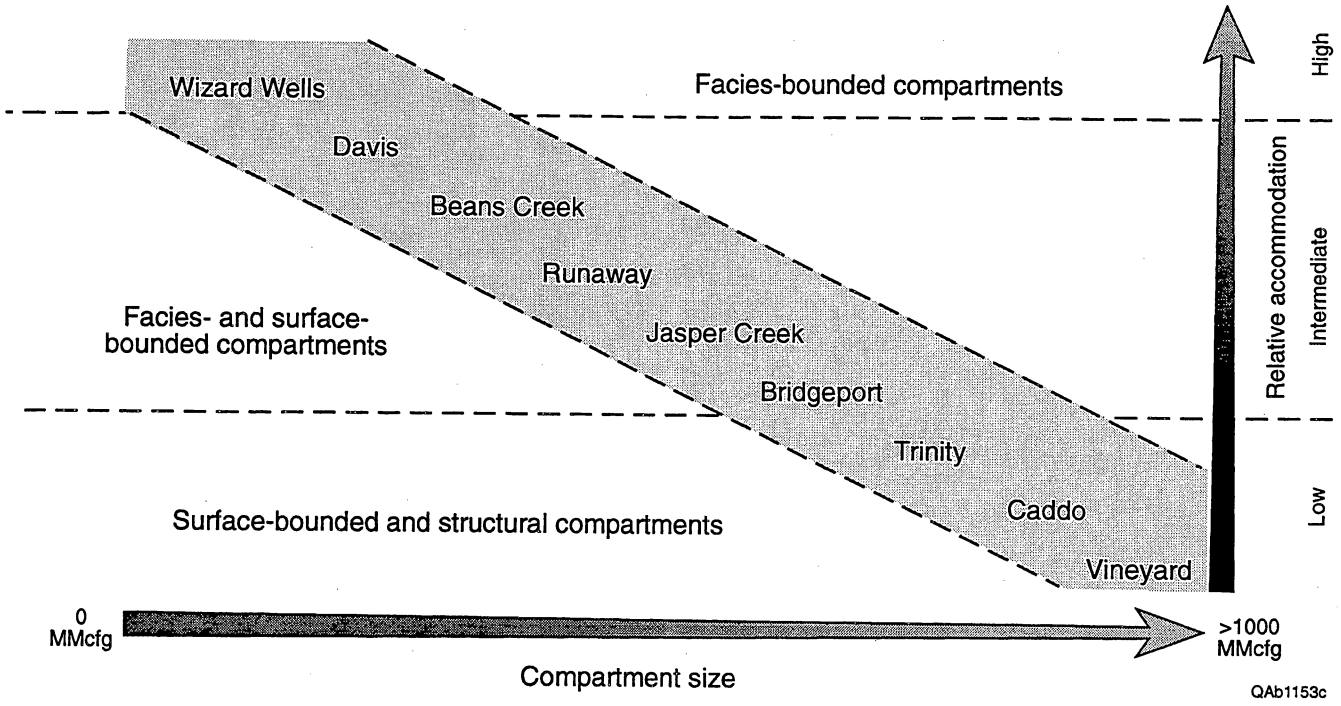

Figure A23. Semiqualitative relationship established between relative accommodation available during deposition of the Boonsville sequences and compartment size in terms of typical, expected gas reserves.

High-Accommodation Example: Wizard Wells Sequence

The Wizard Wells genetic sequence is defined by the interval between maximum flooding surfaces MFS80-MFS70, which averages approximately 200 ft in gross thickness (Fig. 1.5). Despite its great thickness relative to all the other sequences, only a small volume of productive sandstone reservoir occurs in this largely shale prone unit (Fig. A24). The majority of the net reservoir sandstone occurs near the top of the sequences in several discreet lobes in the north-northeastern portion of the project area.

Careful tracing of resistivity patterns indicates that the Wizard Wells is comprised of southward-dipping clinoforms representing a highstand delta prograding south-southeastward into a relatively deep body of water (Fig. A25). Local erosion surfaces that probably represent channel-cut diastems can be identified in the sandstone-rich lobes in the northwest quadrant of the project area, but there is not a single, through-going erosion surface as is typical of many other Boonsville sequences. Low net-reservoir volume, preservation of several small facies-bounded sandstone bodies, very high gross thickness, and overwhelming predominance of mudstones suggest that a relatively high amount of accommodation was available during Wizard Wells deposition.

Intermediate-Accommodation Example: Jasper Creek Sequences

The Jasper Creek sequences represent an intermediate relative accommodation example in the comparative examination of reservoir types found within Bend Conglomerate sequences. Intermediate relative accommodation type reservoirs are the most attractive targets for future gas reserve growth because they are highly compartmentalized and thus likely to contain untapped reserves. In addition, the upside potential for finding relatively large compartments is high: several wells—for example, the Billie Yates No. 2 (Runaway) and the Billie Yates No. 3 (Lower Jasper Creek)—have produced more than 1 Bcfg in these types of compartments.

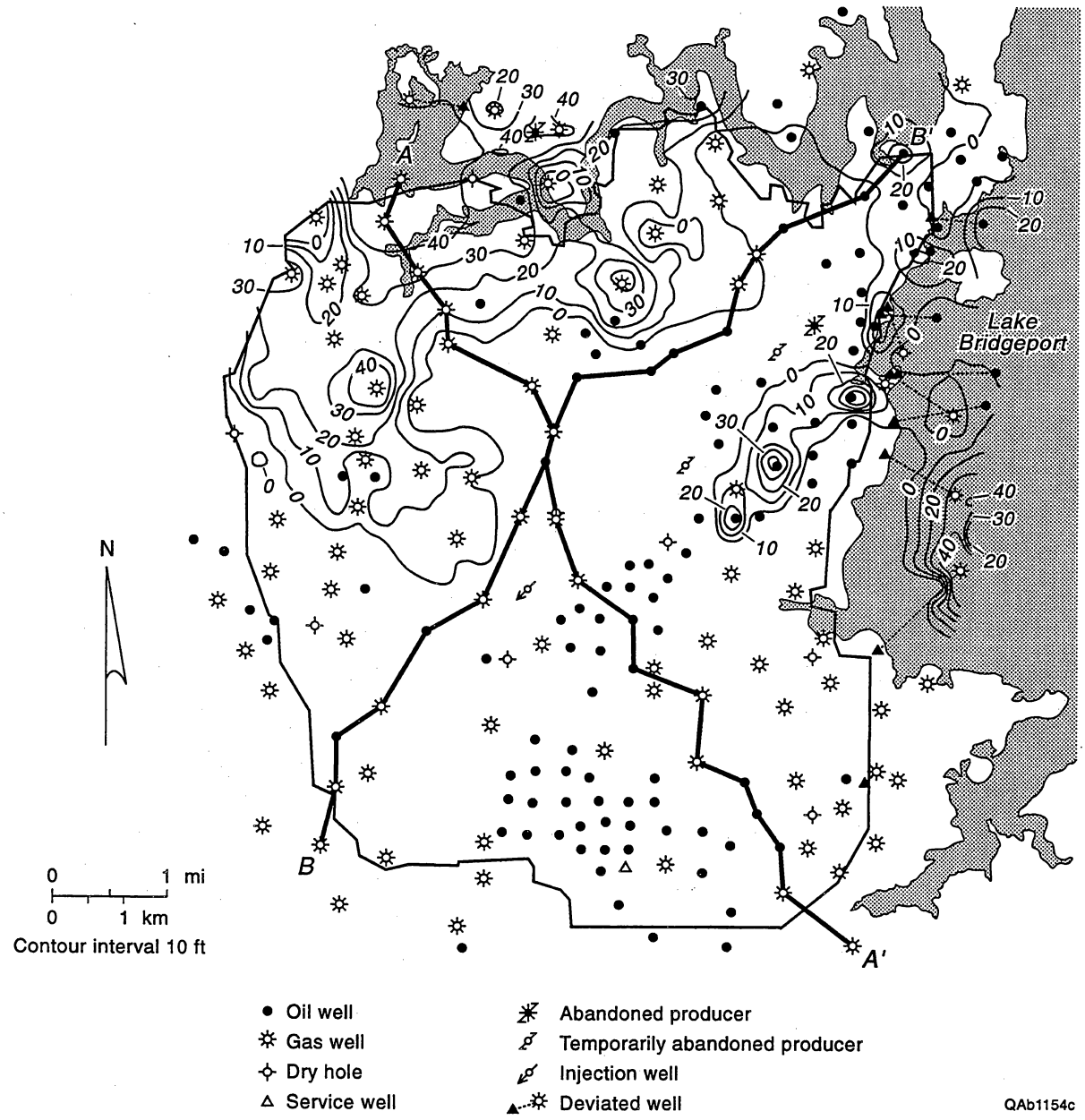

Figure A24. Wizard Wells genetic sequence net reservoir isopach (MFS80–MFS70). Net reservoir cutoffs: SP < –30 mv; Res > 10 ohmm.

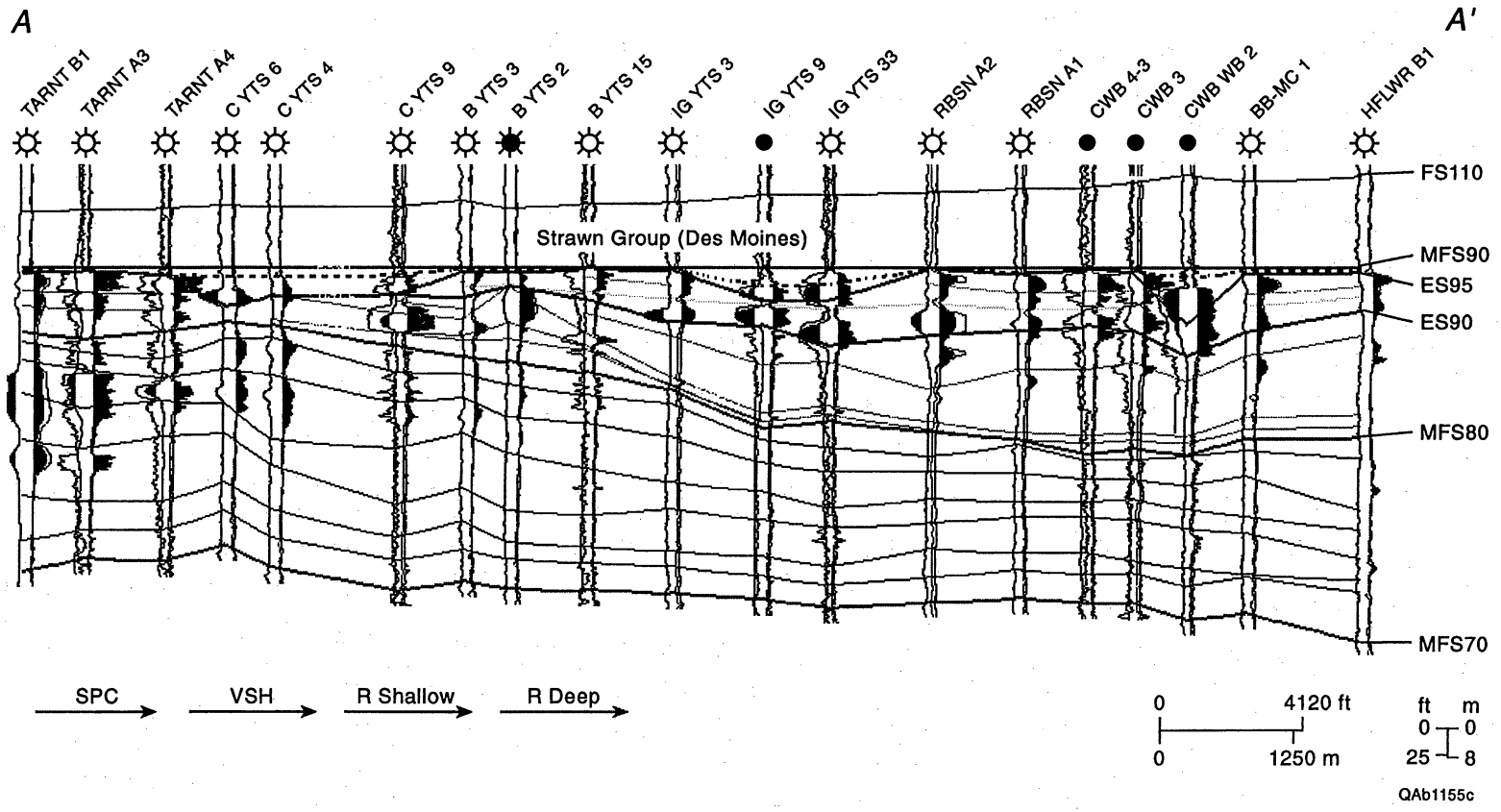

Figure A25. Stratigraphic cross section A–A′ of Wizard Wells genetic sequence (MFS80–MFS70) illustrating clinoforms (thin black lines between MFS80–MFS70) comprising this highstand delta system. Stratigraphic datum = MFS90.

The Jasper Creek sequence is a thick, erosion-surface-bounded sequence that consists of four subsequences, each one of which contains sinuous belts of reservoir sandstone (Figs. A26, A27). Severe erosional truncation of the uppermost Jasper Creek sequences by the ES40 (Beans Creek) occurs in the northern part of the project area (Fig. A28). Oldest to youngest, these ES-based subsequences are Lower (ES30-ES34), Middle (ES34-ES36), Upper (ES38-ES36), and 4th Jasper Creek (FS39-ES38). The bases of the ES30 and ES34 exhibit significant erosional truncation across the project area, suggesting they represent unconformities. The thick uppermost Jasper Creek strata (above FS34) contain numerous upward-shoaling lobes (parasequences), and it is more difficult to trace erosion surfaces (ES36, ES38) in areas where sharp-based, channel-fill sandstones are absent, suggesting that the ES36 and ES38 may be local diastems. Review of individual Jasper Creek net reservoir sandstone isopachs (Figs. A29 through A32) indicates a progressive upward decrease in net reservoir sandstone volume, suggesting that a large-scale transgressive event occurred during Jasper Creek deposition.

Reservoir compartments in the Jasper Creek sequences are mostly surface-bounded valley-fill deposits, with varying degrees of internal facies- and cement-bounded barriers. The Jasper Creek net reservoir sandstone isopach in Figure A27 contains a greater area where net reservoir is present (exceeds zero) as compared with the Wizard Wells isopach (Fig. A24), which has a vast area containing no reservoir rock, showing that a decrease in accommodation favors greater lateral distribution of sand in the depositional system. Both sequences are similar in that they contain several discrete sandstone bodies; however, the Jasper Creek sequences are dominated by fluvio-deltaic valley-fill and distributary-channel deposits (Fig. A33), several of which may represent entirely different base-level cycles, whereas the Wizard Wells sandstone bodies appear to be the result of shifting of lower energy deltaic environments within a large-scale progradational event during the highstand of a single base-level cycle.

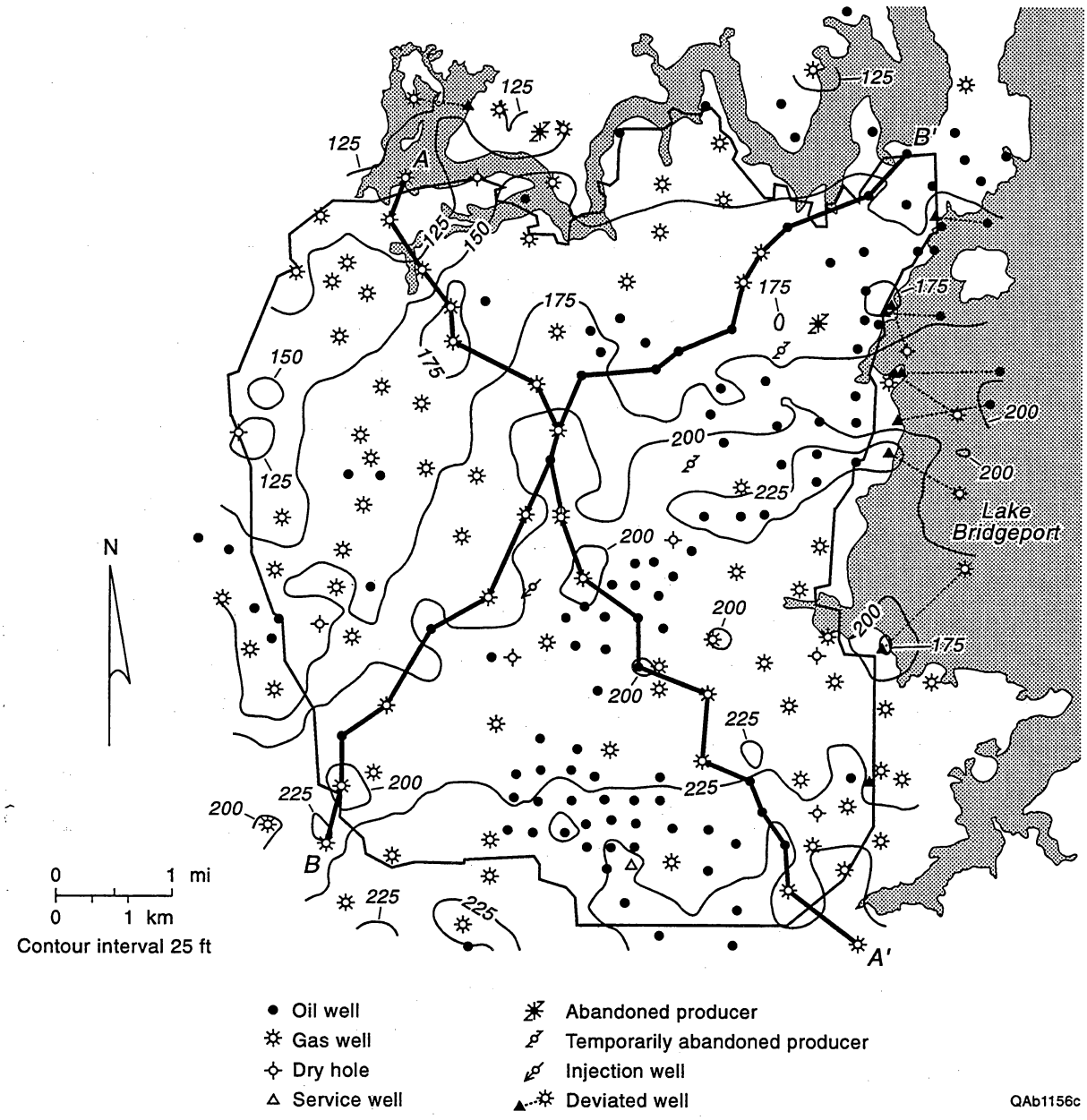

Figure A26. Jasper Creek "Exxon" sequence total gross interval isopach (ES40–ES30).

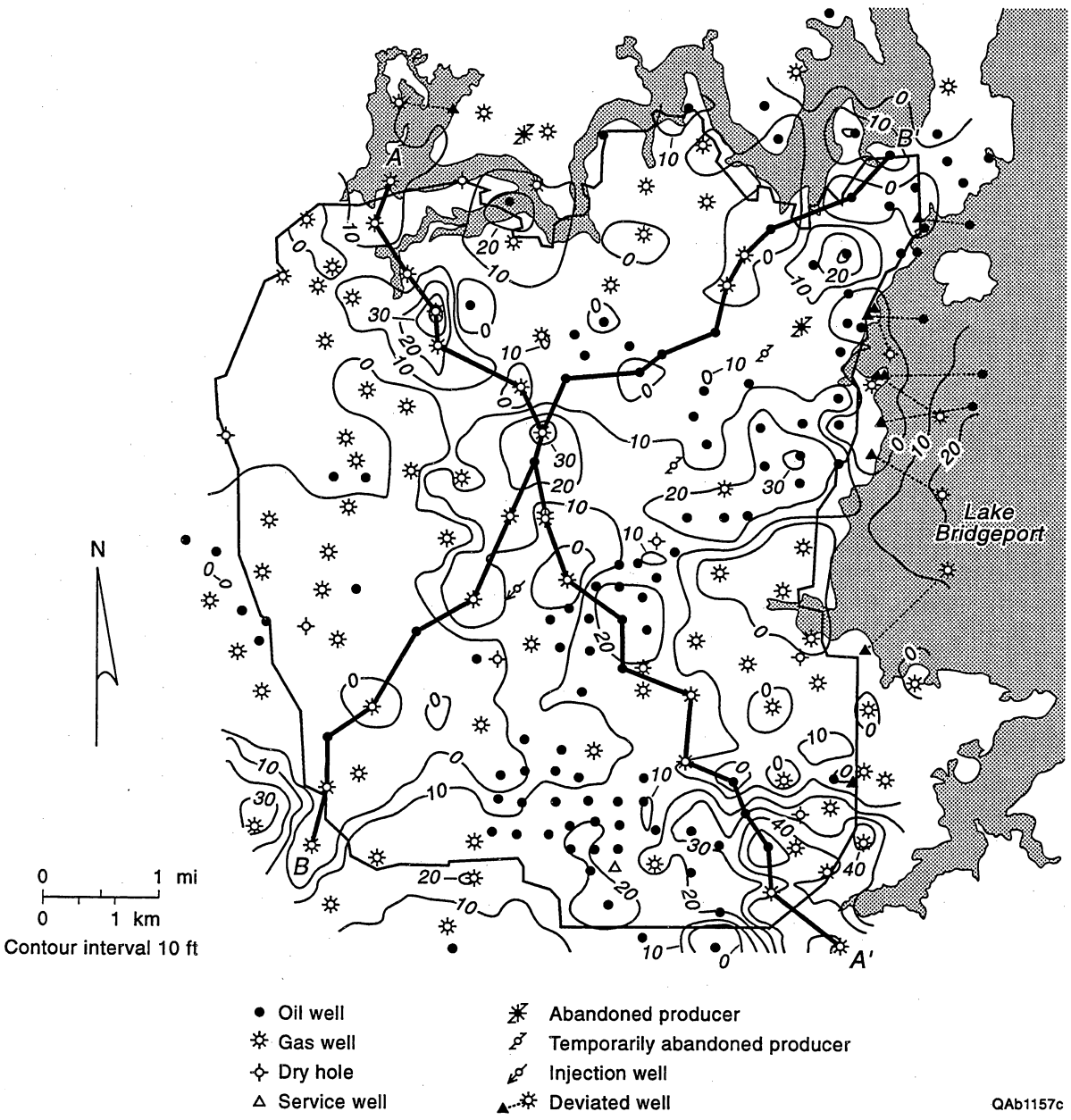

Figure A27. Jasper Creek "Exxon" sequence total net reservoir isopach (ES40–ES30). Net reservoir cutoffs: SP < –30 mv; Res > 10 ohmm.

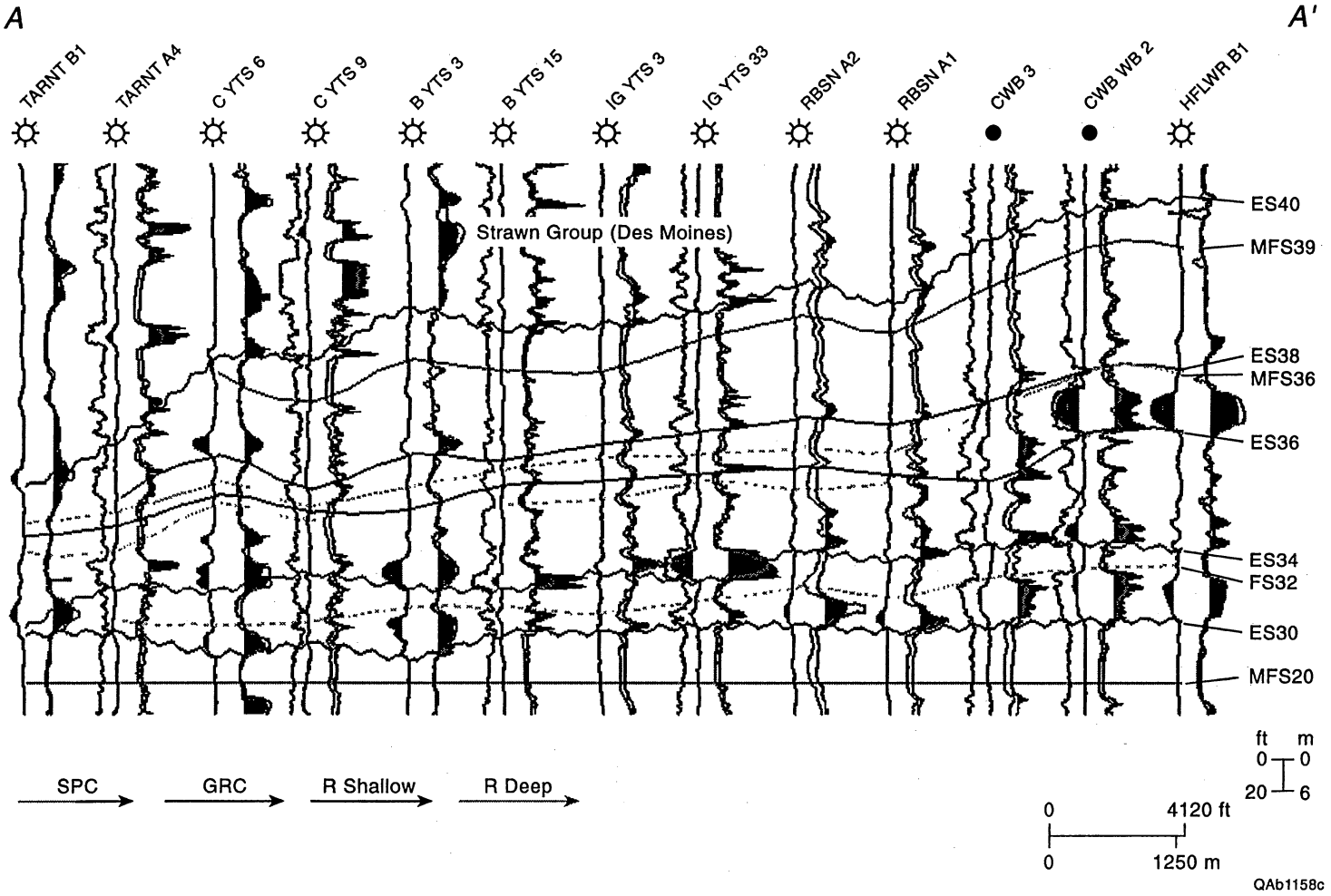

Figure A28. Stratigraphic cross section A–A′ illustrating the Jasper Creek "Exxon" sequence (ES30–ES40). The Jasper Creek sequence contains four subsequences in which sinuous belts of reservoir sandstone occur. Note the severe erosional truncation of Jasper Creek sequences by the ES40 (Beans Creek) in the north part of the project area. Stratigraphic datum = MFS20.

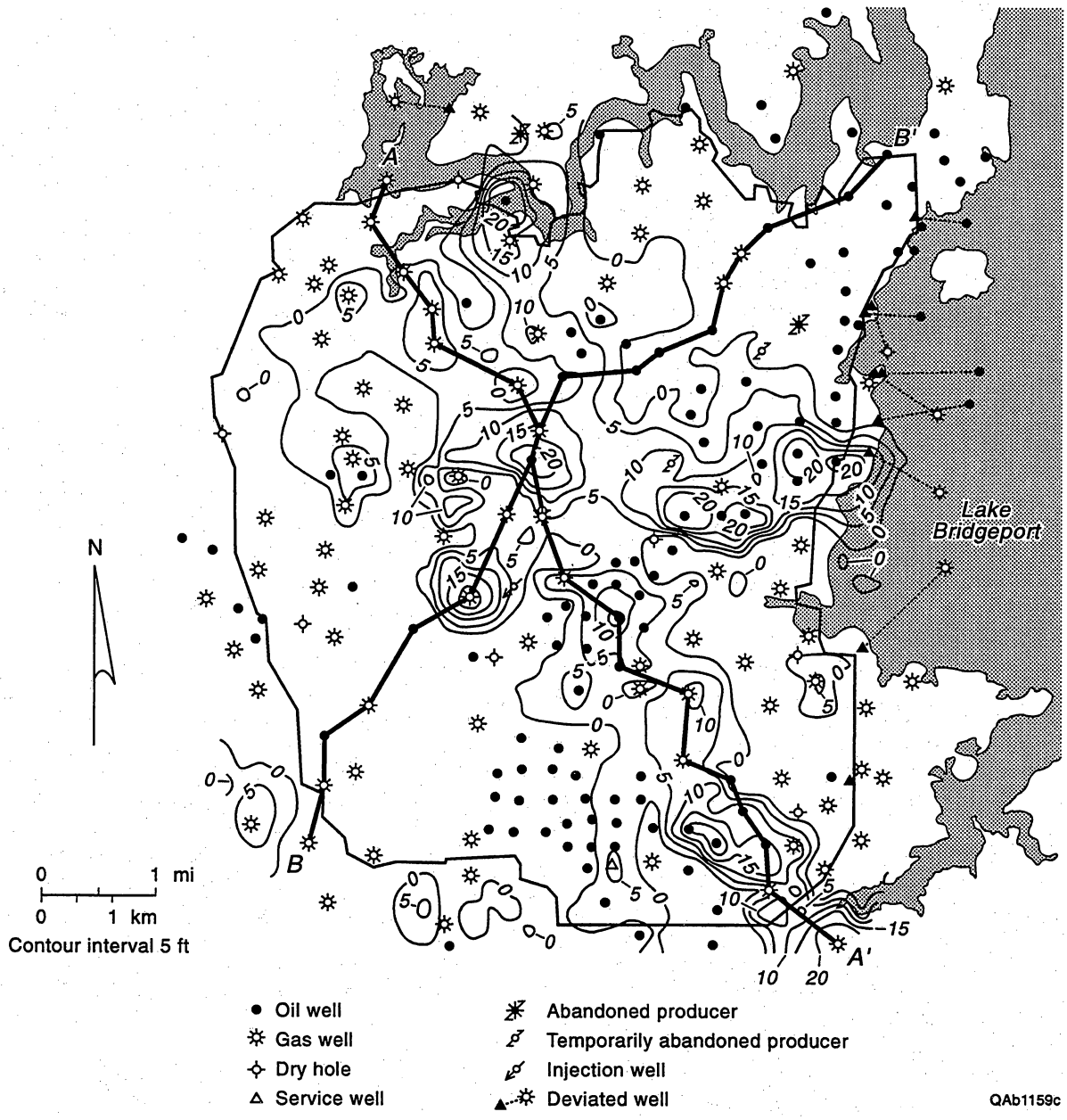

Figure A29. Lower Jasper Creek "Exxon" sequence total net reservoir isopach (ES34–ES30). Net reservoir cutoffs: SP < –30 mv; Res > 10 ohmm.

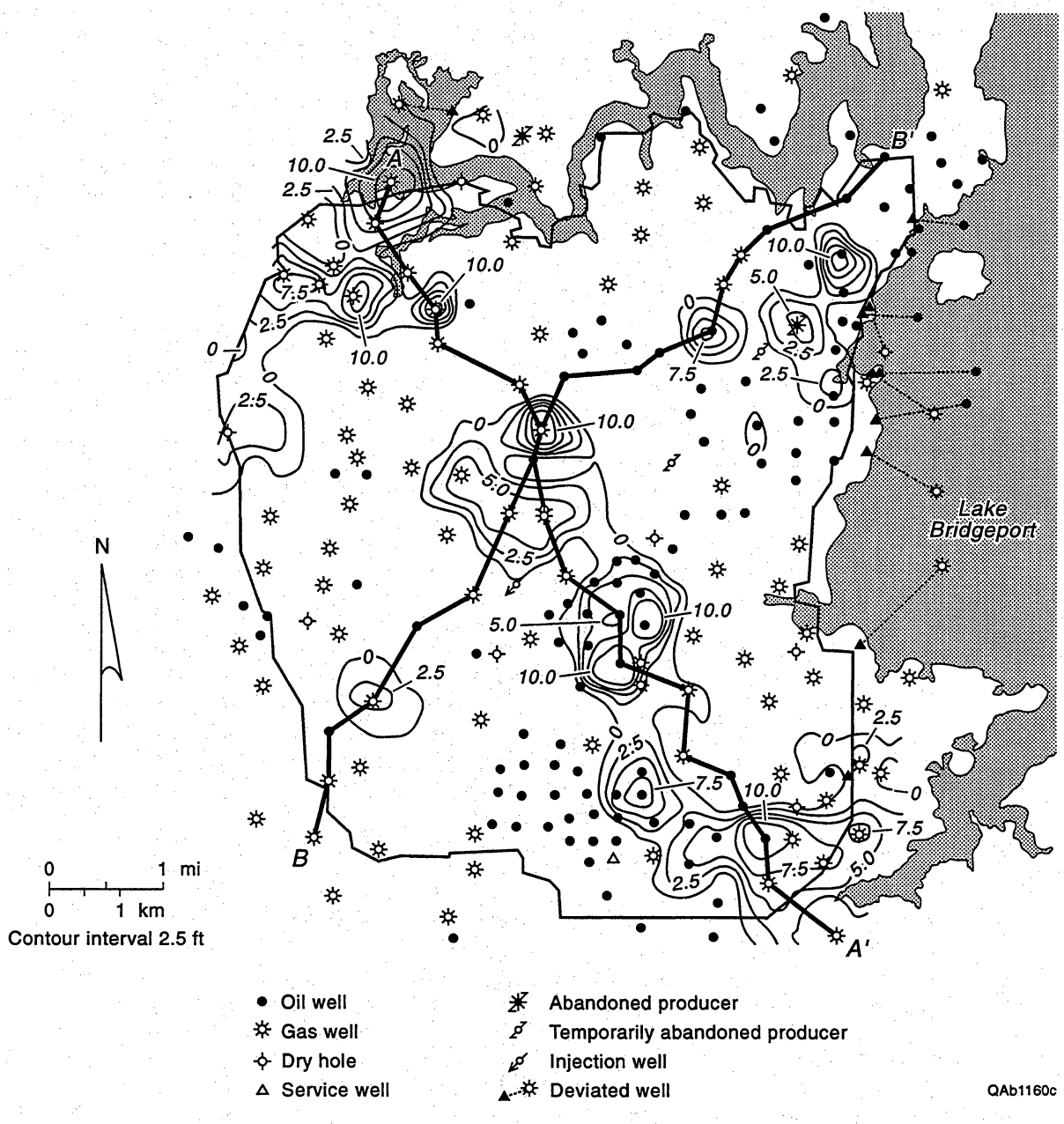

Figure A30. Middle Jasper Creek lowstand valley fill net reservoir isopach (FS34–ES34). Net reservoir cutoffs: SP < –30 mv; Res>10 ohmm.

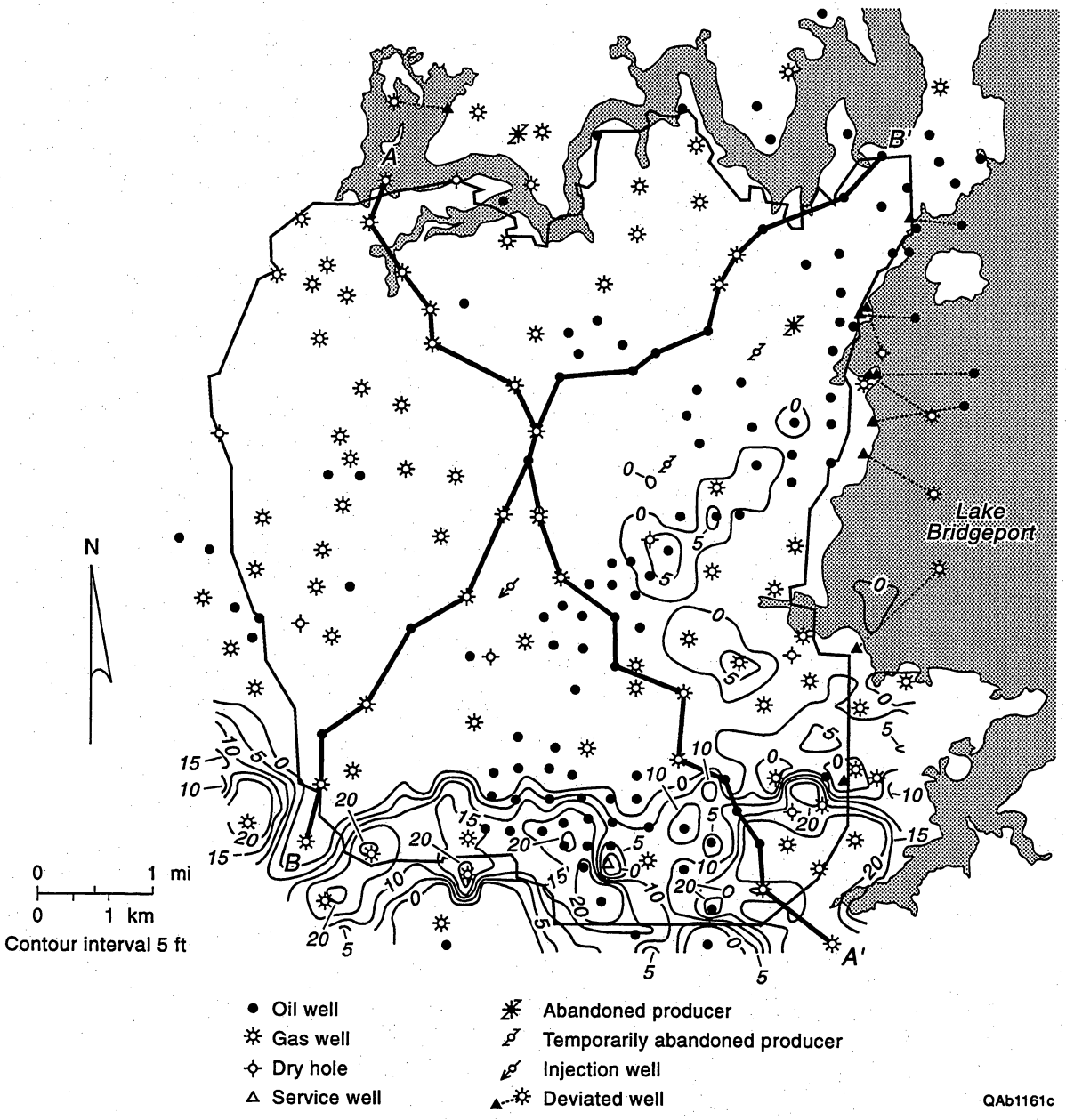

Figure A31. Upper Jasper Creek "Exxon" sequence net reservoir isopach (ES38–ES36). Net reservoir cutoffs: SP < –30 mv; Res > 10 ohmm.

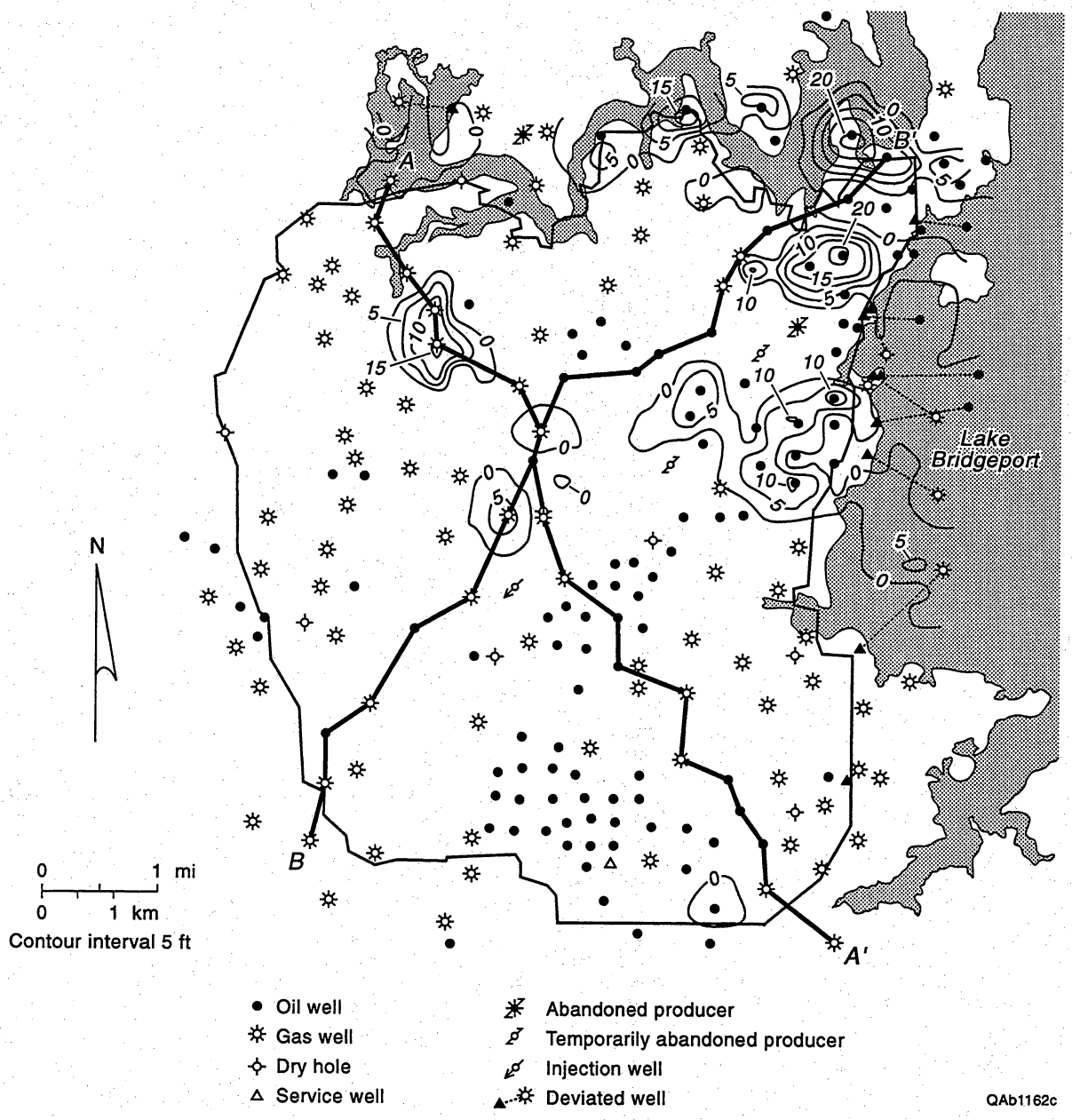

Figure A32. Fourth Jasper Creek "Exxon" sequence net reservoir isopach (ES40–ES38). Net reservoir cutoffs: SP < –30 mv; Res > 10 ohmm.

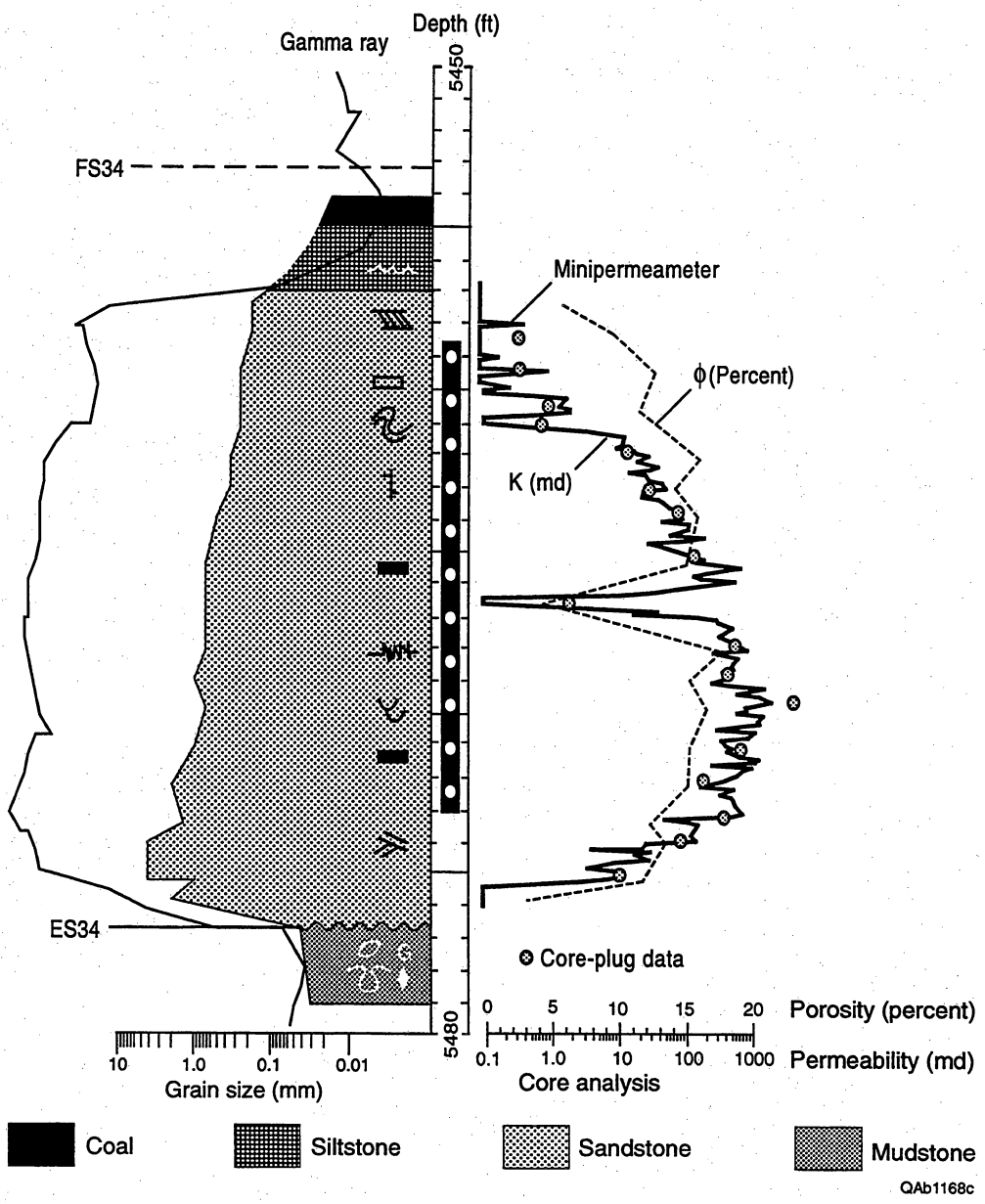

Figure A33. Middle Jasper Creek genetic sequence from Threshold Development I. G. Yates No. 33 core.

Low-Accommodation Example: Caddo

In contrast to the Wizard Wells and Jasper Creek isopachs (Figs. A24 and A27), the total Caddo net reservoir sandstone isopach in Figure A34 illustrates a more widespread sandstone distribution typically found in a relatively low accommodation setting. The Caddo contains only two discrete sandstone bodies that occur within a Lower Caddo highstand systems tract (MFS80-ES95) and an Upper Caddo lowstand systems tract (MFS90-ES95). Judging from clinoform geometries, rock types and high feldspar contents, and FMI paleocurrent indicators, Caddo sediment transport is inferred to have been southward from Red River (Electra) and Muenster granitic terrains.

The Lower Caddo is a southward-prograding deltaic system, exhibiting low-angle, shingled clinoforms (Fig. A35). "The Caddo Limestone" in the project area actually comprises two separate carbonate units representing the abandonment and transgression of two distinct delta-lobe platforms. Figure A36 shows a northeast-trending net reservoir thick in the south half of the project area that is interpreted to be a strike-oriented, delta-front deposit. Sinuous, south-trending ribbons of thin sandstone north of the delta front sandstone may represent minor fluvial or distributary channels. The Lower Caddo is an oil-productive zone and it occurs in the area of highest structural elevation at the Caddo level (Fig. A17).

The Upper Caddo sandstone is a broad southeast-trending belt of sandstone with several smaller sinuous fingers extending from it to the south and southwest (Fig. A37). Overall, the Upper Caddo represents a large incised valley-fill system that was filled by high-energy fluvial and deltaic-channel deposits.

The Upper Caddo overlies a conspicuous erosional surface, ES95, which is inferred to be an unconformity. Caddo limestones do not occur above the sharp-based, blocky to upward-fining Upper Caddo sandstone (Fig. A38), and sharp-based upward-fining sandstones are generally not present below Caddo limestones. In the northeastern part of

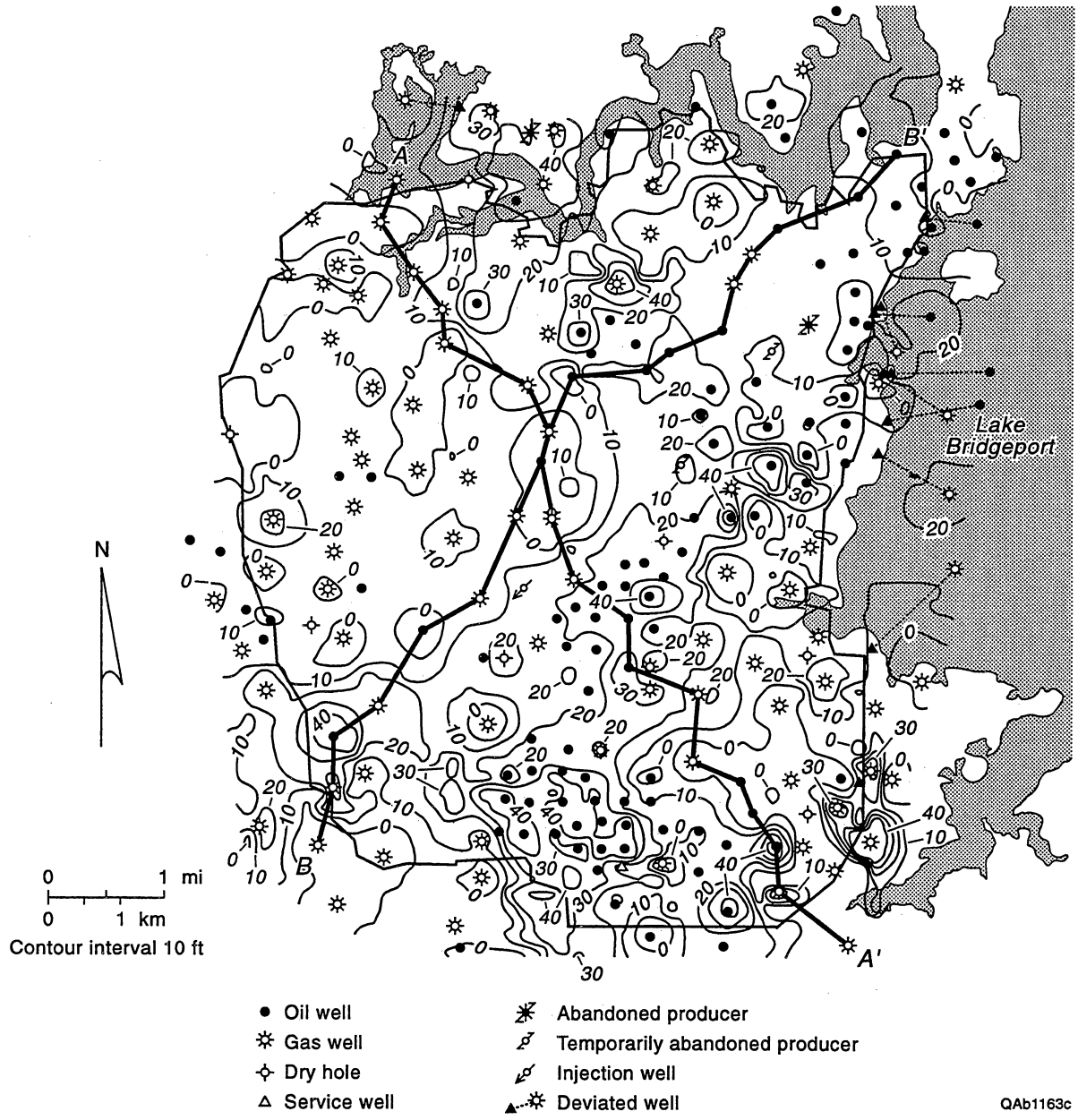

Figure A34. Caddo genetic sequence total net reservoir isopach (MFS90–MFS80). Net reservoir cutoffs: SP < –30 mv; Res >10 ohmm.

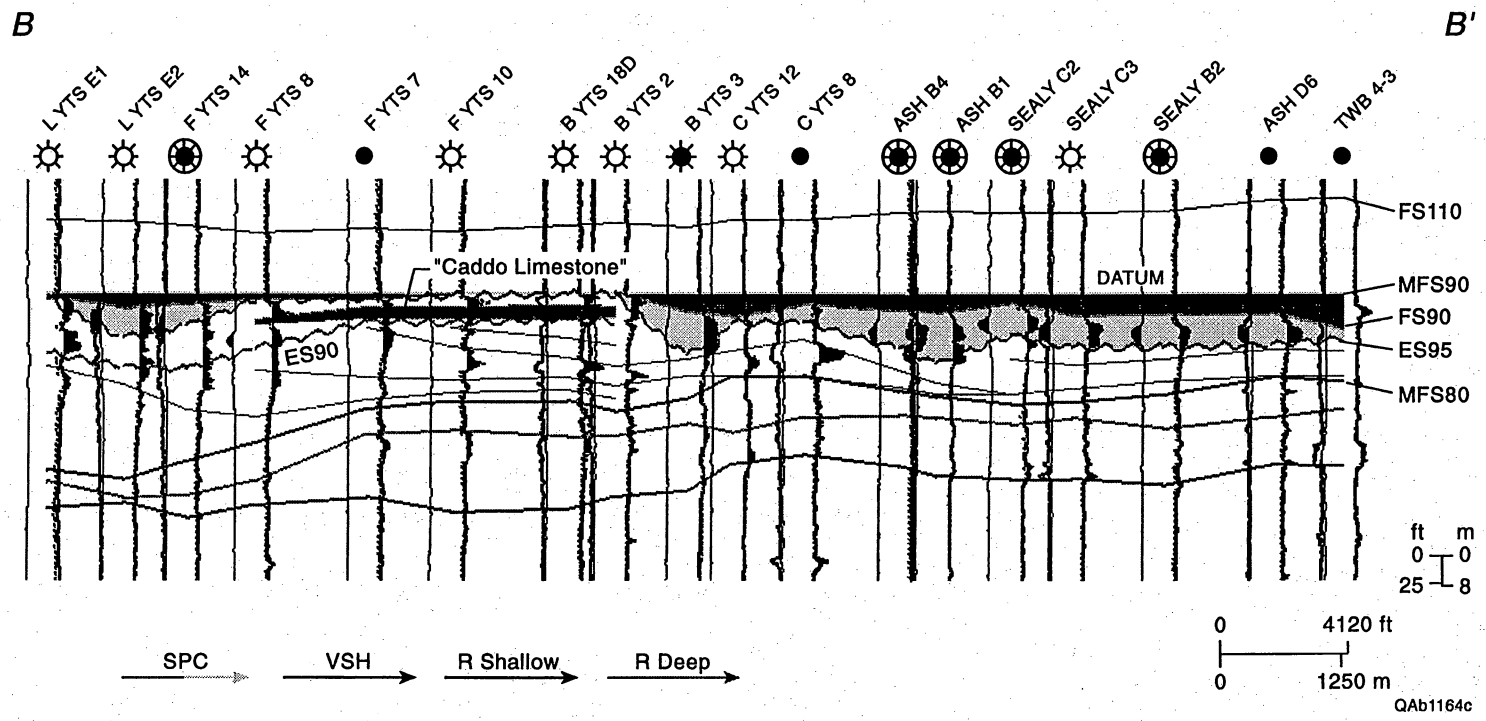

Figure A35. Stratigraphic cross section B–B′ illustrating Lower Caddo shingling clinoforms and limestone erosionally truncated by ES95. Upper Caddo valley-fill reservoirs shaded in light gray. Stratigraphic datum = MFS90.

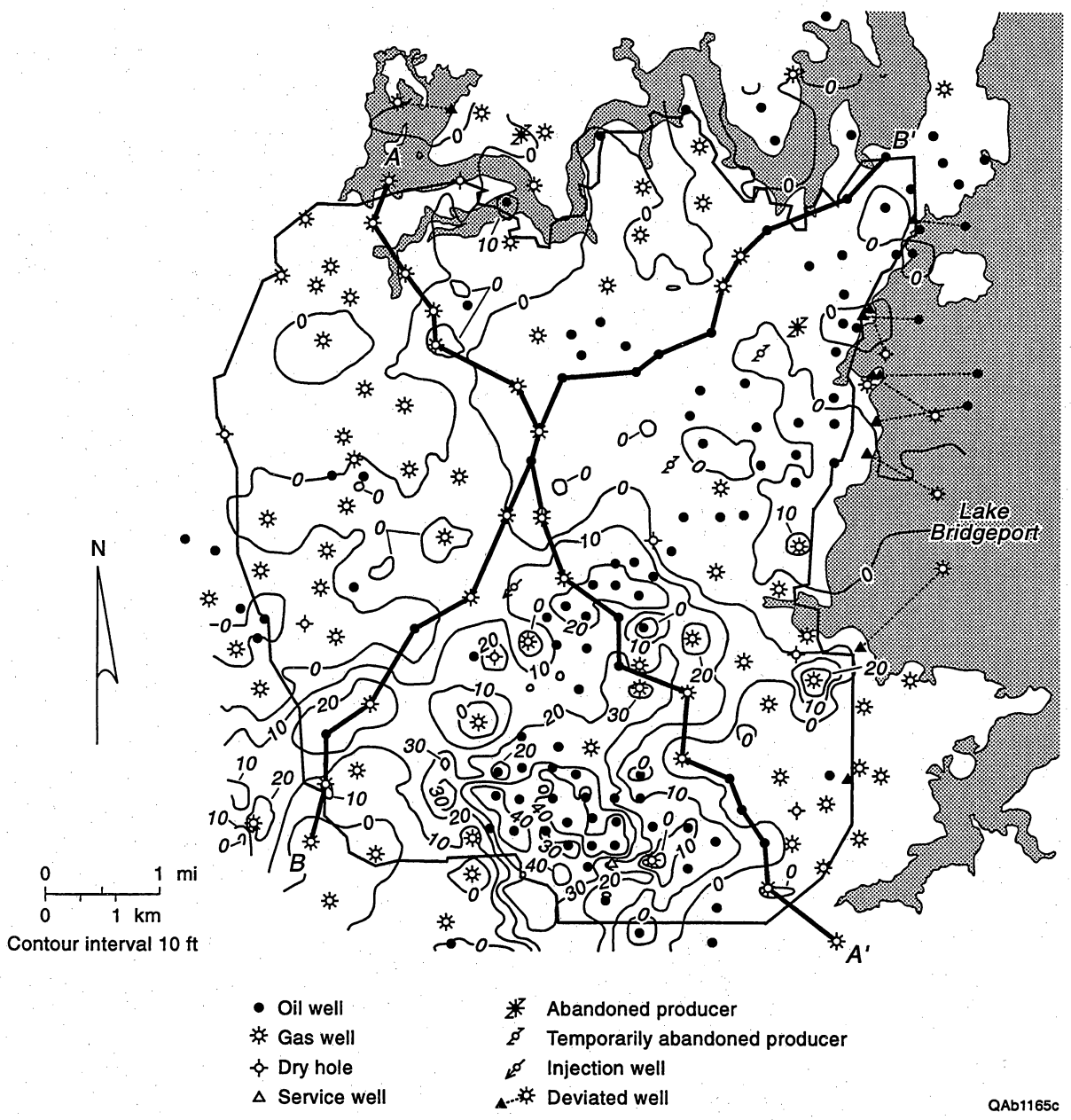

Figure A36. Lower Caddo lowstand wedge net reservoir isopach (ES95–MFS80). Net reservoir cutoffs: SP < –30 mv; Res > 10 ohmm.

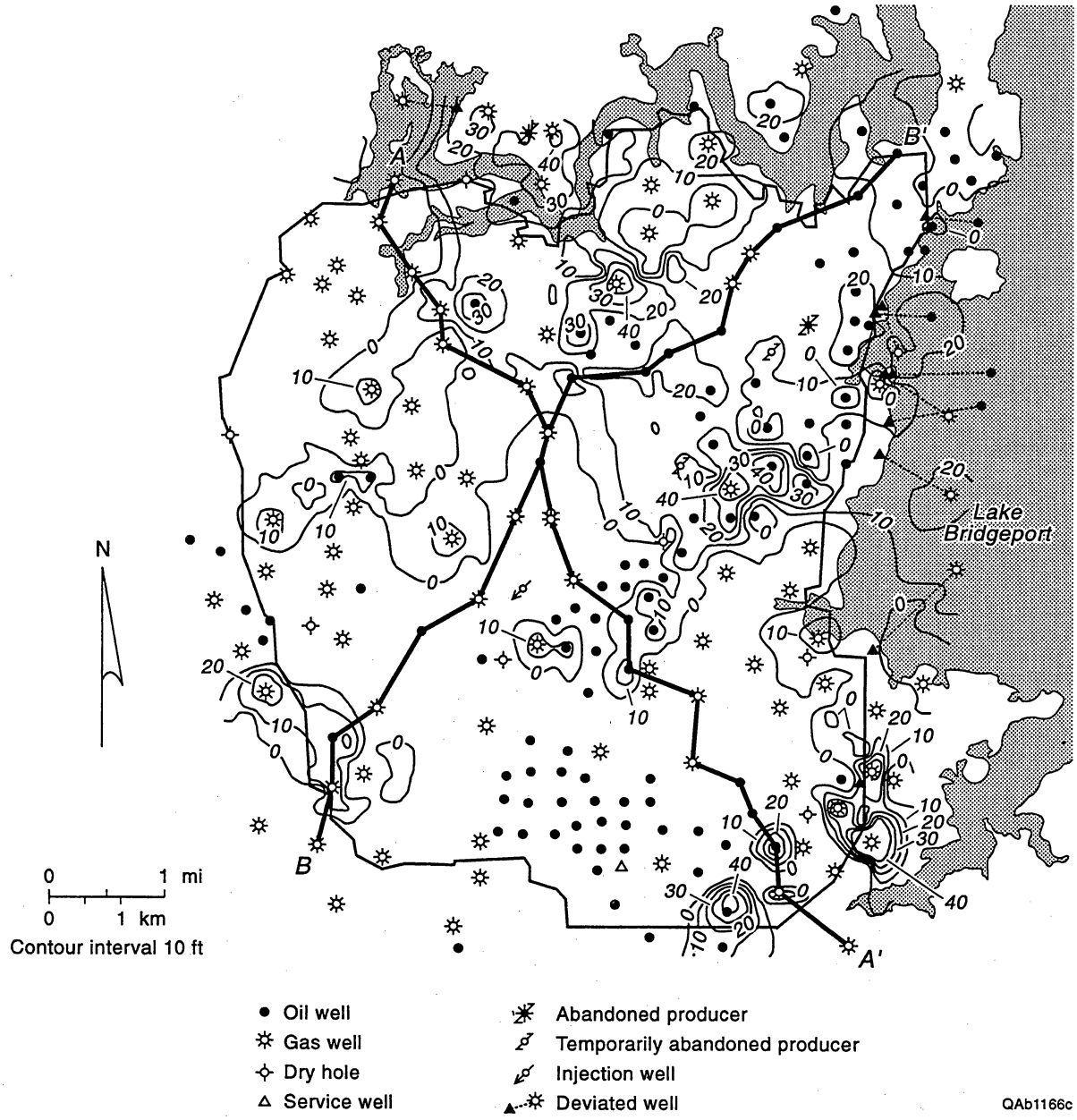

Figure A37. Upper Caddo genetic lowstand wedge net reservoir isopach (MFS90–ES95). Net reservoir cutoffs: SP < –30 mv; Res > 10 ohmm.

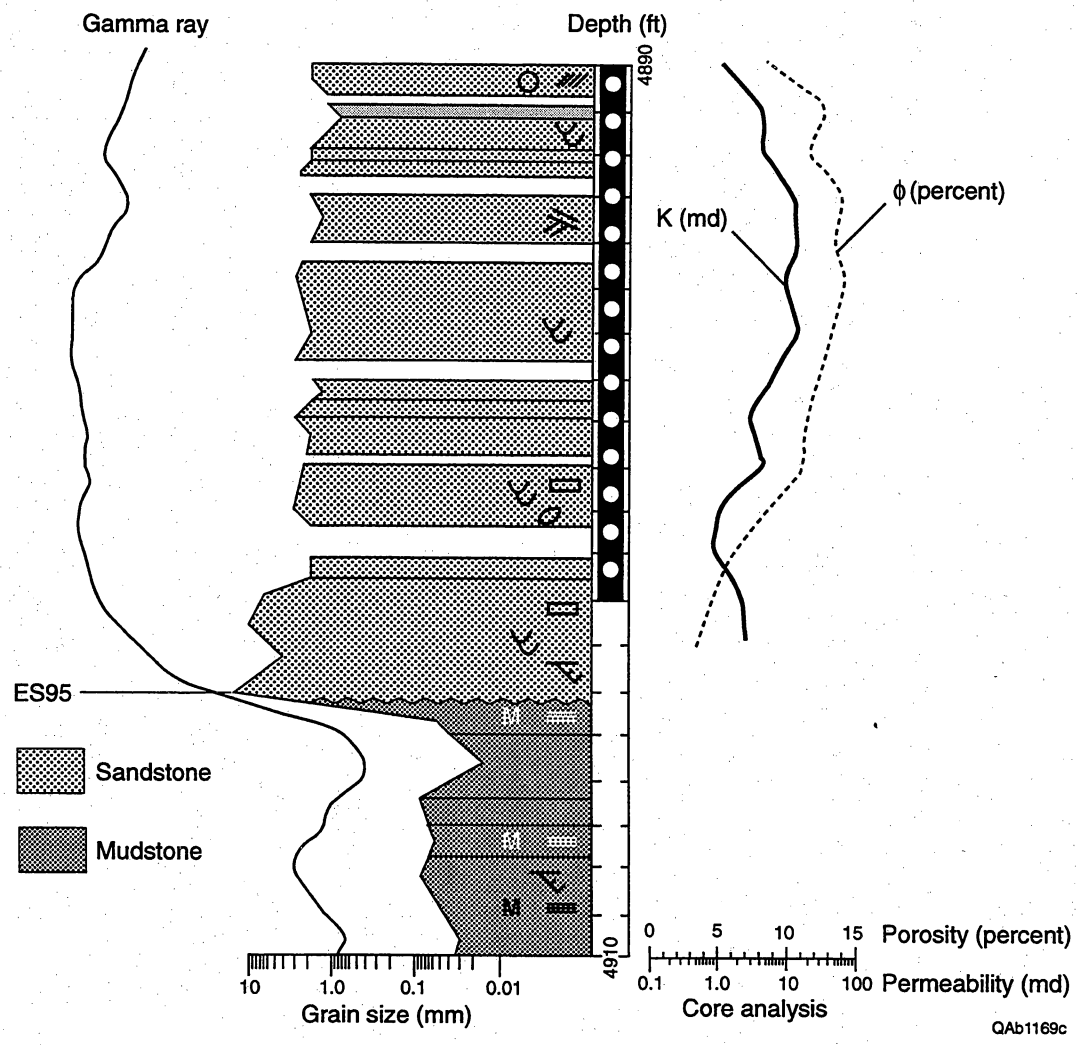

Figure A38. Upper Caddo sequence from OXY, U.S.A., Sealy C No. 2 core.

the project area, Upper Caddo sandstone sharply overlies shelf mudstones, a marked facies dislocation suggesting that erosional stripping of units has occurred.

Although most of the Caddo production in the project area is oil, significant gas reserves have been found in Upper Caddo wells (for example, Sealy "C" No. 2 and "C" No. 3) located structurally downdip relative to the Lower Caddo oil accumulation in the south, indicating that the two units are physically separate reservoir compartments. The Upper and Lower Caddo Sandstones occur in distinctly different systems tracts and provide an excellent example of surface-bounded reservoir compartmentalization on a fieldwide scale.

Summary and Conclusions of Geologic Evaluation

A computer-based geologic evaluation of well log curves and cores from an approximately 30-m^2 portion of Boonsville (Bend Conglomerate Gas) field was conducted by part of an interdisciplinary team assigned the task of developing infill drilling strategies to increase natural gas reserves in the mature Midcontinent region. The following has been uncovered as a result of this endeavor:

- Late Paleozoic strata of the U.S. Midcontinent region, including those containing hydrocarbon reservoirs, represent the thin, updip stratigraphic remnants of sea-level highstands deposited in stable cratonic areas. These rocks can be described as surface-dominated strata; there is relatively more geologic time represented by surfaces than by preserved strata.
- Surface-dominated, terrigenous clastic strata are typically thin and commonly contain sand-prone, lowstand systems tracts that are rarely fully preserved. The Fort Worth Foreland Basin provided a mixed-accommodation setting into which Atokan surface-dominated strata were deposited.
- When performing geological correlations in surface-dominated, Midcontinent reservoirs, researchers must recognize major erosional features that have cut out

previously deposited sequences and shingling, clinoform geometries in which several individual sandstone compartments can occur that appear to be one unit in well log cross sections.

- The Bend Conglomerate stratigraphic interval averages 1,100 ft in thickness in the Boonsville Project Area and consists of sandstone, limestone, and mudstone deposits representing the 2- to 7-million-yr-long Atoka Epoch, which is part of the Early Middle Pennsylvanian Period (Carboniferous Upper Westphalian Series).
- The Boonsville Bend Conglomerate stratigraphic interval is composed of 10 genetic stratigraphic sequences (or genetic sequences) that average about 100 ft in gross thickness. The genetic sequences are defined and bounded by impermeable, deep-shelf shales that represent relative maximum flooding events. Genetic sequences are similar to cycles or cyclothems used by many workers to describe repetitive stratigraphic successions in upper Paleozoic strata.
- Individual genetic sequences contain a well-defined succession of *depositional systems tracts*, including *highstand*, *lowstand*, and *transgressive* tracts. The inferred systems tracts are defined and bounded by key chronostratigraphic surfaces, namely *maximum flooding surfaces* (MFS), *erosion surfaces* (ES), and transgressive *flooding surfaces* (FS). Highstand, lowstand, and transgressive systems tracts are inferred to coincide broadly with high and falling base level, base-level minima and early-phase base-level rise, and rising base level, respectively.
- Thickness and lithologic trends in Bend Conglomerate genetic sequences suggest that eustasy may have been the dominant variable controlling base-level cycles that created the complex stratal architecture. Atokan relative sea-level interpretations of Ross and Ross (1988) indicate an overall increase in eustatic sea level punctuated by high amplitude (100 to 300 m) and high-frequency (100,000 to 400,000 yr) sea-level cycles. The Boonsville Project Area was probably alternately subaerially

exposed then inundated by marine waters at least 6, and perhaps as many as 10, times during Atoka time.

- Natural gas reservoirs at Boonsville occur predominantly as lowstand, valley-fill conglomeratic sandstones; they owe their existence to erosional downcutting (incisement), which occurs during relative base-level lowstands, followed by subsequent aggradation during the early phase of relative base-level rises. Highstand deltaic and shoreface sandstones are also important reservoirs that occur as progradational lobes. Lowstand fluvial and deltaic deposits overlie and erosionally truncate highstand deposits; however, their respective reservoir sandstone bodies typically occur as separate compartments.
- Many small-scale, near-vertical fault zones, which cannot be mapped without 3-D seismic data, have oval or circular patterns on time-structure maps. Most of these high-angle normal and reverse faults have less than 100 ft of displacement; they rarely penetrate the overlying Strawn Group; and they are closely associated with karst collapse features in the underlying Paleozoic platform carbonate units.
- In map view, the karst collapse features occur in broadly defined, dominantly north-northwesterly linear groups, suggesting a genetic relationship between karst-dissolution processes and preexisting, subtle basement faulting.
- Isopach mapping of the sum of all net reservoir (i.e., total Atoka net reservoir) contained in the Bend Conglomerate within the project area indicates a strong relationship between sandstone-reservoir distribution and structurally low areas on the pre-Atoka, seismic time-structure surface. This fact implies that subtle differences in structural elevation at the pre-Atoka, Paleozoic carbonate stratigraphic level controlled the geographical locations of incised valleys, fluvial and fluvio-deltaic axes in which high-energy reservoir facies were concentrated. Many of the thickest valley-fill sandstone reservoirs occur above or immediately adjacent to vertically faulted, karst collapse zones.

- The predominant compartmentalization mechanisms observed in the Boonsville project area are (1) stratigraphic, comprising surface-bounded, facies-bounded and cement-bounded compartments; (2) structural, mainly fault-bounded compartments; and perhaps the most common type encountered at Boonsville, (3) a combination of stratigraphic and structural mechanisms.
- Three types of stratigraphic compartmentalization mechanisms occur in the Boonsville project area. Surface-bounded compartments result from the juxtaposition of reservoir sandstones and impermeable facies at key chronostratigraphic surfaces. Facies-bounded compartments result from high-frequency autocyclic processes within the depositional systems tract. Diagenetic cements can occlude porosity in Midcontinent reservoir sandstone units to the extent that cement-bounded compartments arise.
- Accommodation varied through Atoka time such that each of the Bend Conglomerate sequences was deposited under unique conditions that controlled compartment size. Geological parameters such as gross thickness, average net reservoir sandstone thickness, average net:gross ratio, and number of individual sandstone beds per zone can help provide a comparative estimate of the relative amount of space available during deposition of each reservoir-bearing sequence, and an estimate of expected compartment sizes can be made and used as a screening tool.
- Seismic attribute analysis of confidently interpreted reservoir zones (i.e., genetic sequences) holds great promise for identifying stratigraphic prospects in some of the thicker, low-accommodation reservoir zones, such as the Caddo. Although attribute analysis can in some instances provide startling, magic-bullet identification of interwell reservoir properties, in Midcontinent thin-bed reservoirs, it is an advanced task requiring very accurate horizon interpretations and expert

workstation data-manipulation techniques that go well beyond a quick-look interpretation of the 3-D data.

References

Ammentorp, A. D., and Cleaves, A. W., 1990, Depositional systems, petrography, and hydrocarbon entrapment in the upper Atokan "Caddo" clastics interval on the northwestern margin of the Fort Worth Basin: Transactions of the American Association of Petroleum Geologists, Southwest Section, 1990 Annual Convention &, & eds., p. 121–130.

Berger, A., 1988, Milankovitch theory and climate: Reviews of Geophysics, v. 26, no. 4, p. 624–657.

Blanchard, K. S., Denman, O., and Knight, A. S., 1968, Natural gas in Atokan (Bend) section of northern Fort Worth Basin, *in* Beebe, B. W., and Curtis, B. F., eds., Natural gases of North America: American Association of Petroleum Geologists Memoir 9, v. 2, p. 1446–1454.

Boardman, D. R., II, and Heckel, P. H., 1989, Glacial-eustatic sea-level curve for early Late Pennsylvanian sequence in north-central Texas and biostratigraphic correlation with curve for midcontinent North America: Geology, v. 17, no. 9, p. 802–805.

Brown, L. F., Jr., and W. L. Fisher, 1977, Seismic-stratigraphic interpretation of depositional systems: examples from Brazilian rift and pull-apart basins, *in* Payton, C. E., ed., Seismic stratigraphy—applications to hydrocarbon exploration: American Association of Petroleum Geologists Memoir 26, p. 213–248.

Brown, L. F., Jr., Solis-Iriate, R. F., and Johns, D. A., 1990, Regional depositional systems tracts, paleogeography, and sequence stratigraphy, Upper Pennsylvanian and

Lower Permian strata, north- and west-central Texas: The University of Texas at Austin, Bureau of Economic Geology Report of Investigations No. 197, 116 p.

Caputo, M. V., and Crowell, J. C., 1985, Migration of glacial centers across Gondwana during the Paleozoic Era: Geological Society of America Bulletin, v. 96, no. 8, p. 1020–1036.

Cheney, M. G., and Goss, L. F., 1952, Tectonics of central Texas: American Association of Petroleum Geologists Bulletin, v. 36, no. 12, p. 2237–2265.

Collins, E. W., Laubach, S. E., Dutton, S. P., and Hill, R. E., 1992, Depositional environments, petrology and fractures of the Atoka Davis Sandstone: a low-permeability gas-bearing sandstone of the Fort Worth Basin, north-central Texas, *in* Cromwell, D. W., Moussa, M. T., Mazzullo, L. J., eds., Transactions of the American Association of Petroleum Geologists, Southwest Section, Publication 92-90, p. 221–230.

Connolly, W. M., and Stanton, R. J., Jr., 1992, Interbasinal cyclostratigraphic correlation of Milankovitch band transgressive-regressive cycles: correlation of Desmoinesian–Missourian strata between southeastern Arizona and the midcontinent of North America: Geology, v. 20, no. 11, p. 999–1002.

Cross, T. A., 1988, Controls on coal distribution in transgressive-regressive cycles, Upper Cretaceous, Western Interior, U.S.A., *in* Wilgus, C. K., Hastings, B. S., Ross, C. A., Posamentier, H., Van Wagoner, J., and Kendal, C. G. St. C., eds., Sea-level changes: an integrated approach: Society of Economic Paleontologists and Mineralogists Special Publication No. 42, p. 371–380.

Crowell, J. C., and Frakes, L. A., 1970, Phanerozoic glaciation and the causes of ice ages: American Journal of Science, v. 268, no. 3, p. 193–224.

_____ 1975, The Late Paleozoic glaciation, *in* Campbell, K. S. W., ed., Gondwana geology: papers presented at the third Gondwana symposium, Canberra, Australia, 1973, p. 313–331.

Crowley, T. J., and Baum, S. K., 1991, Estimating Carboniferous sea-level fluctuations from the Gondwanan ice extent: Geology, v. 19, no. 10, p. 975–977.

Donovan, D. T., and Jones, E., 1979, Causes of world-wide changes in sea level: Journal of the Geological Society of London, v. 136, p. 187–192.

Fisher, W. L., and McGowen, J. H., 1967, Depositional systems in the Wilcox Group of Texas and their relationship to occurrence of oil and gas, *in* Gulf Coast Association of Geological Societies Transactions, v. 17, p. 105–125.

Flawn, P. T., Goldstein, A. G., Jr., King, P. B., and Weaver, C. E., 1961, The Ouachita System: University of Texas, Austin, Bureau of Economic Geology Publication No. 6120, 401 p.

Galloway, W. E., 1989, Genetic stratigraphic sequences in basin analysis I: architecture and genesis of flooding-surface bounded depositional units: American Association of Petroleum Geologists Bulletin, v. 73, no. 2, p. 125–142.

Gardner, M. H., 1995, Tectonic and eustatic controls on the stratal architecture of Mid-Cretaceous stratigraphic sequences, Central Western Interior Foreland Basin of North America, *in* SEPM (Society for Sedimentary Geology) Special Publication No. 52, p. 243–281.

Gardner, M. H., and Cross, T. A., in preparation, Time-space partitioning of sediment volumes in facies tracts: a primary control on stratal geometry and facies architecture of depositional sequences.

Glover, G., 1982, A study of the Bend Conglomerate in S. E. Maryetta Area, Boonesville [sic] Field, Jack County, Texas: Dallas Geological Society &

Goldhammer, R. K., Oswald, E. J., and Dunn, P. A., 1991, Hierarchy of stratigraphic forcing: example from Middle Pennsylvanian shelf carbonates of the Paradox Basin, *in* Franseen, E. K., and others, eds., Sedimentary modeling: computer simulations and methods for improved parameter definition: Kansas Geological Survey Bulletin No. 233, p. 361–413.

Heckel, P. H., 1977, Origin of phosphatic black shale facies in Pennsylvanian cyclothems of mid-continent North America: American Association of Petroleum Geologists Bulletin, v. 61, no. 7, p. 1045–1068.

_____ 1980, Paleogeography of eustatic model for deposition of midcontinent Upper Pennsylvanian cyclothems, *in* Fouch, T. D., and Magathan, E. R., eds., Paleozoic paleogeography of the west-central United States: Rocky Mountain Section of the Society of Economic Paleontologists and Mineralogists, Rocky Mountain Paleogeography Symposium 1, p. 197-215.

_____ 1986, Sea-level curve for Pennsylvanian eustatic marine transgressive-regressive depositional cycles along midcontinent outcrop belt, North America: Geology, v. 14, no. 4, p. 330–334.

_____ 1989a, Implications for Texas of glacial eustatic control over Middle and Upper Pennsylvanian cyclothems in midcontinent North America (abs.): Geological Society of America Abstracts with Programs, South-Central Section, v. 21, no. 1, p. 14.

_____ 1989b, Updated Middle-Upper Pennsylvanian eustatic sea level [sic] curve for midcontinent North America and preliminary biostratigraphic characterization: XI^{e}

Congrés International de Stratigraphie et de Géologie du Carbonifère Beijing 1987, Comptes Rendu, v. 4, p. 160–185.

Jervey, M. T., 1988, Quantitative geological modeling of siliciclastic rock sequences and their seismic expression, *in* Wilgus, C. K., Hastings, B. S., Ross, C. A., Posamentier, H., Van Wagoner, J., and Kendal, C.G.St.C., eds, Sea-level changes: an integrated approach: Society of Economic Paleontologists and Mineralogists Special Publication No. 42, p. 47–69.

Lahti, V. R., and Huber, W. F., 1982, The Atoka Group (Pennsylvanian) of the Boonsville Field area, north-central Texas, *in* Martin, C. A., ed., Petroleum geology of the Fort Worth Basin and Bend Arch area: Dallas Geological Society, p. 377–399.

Lovick, G. P., Mazzini, C. G., and Kotila, D. A., 1982, Atokan clastics—depositional environments in a foreland basin: Oil and Gas Journal, v. 80, no. 5, p. 181–199.

Masters, J. A., 1979, Deep basin gas trap, Western Canada, American Association of Petroleum Geologists Bulletin, v. 63, p. 152–181.

McElhinny, M. W., 1973, Palaeomagnetism and plate tectonics: Cambridge, Cambridge University Press, 358 p.

Meckel, L. D., Jr., Smith, D. G., Jr., Wells, L. A., 1992, Ouachita foredeep basins: regional paleogeography and habitat of hydrocarbons, Chapter 15, p. 427–444.

Moore, R. C., Wanless, H. R., Weller, J. M., Williams, J. S., Read, C. B., Bell, W. A., Ashley, G. H., Cheney, M. G., Cline, L. M., Condra, G. E., Dott, R. H., Dunbar, C. O., Elias, M. K., Glenn, L. C., Grene, F. C., Hendricks, T. A., Jewett, J. M., Johnson, J. H., King, P. B., Knight, J. B., Levorsen, A. I., Miser, H. D., Newell, N. D., Plummer, F. B., Thompson, M. L., Tomlinson, C. W., and Westheimer, J.,

1944, Correlation of Pennsylvanian formations in North America: Geological Society of America Bulletin, v. 55, no. 6, p. 657–706.

Morel, P., and Irving, E., 1978, Tentative paleocontinental maps for the Early Phanerozoic and Proterozoic: Journal of Geology, v. 86, no. 5, p. 535–561.

Mulholland, J. W., 1994, Sequence stratigraphic correlation of well-log cross sections: Mountain Geologist, v. 31, no. 3, p. 65–75.

Nassichuk, W. W., and Bamber, E. W., 1978, Middle Pennsylvanian biostratigraphy, eastern Cordillera and Arctic islands, Canada—a summary, *in* Stelck, C. R., and Chatterton, B. D. E., Western and Arctic Canadian biostratigraphy: Geological Society of Canada Special Paper 18, p. 395–413.

Ng, D. T. W., 1976, Subsurface study of Atoka (Lower Pennsylvanian) clastic rocks, North-Central Texas, *in* Henry, G. E., ed., Basins of the Southwest: Phase III: compiled for the North Texas Geological Society, p. 155–191.

Ng, D. T. W., 1979, Subsurface study of Atoka (Lower Pennsylvanian) clastic rocks in parts of Jack, Palo Pinto, Parker, and Wise Counties, North-Central Texas: American Association of Petroleum Geologists Bulletin, v. 63, p. 50–66.

Phillips, T. L., and Peppers, R. A., 1984, Changing patterns of Pennsylvanian coal-swamp vegetation and implications of climatic control on coal occurrence: International Journal of Coal Geology, v. 3, no. 3, p. 205–255.

Quinlan, G. M., and Beaumont, Christopher, 1984, Appalachian thrusting, lithospheric flexure, and the Paleozoic stratigraphy of the Eastern Interior of North America: Canadian Journal of Earth Sciences, v. 21, no. 9, p. 973–996.

Railroad Commission of Texas, 1991, Field rules, Section VI, Boonsville Field (Bend Conglomerate Gas), Order No. 9-36, 420.

Ramsbottom, W. H. C., 1979, Rates of transgression and regression in the Carboniferous of NW Europe: Journal of the Geological Society of London, v. 136, no. 2, p. 147–153.

Ross, C. A., and Ross, J. R. P., 1985, Late Paleozoic depositional sequences are synchronous and worldwide: Geology, v. 13, no. 3, p. 194–197.

_____ 1988, Late Paleozoic transgressive-regressive deposition, *in* Wilgus, C. K., Hastings, B. S., Ross, C.A., Posamentier, H., Van Wagoner, J., and Kendal, C. G. St. C., eds, Sea-level changes: an integrated approach: Society of Economic Paleontologists and Mineralogists Special Publication No. 42, p. 227–247.

Saunders, W. B., Ramsbottom, W. H. C., and Manger, W. L., 1979, Mesothermic cyclicity in the mid-Carboniferous of the Ozark shelf region?: Geology, v. 7, no. 6, p. 293-296.

Scotese, C. R., Bambach, R. K., Barton, C., Van der Voo, R., and Zeigler, A. M., 1979, Paleozoic base maps: Journal of Geology, v. 87, no. 3, p. 217–277.

Shanley, K. W., and McCabe, P. J., 1994, Perspectives on the sequence stratigraphy of continental strata: American Association of Petroleum Geologists Bulletin, v. 78, p. 544–568.

Srivastava, G. S., 1994, Interactive software integrates geological and engineering data: Oil and Gas Journal, September, p. 85–91.

Thompson, D. M., 1982, Atoka Group (Lower to Middle Pennsylvanian), Northern Fort Worth Basin, Texas: terrigenous depositional systems, diagenesis, and reservoir

distribution and quality: The University of Texas at Austin, Bureau of Economic Geology Report of Investigations No. 125, 62 p.

_____ 1988, Fort Worth Basin, *in* Sloss, L. L., ed., The geology of North America: Boulder, Geological Society of America, v. D-2, p. 346–352.

Turner, G. L., 1957, Paleozoic stratigraphy of the Fort Worth Basin, *in* Bell, W. C., ed., Abilene and Fort Worth Geological Societies 1957 Joint Field Trip Guidebook, p. 57–77.

Vail, P. R., Mitchum, R. M., Thompson, S., III, 1977, Seismic stratigraphy and global changes of sea level, part 4: global cycles of relative changes of sea level, *in* Payton, C. E., ed., Seismic stratigraphy—applications to hydrocarbon exploration: American Association of Petroleum Geologists Memoir 26, p. 83–97.

Van Wagoner, J. C., Mitchum, R. M., Campion, K. M., and Rahmanion, V. D., 1990, Siliciclastic sequence stratigraphy in well logs, cores, and outcrops: concepts for high-resolution correlation of time and facies: American Association of Petroleum Geologists Methods in Exploration Series, No. 7, 55 p.

Walper, J. L., 1977, Paleozoic tectonics of the southern margin of North America, *in* Gulf Coast Association of Geological Societies Transactions, v. 27, p. 230–239.

Wanless, H. R., and Weller, J. M., 1932, Correlation and extent of Pennsylvanian cyclothems: Geological Society of America Bulletin, v. 43, p. 1003–1016.

Wickham, J., Roeder, D., and Briggs, G., 1976, Plate tectonic models for the Ouachita foldbelt: Geology, v. 4, no. 2, p. 173–176.

Youle, J. C., Watney, W. L., and Lambert, L. L., 1994, Stratal hierarchy and sequence stratigraphy—Middle Pennsylvanian, southwestern Kansas, U.S.A., *in* Klein, G. D.,

ed., Pangea: paleoclimate, tectonics, and sedimentation during accretion, zenith, and breakup of a supercontinent: Boulder, Colorado, Geological Society of America Bulletin Special Paper 288.

APPENDIX B

RESERVOIR ENGINEERING ANALYSIS OF THE BOONSVILLE PROJECT AREA

Introduction

This appendix highlights key results and conclusions derived from the reservoir engineering analysis conducted in the 26-mi^2 project area in Boonsville (Bend Conglomerate Gas) field in Wise and Jack Counties, Texas. Reservoir engineering plays an important role in an integrated study such as the one conducted in this project. The reservoir engineer must review available well-completion and well-performance data to establish the existence (or lack thereof) of compartmented or incompletely drained reserves and then to estimate the incremental gas reserves that may be expected from additional development. Well-test and production-data analysis and reservoir simulation can then be used to estimate reservoir properties and reservoir size, and, in some instances, to determine reservoir geometry. Reservoir properties may be mapped for regional trends that correlate with larger scale geologic and geophysical analyses; likewise, detailed reservoir engineering analyses of individual wells can provide valuable insight into reservoir architecture. Ultimately, the role of the reservoir engineer is to help focus and refine geological/geophysical interpretations being developed. Any geological/geophysical interpretations of reservoir geometry and reservoir compartmentalization must honor the known well-performance data.

As a result of the engineering analysis conducted in this project area, the following observations were made:

1. Engineering data, particularly pressure and production data, provide evidence of compartmented or incompletely drained gas in the Boonsville project area.

2. The expected gas volumes associated with these isolated compartments or poorly drained areas in most individual stratigraphic intervals will be small (200 MMscf or less on average), and multiple completion opportunities will typically be needed to achieve economic success in new infill wells.
3. Production and well test data can be used in many instances to estimate reservoir properties and to focus and refine the geological and geophysical interpretations of reservoir size and geometry.
4. Careful, strategic targeting of new wells will be the key to maximizing economic success.

Evidence of Compartmented or Incompletely Drained Gas

As part of the general overview of the Boonsville project, Figure 1.5 (see Overview section) presents a typical log through the Bend Conglomerate interval. As that figure shows, there are numerous, potentially productive sequences throughout the Bend Conglomerate. Of these intervals, the Upper Caddo and the Vineyard have been by far the most prolific producing reservoirs in the project area, although there have been completions in all the major sequences. In addition, the Upper and Lower Caddo are primarily oil-productive, although there is some gas production in both sequences.

Of particular importance to the engineering evaluation is that the Bend Conglomerate is treated as a common source of supply, and wells completed in more than one of the Bend productive sequences may be commingled and produced from a single wellbore. This poses particular problems in trying to determine total production volumes that can be attributed to specific stratigraphic sequences and in estimating interval-by-interval reservoir properties. Recently the Railroad Commission of Texas has also granted operators permission to commingle production from the Caddo and the Bend intervals in some instances.

The engineering analysis conducted in this project area included all wells drilled to the Caddo or deeper (total depth greater than 4,000 ft) within the 26^2-mi area where the 3-D data were shot and wells adjacent to, but just outside, the 3-D area. There are just over 200 wells in the 3-D area and approximately 350 wells in the engineering data base. Well logs were available for almost all of the wells in the 3-D area. Completion information and production history were also obtained for the additional wells in the engineering data base.

As additional background to the completion history in the Boonsville project area, Figure B1 illustrates the relative completion frequency of wells in the various Bend sequences. This summary includes all completions from the early 1950's to the mid-1990's for wells with log data. This figure shows all completions in the particular sequences, taking into account that one well is often completed in more than one interval. In fact, in the project area, an average of about three sequences are completed per well. The figure shows both producing and attempted completions in each interval; not all sands completed and tested in each interval were subsequently produced.

The basal Vineyard conglomerate has been the most widely completed sequence in the project area because the Vineyard is encountered throughout the project area, and it typically has 20 to 25 ft or more of net pay. Almost 70 percent of the wells in the project area have been completed in the Vineyard at some point. Quite a few wells have also tested, but not produced, the Vineyard interval. Most of these nonproductive Vineyard zones are located in the northeast portion of the project area, where the Vineyard, although thick, is deeper and has less porosity, higher water saturation, and apparently, much lower permeability.

Both the Caddo sequences and the Trinity have also been widely completed across the project area. The Bridgeport, Runaway, and Jasper Creek intervals have been completed in 15 to 30 percent of the project area wells. The other sands, including the

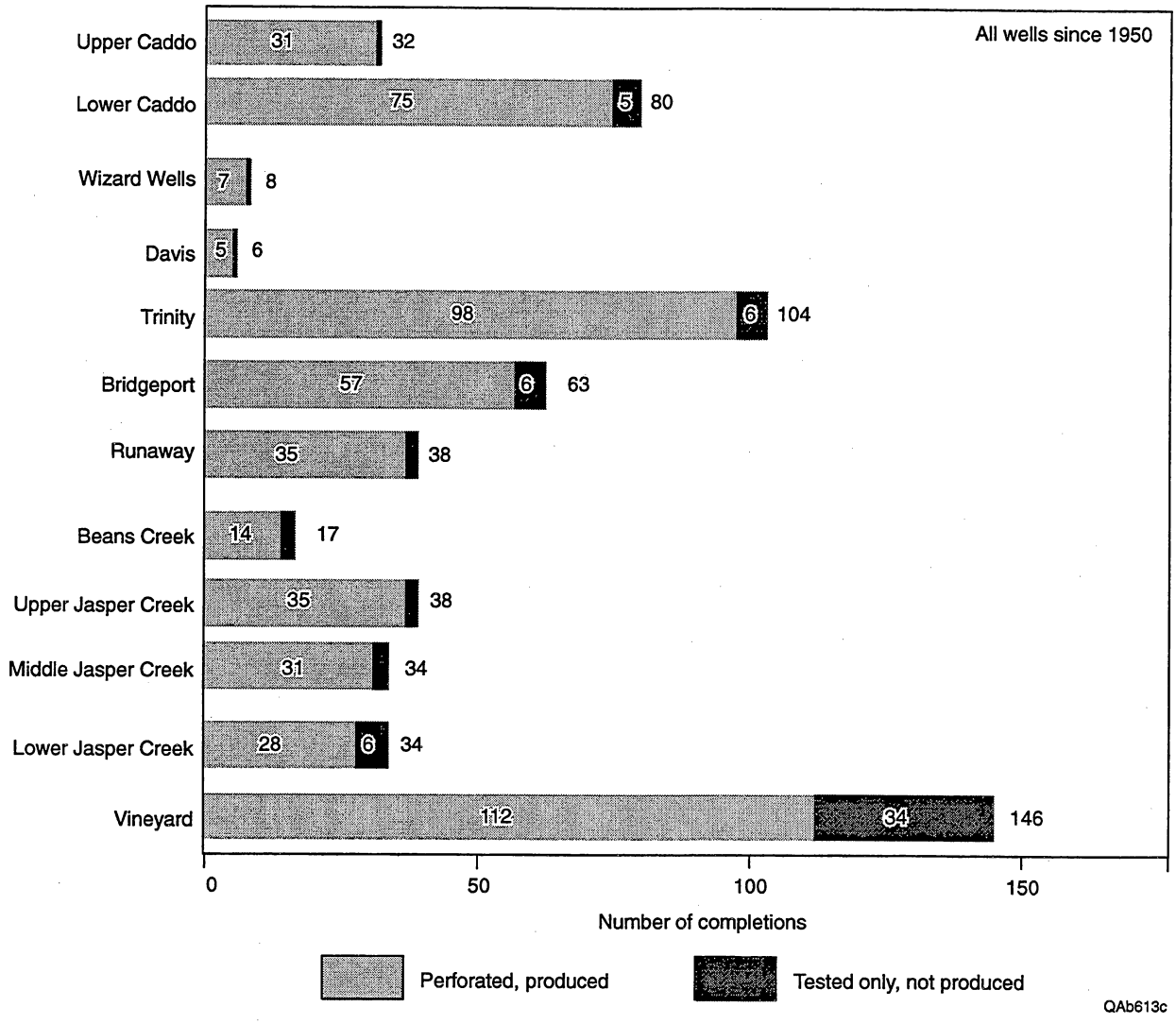

Figure B1. Completion frequency in various stratigraphic sequences for all wells in the Boonsville project area.

Wizard Wells, the Davis, and the Beans Creek are encountered only sparsely throughout the project area, as reflected in the small number of completions recorded.

As infill wells have been added at closer spacings, operators have completed in the sequences above the Vineyard with relatively greater frequency. This is illustrated in Figures B2 and B3 for wells drilled since 1980 and 1990, respectively. The Vineyard is now widely depleted across the project area, and reservoir pressures of 500 psi or less are often encountered in this sequence. As described later, the higher pressures associated with poorly drained or isolated reservoirs are found in the sequences above the Vineyard in the newer wells, accounting for the greater frequency of completion in these intervals.

With this understanding of well-completion history, one of the first steps undertaken in the engineering analysis was to look for evidence of compartmented or incompletely drained gas in the Boonsville project area. Figure B4 is a plot of initial pressures reported for wells in the project area as a function of time. These pressures are taken from multiple sources, including operator well files, state completion records, and commercial services such as Dwight's and Petroleum Information. These pressures may represent single or multiple commingled completions in different intervals throughout the Bend. In some cases, it is almost certain that these pressures are not fully built up and represent lower bound estimates of initial pressure. In all cases, however, these are the best estimates of initial pressure available for wells in the project area, and these data do provide at least a qualitative idea of the pressure history in the Bend Conglomerate over time.

In the 1950's, when most initial drilling occurred, most initial pressures reported ranged from about 1,500 to about 2,200 psi. The cluster of pressures reported in the 2,000- to 2,200-psi range reported in the mid- to late 1950's reflects the fact that most of the deeper Vineyard wells were drilled and completed during this time. As the figure shows, however, a number of the more recent wells drilled in the 1980's and 1990's still encounter initial pressures that are at or near the pressures measured in the 1950's. Clearly, there is additional scatter in the more recent data, indicating that many new wells

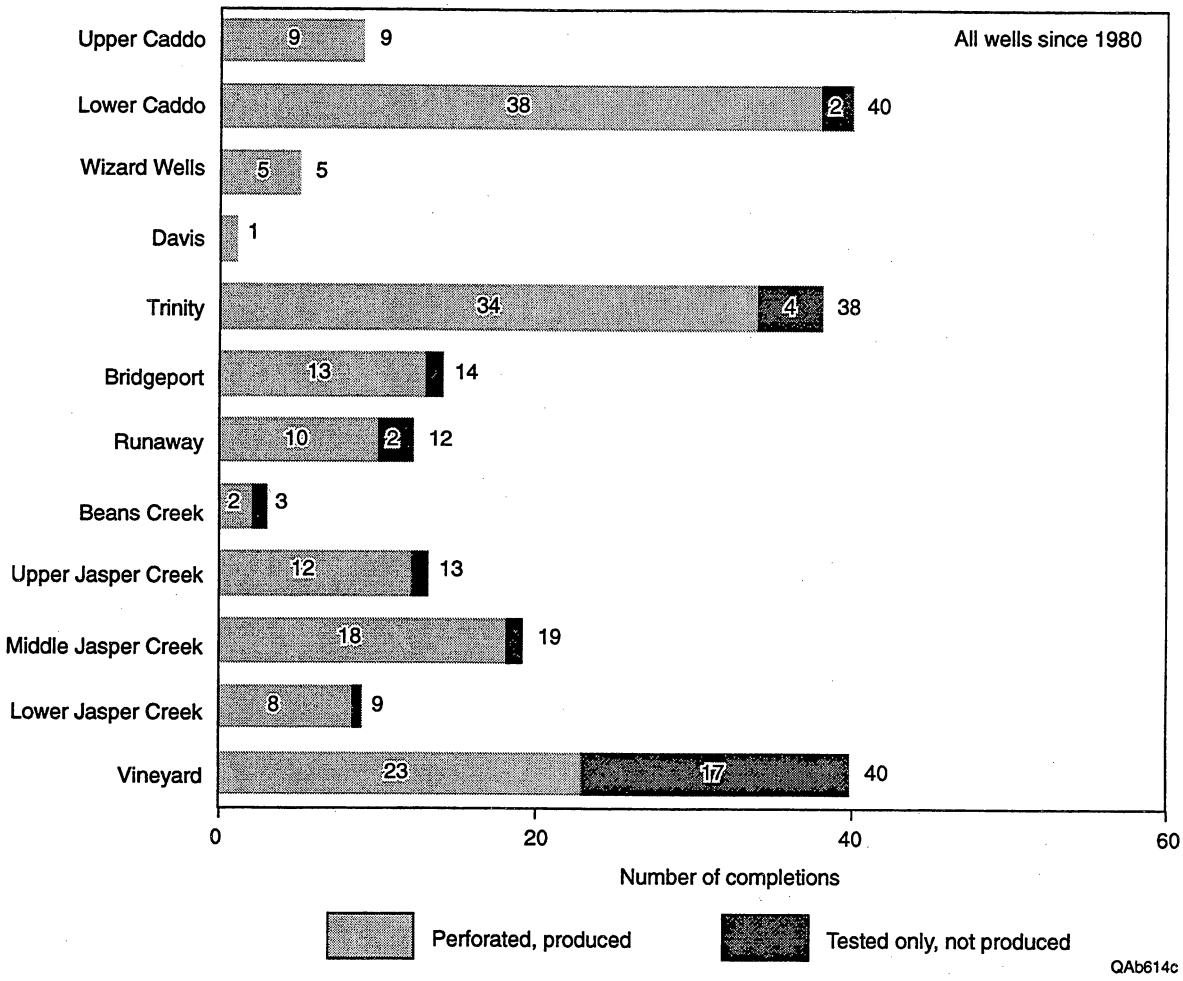

Figure B2. Completion frequency in various stratigraphic sequences for wells drilled since 1980 in the Boonsville project area.

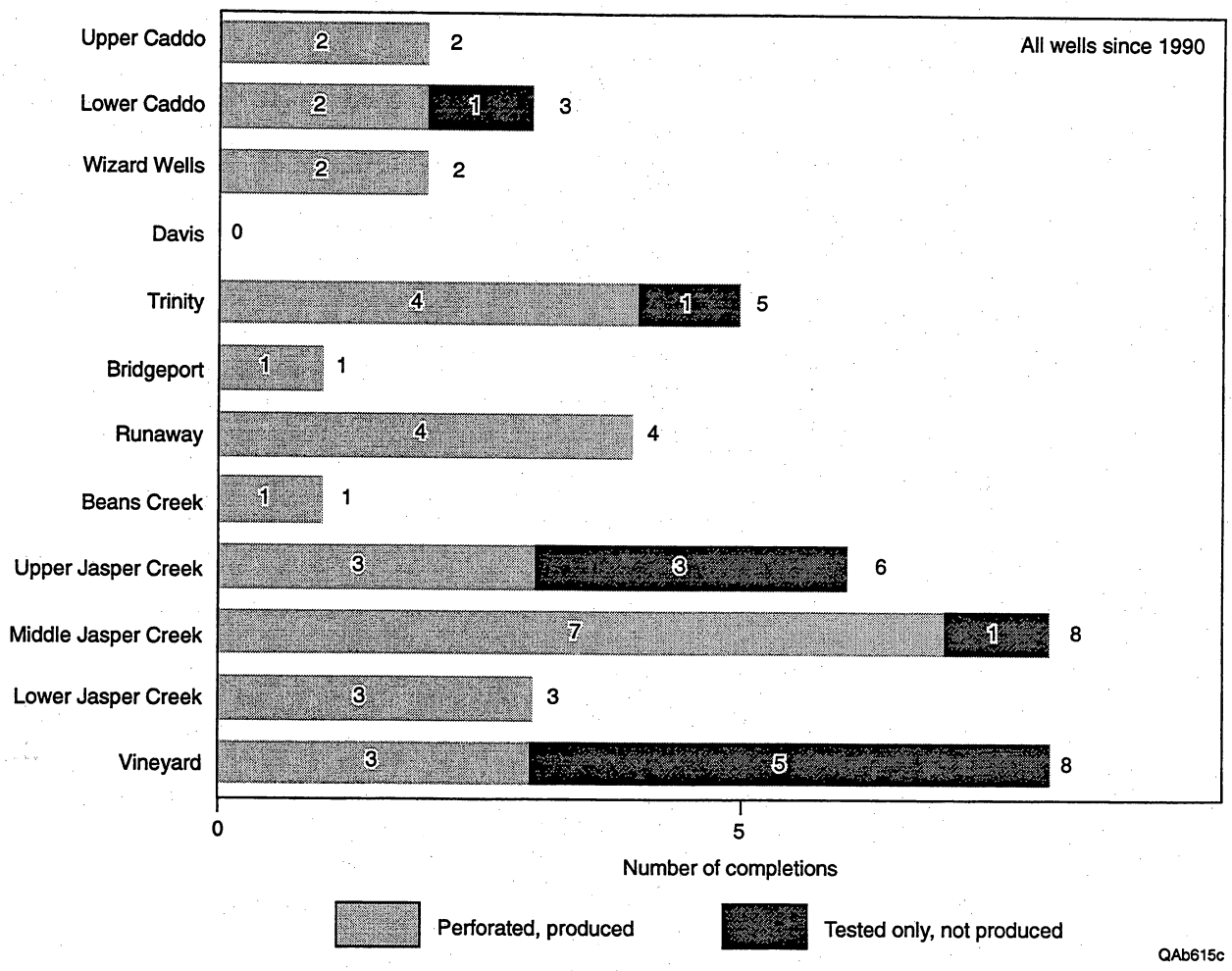

Figure B3. Completion frequency in various stratigraphic sequences for wells drilled since 1990 in the Boonsville project area.

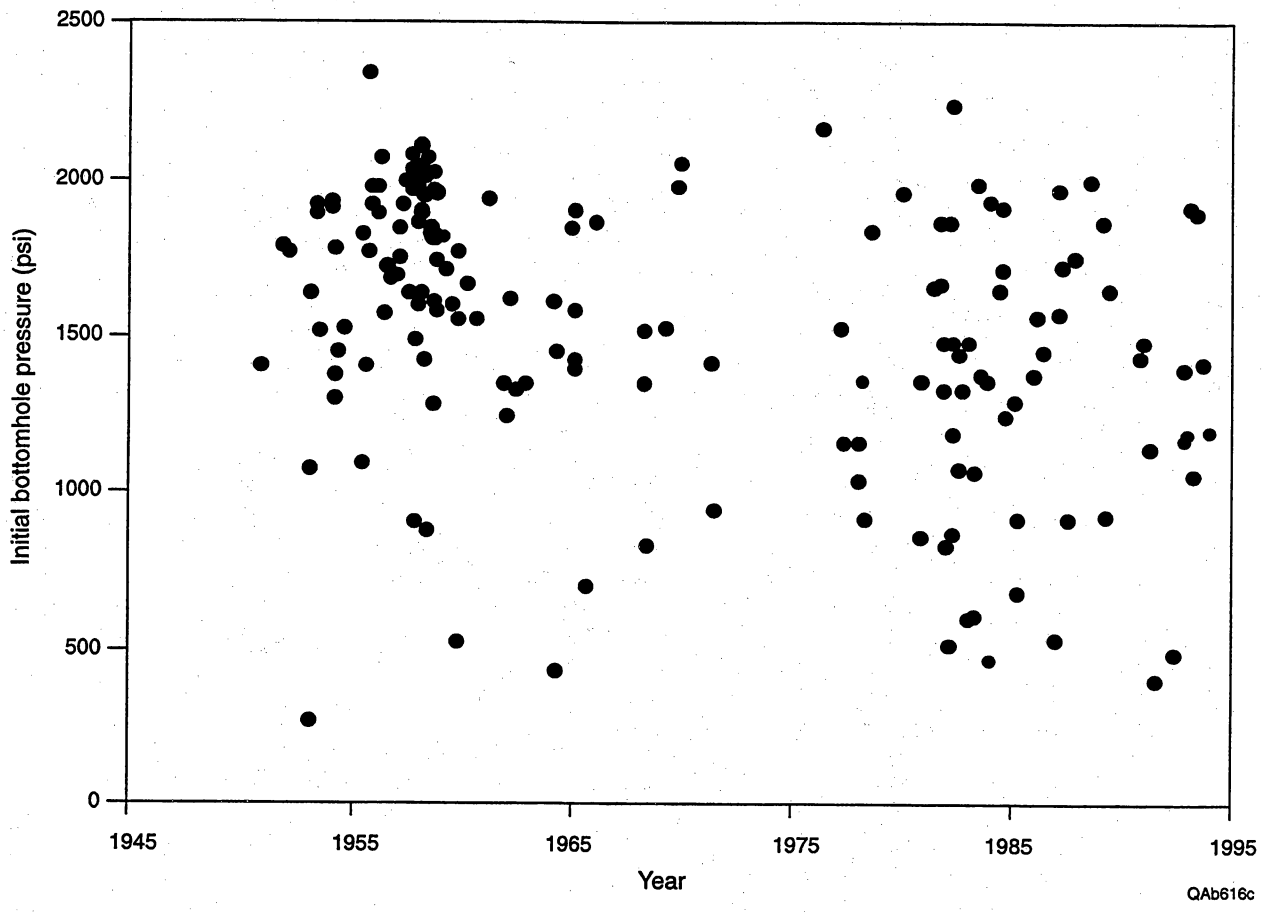

Figure B4. Best estimates of original pressure available from wells in the Boonsville project area. A number of new wells still encounter pressures near the original pressures measured 40 yr ago.

also encounter partially or significantly depleted areas in these reservoirs. Still, these higher pressures indicate that isolated, untapped reservoir compartments and poorly drained areas of the Bend Conglomerate reservoirs can still be found today.

This behavior is encountered widely throughout the Bend section. Figures B5 and B6 show similar plots generated for the Upper Caddo and the Jasper Creek sequences. In both cases, the initial pressures measured in several of the more recent completions in these intervals are comparable to original pressures reported in wells drilled 40 yr ago. Again, these data indicate that within individual stratigraphic sequences, there still appear to be isolated reservoir compartments or, at a minimum, very poorly drained areas of these reservoirs.

Figure B7 presents a summary of pressures measured by interval in wells drilled since 1990. These pressures also come from a variety of sources, including RFT's run during logging, actual wells tests, and completion records. Because the RFT (see Appendix C for discussion of RFT tool) has been used routinely by operators in the project area to measure pressure in potential completion intervals, a number of pressure measurements are available throughout the section, even in intervals that were not subsequently completed. In almost every sequence, pressures have been measured at or very near the expected original reservoir pressure for that interval, indicating poorly drained or compartmented gas reserves in these intervals. Generally, a wide range of pressures are recorded in many of these sequences, and even those where higher pressures have been measured also show evidence of significant depletion in other instances—e.g., Upper Caddo, Trinity, Bridgeport, and Jasper Creek intervals.

In two intervals, the Lower Caddo and the Vineyard, no pressures have been measured in recent wells in the project area that could be considered initial reservoir pressure. The initial pressure in the Vineyard is on the order of 2,200 psi, but the highest pressure measured in any well drilled since 1990 in the project area is about 1,500 psi. Most are significantly lower, in the range of 500 psi or less. The same is true in the

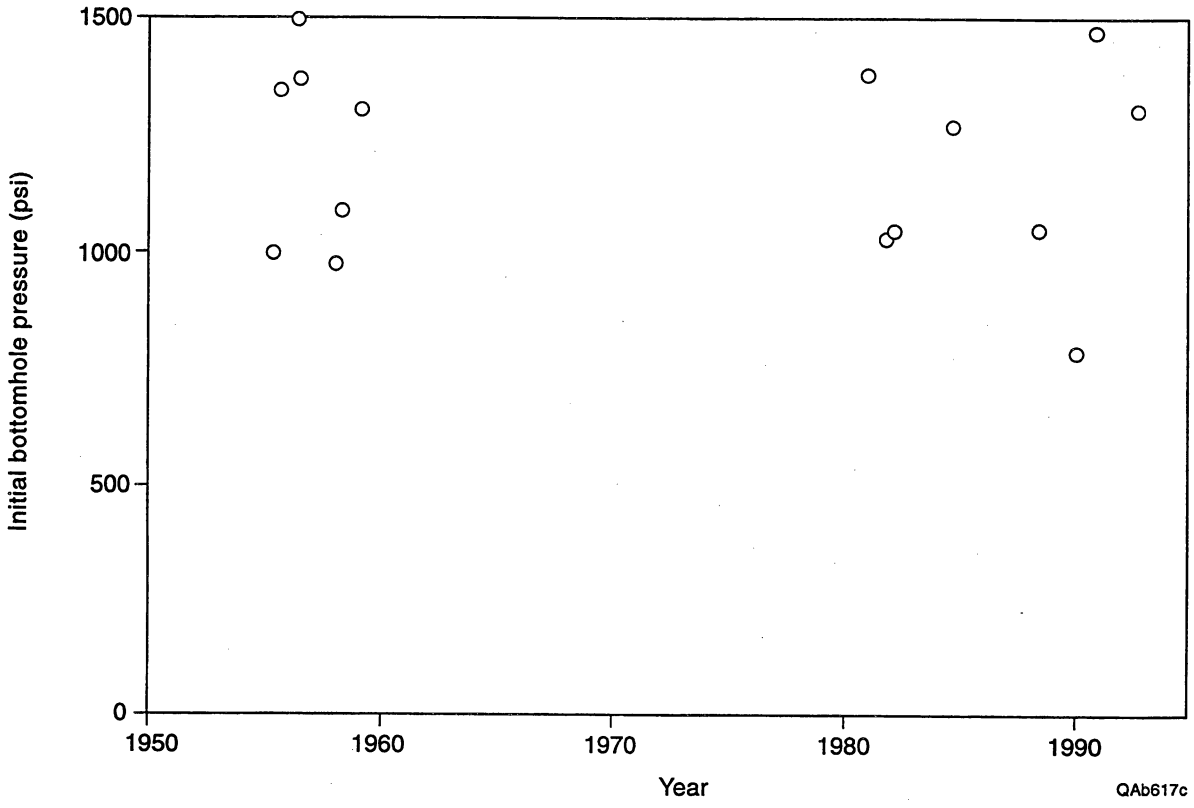

Figure B5. Comparison of initial pressures measured in more recent Upper Caddo completions to original pressures reported in the Upper Caddo sequence in the 1950's.

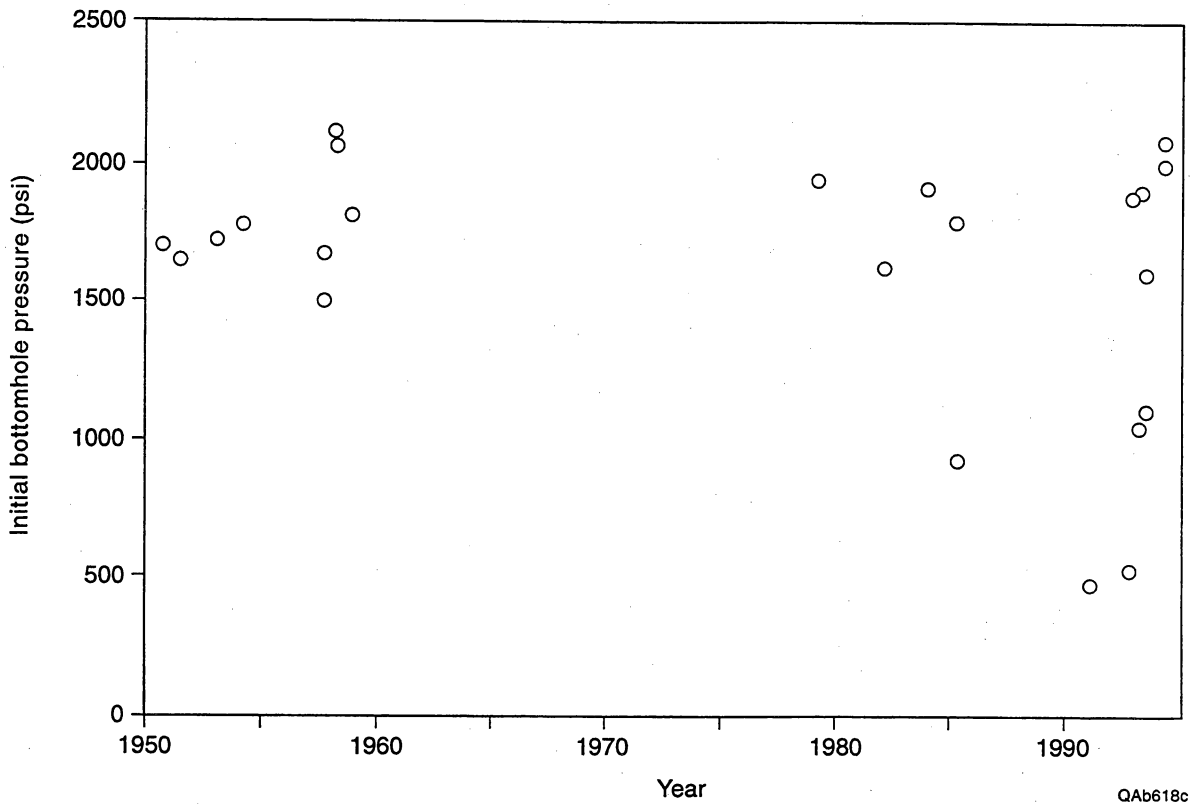

Figure B6. Comparison of initial pressures measured in more recent Jasper Creek completions to original pressures reported in the Jasper Creek sequence in the 1950's.

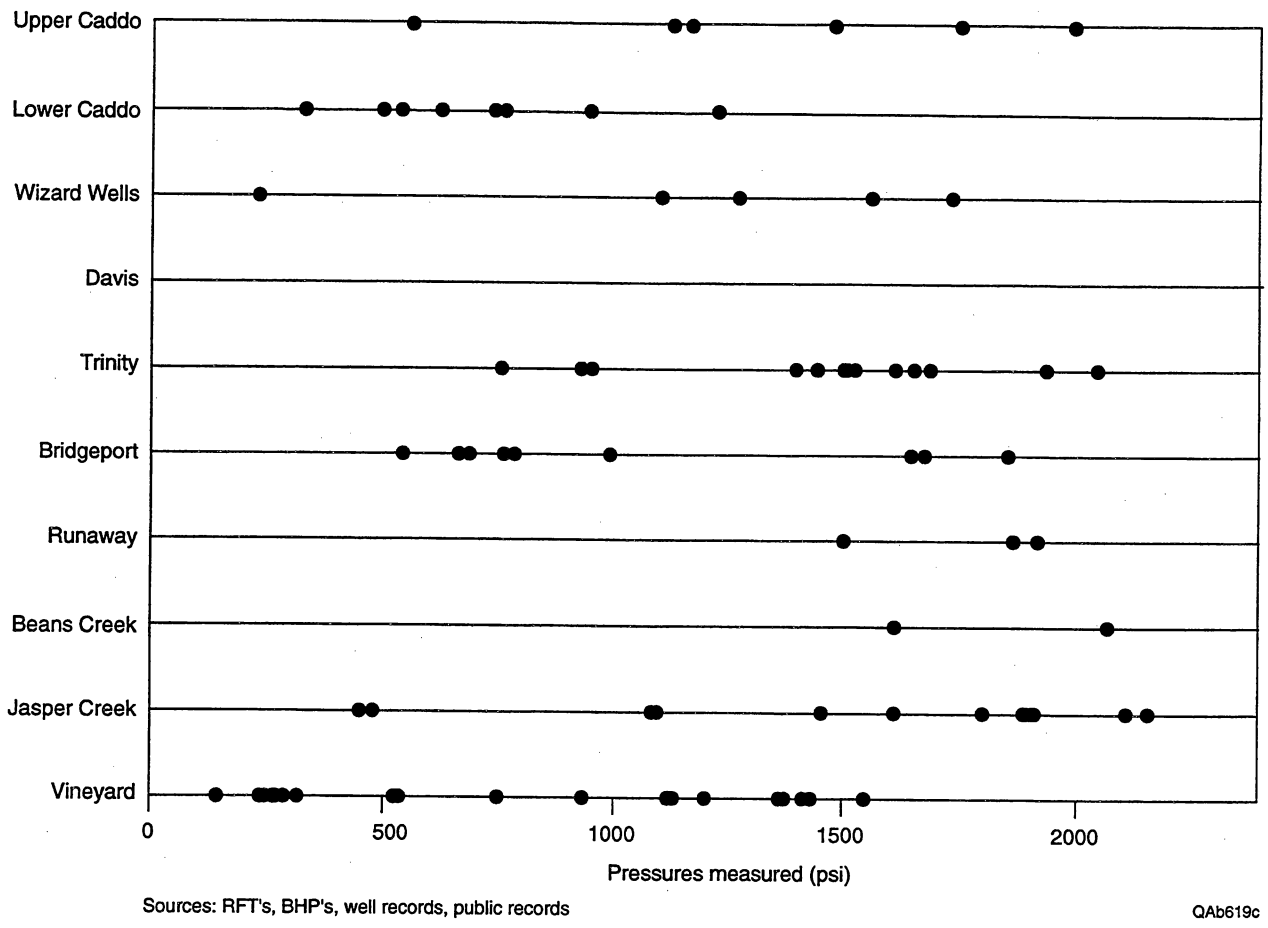

Figure B7. Pressures measured in various stratigraphic sequences in wells drilled since 1990 in the Boonsville project area. With the exception of the Lower Caddo and Vineyard sequences, original or near-original pressures have been found in almost all sequences.

Lower Caddo, where most pressures measured in recent wells have been far less than the estimated original pressure of about 1,600 to 1,700 psi. This behavior in the Vineyard and the Lower Caddo is not surprising. As mentioned earlier, these intervals have been the best producing intervals in the area historically, and, as described in the geologic analysis (see Appendix A), these sequences were deposited in a low accommodation space environment suggesting less likelihood of compartmentalization, especially at spacings of less than 160 acres.

Although the pressure data indicate that isolated or poorly drained gas reserves are still encountered in the Bend Conglomerate, a look at the production statistics in the project area indicates that these pressures are associated with decreasing gas volumes. Figure B8 plots the estimated ultimate gas recovery from project area wells drilled between the 1950's and 1970's as a function of the probability of occurrence; this was the first phase of drilling when wells could only be drilled on 320-acre units. There has been a wide range of gas recoveries from these wells, from as little as less than 10 to 20 MMscf to as much as 8 Bscf. The median ultimate gas recovery from wells drilled in this time period (the value occurring at a 50-percent probability) is 1.55 Bscf.

When the spacing requirements were reduced in 1980, permitting wells on optional 160-acre spacing, a number of new wells were drilled. Figure B9 presents the estimated gas recovery from these wells. These values again range from less than 50 MMscf to between 2 and 3 Bscf. The median gas recovery from wells drilled in this time period is expected to be about 600 MMscf. This decrease in expected ultimate recovery is largely influenced by the fact that more wells were completed in the Vineyard early in the development of this area. As mentioned previously, by the 1980's drilling phase, the Vineyard was already widely produced and substantially depleted in many areas. Because of this, it was completed less frequently, and when it was, it was less of a contributor to overall well performance. Thus, the gas recoveries shown in this figure are more

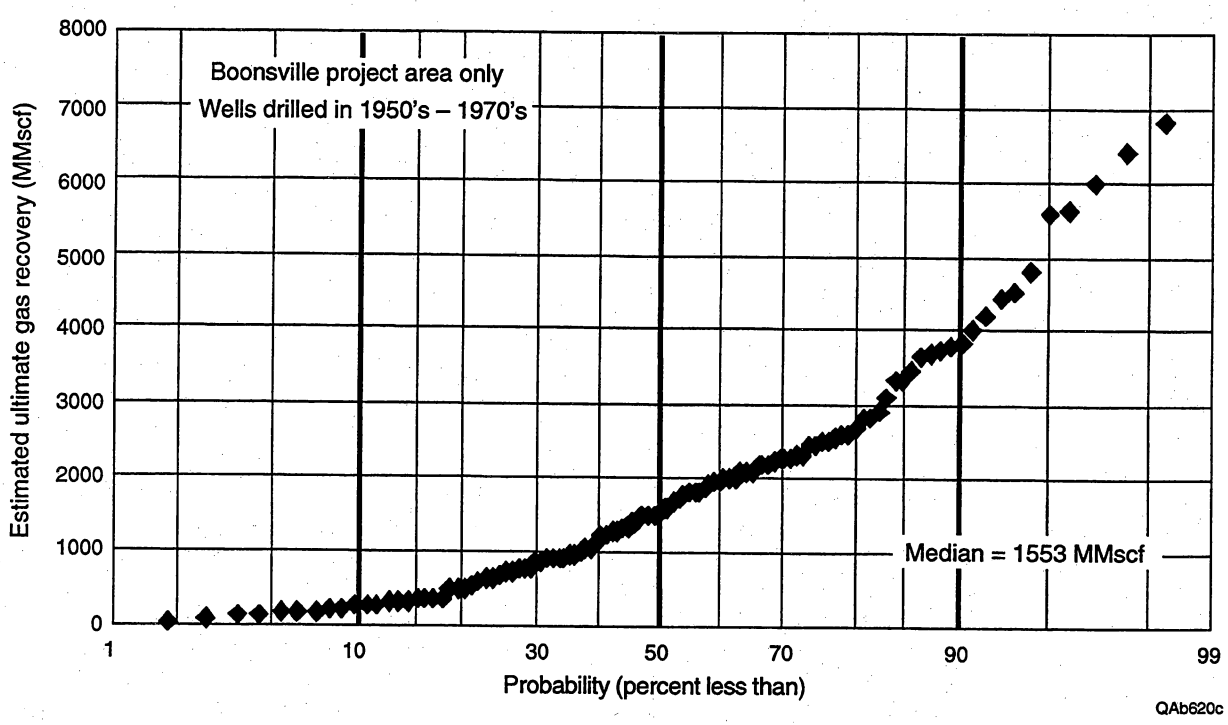

Figure B8. Distribution of estimated ultimate gas recoveries from wells in the project area drilled in the late 1950's through 1970's. The median gas recovery is about 1.5 Bscf.

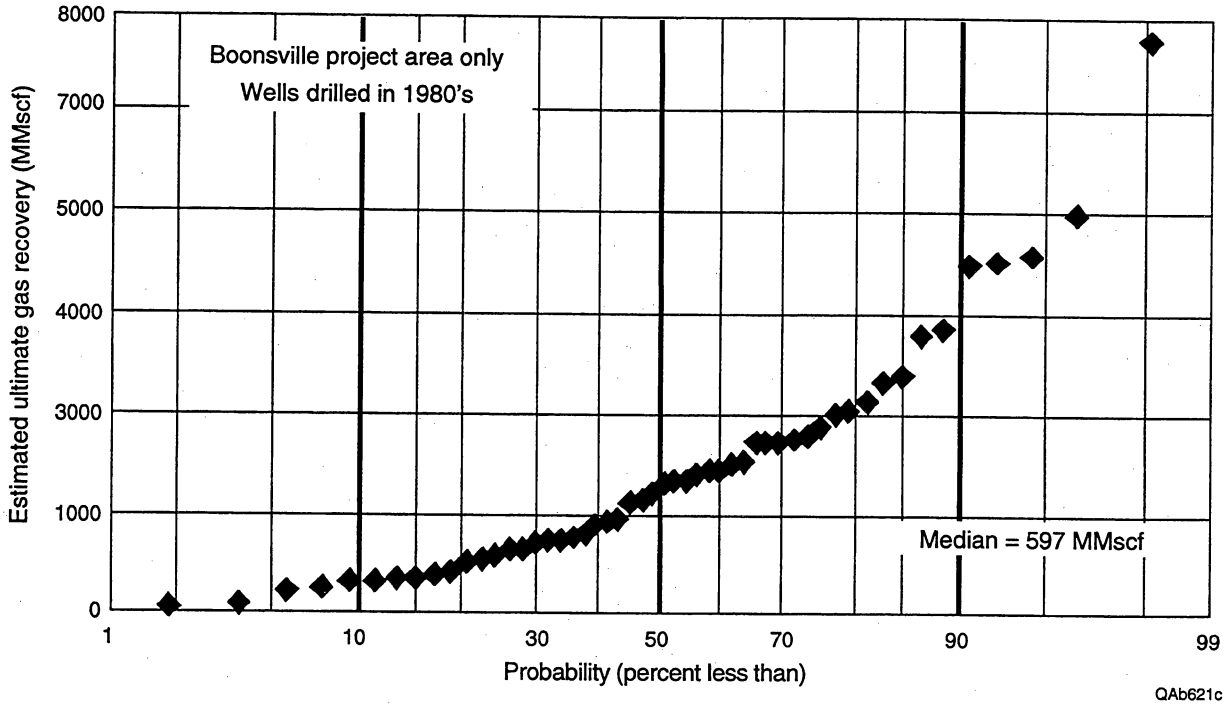

Figure B9. Distribution of estimated ultimate gas recoveries for wells in the project area drilled in the 1980's. The median gas recovery is about 600 MMscf.

reflective of the contributions of uphole sequences, including especially the Trinity, Bridgeport, Runaway, and Jasper Creek.

Figure B10 shows estimated gas recoveries from wells drilled since 1990 in the immediate project area. Current field rules permit wells to be drilled on optional 80-acre units, but some wells shown in this figure have somewhat larger well spacings. Not many wells have been drilled in the project area since 1990, but those that have been drilled have estimated ultimate gas recoveries ranging from less than 100 MMscf to about 700 MMscf. Unlike the previous two figures, these estimated gas recoveries include only the zones currently producing; several still have behind pipe completion opportunities that may contribute additional gas to the overall well recovery. In Figures B8 and B9, there are almost no remaining behind-pipe opportunities in those wells; essentially all potential reservoirs have been completed and tested.

Based on currently producing zones, the median recovery from these recently drilled wells is only about 250 MMscf from the Bend Conglomerate. Again, however, this value is low, and the dashed line in Figure B10 is intended to suggest that behind-pipe opportunities will raise this distribution somewhat, although it is unlikely to go much above about 400 MMscf. Gas reserves of 300 to 400 MMscf are at the lower end of what operators in this field need for wells to be attractive investments. The goal of this project is to improve the overall distribution of ultimate gas recoveries through strategic targeting of new infill wells. Through strategic targeting, it is anticipated that poorer wells can be eliminated and that better wells will be drilled more routinely; this, in turn, will shift the distribution of gas recoveries to the right and up, into a range of gas recovery that is economical and that pays for the technology necessary to achieve it.

All of the wells represented in Figure B10 were completed initially in one or more reservoirs with a measured pressure at or near the expected original pressure. In several instances, these wells were tested at 1 to 2 MMscf/d, but both reservoir pressure and gas flow rates decline rapidly with time (see case histories on the I. G. Yates 33 area and the

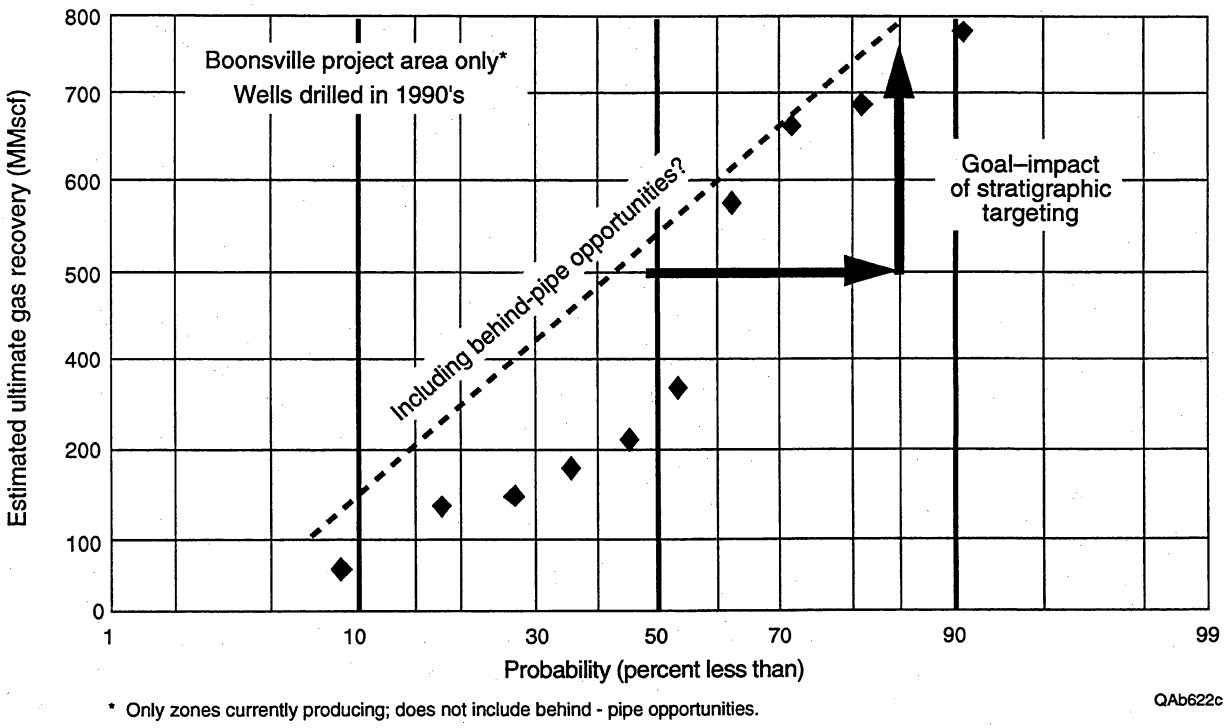

Figure B10. Distribution of estimated ultimate gas recoveries, not including behind-pipe opportunities, for wells in the project area drilled in the 1990's. The goal of the secondary gas recovery research is to increase gas recovery through strategic targeting of new wells.

B Yates 18D in the main body of the report). Ultimately the gas reserves associated with these higher pressures in a particular stratigraphic sequence were quite small—less than 100 MMscf in several cases. On the other hand, two recent wells drilled and completed in the Upper Caddo and also included in Figure B10, the Sealy C-2 and Sealy B-3 wells (see case history in the main body of the report), are projected to have ultimate gas recoveries of 500 to 600 MMscf from the Upper Caddo alone.

This is the reality faced by operators in this area as wells are drilled on closer spacings. Sometimes these higher (original or near original) pressures are associated with significant gas volumes, resulting in economically successful wells. At other times, however, these higher pressures occur in reservoirs of very limited size. These results point to the need for a better understanding of reservoir architecture and a more strategic approach to targeting new wells.

Hydrocarbon Distribution and Volumetric Estimates

Pressure data establish the existence of compartmented or poorly drained gas reserves throughout much of the Bend Conglomerate interval. The next step in the engineering analysis is to look at how the hydrocarbons are distributed within the Bend interval and to establish the expected size of the infill well reserves. To do this, a detailed petrophysical evaluation of the well log data was conducted as explained in Appendix C. Using the quantitative results of this log analysis, useful information was developed about the distribution of hydrocarbons and reservoir size within the Bend sequences.

Figure B11 illustrates the distribution of net pay and net hydrocarbon feet among the Bend intervals. As used in this analysis, net pay is defined as the hydrocarbon-bearing portion of the reservoir having a shale volume of less than 50 percent, a porosity of greater than 4 percent, and a water saturation of less than 60 percent. Net hydrocarbon feet is defined as the product of net pay, porosity, and hydrocarbon saturation (one minus the water saturation).

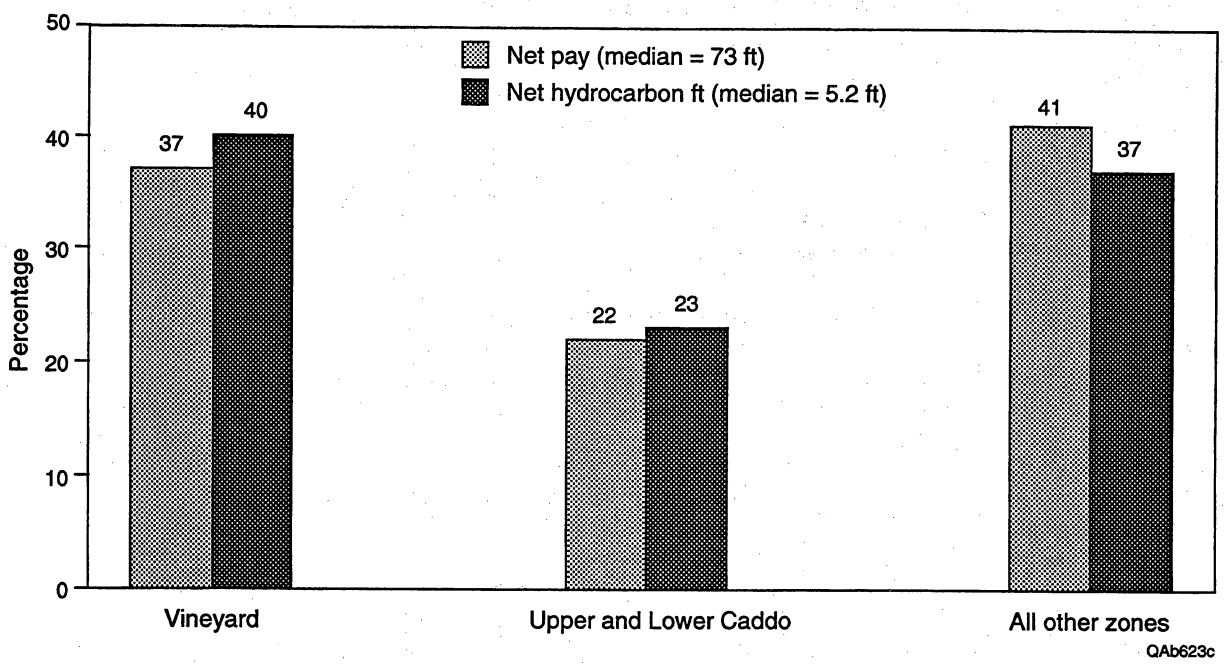

Figure B11. Distribution of net pay and net hydrocarbons among the Bend intervals in the project area.

As the figure shows (and as has been alluded to previously), the Vineyard sequence alone contains about 40 percent of the total net hydrocarbons found between the top of the Caddo and the base of the Vineyard in the project area. The combined Upper and Lower Caddo zones contribute another 20 percent to the total. All other intervals combined, from the Wizard Wells through the Lower Jasper Creek, make up the remaining 40 percent of the net pay and net hydrocarbon feet. The median net pay for wells in the project area is 73 ft; the median value of net hydrocarbon is 5.2 ft.

The pressure data in Figure B7 demonstrated that most high pressures measured that are indicative of original reservoir pressure have been found in the intervals between the Lower Caddo and the Vineyard. Thus, although there is recent evidence of compartmented gas reserves in the Upper Caddo, it appears likely that most isolated or poorly drained gas in the project area will be found in the sequences between the Lower Caddo and the Vineyard. Because of this, most of the subsequent analyses considered only those zones between the Lower Caddo and the Vineyard.

That said, however, the Vineyard may still be a viable completion target in certain infill wells drilled within the project area, even if it is substantially depleted. Because of the Vineyard's overall reservoir quality—large net pays (20 to 30 ft), low water saturations (20 to 25 percent), and good permeabilities (0.5 to 5 md), this zone may still produce as much as 100 to 300 MMscf, depending on its effective drainage area, even if the average reservoir pressure is as low as 500 psi. Often, because many earlier Vineyard completions have been abandoned, newer wells drilled to the Vineyard may drain substantial areas. Clearly these reserves are neither isolated nor compartmented, but they should not be overlooked in planning the completion strategy for future infill wells. In some cases, these potential reserves may represent as much as half of the gas recovery needed to make an infill well in this area successful economically. One word of caution is appropriate, however; these low pressure intervals in the Bend Conglomerate are easily

damaged by fluid contact, so operators must be careful to minimize exposure to fluids when attempting completions in these zones (Darden, 1994).

Figures B12 and B13 show the distribution of total net pay and total net hydrocarbon feet in the intervals between the Lower Caddo and the Vineyard. Total net pay in these intervals, when present, ranges from as little as 1 ft to more than 110 ft, but the median value is 30 ft. This means that, historically, half the wells drilled in the project area have found less than a total of 30 ft of net pay and half the wells have found greater than 30 ft of net pay between the Lower Caddo and Vineyard sequences. The median value for net hydrocarbon is 1.9 ft.

As Figures B12 and B13 illustrate, significantly less net pay and net hydrocarbon are found between the Lower Caddo and the Vineyard on the west side of the project area as compared with the east side. As demonstrated in the geologic evaluation of the project area (see Appendix A), the west portion of the project area is structurally higher than the east side. Because of this, overall less sand was deposited on the west side of the project area (see Figure A14 in Appendix A).

As a result, the west side of this area has a median total net pay and net hydrocarbon between the Lower Caddo and the Vineyard of only 21 and 1.3 ft, respectively, compared with values of 40 and 2.2 ft to the east. This superior distribution of net pay and net hydrocarbon to the east may suggest better infill opportunities in that part of the project area. Conversely, the lack of net pay to the west may suggest conditions more favorable to additional reservoir isolation.

Operators in and near the project area have indicated that gas reserves of 300 to 500 MMscf are needed for new Bend wells to be economically viable; the exact value depends on the operator's drilling and completion practices. Wells drilled through the Bend cost about $200,000 to $250,000 to drill and complete on average, but this can vary considerably among operators. For purposes of this evaluation, an ultimate recovery per well of 400 MMscf has been used as an economic infill well target.

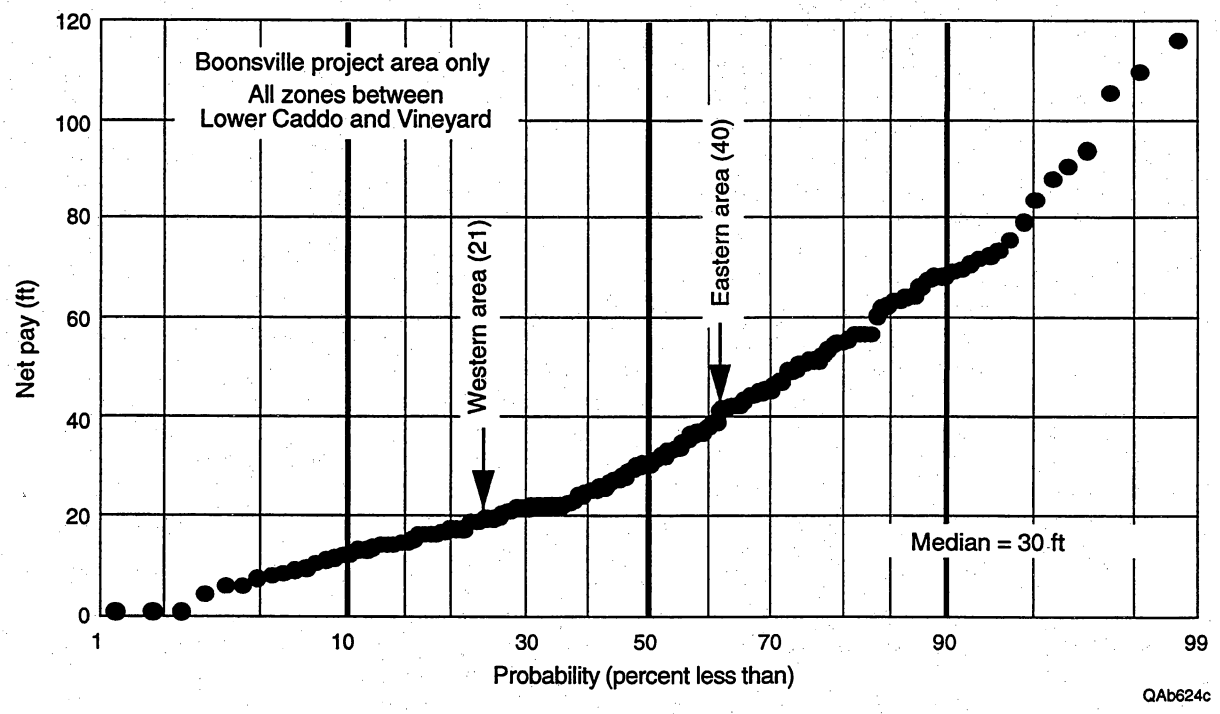

Figure B12. Distribution of net pay thickness in all zones between the Lower Caddo and the Vineyard; the median net pay is 30 ft.

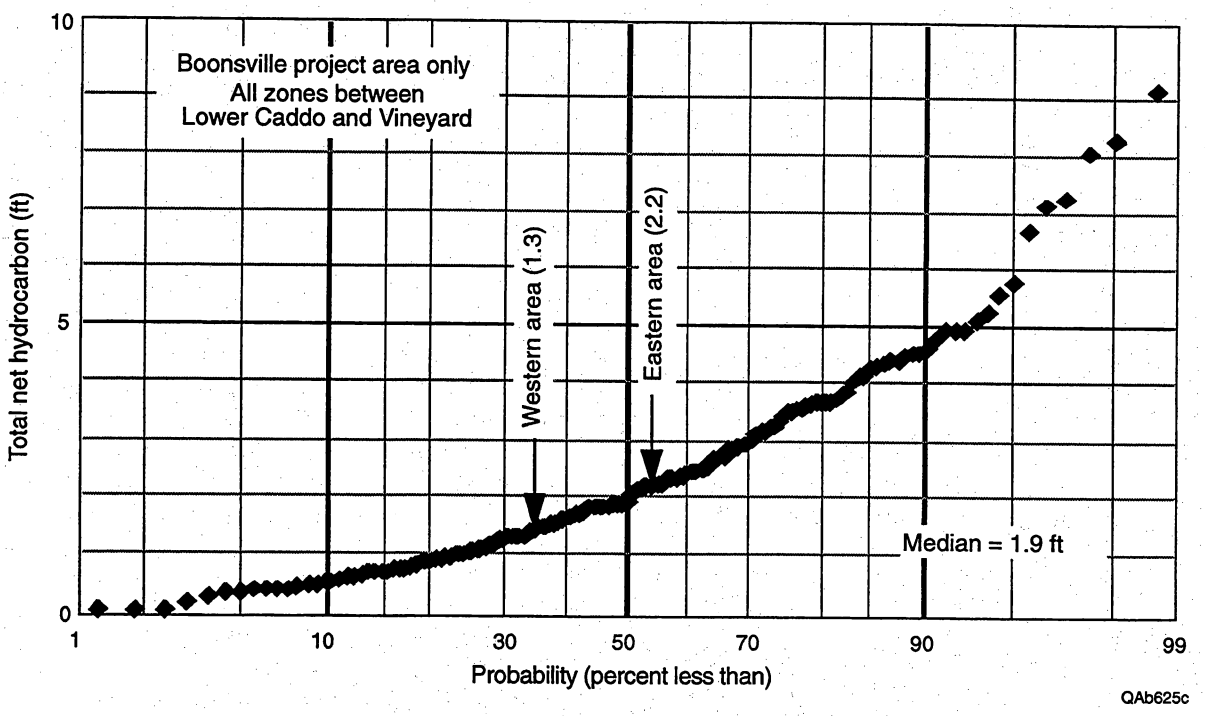

Figure B13. Distribution of net hydrocarbon thickness in all zones between the Lower Caddo and the Vineyard; the median net hydrocarbon thickness is 1.9 ft.

Figures B14 and B15 are nomographs prepared for the project area showing total hydrocarbon feet required as a function of reservoir pressure and drainage area to yield recoverable gas reserves of 400 MMscf. For drainage areas of 60 to 80 acres and an average reservoir pressure of 1,500 psi, between 1.5 and 2 ft of net hydrocarbon or between 20 and 25 ft of net pay are required to have recoverable gas reserves of about 400 MMscf. As both pressure and drainage area increase, these net pay and net hydrocarbon requirements are less; likewise, if average reservoir pressure and compartment size decrease, even more total net pay and net hydrocarbon feet are needed to have recoverable reserves of 400 MMscf. These values of 1,500 psi for pressure and 60- to 80-acre drainage areas appear reasonable, however, for evaluating potential infill wells to be drilled in the project area.

Figure B16 is a summary of estimated drainage areas computed by completion interval using production data from wells in the project area. As mentioned previously, many wells in this project area are commingled in multiple zones, and it is difficult to allocate production back to specific intervals. This figure, however, is based solely on those completions where the actual production could be attributed to a particular zone with a high degree of certainty. Thus, it should be a reliable indicator of the range of drainage areas to be expected in the project area.

Most of the sequences have quite a wide range of estimated drainage areas. That should not be surprising because some really good wells (greater than 1 Bscf) can be found in almost every major sequence. What the figure shows is that for an interval such as the Trinity, drainage areas range from as small as 10 to 20 acres to in excess of 500 acres, but the median value is about 80 acres. In fact, most median values are in the 50- to 80-acre range for all zones except the Vineyard. The Vineyard has a median drainage area of about 160 acres.

It should be noted that these estimated drainage areas may be somewhat conservative. These values are based on the value of net hydrocarbon feet calculated at

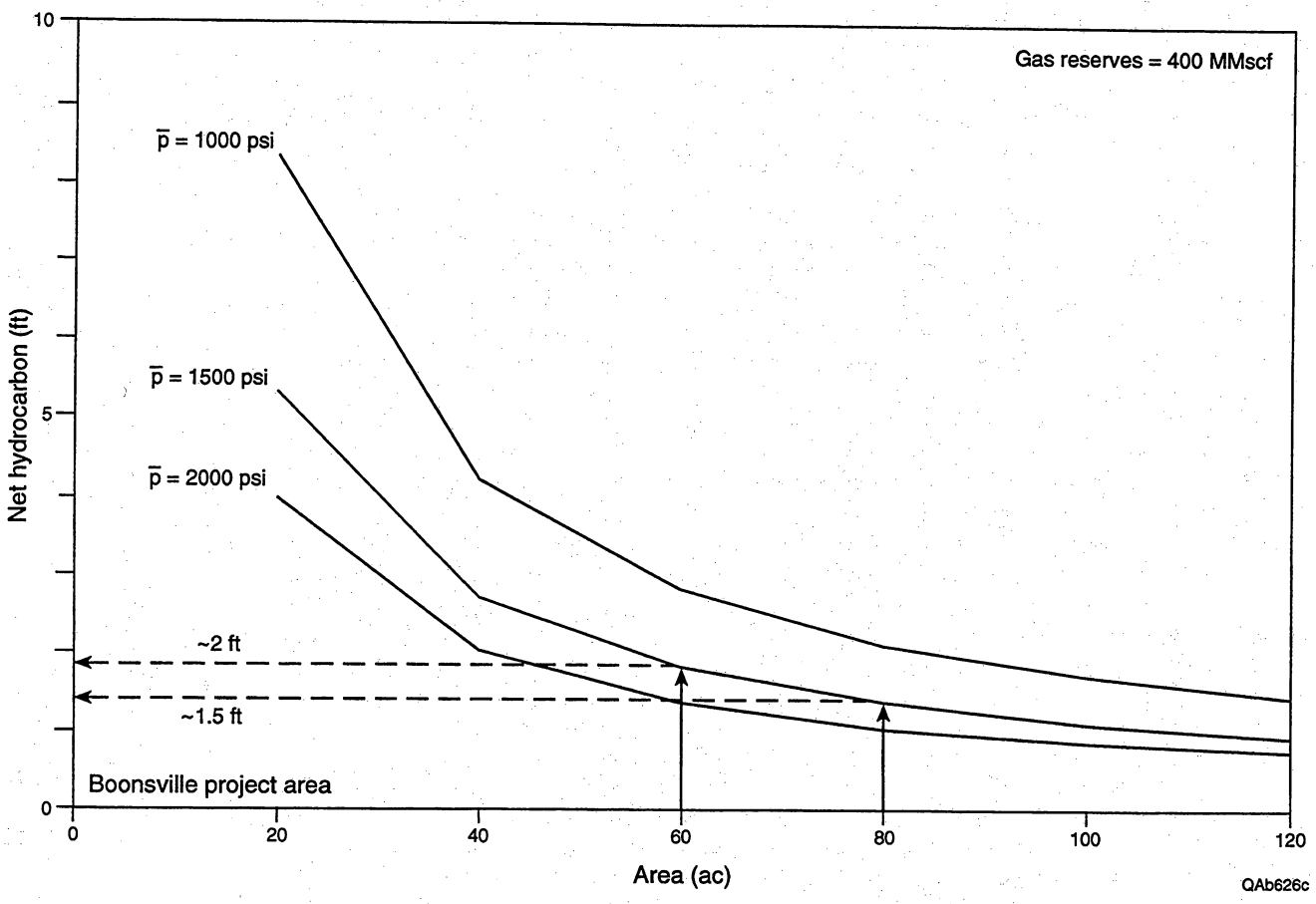

Figure B14. Nomograph for the Boonsville project area, showing the net hydrocarbon feet required as a function of pressure and drainage area to obtain recoverable gas reserves of about 400 MMscf.

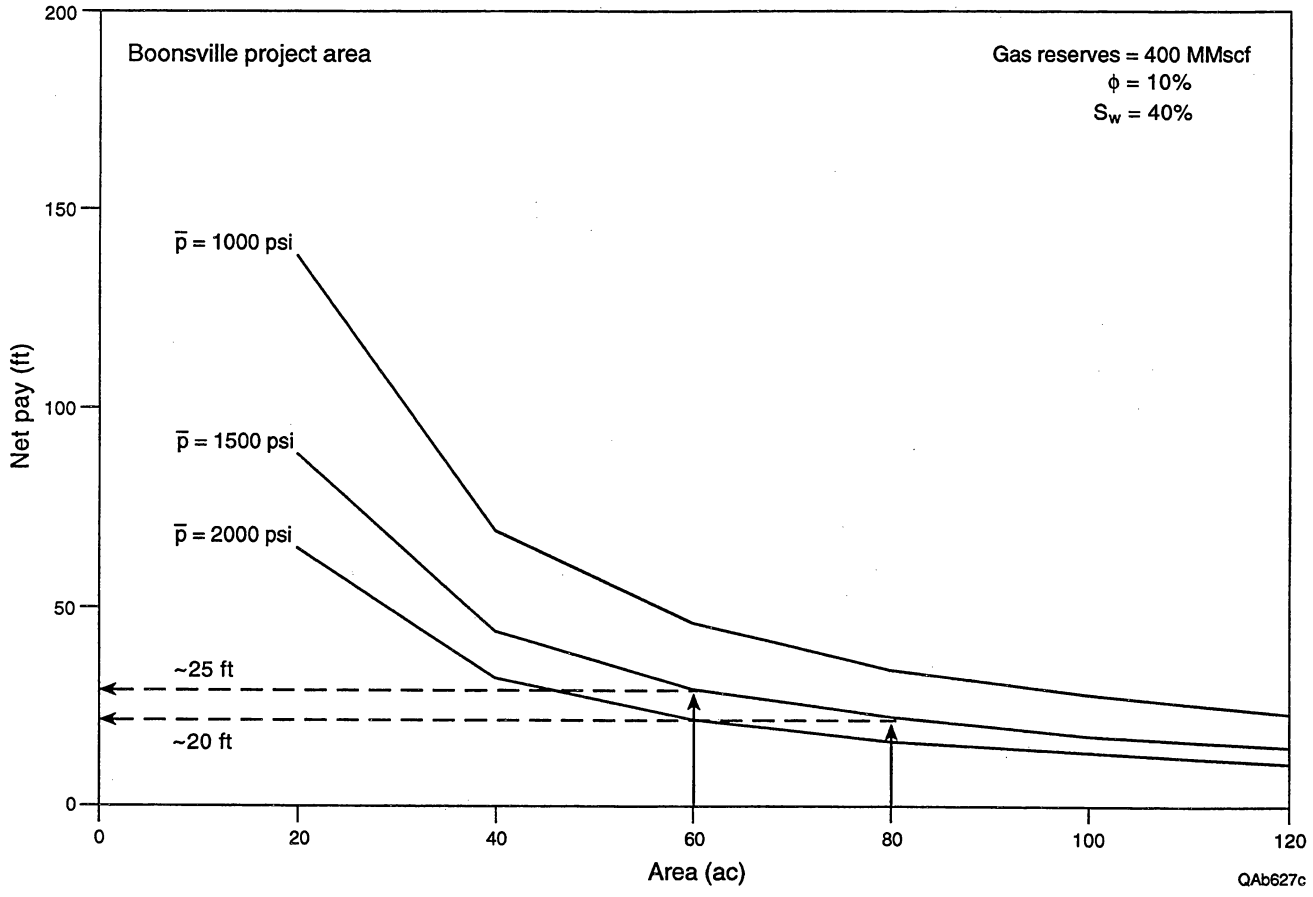

Figure B15. Nomograph for the Boonsville project area showing the net pay required as a function of pressure and drainage area to obtain recoverable gas reserves of about 400 MMscf.

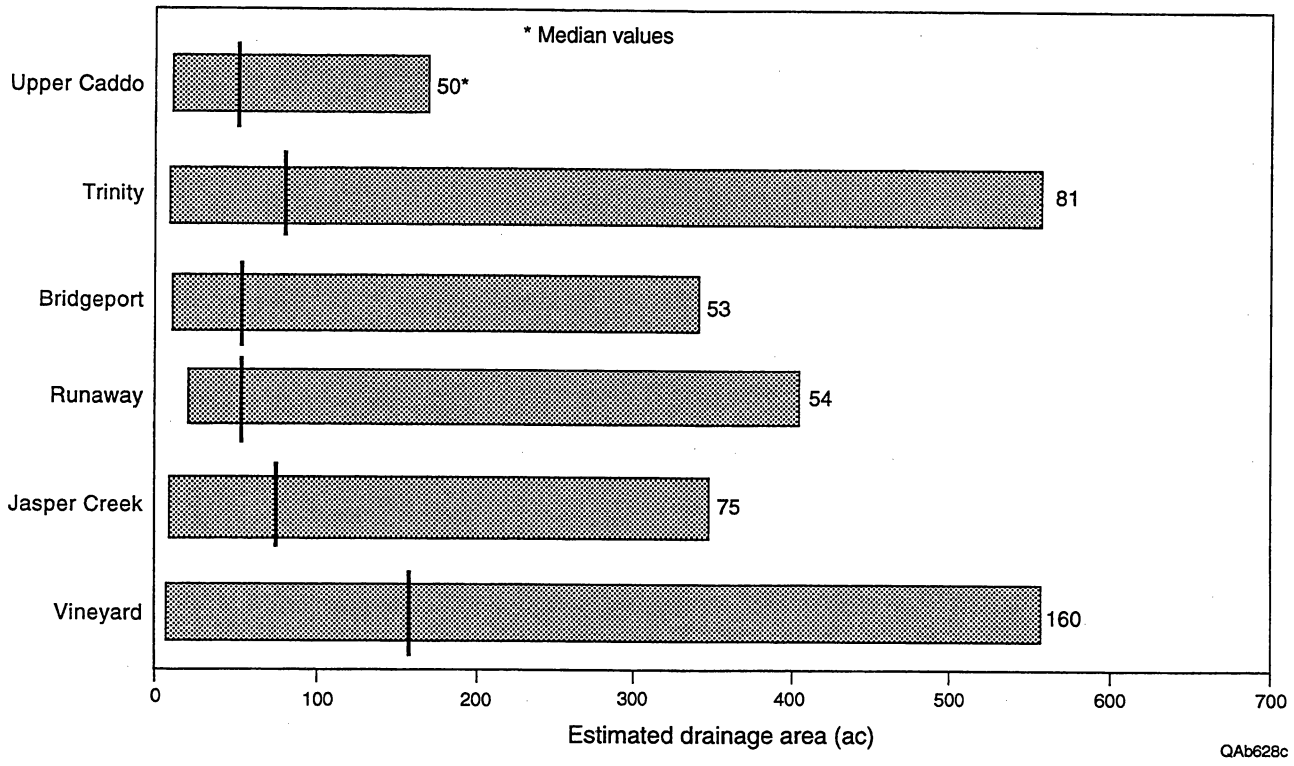

Figure B16. Estimated drainage areas computed for the major stratigraphic sequences using production data from wells in the project area.

the wellbore and assume constant reservoir properties away from the well. To the extent that reservoir quality may decrease away from the wellbore, the calculated drainage areas may be somewhat smaller than they actually are. Nevertheless, these median values and the range of results presented in Figure B16 appear quite consistent with earlier observations that we are more likely to find poorly drained or compartmented reserves in those intervals above the Vineyard as the well spacing is reduced to 80 acres. Likewise, it is not surprising that most Vineyard completions show signs of substantial depletion at spacings of 160 acres and less.

If 20 to 25 ft of net pay and 1.5 to 2 ft of net hydrocarbon are needed in the Bend intervals between the Caddo and the Vineyard for a successful infill well, where will these hydrocarbons be found? Figure B17 provides some insight. This figure plots the range of net pay and net hydrocarbon found in each major sequence throughout the project area. For an interval such as the Trinity, when present, the net pay may range from as little as 1 to about 20 ft; the net hydrocarbon ranges from 0.1 to about 2 ft. The median values are about 10 and 0.6 ft, respectively. Thus, while it is possible to find sufficient net pay and net hydrocarbon in a single completion in most of these sequences, it is far more likely that multiple, stacked completion opportunities will be needed to yield sufficient gas reserves for an economical infill well.

Figure B18 shows this even more clearly. In this figure, the values in Figure B17 were used along with an average drainage area of 80 acres to calculate typical gas reserves by interval. As the figure illustrates, an 80-acre Trinity reservoir may contain gas reserves of up to about 600 MMscf, but gas reserves of about 200 MMscf are more likely. The same is true for the other sequences as well. Thus, on average, it will take multiple, compartmented or poorly drained completion opportunities in those sequences above the Vineyard to result in a successful infill well. This observation should not discourage the use of geological or geophysical information in an effort to identify superior sand development in particular sequences. It does suggest, however, that a reasonable

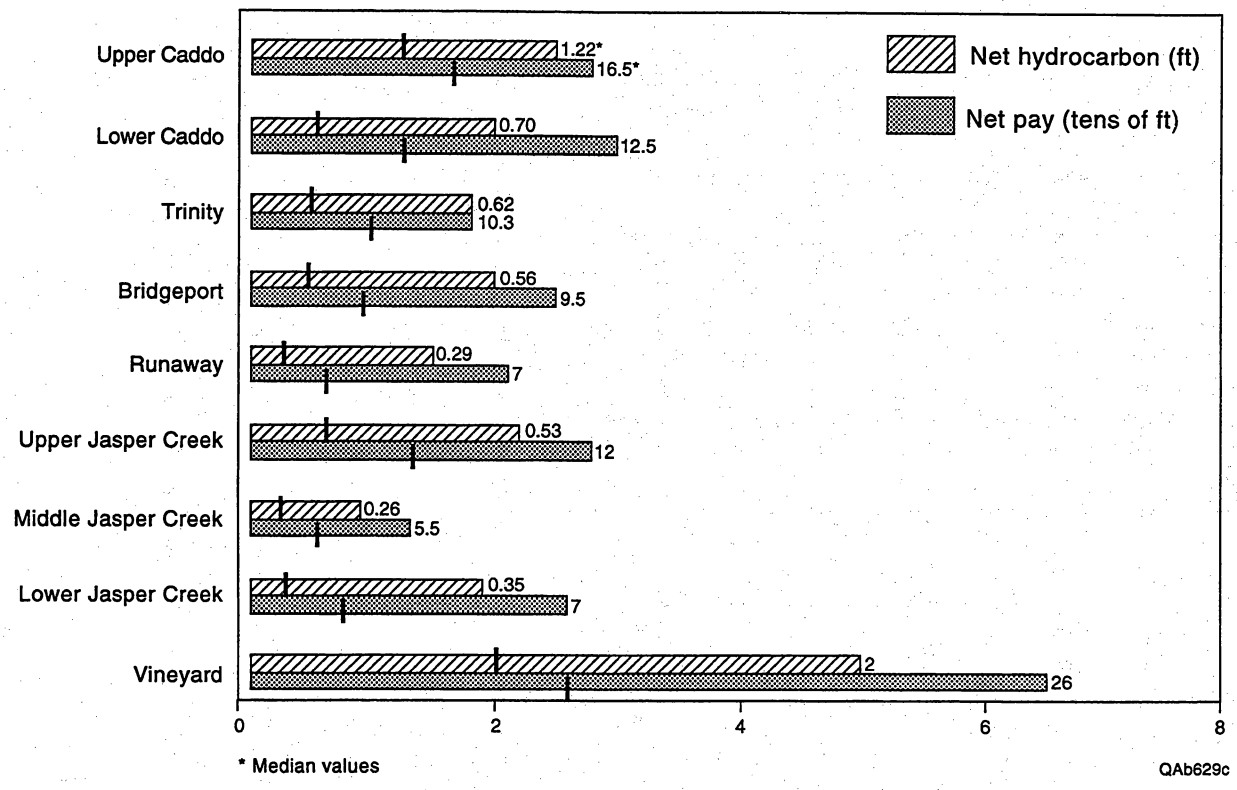

Figure B17. Range of net pay and net hydrocarbons found in each major sequence throughout the project area.

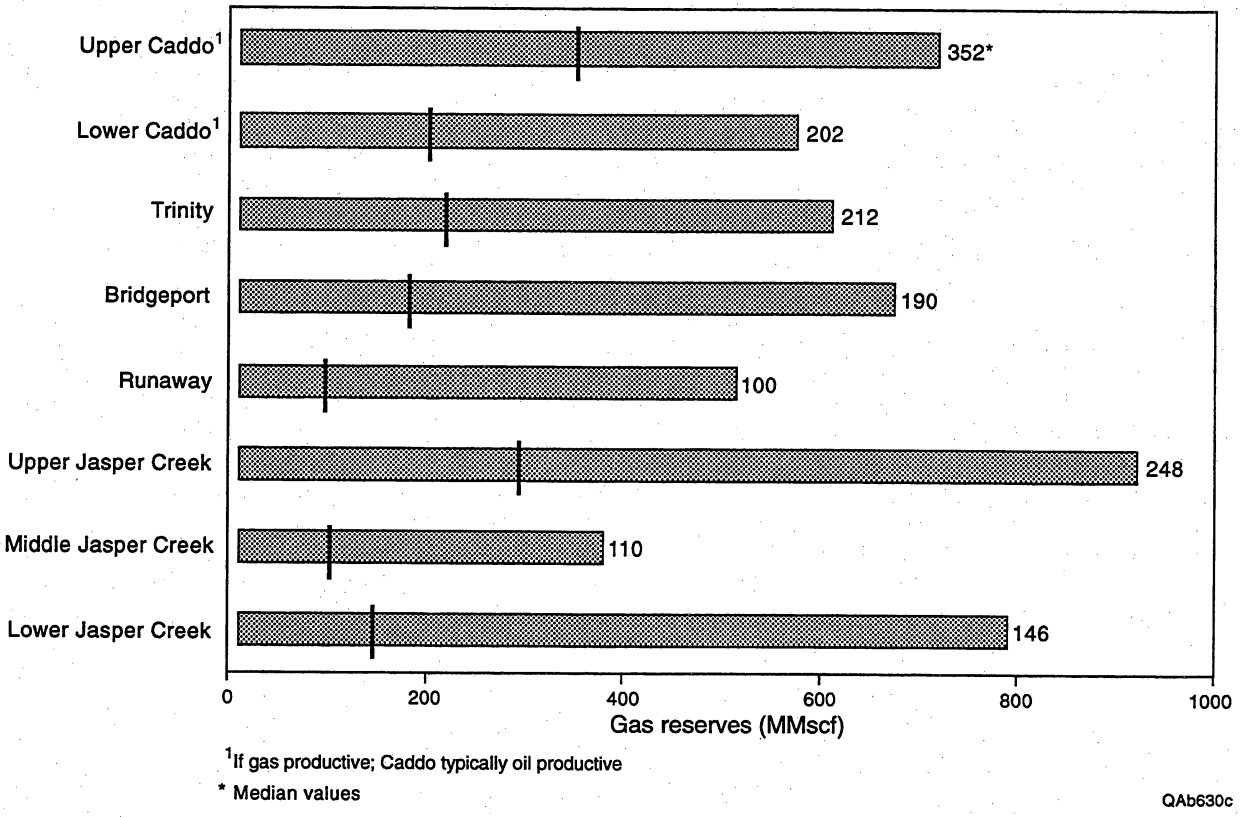

Figure B18. Range of potential gas reserves associated with an 80-acre drainage area in each major sequence throughout the project area.

approach to identifying infill locations may be to focus geological/geophysical evaluation in those areas having the highest likelihood of stacked completion opportunities.

Using that premise, Figures B19 and B20 were prepared. These figures show the distribution of net hydrocarbon and net pay across the project area. Figure B19 highlights those areas, with net hydrocarbon less than 1.5 ft, between 1.5 and 2 ft, and greater than 2 ft between the Caddo and the Vineyard. Figure B20 shows those areas with 3, less than 3, and 4 or more net pay intervals, also between the Caddo and the Vineyard. Comparing these two figures, one can see a band across the center of the project area from east to west that has the highest number of potential pay intervals and the best values of net hydrocarbon feet. This information was provided to both the geologist and the geophysicist in an effort to focus their analyses into areas that appear to have the greatest opportunity for finding multiple, higher volume completion opportunities.

Is there reason to expect that multiple, stacked reservoir compartments (or poorly drained areas) may exist at any one location in the project area? Generally speaking, there probably would not be, but in the Boonsville project area (and perhaps in other Mid-continent reservoirs as well), review of the 3-D seismic data leads to the observation that apparent, stacked, trapping geometries often exist within the 3-D data volume. This is actually one important approach that has been used to identify potential infill well locations (see chapter 6, Siting Boonsville Development Wells—Case Histories—discussion in the main body of the report). Furthermore, the influence of karst-collapse features on Bend Conglomerate stratigraphy as described in the main body of the report also suggests the opportunity and the likelihood for finding multiple, stacked, and at least partially isolated compartments with the Bend.

In fact, these multiple, stacked reservoir compartments have been observed in at least one recent infill well drilled in the project area—the Billie Yates 18D (see discussion in the main body of the report). This well location was actually sited using the 3-D seismic data in an area of both greater than 1.5 net hydrocarbon feet and greater than

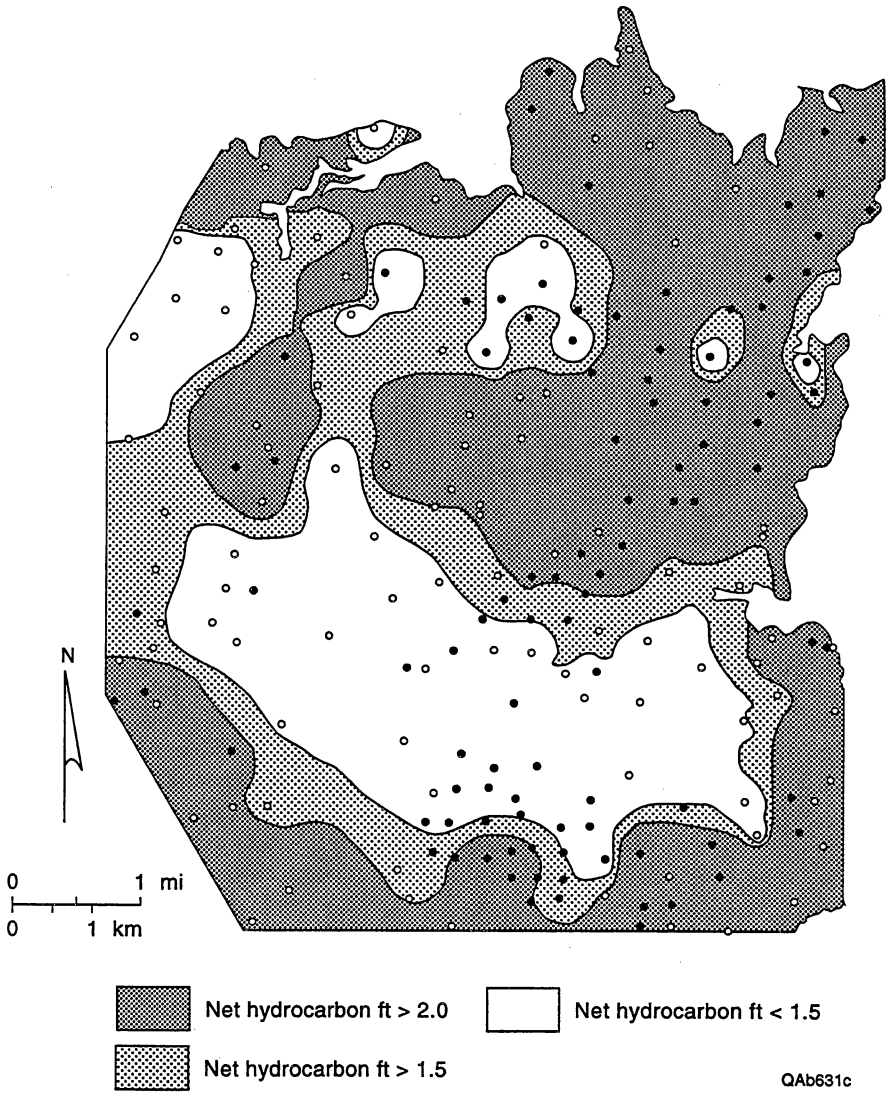

Figure B19. Distribution of net hydrocarbons between the Lower Caddo and the Vineyard mapped across the project area.

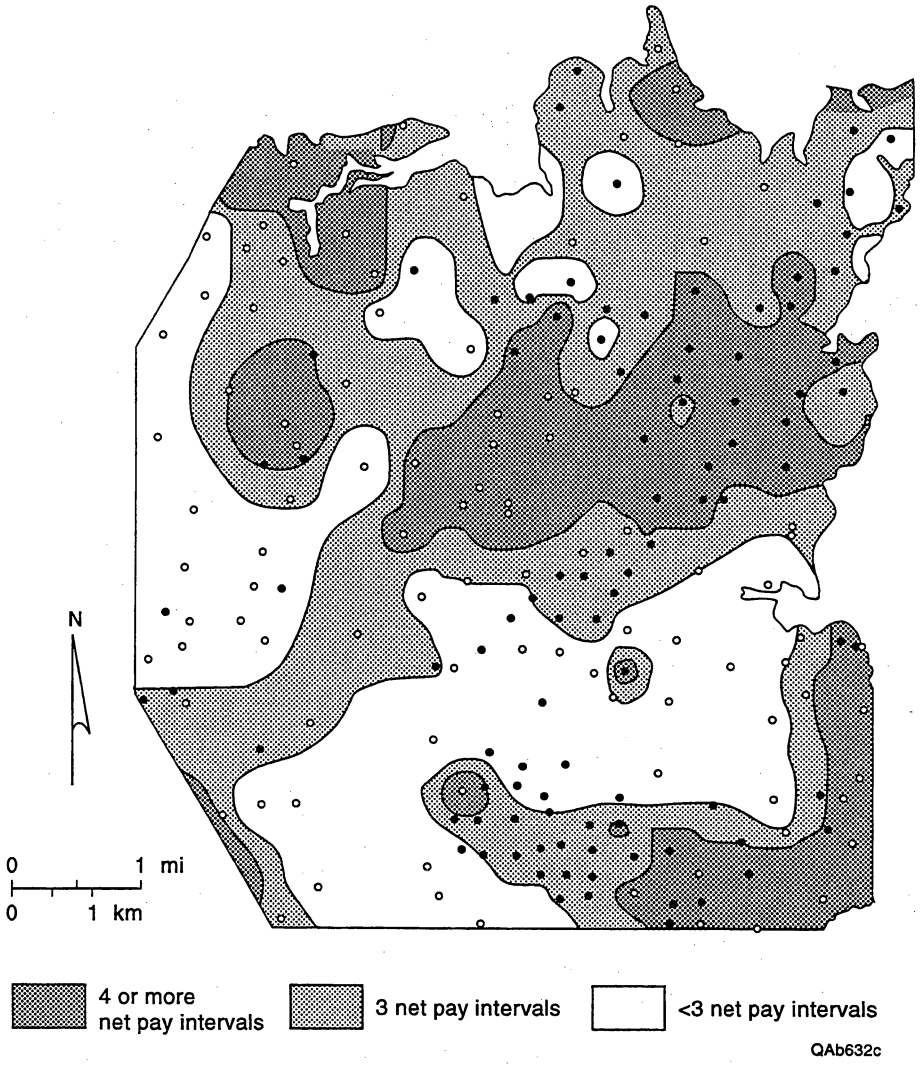

Figure B20. Distribution of the number of net pay intervals between the Lower Caddo and the Vineyard mapped across the project area.

4 net pay intervals according to Figures B19 and B20. When drilled, the well found more than 2 net hydrocarbon feet and 5 net pay intervals between the Lower Caddo and the Vineyard. Four of these intervals encountered original or near-original pressure. Unfortunately, at least one of these intervals, the Upper Runaway, was limited in size (about 8 acres) and produced only about 30 MMscf. Additional high pressure intervals recently completed in the Jasper Creek look more promising, however, having produced about 40 MMscf in just 7 weeks and flowing at 600 Mscf/d, with little decline in flowing tubing pressure.

Estimating Reservoir Characteristics with Pressure, Production, and Well Test Data

Another reservoir engineering goal in an integrated reservoir study of this type is the ability to estimate reservoir properties and reservoir size, and, where possible, to provide some insight about reservoir geometries in order to help focus and refine the geological/geophysical interpretations being developed. To do this, reservoir engineers use these primary sources of data: pressure, production, and well test data.

p/z Analysis

As demonstrated earlier in this appendix, pressure data were used extensively in this analysis to establish the existence (or lack thereof) of isolated or poorly drained reserves in the various stratigraphic sequences that make up the Bend Conglomerate. Another way that long-term pressure data may be used to infer the presence of a partially drained reservoir compartment in communication with an already producing reservoir is by using gas well material balance or "p/z" analysis. This approach has been described elsewhere (Lord and Collins, 1991, 1992), and it was used extensively in the Gulf Coast phase of the Bureau's Secondary Gas Recovery research.

Figure B21 describes how p/z analysis may be used to infer communication with an incompletely drained reservoir compartment. In a volumetric gas reservoir, a plot of average reservoir pressure divided by the z-factor (compressibility factor for real gases) vs. the cumulative gas production will be a straight line whose x-axis intercept is equal to the original gas in place in the reservoir. This behavior is illustrated by the straight line in Figure B21. It should be noted that in order for this straight-line relationship to hold true, the value of pressure used to calculate p/z must be average reservoir pressure.

Often, the only source of long-term reservoir pressure data available in many wells comes from periodic deliverability tests required by State regulatory agencies. These tests may be conducted annually or biannually, and the shut-in periods required during these tests generally range from 24 to 72 h. As Figure B21 shows, as long as these short-term shut-in pressures reflect average reservoir pressure at various times, they can be used to construct a reliable p/z plot. In gas reservoirs, a reservoir permeability of greater than 5 to 10 md is typically required for 24-h shut-in pressures to build up sufficiently to represent average reservoir pressure. This was true of many of the high productivity Gulf Coast sands investigated in the Bureau's earlier research (Levey and others, 1992, 1993).

Sometimes, as shown by the dashed line in Figure B21, the p/z vs. cumulative gas plot may begin to deviate from the straight line and flatten with time. Such behavior may suggest communication between the producing reservoir and an adjacent, supporting reservoir volume or compartment. Flow between these two sands may be restricted by a permeability contrast between the two; thus, it takes some period of depletion in the primary reservoir compartment before the response of the secondary reservoir compartment is observed. As the figure shows, as gas from the secondary compartment migrates into the primary compartment, it acts to maintain the average reservoir pressure at a level higher than would be anticipated, causing the flattening in the p/z curve. In some instances, using these data and the G-WIZ software developed as part of the Gulf Coast research (Lord and Collins, 1991, 1992), quantitative estimates of both primary and

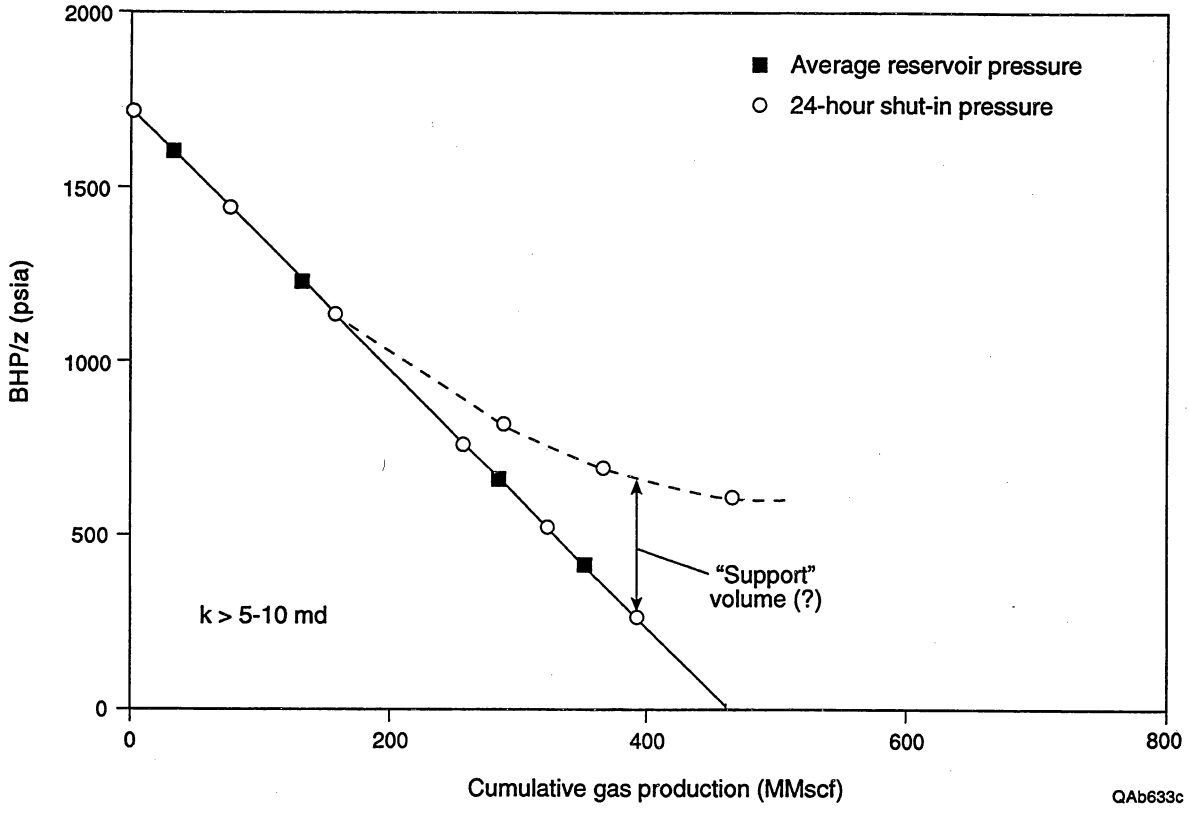

Figure B21. Flattening of the p/z curve with time may suggest communication with an incompletely drained reservoir compartment in high-permeability gas reservoirs (permeability greater than 5 to 10 md). Water drive, production from multiple layers, compaction drive, and even operational changes may also cause this behavior.

secondary reservoir volumes and the degree of communication between the two can be determined.

Although this approach has been used with some success to identify incompletely drained compartments in the Gulf Coast, an engineer must still be cautious when using it. First, as stated previously, it works well only in higher gas permeability reservoirs (5 to 10 md or greater), where the short-term pressures typically used in the p/z plots accurately reflect average reservoir pressure. In addition, the flattening of the p/z curve may be caused by factors other than communication with a secondary reservoir compartment, including water drive, compaction drive, or multiple layers of different permeabilities being produced simultaneously. Even operational changes may result in this type of behavior. Therefore, the inference of a secondary reservoir volume based on a flattening in the p/z curve should also be based on supporting geological and geophysical interpretations.

The p/z curves from wells in the Boonsville project area were not found to be useful for inferring incompletely drained reservoir compartments. As discussed in the Overview section of this report, permeabilities in the Bend Conglomerate reservoirs tended to range between 0.1 and 5 md; thus, the 24-h shut-in pressures typically available for constructing the p/z plots did not represent average reservoir pressure. This is illustrated in Figure B22, for a reservoir with a permeability of 0.5 md. As the figure shows, although the 24-h shut-in pressures do not reflect average reservoir pressure, they do approach the average pressure with time in tighter reservoirs. This behavior, in itself, causes the p/z plot to appear to flatten with time, but it reflects nothing other than the fact that the short-term pressures used to construct the plot do not represent average reservoir pressure.

In addition to the behavior illustrated in Figure B22, many of the wells in the project area have been completed and produced from multiple zones simultaneously. Typically these zones have different pressures, permeabilities, and drainage areas. These variations in interval productivity can also result in a flattening of the p/z curve as the more

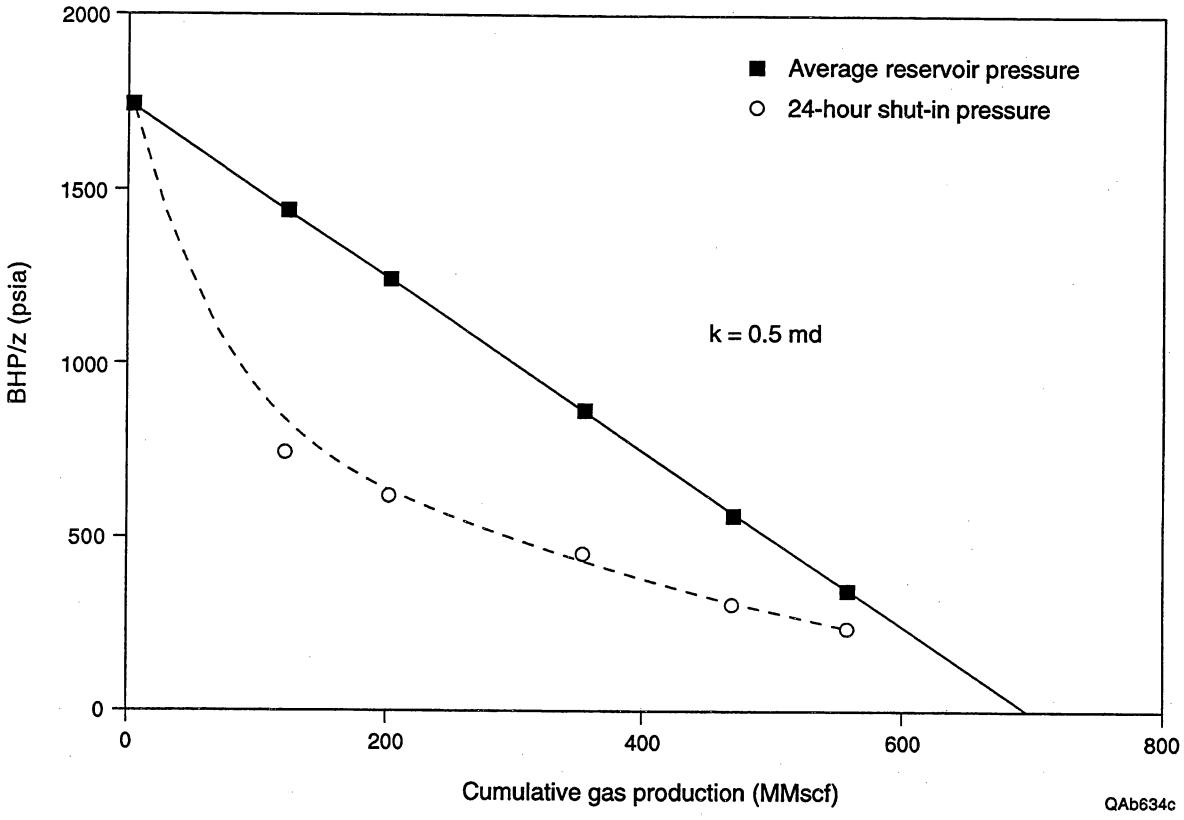

Figure B22. p/z curves may flatten in lower permeability reservoirs but primarily because 24-hr shut-in pressures do not reflect average reservoir pressure. This is true of the Bend Conglomerate reservoirs, where typical permeabilities are 0.1 to 5 md. This flattening behavior may also be due to differential depletion of multiple, commingled producing intervals, which is also common for Bend Conglomerate wells.

permeable intervals dominate the early production and later, the lower productivity intervals begin to contribute more to the overall production. Again, this flattening in the p/z curve is due to reservoir behavior other than communication with a secondary reservoir volume.

Because of the typical permeabilities of the Bend sequences and the way in which many of the wells were completed and produced, the use of p/z analysis to infer secondary reservoir compartments was not a useful technique in this study. This should not rule out the approach in other Midcontinent gas reservoirs, however. In other Mid-continent sands where the permeabilities are a little higher and the reservoirs are completed and produced separately, this p/z analysis may be just as effective in inferring incompletely drained reservoir compartments as in the previous Gulf Coast research.

Production Data Analysis

Production data analysis, or advanced decline curve analysis, was used extensively in the Boonsville engineering analysis to estimate reservoir properties, such as permeability and drainage area, and to evaluate the relative degree of depletion in specific reservoirs. Typically, in any study of this type, production data are usually the most readily available and easily obtained data. Using production data to determine reservoir characteristics is not new, having been introduced by Fetkovich in the early 1970's (Fetkovich, 1973). Still, however, production data, though often used to predict future performance, are not widely used to estimate reservoir properties. The advanced decline-curve analysis methods originally introduced by Fetkovich and extended by others (Fraim and Wattenbarger, 1987; Blasingame and others, 1991; Spivey and others, 1992; Spivey and Lee, 1993; Spivey and Frantz, 1994) enable production data to be analyzed in a manner similar to that used for well test data to estimate reservoir properties such as permeability, the degree of damage or stimulation (skin factor), and drainage area.

Figure B23 presents the Fetkovich type curves, which are composites of both analytical and empirical curves. These type curves combine analytical solutions for the radial flow equation describing transient flow, with empirical decline curve equations describing pseudo-steady-state or boundary-dominated flow. The curves are log-log plots of dimensionless rate, q_{Dd}, vs. dimensionless time, t_{Dd}, and assume constant bottomhole pressure production. The early stems are functions of dimensionless wellbore radius, r_D (ratio of drainage radius to effective wellbore radius), which is an indicator of damage or stimulation; the smaller the value of r_D, the greater the degree of stimulation. The later stems are functions of the decline exponent "b," also known as the Arps exponent (Arps, 1945), where a b value of zero indicates exponential decline and a b value of 1 represents harmonic decline. The evenly spaced b stems in between represent different types of hyperbolic decline. A b value between 0 and 0.7 is most common. For gas wells, Fraim and Wattenbarger (Fraim and Wattenbarger, 1987) showed that when gas reservoir properties are evaluated properly with time, all gas production data will follow the b stem of 0 on the type curve. This is particularly useful when analyzing gas well data quantitatively.

As Figure B23 shows, when the production data are plotted as log rate vs. log time, two important flow periods can be identified: transient flow and depletion or boundary-dominated flow. The transient flow period occurs first and is characterized by no influence from the reservoir boundaries. During this time, reservoir performance does not depend on reservoir size, but rather on permeability and the degree of damage or stimulation of the reservoir. This portion of the data can be used to estimate permeability and skin factor. Once reservoir boundaries begin to influence well performance, the log-log plot of flow rate vs. time begin to take on a concave downward shape. This portion of the data can be used to estimate ultimate recovery and drainage area.

Analyzing gas well data using the type curves is quite simple. First, a log-log plot of actual gas flow rate vs. time is generated as shown in Figure B24 at the same scale as the

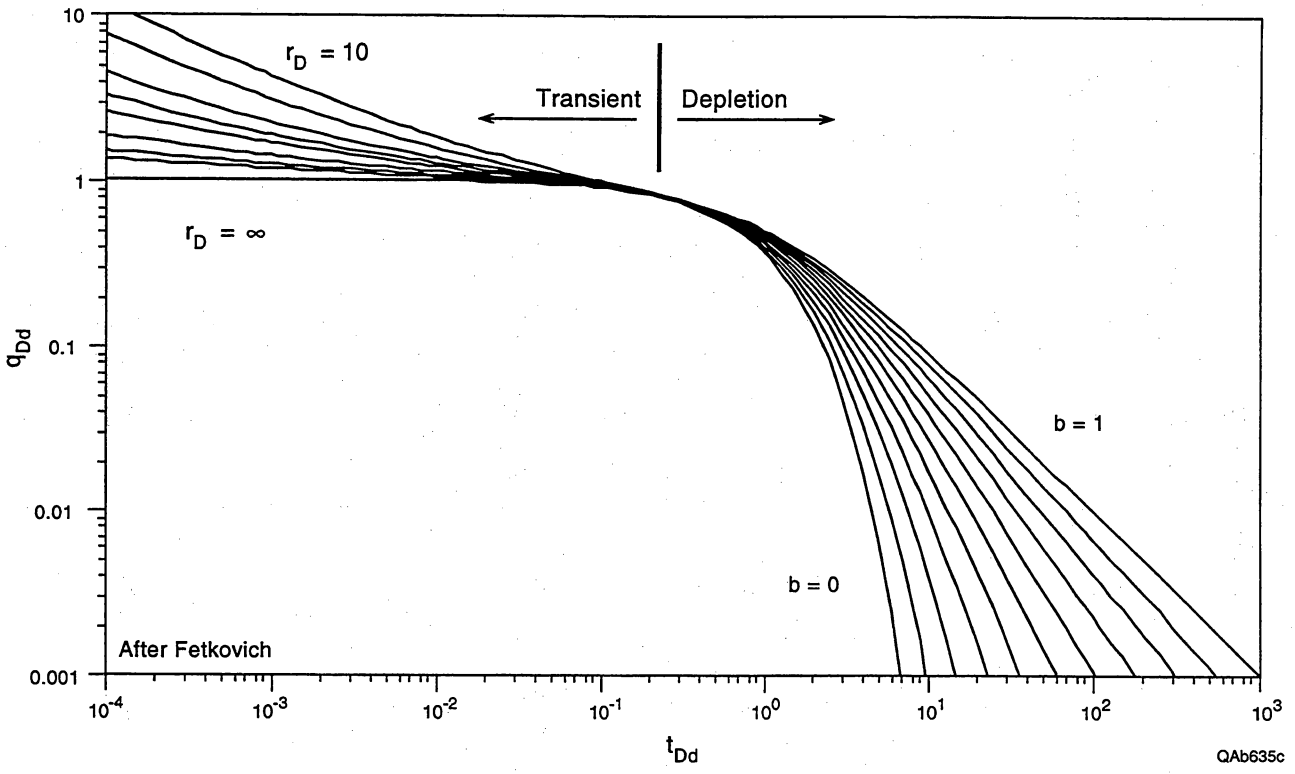

Figure B23. Example of a Fetkovich type curve that can be used for quantitative production data analysis to estimate reservoir properties, predict drainage area and gas in place, and forecast future performance.

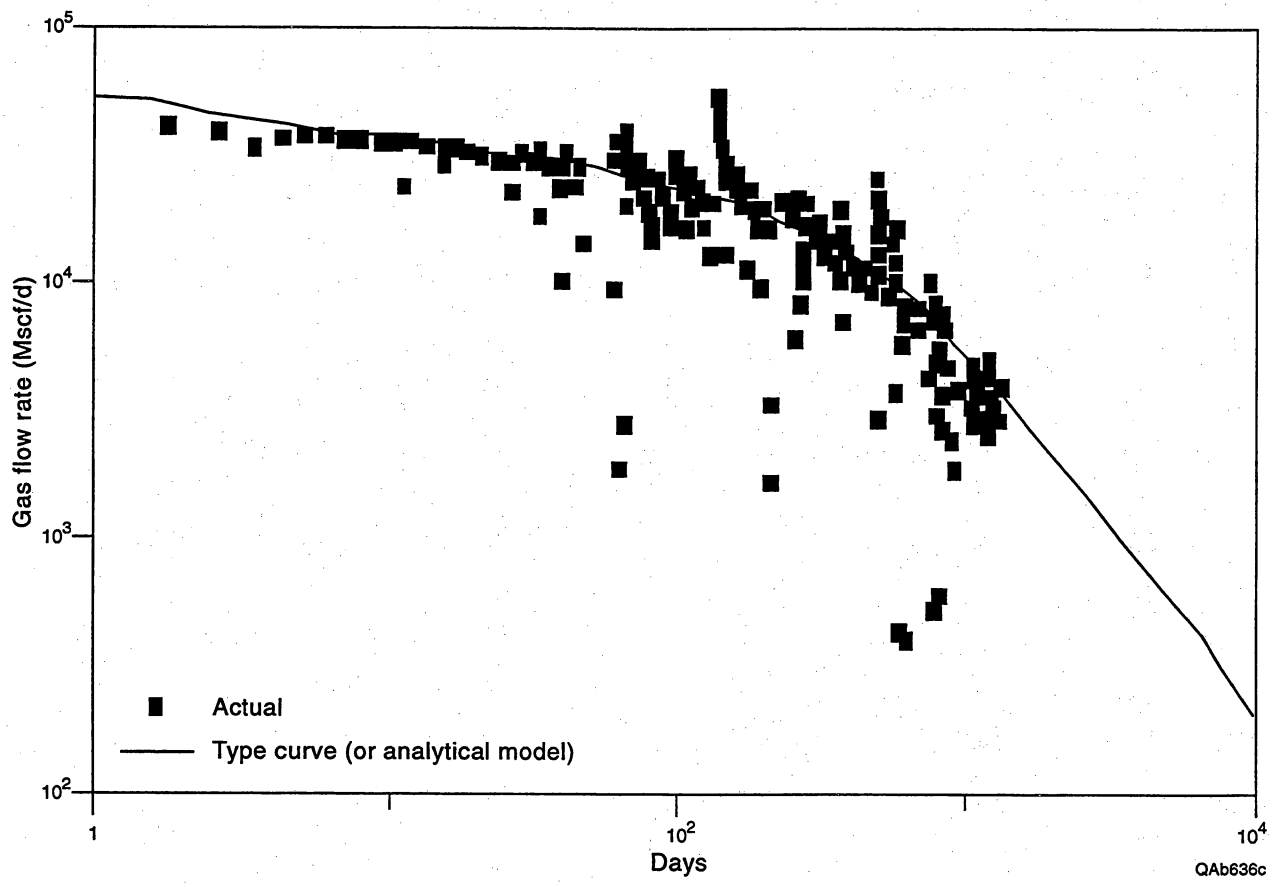

Figure B24. Example production data analysis using the Fetkovich type curves (or an equivalent analytical model).

type curve plot. Then the actual data are moved up and down and left to right until the best match of the production history is achieved with one of the type curves. From this match, values of permeability, skin factor, ultimate gas recovery, and drainage area can be estimated. This analysis can be accomplished by hand (Fetkovich, 1973), but automated Fetkovich-type analyses are also included in many popular decline-curve analysis software packages available in the petroleum industry today.

For analyzing production data from several hundred wells in a project such as this, however, an automated form of production data analysis is preferred. In this study, the production data analysis was actually accomplished using a GRI-developed software package known as PROMAT (Watson and Lee, 1986; Murtha and others, 1987; PROMAT, 1992). PROMAT is a single-phase production data analysis and forecasting tool developed as part of previous GRI research. The software includes a wide variety of analytical solutions modeling a number of different reservoir types and inner and outer boundary conditions. PROMAT is particularly useful because it includes an automatic history matching option that allows the engineer to enter and match actual production data easily and quickly to obtain estimates for reservoir permeability, skin factor, drainage area, and other reservoir properties, such as the degree of fracture storage and matrix-to-fracture transmissibility in naturally fractured reservoirs. PROMAT also permits variable flowing bottomhole pressures to be modeled over the life of a well (Spivey and Frantz, 1994), which can be important when trying to capture a known flowing bottomhole pressure history and operational events such as curtailment and compression.

Production data from all wells in the Boonsville project area were analyzed using PROMAT to estimate reservoir properties. Wherever possible, production from individual sequences was analyzed separately to develop estimates for reservoir characteristics by stratigraphic interval. Often, however, production from multiple zones had always been commingled, and it was not possible to allocate production back to

individual sequences. In these instances, total production from all zones was analyzed as a single zone, but with the knowledge that only estimates of overall gas recovery were generally reliable and not the reservoir properties themselves.

Age of the wells was also a problem in analyzing some Boonsville production data. Many wells in the project area were drilled in the 1950's, before the public data sources such as Dwight's and Petroleum Information began keeping records. In addition, the operators of these wells changed over the years in many cases, and much of the early production records are no longer available. Thus, in a number of the older wells, the first 5 to 10 yr of production data were missing. Again, this impacts the reliability of the estimates for reservoir permeability and especially skin factor in some cases, but the estimates for ultimate recovery and reservoir size should be largely unaffected.

As an example of how the production data were analyzed, Figure B25 shows the Trinity-only production history from the Threshold C Yates 9 well (see case history in the main body of the report). This decline behavior is typical of many project area wells. This well was completed in the Trinity sequence in June 1971 and produced about 1.9 Bscf from this interval through September 1989. The well came on line making about 2.5 MMscf/d and declined to about 20 Mscf/d over the 18 yr of production. This zone is still producing but is now commingled with the Vineyard reservoir below.

Figure B26 shows the more diagnostic log-log plot of the flow rate vs. time data. This plot suggests a period of transient flow for the first year or so; then the concave downward shape of the production data thereafter indicates boundary-dominated flow during most of the well's producing life. Using the analytical model (PROMAT) to history-match the production data, we estimated the Trinity reservoir to have a permeability of 3.3 md and a drainage area of about 300 acres. The estimated gas in place was 2.1 Bscf. Thus, the Trinity reservoir at this location has been essentially depleted by this well.

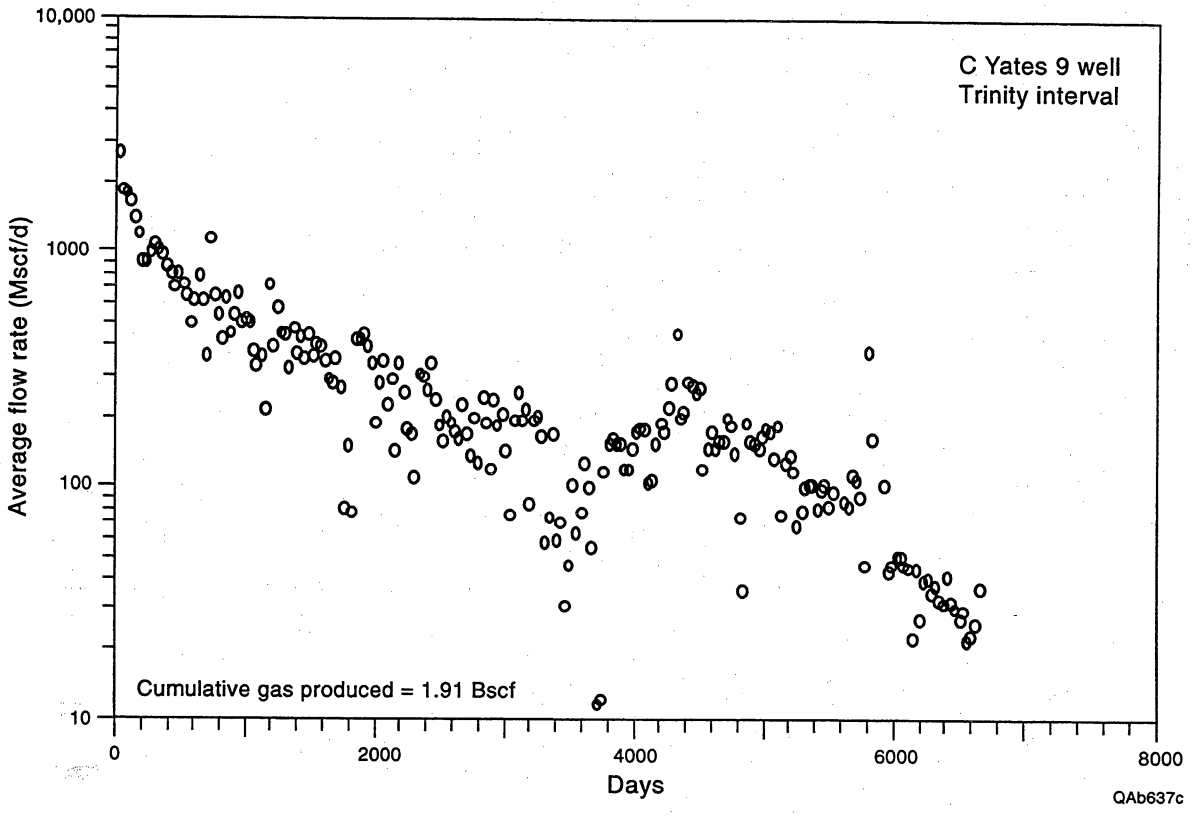

Figure B25. Semilog plot of flow rate vs. time for the Trinity interval in the C Yates 9 well; this production decline behavior is typical of many wells in the project area.

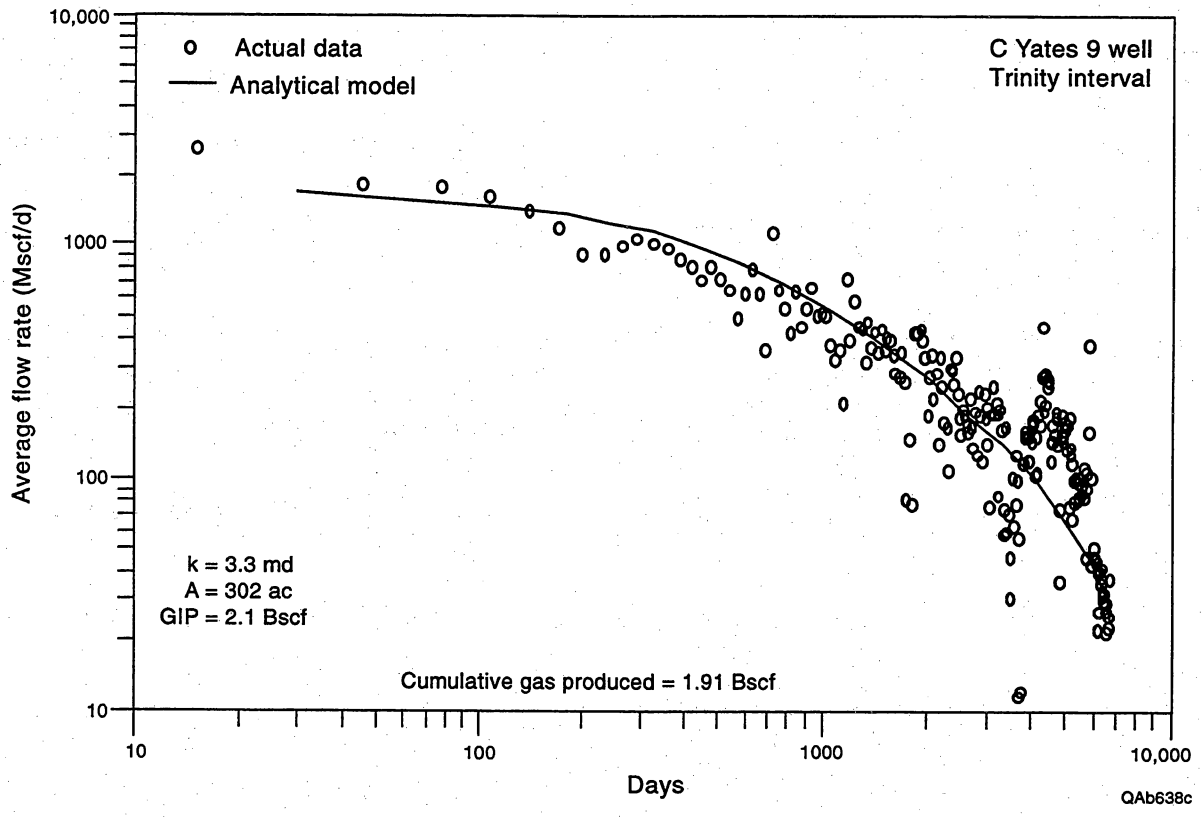

Figure B26. Log-log plot of production data from the C Yates 9 well showing significant depletion of the Trinity reservoir. A history match using an analytical model yields estimates for permeability, drainage area, and gas in place.

This same type of behavior can be seen throughout the project area. Figure B27 is another example of long-term production data analysis from the Upper Jasper Creek reservoir in the Threshold F Yates 9 well; this well produced for over 30 yr from this interval. Using the analytical reservoir model to history-match the production data, we found the Upper Jasper Creek reservoir to have a permeability of 0.33 md, a gas in place of 2.4 Bscf, and a drainage area of 232 acres. Again, the data suggest that this reservoir is substantially depleted.

Although the vast majority of production histories evaluated suggest substantial reservoir depletion, as shown in Figures B26 and B27, not all do. Figure B28 is a semilog plot of average flow rate vs. time from the Threshold B Yates 2 well. This well was completed in the Runaway sequence in 1956 and has produced for almost 40 yr from this reservoir alone. Although much of the first 10 yr of production history is unavailable, completion records suggest that the well came on production making 700 to 800 Mscf/d. Over time, however, the well has declined slowly and has maintained an average flow rate of about 50 to 100 Mscf/d over the last 30 yr. Overall, the decline is much flatter than observed in most project area wells.

In the late 1960's, the B Yates 2 was shut in and apparently curtailed for a couple of years. Once the well came back on line, however, the production jumped up to 400 to 500 Mscf/d and then declined back to a 50 to 100 Mscf/d average rate. The same was true following another apparent period of curtailment in the late 1970's.

When plotted on a log-log plot, as shown in Figure B29, the production data show only limited influence of boundary-dominated flow. This suggests that the B Yates 2 well is in communication with a larger gas volume than it can drain efficiently. Using the analytical model, we estimated the Runaway reservoir to have a permeability of 0.34 md, a gas in place of about 2.6 Bscf, and a drainage area of almost 600 acres. Because the B Yates 2 well has produced about 1.13 Bscf to date and is currently making about

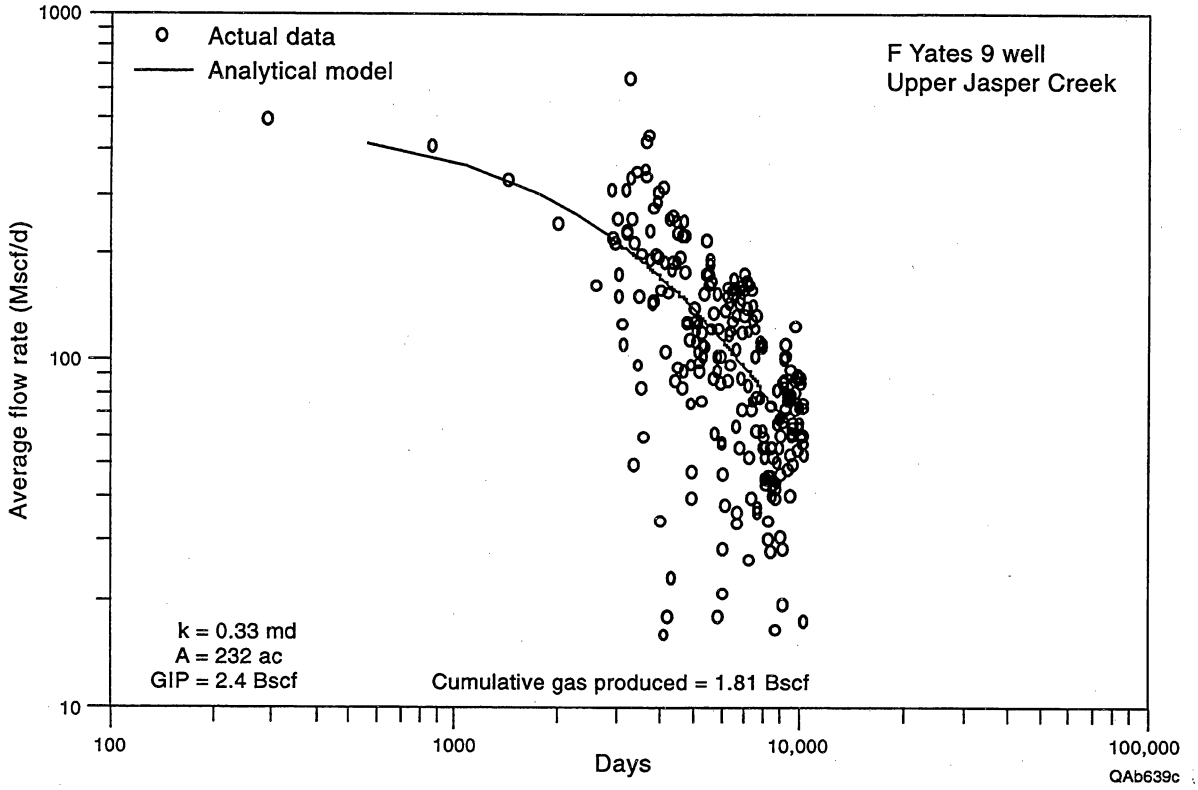

Figure B27. Log-log plot of production data from the F Yates 9 well showing significant depletion of the Upper Jasper Creek reservoir. A history match using an analytical model yields estimates for permeability, drainage area, and gas in place.

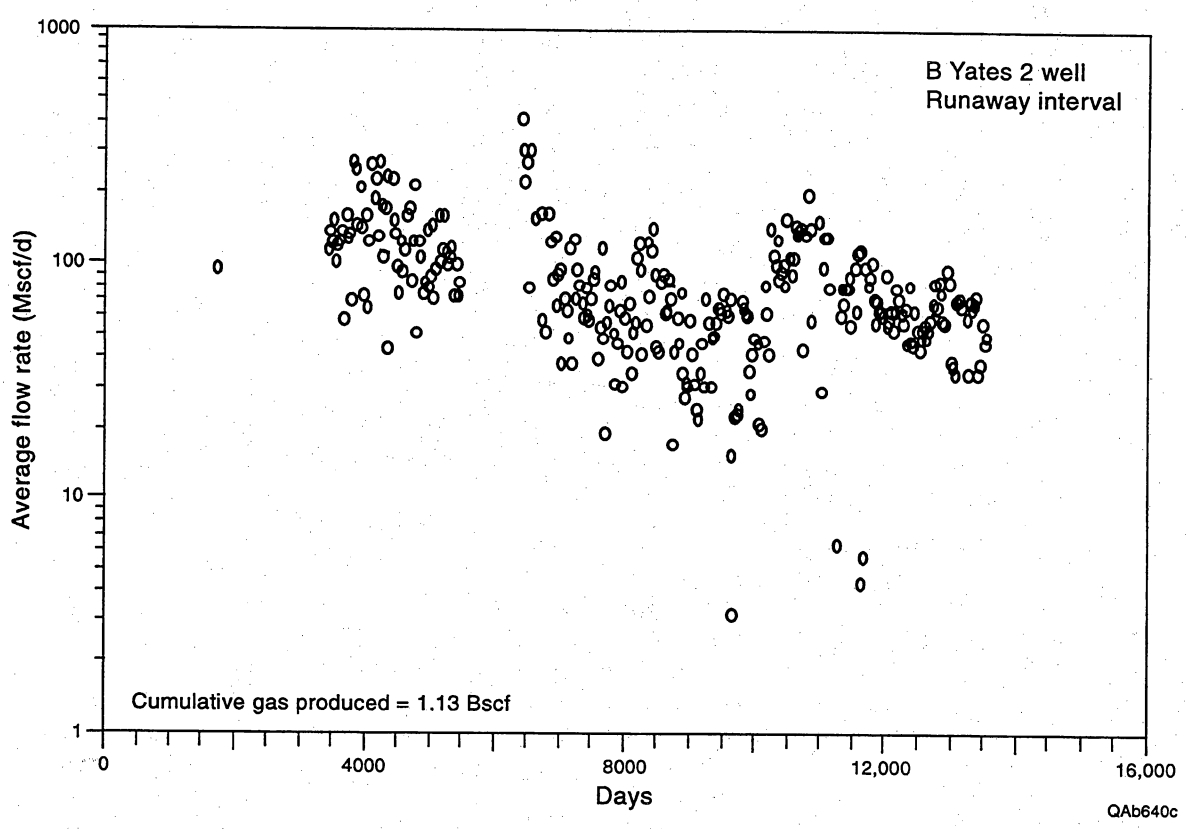

Figure B28. Production data from the Runaway interval in the B Yates 2 well. Note the relatively small decline in flow rate over time, over about 40 yr, which is atypical of most Bend completions.

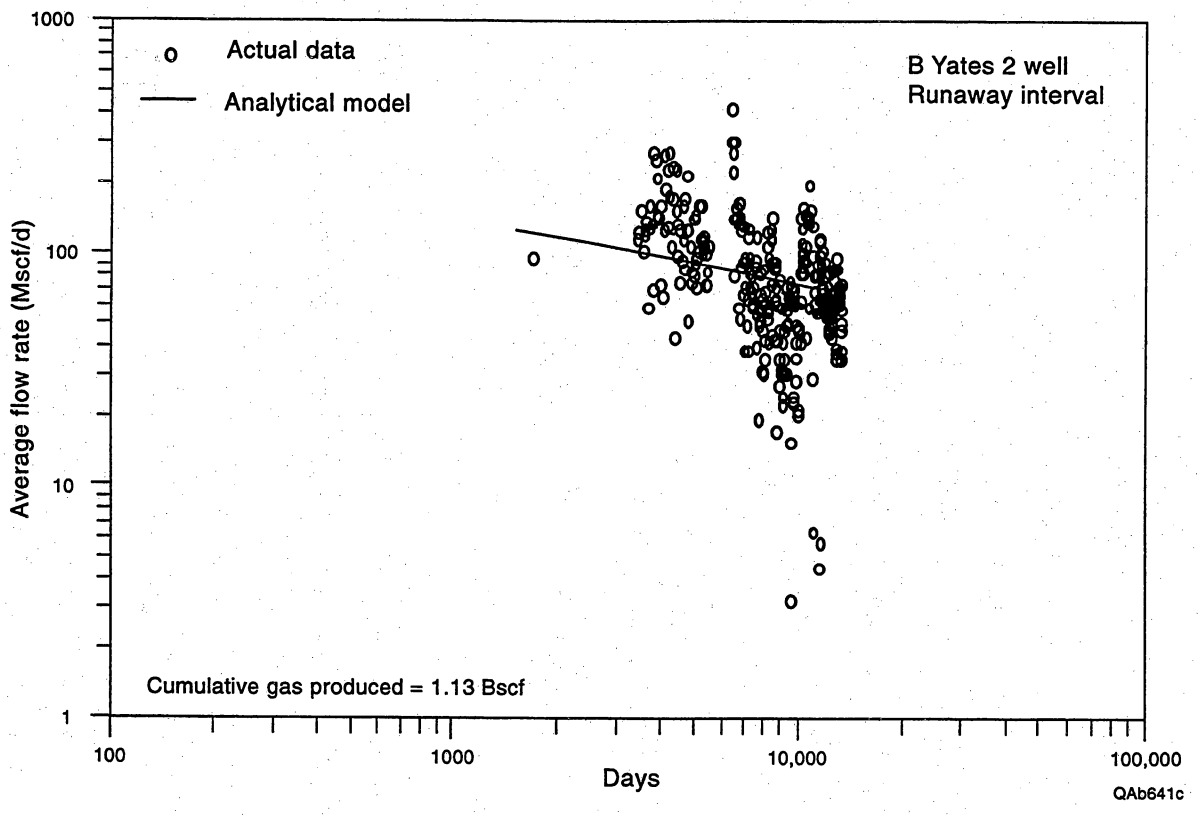

Figure B29. History match of production data from the Runaway interval suggests that the B Yates 2 well may be in communication with a larger gas volume than it can drain effectively.

50 Mscf/d, this evaluation suggests that another well may be needed to produce the gas from this reservoir effectively (or perhaps that this well should be restimulated).

Observations of this type signal areas where additional geological and geophysical interpretation should be focused. If, as the production data suggest, a reasonably large Runaway reservoir is communication with the B Yates 2 and a second well is needed, this area needs to be mapped and evaluated using the 3-D seismic data to both identify the reservoir extent and the optimal location for an additional well. Clearly this analysis does not infer the existence of an isolated reservoir compartment in the Runaway, but it does suggest an incompletely drained reservoir that may benefit from an additional well to accelerate the production of gas reserves in a more timely and economical manner.

Other uses of production data analysis results have been to map certain key properties across the project area and to compare the results with those from other disciplines. Figure B30 shows one such plot of drainage areas estimated for Middle Jasper Creek completions from production data analysis. The Middle Jasper Creek is a valley-fill sandstone that runs diagonally from northwest to southeast across much of the project area. Interestingly, in the central and southeast parts of the project area, the Middle Jasper Creek is characterized by smaller drainage areas on the order of 60 acres or less, whereas much larger drainage areas (up to about 300 acres) are found in the northwest part of the project area. Similar maps were prepared for other sequences and were provided to aid and refine the geological and geophysical interpretations of these sequences.

The Boonsville 3-D seismic data show that south and southeast of the B Yates 18D well, that the Jasper Creek interval is much more compartmentalized than it is north of the B Yates 18D. This change in compartment size is best seen on time slices of instantaneous seismic frequency (Fig. B31). A seismic interpretation principle that is emphasized in Appendix E is that instantaneous frequency is the seismic attribute that is probably the most sensitive to structural and stratigraphic discontinuities, particularly

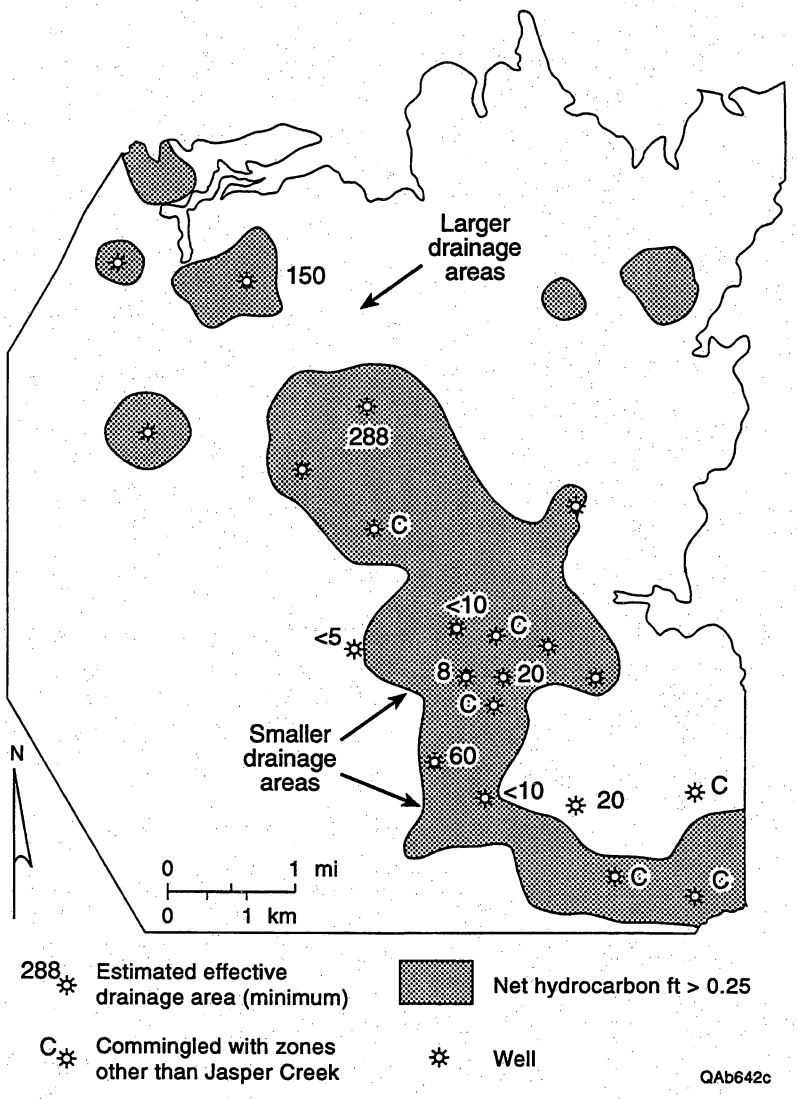

Figure B30. Map showing drainage areas estimated for Middle Jasper Creek completions from production data analysis.

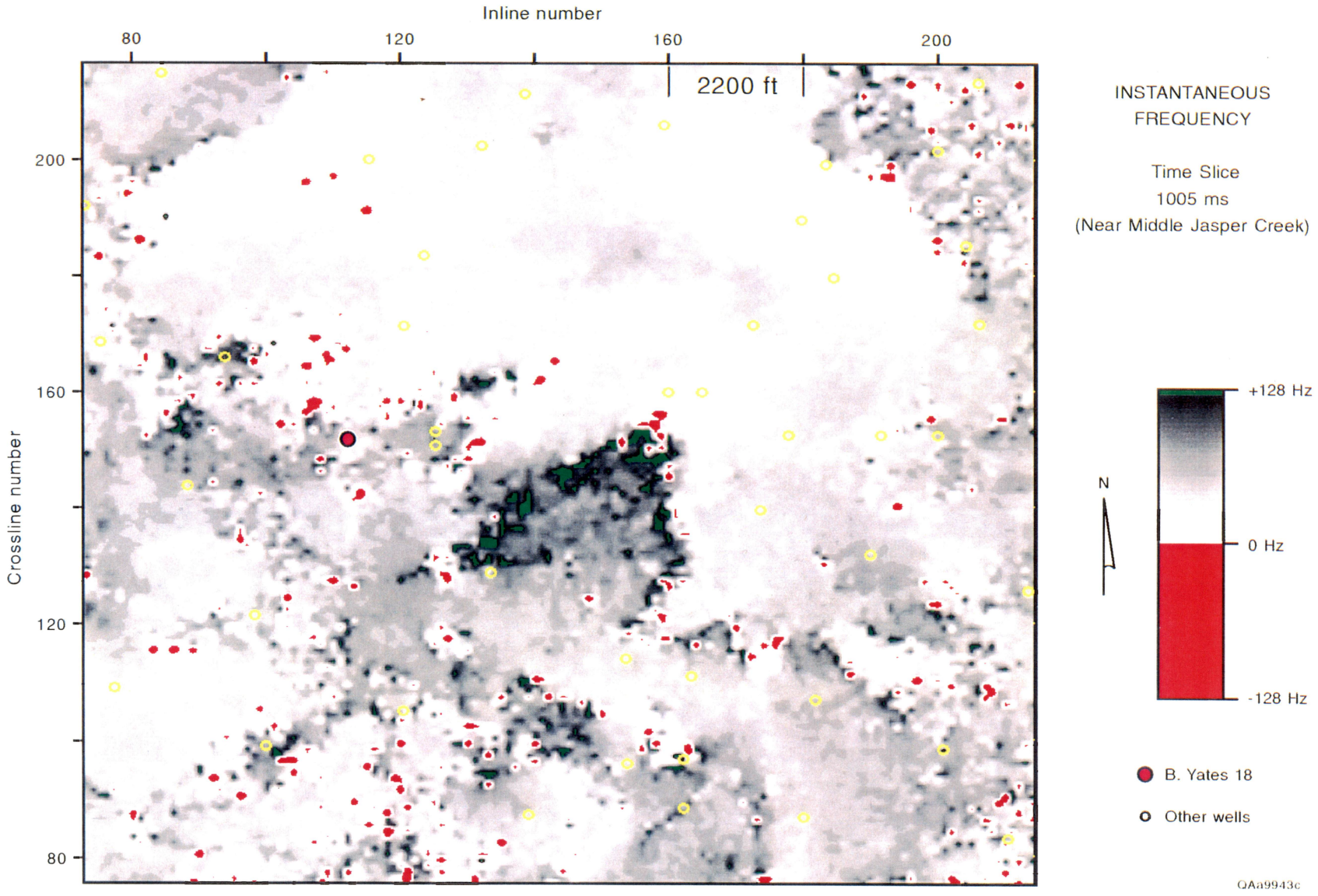

Figure B31. Time slice of instantaneous seismic frequency. The B Yates 18D well is identified by the large purple dot at (approximately) crossline coordinate 150 and inline coordinate 110. The time slice cuts through the Middle Jasper Creek sequence in the B Yates 18D well (at approximately 1.005 s). The color bar is chosen so that anomalous frequency values are red or green (see App. E for an explanation). An interpretation principle that is stressed in this work is that these anomalous frequencies commonly align in narrow trends along boundaries where structural and stratigraphic discontinuities occur. On the basis of this interpretational principle, we interpret the area south and southeast of the B Yates 18D well to be much more compartmentalized than the area north of the 18D well.

when these discontinuities are subtle. Thus, any reservoir compartmentalization that is caused by stratigraphic terminations or small faults can usually be readily seen in time slices (and horizons) that show the numerical behavior of instantaneous frequency and that use an appropriate color bar to emphasize anomalous frequency values.

The instantaneous frequency time slice in Figure B31 cuts through the 3-D data at a two-way time of 1.005 s, which is close to the Middle Jasper Creek sequence boundary at the B Yates 18D well. Away from the 18D well, this time slice does not follow the Middle Jasper Creek sequence exactly because that sequence boundary has some amount of time structure relief. However, the time slice does allow an interpreter to acquire a general sense of how often the Jasper Creek section is structurally or stratigraphically disrupted and where these disruptions are located. Inspection of the figure shows that north and northeast of the 18D well, the instantaneous frequency is smooth and continuous, implying that the Jasper Creek section is not severely compartmentalized in this region (see App. E for concept). In contrast, to the south and southeast of the 18D location, the instantaneous frequency map has many numerical discontinuities, suggesting that the Jasper Creek interval has numerous structural and/or stratigraphic disruptions in this part of the 3-D image (App. E). Apparently many of these discontinuities, barriers to horizontal fluid flow, create smaller Jasper Creek reservoir compartments south of the B Yates 18D well, which supports the segregation of compartment sizes documented in Figure B30.

Figure B32 presents another example of how the results of production data analyses were integrated with analyses from the other disciplines. This figure presents cumulative gas production as a function of time from the OXY Sealy B-3 and Sealy B-2 wells, both drilled since 1991 and completed in the Upper Caddo (see case history in the main body of the report). Both wells encountered near-original pressures upon completion in the Upper Caddo. As shown in the figure, both wells recovered about 350 MMscf through

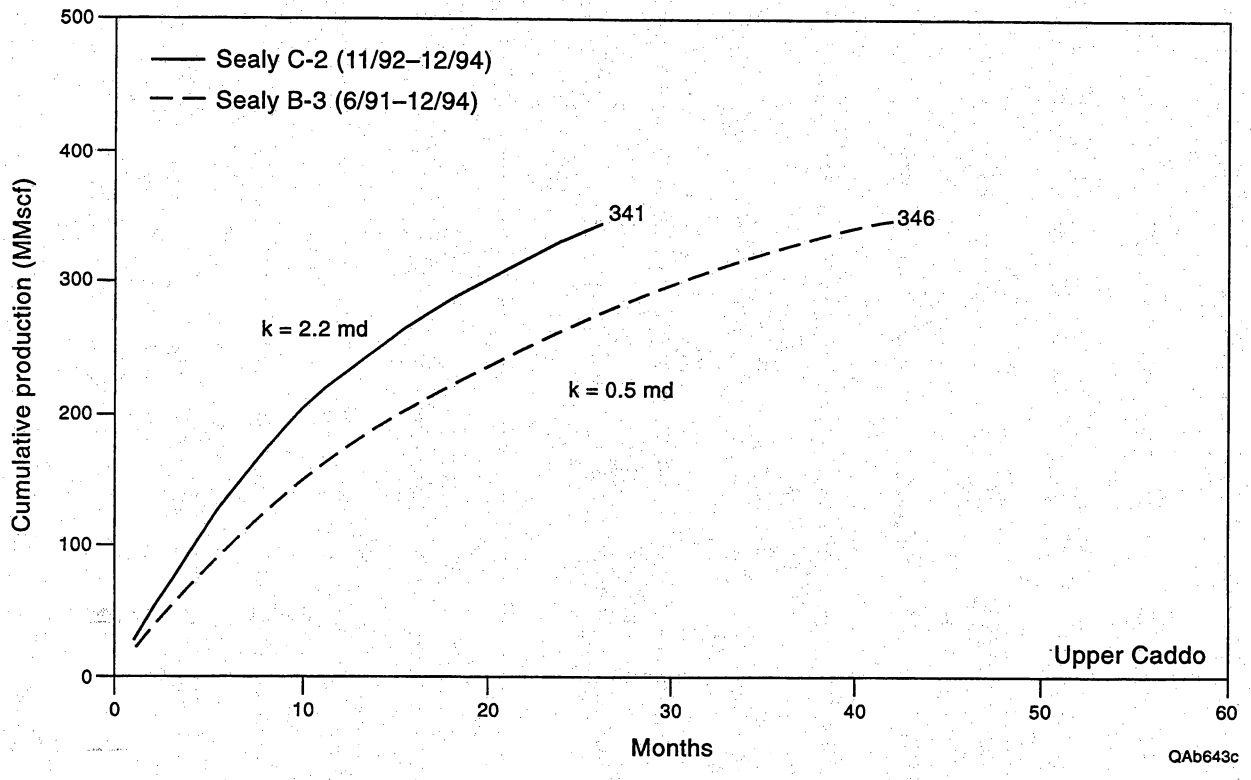

Figure B32. Comparison of well performance and permeabilities determined from production data analysis for the Sealy C-2 and Sealy B-3 wells; both are Upper Caddo completions.

the end of December 1994; the Sealy C-2 well has produced at somewhat higher flow rates than the Sealy B-3.

Also shown in Figure B32 are the values of permeability estimated for the Upper Caddo reservoir in each well from production data analysis. Permeabilities of 2.2 and 0.5 md were determined for the Sealy C-2 and Sealy B-3 wells, respectively. These permeabilities were then compared with those of the facies calculated for the Upper Caddo in both wells as determined from the petrophysical analysis (see Appendix C). The Upper Caddo facies determined for the Sealy C-2 well was "E," indicative of the cleanest sand in the Boonsville project area; the facies in the Sealy B-3 was found to be "E2," the shalier, lower quality productive sand type in the area. The permeability contrast between the two wells correlated nicely with this change in facies. In fact, additional comparisons between calculated facies and permeabilities suggest that a permeability of about 1 md may distinguish E from E2 facies in the project area. That is, E facies sands appear to have permeabilities greater than 1 md, whereas E2 facies reservoirs appear to have permeabilities of less than 1 md.

Well Test Analysis

Another useful source of reservoir information in a study of this type is well test data, particularly from pressure buildup tests. Well tests, when available, should provide superior estimates of permeability and skin factor (the degree of near-well damage or stimulation) as compared with production data because the test data are more concentrated at early times when transient flow generally dominates well performance. In some instances, depending on reservoir properties, pressure buildup tests may also provide insight into reservoir size and shape. This information about reservoir geometry can then be integrated with corresponding geological and geophysical interpretations to develop a better understanding of reservoir architecture.

Unfortunately, in an old field such as Boonsville (and, no doubt, many other older Mid-continent fields), not many well tests are available. Pressure buildup tests were rarely run in wells in the project area, and even when they were, many of the older test data were not always preserved. During the course of the research, however, several pressure buildup tests were run. Figure B33 presents the results from one of the well tests conducted in the Threshold I. G. Yates 33 well.

The I. G. Yates 33 well was drilled in April 1993 and completed in a high-permeability, 17-ft sand in the Middle Jasper Creek (see chapter 4). RFT's run during openhole logging recorded pressures of about 1,900 psi in the Middle Jasper Creek, leading to the conclusion that this was a previously untapped reservoir compartment. The well flowed at rates above 2 MMscf/d initially without stimulation, but both flow rate and flowing tubing pressure declined very quickly, indicating a small reservoir volume. The Middle Jasper Creek interval made only about 60 MMscf of gas and some oil prior to being abandoned in September 1994.

The well test presented in Figure B33 was run only several days after the I. G. Yates 33 well was placed on production, but it provided early evidence of the limited reservoir size. Figure B33 is a semilog plot of the test data. From a quantitative analysis of the data, a permeability of 28 md was calculated for the Middle Jasper Creek reservoir. This permeability was higher than generally observed in the Bend intervals in this area, but this value was consistent with the abnormally high permeabilities measured from core analysis in this well. At a shut-in time of only about 0.5 h, a sharp upturn in the pressure data was observed, indicating that a near-well boundary had been encountered. The estimated average reservoir pressure of 1,560 psi was about 350 psi below the initial measured pressure of approximately 1,900 psi in this reservoir, after only less than 10 MMscf of gas had been produced. Again, these results suggested a very small reservoir volume.

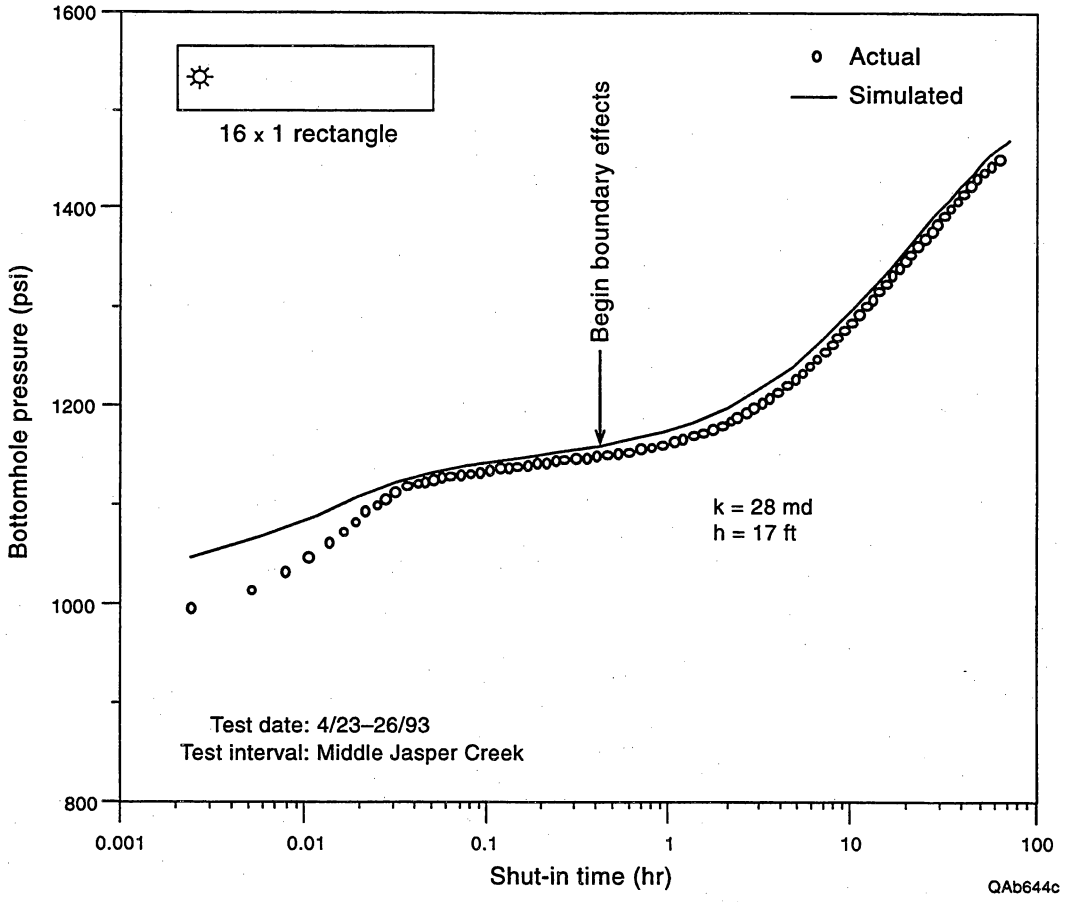

Figure B33. History match of the pressure buildup test data from the April 1993 well test conducted on the I. G. Yates 33 well.

Figure B33 also presents a history-match of the pressure buildup test data generated by a reservoir simulator. Although several different reservoir descriptions were tried, the best match of the actual test data was obtained using a long, narrow (16×1) rectangular reservoir, with the well located near one end of the drainage area. The permeability used in generating the simulated test data was also 28 md, and the total reservoir size was about 8 acres. This high permeability and rectangular shape, as deduced from the well test analysis, were consistent with subsequent well performance, and, ultimately, with the geologic description of the complex Middle Jasper Creek stratigraphy in this area.

Well tests run in other project area wells were analyzed in a similar fashion to provide estimates of reservoir permeability, skin factor, reservoir size, and reservoir geometry for integration with the corresponding geological and geophysical interpretations. The results of several of these interpretations are included in the discussions found in the main body of this report.

Summary

In summary, engineering data, particularly pressure and production data, confirm the existence of compartmented or poorly drained gas reserves throughout much of the Bend Conglomerate interval in the project area. New wells drilled through the Bend Conglomerate still frequently encounter pressures in one or more of the Bend sequences that are at or near the original pressures encountered more than 40 yr ago. Most of these compartmented or poorly drained gas reserves are found between the Lower Caddo and the Vineyard intervals, particularly in the Trinity, Bridgeport, Runaway, and Jasper Creek sequences. Median drainage areas in these sequences were found to be 80 acres or less, further confirming the likelihood that compartmented or poorly drained gas reserves will continue to be found as well spacing is reduced to 80 acres.

Although higher pressures are still being found, the gas volumes associated with these pressures are the key to successful infill development. On the basis of the

hydrocarbon distribution in the project area, we expect gas volumes associated with these isolated compartments or poorly drained areas (i.e., higher pressures) in most stratigraphic intervals will be small, on the order of 200 MMscf or less on average (using an estimated drainage of 80 acres and typical volumetric properties). Recent wells having pressures at or near original in various sequences have found gas reserves in these zones ranging from less than 50 MMscf to about 700 MMscf. Thus, whereas it is possible that any single Bend sequence may include gas reserves sufficient to be economically attractive as well spacing is reduced, it is more likely that multiple, stacked completion opportunities will be needed to yield gas reserves sufficient for an economical infill well. More careful strategic targeting of new wells, incorporating insight gained from 3-D seismic and supporting geologic analysis, will therefore be needed to maximize economic success in Boonsville field.

Petrophysical, production, and well test data were analyzed wherever available throughout the Boonsville project area to estimate reservoir properties, drainage areas, and reservoir geometries. These results, in turn, were used to focus and refine the geological and geophysical interpretations developed. In particular, engineering estimates of reservoir size and geometry proved particularly important in understanding the stratigraphic complexities of the Bend Conglomerate and in calibrating 3-D seismic interpretations.

Review of 3-D seismic data in the project area leads us to the conclusion that apparent, stacked, trapping geometries often exist within the 3-D data volume. Further, influence of karst-collapse features on Bend Conglomerate stratigraphy also suggests the opportunity and likelihood for finding multiple, stacked, and at least partially isolated compartments. In the absence of clear geologic or seismic evidence of undeveloped reservoirs, a reasonable approach to identifying infill well locations may therefore be to focus 3-D seismic evaluation on these apparent, stacked, trapping geometries in those

areas having the highest likelihood of multiple completion opportunities (i.e., multiple net pay zones).

References

Arps, J. J., 1945, Analysis of decline curves: Transactions of the American Institute of Mining, Metallurgical, and Petroleum Engineers, v. 160, p. 228.

Blasingame, T. A., McCray, T. C., and Lee, W. J., 1991, Decline curve analysis for variable pressure drop/variable flowrate systems: Society of Petroleum Engineers, Paper SPE 21513.

Darden, D. P., 1994, Plunger lift applications in wells with set packers or permanent tubing (abs.): Journal of Petroleum Technology, January, p. 6.

Fetkovich, M. J., 1973, Decline curve analysis using type curves: Society of Petroleum Engineers, Paper SPE 4629.

Fraim, M. L., and Wattenbarger, R. A., 1987, Gas reservoir decline-curve analysis using type curves with real gas pseudopressure and normalized time, *in* Society of Petroleum Engineers Formation Evaluation, p. 671–682.

Levey, R. A., and others, 1992, Infield gas reserve growth potential: Gulf Coast sandstone reservoirs (Frio, Vicksburg, Wilcox): The University of Texas at Austin, Bureau of Economic Geology, short course notes prepared for the Gas Research Institute, U.S. Department of Energy, and State of Texas, 392 p.

Levey, R. A., Hardage, B. A., Langford, R. P., Scott, A. R., Finley, R. J., Sippel, M. A., Collins, R. E., Vidal, J. M., Howard, W. E., Ballard, J. R., Grigsby, J. D., and Kerr, D. R., 1993, Secondary natural gas recovery: targeted technology applications for infield reserve growth in fluvial reservoirs, Stratton field, South Texas: The

University of Texas at Austin, Bureau of Economic Geology topical report prepared for the Gas Research Institute and the U.S. Department of Energy, GRI-93/0187, GRI Contract No. 5088-212-1718 and DOE Contract No. DE-FG21-88MC25031, 244 p.

Lord, M. E., and Collins, R. E., 1991, Detecting compartmented gas reservoirs through production performance: Society of Petroleum Engineers, Paper SPE 22941, p. 575–581.

_____ 1992, Simulation system for compartmented gas reservoirs: targeted technology applications for infield reserve growth: Research & Engineering Consultants, Inc., topical report prepared for the Gas Research Institute and the U.S. Department of Energy, GRI-92/0104, GRI Contract No. 5088-212-1718 and DOE Contract No. DE-FG21-88MC25031.

Murtha, J. A., Gatens, J. M., Lancaster, D. E., Lane, H. S., Lee, W. J., Olarewaju, J. S., and Watson, A. T., 1987, Practical analysis methods for well test and production data: S. A. Holditch & Associates, Inc., topical report prepared for the Gas Research Institute, GRI-88/0017, GRI Contract No. 5084-213-0980.

PROMAT, 1992, A production data history matching and performance forecasting program for oil and gas wells: S. A. Holditch & Associates, Inc., User's Manual, Version 3.1.

Spivey, J. P., and Frantz, J. H., 1994, History matching production data using analytical solutions for linearly varying bottomhole pressure: Society of Petroleum Engineers, Paper SPE 29167.

Spivey, J. P., Gatens, J. M., Semmelbeck, M. E., and Lee, W. J., 1992, Integral type curves for advanced decline curve analysis: Society of Petroleum Engineers, Paper SPE 24301.

Spivey, J. P., and Lee, W. J., 1993, Production data analysis for wells that have been subject to periodic curtailment: Society of Petroleum Engineers, Paper SPE 26182.

Watson, A. T., and Lee, W. J., 1986, A new algorithm for automatic history matching production data: Society of Petroleum Engineers, Paper SPE 15228.

APPENDIX C

PETROPHYSICAL ANALYSIS OF THE BOONSVILLE PROJECT AREA

Petrophysical Data

Two major Bend Conglomerate petrophysical data bases were created from log data recorded in wells within and immediately surrounding the Boonsville 3-D seismic survey, using two different software packages—Scientific Software-Intercomp's WorkBench* and Occidental Petroleum's Stacked Curves (SCPC)*.

WorkBench is a reservoir management tool kit that includes a reservoir description module. The reservoir description module produces base maps and cross sections and performs advanced log analysis, summation calculations, and contouring. This system was used to edit the log data, depth-shift the various log suites to a common depth (usually on the basis of the resistivity suite), and perform environmental corrections before any log analyses were performed. Geological markers generated by SCPC were imported into WorkBench before summations were calculated for each of the layers. The summation results were contoured using several different software packages, including WorkBench.

Wireline Logs—A Historical Perspective of Available Data

Log analysis of Boonsville field involved interpreting several different types of log suites. Wells were logged from the discovery of the field in 1945 until the present time. During that period, the wireline logging industry developed and introduced a number of new logs and replaced older logging tools with newer tools. Figure C1 shows a rough

*The Bureau of Economic Geology (BEG), the Gas Research Institute (GRI), and the U.S. Department of Energy (DOE) do not endorse in any way the software, hardware, or any other commercial or noncommercial products mentioned in this report. Any references to these products should not be construed as such an endorsement.

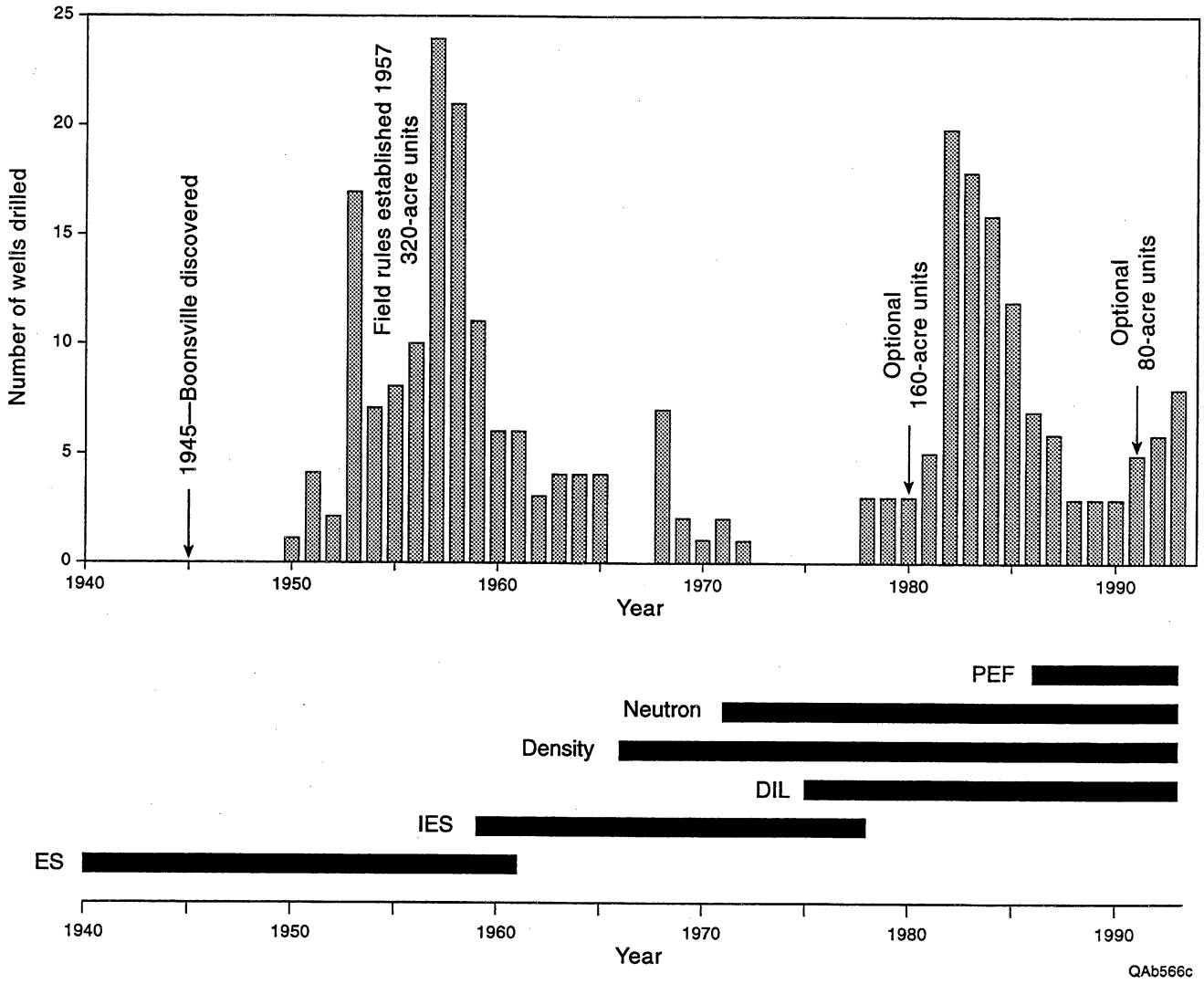

Figure C1. Time line showing available tool types and a graph of the drilling activity in the general area of the study.

time line of the available tool types along with a graph of drilling activity in the general area of study. Peaks of activity occurred when the field was first drilled at 320-acre spacing, then at 160-acre spacing, and most recently when 80-acre spacing was authorized.

In the 1940's and 1950's, only resistivity measurements were available. At first, these data consisted of electric sonde logs (ES logs), which made four measurements: Spontaneous Potential (SP), 16-inch Short Normal (SN), 64-inch Long Normal (LN), and 18-ft, 8-inch Lateral Log (LAT). An additional log that was commonly run in Boonsville field was the microlog, which provided three measurements: Caliper, Micro Normal (2 inches), and Micro Inverse (1 inch × 1 inch). Later this microlog was sometimes replaced with newer devices such as Proximity logs, MicroLaterlog logs, and MicroSFL logs. These micrologging tools were used to find permeable zones in a qualitative way, on the basis of the concept that the curve cross-over that occurs when the resistivity is below 20 ohm-ms is a good indication of a permeable sand.

The Lateral Log measured resistivity values that were close to the true resistivity only in sandstones that were at least five times as thick as the measure length (18 ft, 8 inches) of the tool; most sands in the Bend Conglomerate are not this thick. The asymmetrical nature of the Lateral Log measurement thus made it difficult to estimate true resistivity of the noninvaded sandstones. This log was later replaced by the Induction Log.

The first induction tools that were used in Boonsville field were the Induction Electric Logs (IES logs), which provided three measurements: Spontaneous Potential (SP), 16-inch Short Normal (SN), and Deep Induction (ILD). Most of these logs were provided by Schlumberger Well Services, but several new wireline vendors soon appeared and offered their own versions of these logs. The differences in the tools of the various vendors are not enough to make any substantial difference to the water-saturation

calculations; however, we did correct for differences using the automatic environmental corrections module of WorkBench.

In the late 1960's, the Short Normal was replaced by focused shallow resistivity tools, such as the Spherically Focused Log (SFL). The new resistivity tool was then known as the Induction SFL (I/SFL) tool and was often run with the newly developed borehole compensated sonic (BHS) tool and the gamma ray (GR) tool. The combined tool suite was referred to as the ISF/Sonic suite by Schlumberger. Other logging companies had different tool mnemonics, but the tools provided similar measurements.

In the 1970's, two new tools, the Compensated Neutron (CNL) and the Compensated Formation Density (FDC) devices, became commonly used. These tools were used to estimate porosities and lithologies of the formation, and they usually replaced sonic tools in Boonsville field. In fact, few sonic tools were run in the study area because at the time when these tools were popular, the area was not being drilled (see Figure C1).

In the 1980's, the density tool was enhanced to include a photoelectric effect measurement (PEF) that is very useful in determining lithology, particularly for detecting the presence of calcite. This density tool uses gamma rays at two different energies. The lower energy gamma rays interact with the formation by Compton scattering of the outer electron shells in component atoms, thus giving a measure of electron density which, in turn, allows the bulk density to be estimated. The higher energy gamma rays interact with the atoms by the photoelectric effect.

Other recently developed tools that have been used in Boonsville field include the microwave absorption tool (EPT) and formation scanning tools (FMS and FMI). The FMI, in particular, was used in three recent cooperative wells—the B Yates 17D, the B Yates 18D, and the I. G. Yates 33 wells. The microwave tool is used to measure water in the invaded zone, allowing invasion and porosity calculations to be performed. The FMS and FMI imaging tools use a series of microresistivity buttons on four calipers, and

sophisticated processing of their resistivity data produces resistivity images covering about 80 percent of the surface of the borehole. These images are valuable in determining the stratigraphic and structural environment of the formation.

Repeat Formation Tester

The Repeat Formation Tester (RFT) was run in many wells in the study area. This device is one of the most important wireline tools because it can measure pressure in formations having permeability down to about 0.1 md before running the risk of differential sticking. Pressure data are a good first indicator of whether a reservoir has been produced from another well or whether it resides in its own untapped compartment. Pressure data provided the first evidence of compartmented or incompletely drained gas in the Bend Conglomerate (see Appendix B).

The RFT tool estimates formation pressure and permeability by mechanically placing a probe against the formation and sealing it to the mud cake. A small prechamber is opened, creating a vacuum that the formation fluid will tend to fill if the fluid is capable of moving. The prechamber volume can be as large as 20 cm^3. Smaller prechambers are used in lower permeability zones. In the Bend sandstones, 2- to 5-cm^3 prechambers are commonly used. With this small prechamber, the tool is being influenced by the invaded zone, not by the virgin formation. The invaded zone is often damaged by invading fluids (mud filtrate), so the permeability data obtained using an RFT tool must be used with care. The permeability value obtained with the tool is usually pessimistic compared with the values determined by a full drill-stem test. The RFT pressure data can provide a good estimate of formation pressure, however, if sufficient time is allowed for pressure to build up to a value that is close enough to actual formation pressure to allow an accurate extrapolation.

Although the RFT tool is capable of obtaining fluid samples from the formation, this option is normally used only in zones of sufficiently high permeability that allow the samples to be obtained within a few minutes. Permeabilities in the Bend Conglomerate are not high enough to permit retrieving a fluid sample before running the risk of sticking the tool in the borehole.

Care must be taken to ensure that the probe of the RFT tool remain clean because the probe includes a fine filter that can easily become clogged. In the Bend Conglomerate, there are some potential "lost circulation" zones, particularly near the top of Marble Falls. When these lost circulation zones are penetrated, it is sometimes necessary to add fluid-loss materials to the mud to regain control of the mud column. This lost circulation material is usually some type of fibrous material, such as cottonseed hulls, which is designed to form a seal over higher permeability features (such as fractures and vugs), so that a mud cake can be formed at the borehole. Unfortunately, this material can also clog the filter and/or probe of the RFT tool.

If the probe becomes clogged by lost circulation material, the operator must normally pull the tool to the surface and clean the tool. Occasionally the probe can be cleaned by moving the tool to a high-permeability zone and allowing the formation fluid to move through the probe (as was done in the OXY Sealy C-3 well using the Upper Jasper Creek sand). In order to reduce the problem of lost circulation material clogging the RFT probe, we recommend that the mud be altered to a high viscosity and then circulated out from the bottom up for 2 h or more before pulling the drill string out of the hole for logging.

Core Data

Cores were obtained in four cooperative wells:

Well Name	Depths (ft)
I. G. Yates 33	5446-5472
Sealy C-2	4891-4910
Craft Tarrant Water Board 3	5370-5518
Tarrant A-4	4715-4750
Tarrant A-4	4800-4841
Tarrant A-4	5497-5566

The core data were divided into the 12 different facies shown in Table C1. Each facies is identified by a letter and is assigned a number that roughly describes the hardness of that facies. This hardness number is used in cross sections to graphically show the facies described from core and calculated from wireline logs.

Sample plugs were taken from representative zones and analyzed for porosity and permeability. Samples were taken from cores in both permeable and nonpermeable rock and analyzed for mineralogy by infrared (IR) spectroscopy. The results of this analysis are listed in Table C2 and show that the primary components of the samples are quartz, calcite, and clays. Note that although numbers are quoted for pyrite (all zeroes), the spectrometer was not capable of detecting pyrite. However, pyrite was seen visually in many parts of the cores. Thin sections were also prepared and petrographic analysis performed.

Table C1. The 12 primary facies identified from the core data for the Bend Conglomerate. The facies number is loosely based on the hardness of each facies. This number is used to display the facies on cross sections when the facies is derived from core or logs.

Facies name	Facies no.	Description	Interpretation
A	2	Fissile mudstone	Maximum flooding shale—outer shelf
B	3	Fossiliferous mudstone	Shelf, prodelta
C	8	Interbedded fossiliferous, calcareous sandstones and mudstones	Lower shoreface, distal delta front
D	15	Fossiliferous, calcareous sandstones (+conglomerate)	Upper shoreface
E	20	Conglomeratic sandstones	Active fluvial/deltaic channel fill
E2	18	Muddy, fine-grained sandstones	(High sinuosity?) fluvial channel fill
G	6	Burrowed, poorly fossiliferous interbedded sandstones and mudstones	Estuary or restricted bay fill
G2	9	Burrowed, poorly fossiliferous fine-grained sandstones	Estuarine channel fill
H	4	Carbonaceous, coaly mudstone	Marsh / swamp
I	13	Bioturbated calcareous fine sandstones	Transgressive shoreface
J	10	Bioturbated muddy skeletal wackestone	Interdeltaic shelf, lower shoreface
K	17	Skeletal packstone, wackestone	Shelf carbonate

Table C2. Results of infrared (IR) spectroscopy analysis on selected core samples. Note that although pyrite numbers were quoted, the spectrometer could not detect pyrite. The wells used were Sealy C-2 (SC2), I. G. Yates 33 (IGY33), and Craft TWB 3 (CTWB3). The minerals listed are Qtz (quartz), Plg (plagioclase), Ksp (K-feldspar), Cal (calcite), Dol (dolomite), Pyr (pyrite), Anh (anhydrite), Sid (siderite), Alb (albite), Arg (aragonite), Kao (kaolinite), Chl (chlorite), Ill + Smc (illite and smectite). The grain densities are calculated using average densities of the minerals detected.

Well	Depth (ft)	Grain density (gm/cm^3)	Qtz	Plg	Ksp	Cal	Dol	Pyr	Anhy	Sid	Alb	Arg	Total clay	Kao	Chl	Ill+Smc
SC2	4,890.5	2.66	44	0	10	14	9	0	0	0	13	0	10	6	0	4
SC2	4,893.5	2.65	46	0	3	16	3	0	0	0	27	0	5	2	0	3
SC2	4,896.2	2.63	52	0	3	3	0	0	0	0	37	0	5	3	0	2
SC2	4,897.6	2.63	56	0	5	1	0	0	0	0	36	0	2	0	0	2
SC2	4,901.5	2.66	49	0	9	13	8	0	0	0	15	0	6	4	0	2
SC2	4,903.9	2.71	38	2	2	28	3	0	0	5	11	0	11	4	4	3
SC2	4,906.0	2.68	20	1	1	25	9	0	0	1	0	0	43	10	0	33
IGY33	5,457.8	2.66	83	0	0	0	0	0	0	0	2	0	15	0	11	4
IGY33	5,466.7	2.67	65	0	0	11	10	0	0	0	10	0	4	0	1	3
IGY33	5,469.4	2.64	86	0	3	0	0	0	0	0	7	0	4	0	0	4
IGY33	5,476.0	2.66	72	2	0	4	2	0	0	0	7	0	13	0	10	3
IGT33	5,478.0	2.77	54	0	5	4	3	0	0	13	2	0	19	3	7	9
CTWB3	5,371.3	2.69	28	0	0	47	14	0	0	0	0	0	11	3	0	8
CTWB3	5,421.1	2.65	95	0	0	2	0	0	0	0	0	0	3	0	3	1
CTWB3	5,428.1	2.65	60	0	0	0	0	0	0	0	2	0	38	18	2	18
CTWB3	5,440.2	2.66	83	0	0	8	0	0	0	0	1	0	8	2	4	2
CTWB3	5,444.8	2.67	80	0	0	9	1	0	0	0	0	0	10	0	8	2
CTWB3	5,477.7	2.69	49	0	0	37	8	0	0	0	0	0	6	0	4	2
CTWB3	5,483.9	2.69	60	0	0	15	8	0	0	0	0	0	17	0	14	3

Core Analysis

As mentioned earlier, core plug samples were analyzed in most of the sandy intervals. The results of the plug analyses are summarized in Figures C2 and C3 and show three distinct data groupings:

- The first grouping is in the region where porosity is less than 4 percent. These points are associated with the tighter facies that are well cemented, and they probably do not represent reservoir rock. The permeability values are probably the permeabilities related to induced microfractures formed during the coring and plugging processes.
- The second group of points runs generally from porosity = 6 percent, perm = 0.1 md to porosity = 16 percent, perm = 200 md. This group is dominated by a permeable sandstone facies.
- The third group of data is another linear set running from approximate porosity = 6 percent, perm = 0.1 md to porosity = 14 percent, perm = 0.6 md. This group is associated with low-permeability sandstones that may have some measure of cementation or other pore-blocking material.

The second and third groups of data indicate that the productive sands in the Bend Conglomerate are associated with two (or more) different facies. A key objective of the petrophysical analysis was to find a way to calculate the different sandstone facies in order to determine the importance of facies changes in reservoir compartmentalization.

Overview of Log-Analysis Techniques

Data Preparation

Once all the wireline data were located and digitized, the data were brought into the WorkBench environment. The locations of all the wells were entered into the base map

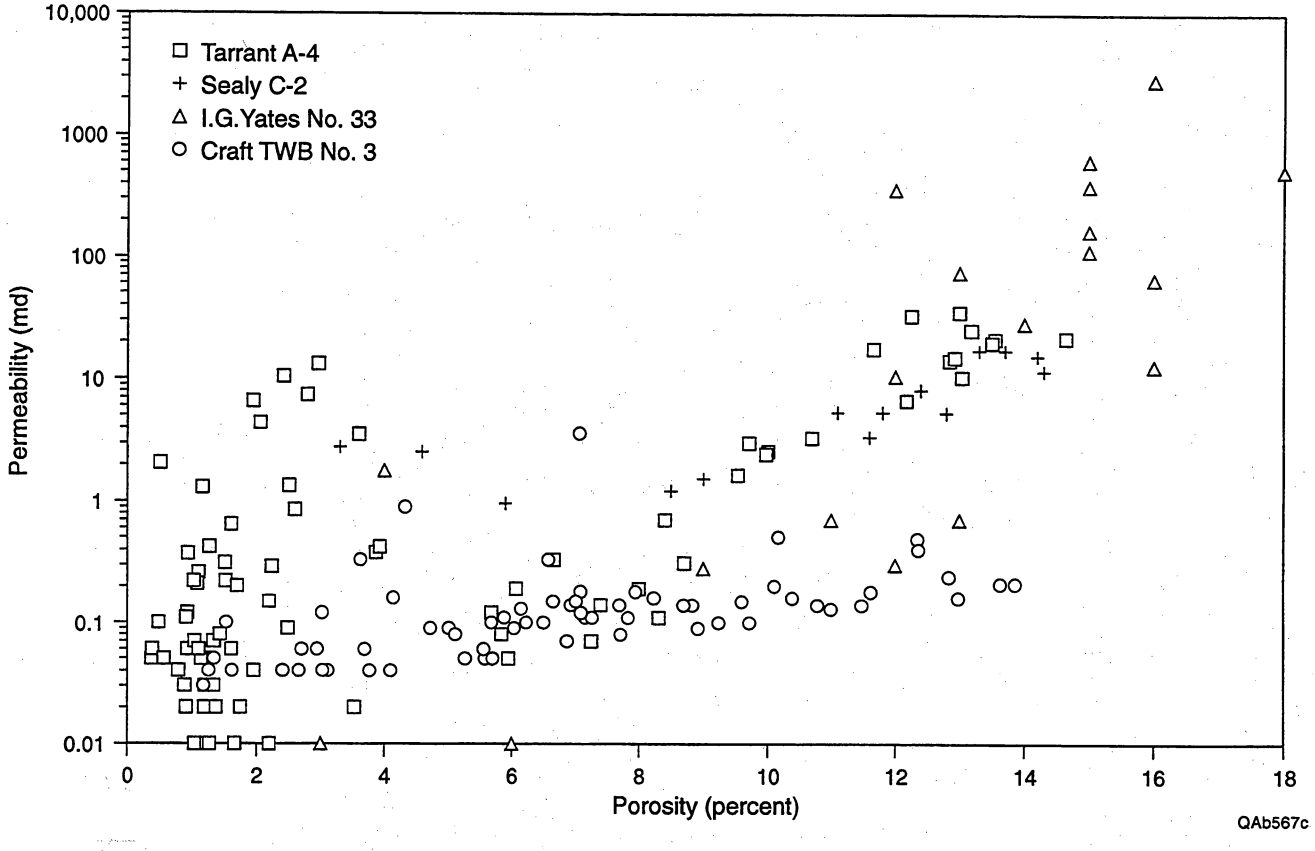

Figure C2. Porosity vs. permeability cross plot of all sample plugs from the four cored wells. The color coding indicates the well from which each plug was taken.

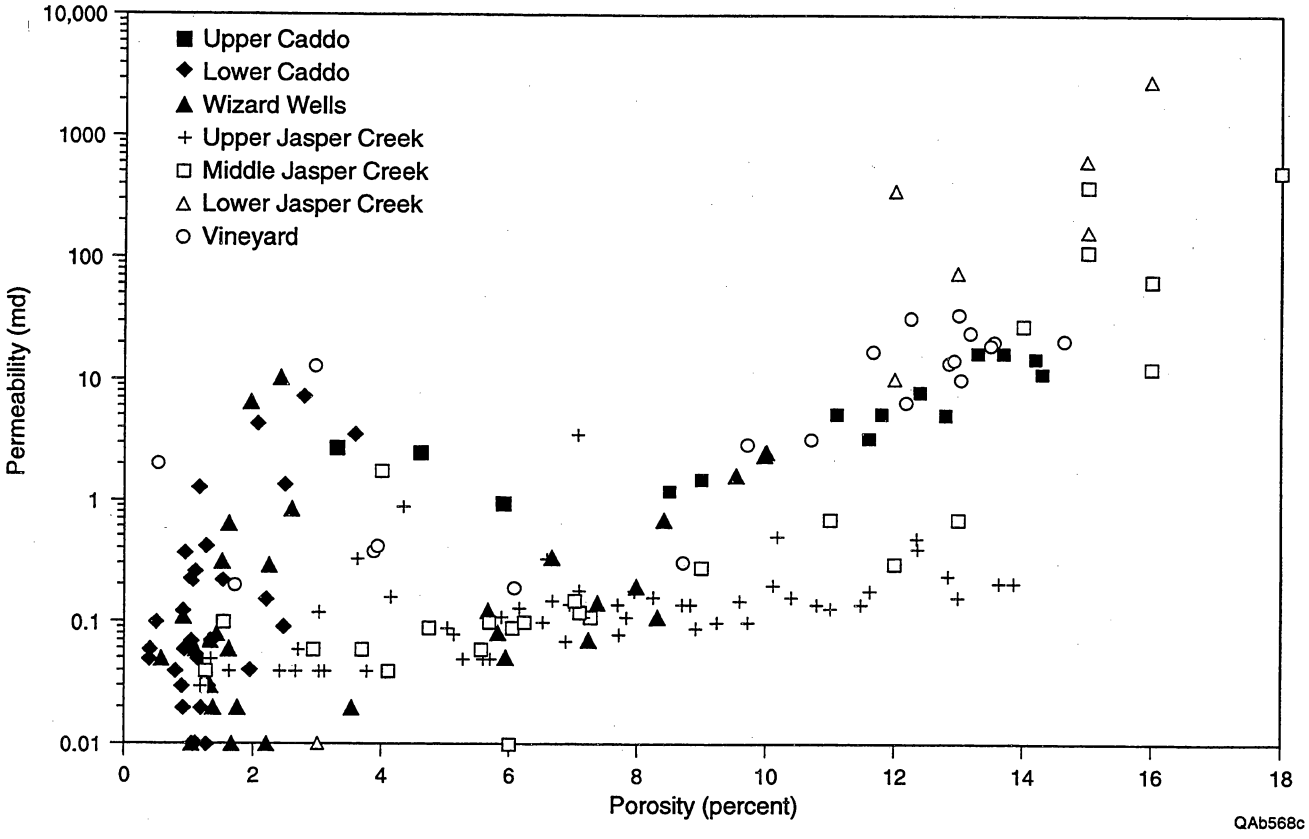

Figure C3. Porosity vs. permeability cross plot of all sample plugs from the four cored wells' zones. The color coding indicates the zone from which the plugs were taken.

system of WorkBench, and appropriate API numbers were attached to each. The log data could then be entered for each well.

The log data were plotted to compare with the original paper logs and checked for digitizing quality. Any editing of the data was then done interactively on the graphic screen or by keyboard entering of data revisions. All the required header data from the logs were also entered into WorkBench. This included information on tool types and wireline vendor. This information was used later by the system for automatic environmental corrections and other operations.

SP base line shift

The Spontaneous Potential (SP) curves were compared for amplitudes, and the variations for sand and shale amplitudes were examined. All wells that penetrated the Bend Conglomerate had at least one sand that was clean and seemed to provide the amplitude of a clean sand for the SP. These wells often had the best sand development for the SP in the Vineyard zone at the bottom of the Bend sequence. Some wells penetrated only the Caddo zone, and, in these cases, the SP examination included the Strawn sequence above the Bend Conglomerate. The SP curves were straightened (i.e., the steady drift to the right was removed) through the Bend Conglomerate sequence for all the wells. The SP curves were then all rescaled to fall into the range of –100 to 0 millivolts. The SP curves needed to be set to the same scales so that meaningful cross sections could be produced in either Stacked Curves or WorkBench. In addition, the facies analysis from logs required all the curves to be normalized (see section after next).

Depth Shift

For wells than had multiple runs, the various runs were depth-shifted to match the resistivity suite to the nearest foot. This was done using sophisticated automatic depth-

shift algorithms in WorkBench. The results of this process were then displayed on the screen for visual verification. In the event that editing of the depth shifts was required, it was done interactively.

Normalization

Many neutron and density curves were found to disagree from one well to another. Crossplots of neutron and density curves were made for each well and then compared with each other. Patterns of lithological origin were easily recognized and showed clusters around tight limestones, clean gas-filled sandstones, and marine shales. Other clusters were recognizable, but either were not present in all wells, or doubt existed as to whether they were a consistent lithological facies across the field. All clusters that could be associated with a known lithological origin were then used for calibration.

Many of the wells gave essentially the same patterns for the calibration clusters, so these values were assumed to be correct and were chosen to be the standard crossplots. The well logs were checked for these wells, and the calibration tails (where available) all showed that these logs had been properly calibrated. The crossplots that deviated from the standard crossplots were then shifted linearly along the density axis and/or the neutron axis to fit the standard. These shifts were then applied to the raw data in the data base for the same well. Some shifts were as high as 10 porosity units. Generally Halliburton and Western Atlas logs required more of this recalibration than did Schlumberger logs.

No attempt was made to normalize the gamma-ray logs (except one well that was obviously grossly miscalibrated in the field). Because the gamma-ray shale and clean sand values were to be picked individually for each well at analysis time, the normalization of the gamma-ray curve was deemed unnecessary.

Environmental Corrections

WorkBench contains all the environmental correction charts for all major wireline vendors. This module corrects neutron, density, and gamma ray data for borehole effects such as temperature, pressure, mud, and washout.

The resistivity data were corrected through the appropriate charts and then used in tornado chart calculations to find a true resistivity of the virgin zone (Rt) and a resistivity of the flushed zone (Rxo), in instances where three or more resistivity curves existed. If only one or two curves existed, the deepest curve was assumed to equal Rt (this is the case on most of the old IES logs).

Dual-Water Method

Examination of the core data indicated that the Bend Conglomerate is composed mostly of fluvial sands and shales, with considerable carbonate material in the form of cements. In addition, marine shales and pure limestones are present. In order to determine the most accurate water saturations, the dual-water method was adopted. The dual-water method accounts for the electrical conductivity of the shales by assuming that the shales are porous and their pores are filled with salty water that may have a salinity different from that of the connate water. A diagrammatic representation of the dual-water model is shown in Figure C4.

Shale porosity is filled with water known as bound water. The resistivity of this water is Rwb. The water in effective porosity (the producible porosity associated with the sands) is filled with free water and any hydrocarbons that may be present. The free water is the same as connate water and has a resistivity of Rwf.

For a rock that has no hydrocarbons, the resistivity of the rock is Ro. Using the dual-water method, this value can be calculated from the equation

$$Ro = a * (Rwf * Rwb) / ((Rwb + Vsh * (Rwf - Rwb)) * PHIT ** m), \qquad (C\text{-}1)$$

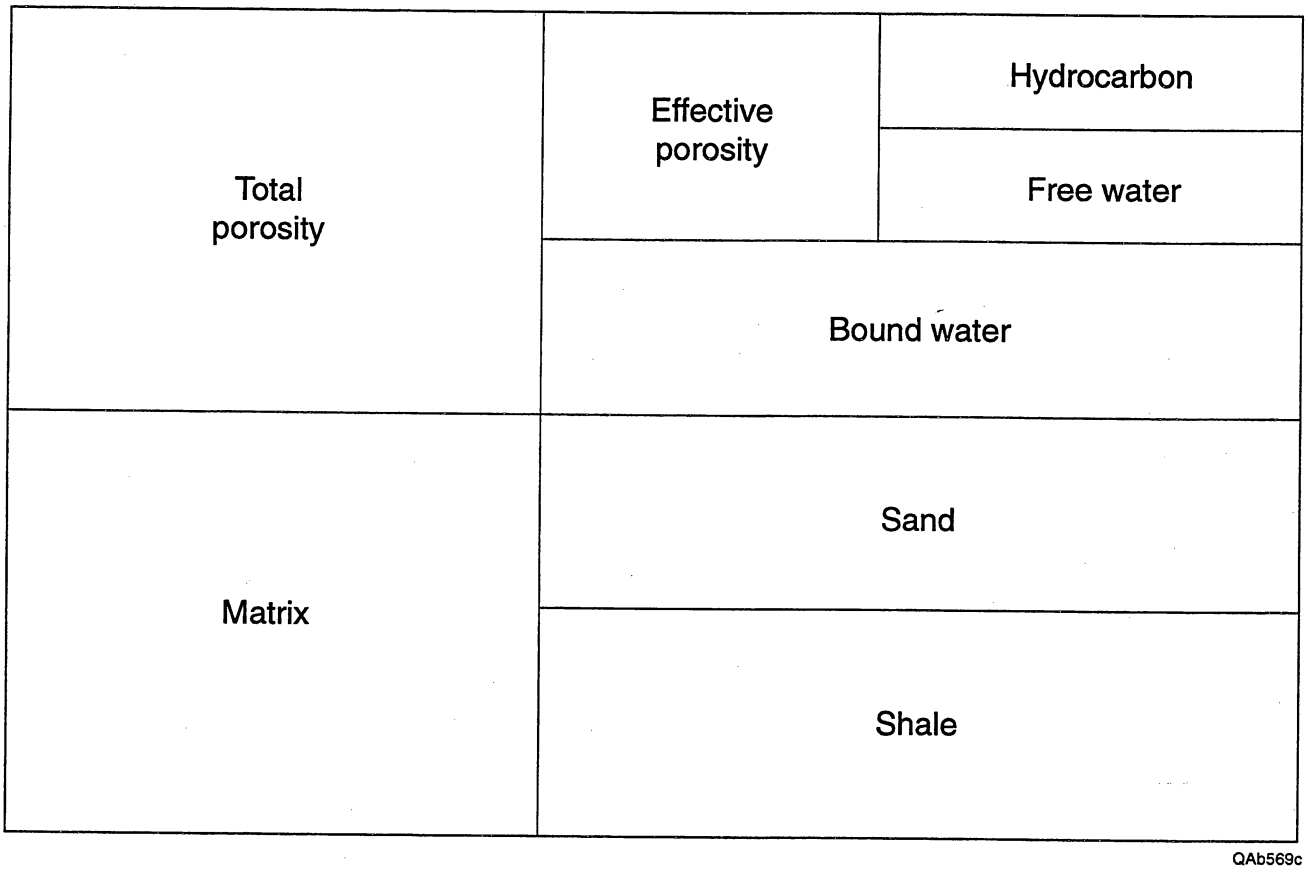

Figure C4. Diagrammatic representation of the dual-water model used to interpret resistivity data for water saturation.

where a = the Archie constant, m = the Archie exponent (cementation exponent), Vsh = the proportion of the matrix that is shale, and PHIT = the total porosity. For this study, Archie parameters were given the values a = 1.0 and m = 2.0.

Total porosity (PHIT) was found to be approximately 15 percent in both the sands and the shales. A lower value of PHIT was found in the carbonates. The observation that the value of the total porosity is constant for the sands and shales has been found to be true in many formations. This observation makes it possible to interpret old wells that have only resistivity logs with reasonable accuracy. This procedure is described in the next section.

IES/ES analysis

Introduction

In fields such as Boonsville that were discovered before the invention of neutron, density, and sonic tools, wells were logged only with resistivity tools. Of the 221 wells used in this study, 55 percent were from older wells that only had resistivity information. Only 45 percent of the well logs could be interpreted for porosity, water saturation, and lithology using standard log analysis techniques. This restriction on the number of interpretable wells represents a limitation in complex clastic reservoirs; therefore, a method had to be developed to interpret the old wells that only had IES logs.

A computer program was developed to interpret induction (IES) logs having deep induction, short normal, and spontaneous potential (SP) curves. The method was developed to interpret zones that consist of three major lithologies: (1) shale, (2) clean, productive sandstone, and (3) tight, carbonate-cemented sandstones and siltstones.

Where possible, the logs must be used to determine the presence of productive sands (along with their characteristics such as porosity, water saturation, etc.) and to understand their structural and stratigraphic settings. Any log analysis that can determine lithologies

and porosities is therefore very valuable. When operators learn to interpret wells containing only resistivity logs, the number of interpreted wells available for geological modeling of the Bend formation in Boonsville field can be more than doubled. The same is true for many other Midcontinent clastic reservoir systems.

Description of the Petrophysical Analysis Technology

A program was developed using a well that had a complete suite of modern well logs. First, the well was interpreted using a standard interpretation program that took advantage of all the curves, including density (RHOB), lithodensity (PEF), and neutron (PHIN) curves. The same well was then interpreted using the new IES technique and recalibrated until the results matched the original analysis as closely as possible. The technique was subsequently used on other wells that had full modern logs. Without any further calibration, the results in these check wells were excellent, indicating that the technique could now be used with confidence in wells having only IES log suites. An example of one of the check wells is illustrated in Figures C5 through C7.

The program uses only two curves: the spontaneous potential (SP) and the deep induction (RILD). From these curves, we calculate the relative proportions of three lithologies, the porosity, and the water saturation. The program uses a dual-water model and assumes that the total porosity (PHIT) is constant through the zone(s) of interest. The total porosity (PHIT) is made up of effective porosity (the porosity associated with productive sands and containing connate water and possibly hydrocarbons) and shale porosity (nonproductive pore space in the shales that contains the bound water). The three lithologies that the program calculates are (1) clean sandstone with porosity, (2) clean calcite cemented (tight) sandstones and (tight) limestones, and (3) shale.

Clean sandstone has porosity and permeability and, therefore, is readily detected by the SP curve. The equations to determine the amount of clean sand and porosity are:

$$VSHS = (SP - SPCL)/(SPSH - SPCL), \qquad (C\text{-}2)$$

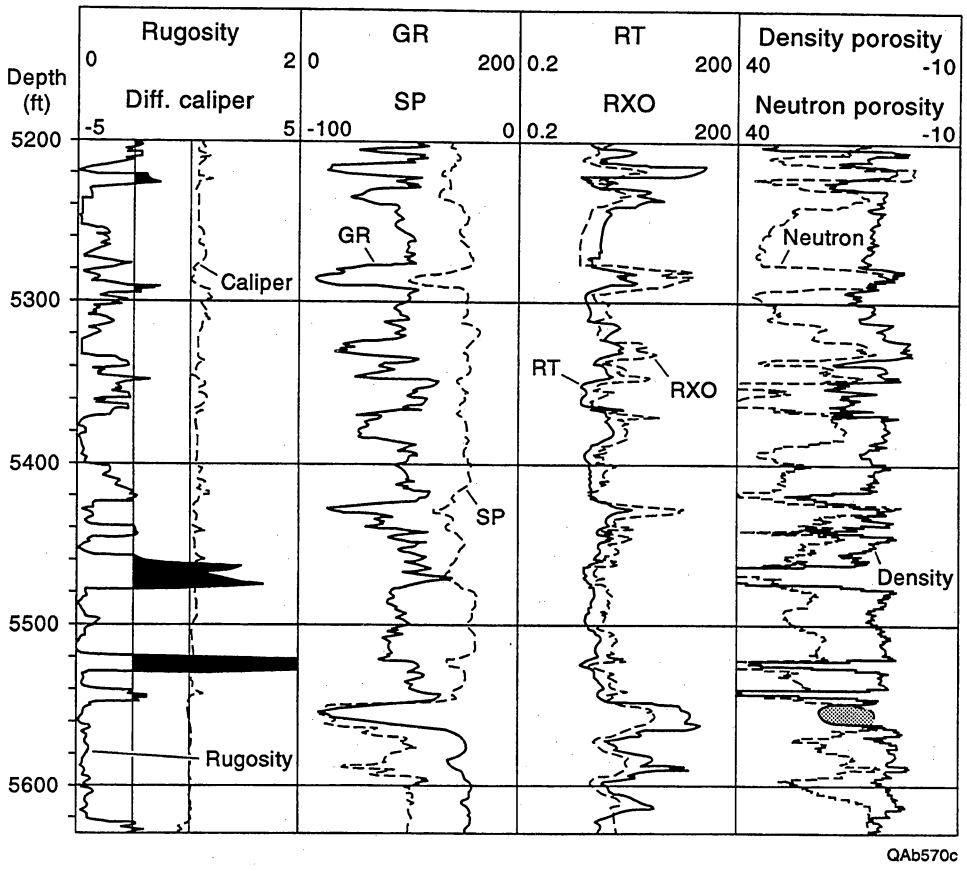

Figure C5. Raw log data from one of the test wells used to develop the IES log-analysis technique. The well is the OXY Tarrant A-4 in the Boonsville project area. The left track contains the caliper and its related bit size curve, in addition to a rugosity curve (shaded above a value of 0.5), which is computed from the caliper. The second track contains an SP curve (generally to the right) and a gamma-ray curve. The third track shows the resistivity curves. The fourth track shows the density porosity (to the right) and the neutron porosity curves. Note that they cross over (shaded area) at a depth of around 5,550 ft.

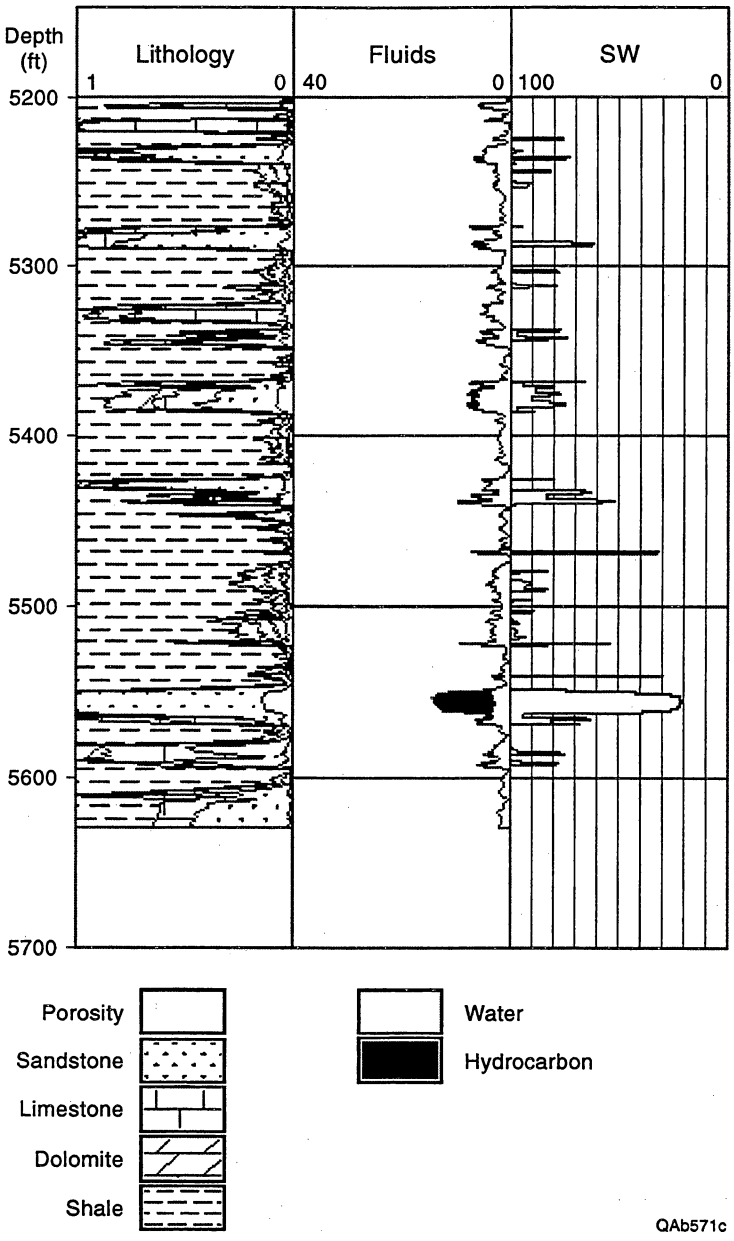

Figure C6. Log interpretation of the Tarrant A-4 well using all available curves in a standard log analysis. The lithology track indicates the proportions of shale, sandstone, calcite, and dolomite. The fluid track shows effective porosity with the hydrocarbons and the water. Water saturations are shown in the fourth track. Note the porous sand at about 5,550 ft, the many tight carbonate cemented sands, and the limestone at about 5,220 ft.

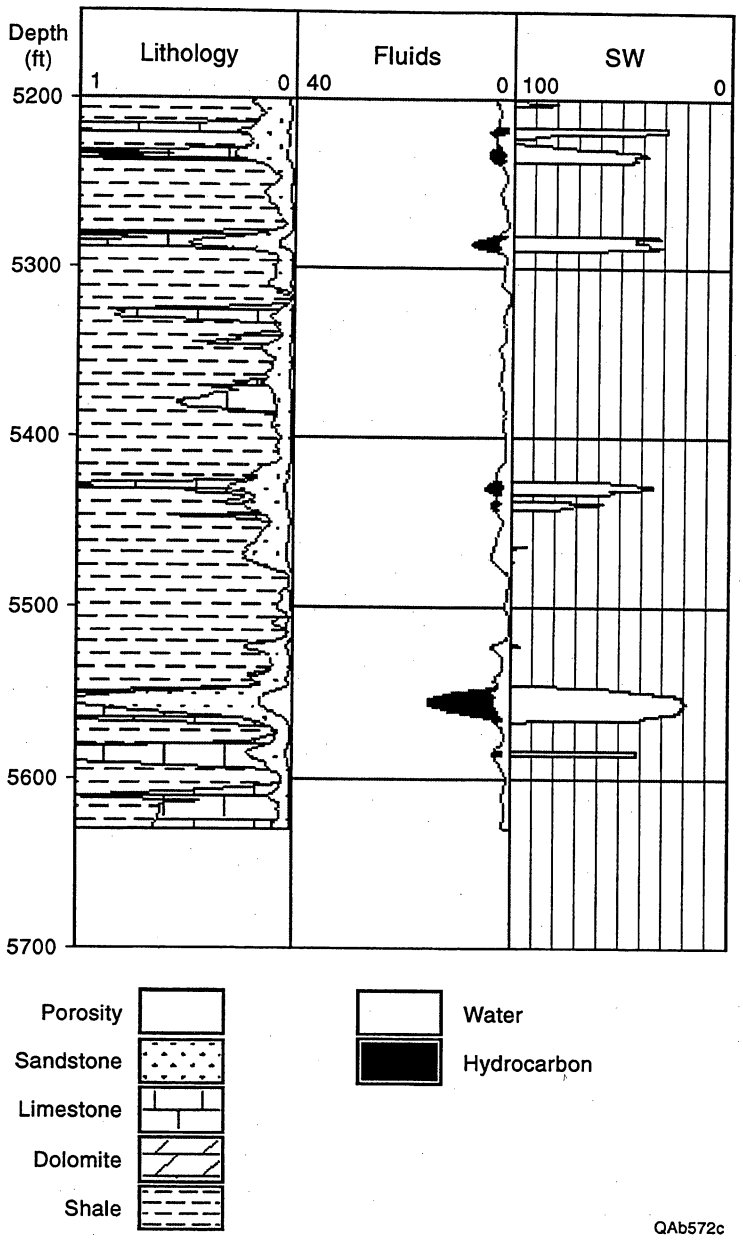

Figure C7. Log interpretation of the Tarrant A-4 well using only the SP and deep resistivity curves in the IES log analysis. Note the porous sand at about 5,550 ft and compare it with the interpretation in Figure C6. Also note that most of the carbonate cemented sandstones shown in Figure C6 are also being found by the IES log-analysis technique.

$$PHIE = PHIT * (1 - VSHS), \text{ and} \quad \text{(C-3)}$$

$$SAND = 1 - PHIE - VSHS, \quad \text{(C-4)}$$

where SPCL = the clean sandstone value for the SP, SPSH = the shale value for the SP, PHIE = the effective porosity, which is the porosity that has the potential to contain movable fluids, PHIT = the total porosity, which must be estimated from nearby wells in the same formation and is generally taken as the maximum value of porosity in the nearby well, SAND = the amount of clean sandstone, and VSHS = the volume of shale in a sand.

Note that estimating the total porosity is a critical step. Total porosity can be determined by performing log analysis on any nearby wells that have neutron and density curves. The maximum PHIE calculated for these wells may be used for the PHIT value in the above equation. Analysts must be careful about using porosities measured by the neutron/density logs in washed-out shales; these are probably too high and will give a false value for PHIT. In the Bend Conglomerate formations, a value of 15 percent was often used during the SGR study. An alternative approach is to use any available core data and to take the maximum value of porosity found in the core analysis for PHIT.

The SPCL value is usually the minimum value of SP found in the zone. The well being studied must have at least one clean sand to obtain a valid interpretation. If the best sand is known to be partially contaminated by carbonate cement, then a lower value of SP must be estimated for the SPCL value.

The second formation type (tight limestones and tight carbonate cemented sandstones) is more difficult to find. Generally these rocks will have no SP response because they have no porosity, but they should have a resistivity higher than the value seen in the shales. The proportion of this facies is determined by:

$$VSHR = 1 - ((RILD - (RSH + 1)) / 12, \quad \text{(C-5)}$$

$$VSH = MIN(VSHS, VSHR), \text{ and} \quad \text{(C-6)}$$

$$CARB = 1 - SAND - VSH - PHIE, \quad \text{(C-7)}$$

where RSH = the value of the deep resistivity in the shales, VSH = the volume of the shale, and CARB = the volume of the carbonate-cemented sandstones.

Note that the numerical divisor in the VSHR equation (the value 12) works well in Boonsville field. In other fields in North and South America, this term can vary from 10 to 20, but is usually close to 12.

Water saturation is then calculated using the dual-water method. This method calculates the theoretical resistivity of the rock as if the rock were 100-percent wet (Ro) as follows:

$$Ro = 1 * (RWF*RWB)/((RWB+VSH*(RWF-RWB))*PHIT^2), \quad \text{(C-8)}$$

where RWF = connate water resistivity, and RWB = resistivity of the bound water (shale water). The program assumes a value of 1.0 for the Archie parameter "a" and a value of 2.0 for the Archie cementation exponent "m."

RWF and RWB are determined by looking at a calculated curve of Rwa. This curve is generated as part of the initial run in the program and is given by the relationship

$$Rwa = RILD * PHIT^2, \quad \text{(C-9)}$$

assuming that a=1 and m=2 for the Archie parameters. RWF is then the Rwa value in a clean wet sand and RWB is the average Rwa value in the pure shales.

Water saturation can now be calculated from the ratio of Ro to RILD.

$$SWR = (R0 / RILD)^(0.5) . \quad \text{(C-10)}$$

Two versions of this IES technique have been programmed—one version for the Macintosh computer and one for Windows 3.1 on MS-DOS computers. These programs are stand-alone versions that will read LAS format files that contain SP and deep resistivity curves and interpret these curves using the technique just outlined. The computed results are displayed on the screen and are also written into an LAS format file for use in other applications. Both source code and executable versions of the IES algorithm may be obtained from GRI or by contacting Robert Elphick with Scientific Software-Intercomp in Denver, Colorado.

ES Logs

ES logs consist of three resistivity measurements: the lateral log (LAT), the short normal (SN), and the long normal (LN). The lateral curve is eccentric and can be used to estimate true resistivity of a sandstone only if the thickness of the bed is at least five times the length of the tool, and the sandstone is homogenous (in terms of its porosity and water saturation). Because the lateral tools were 18 ft, 8 inches long, this requirement means that sandstones would have to be greater than 100 ft thick. Sandstones in the Bend Conglomerate are not this thick and are not homogeneous.

Two different techniques were used to calculate true resistivity from lateral logs. Both techniques involved the use of commercially available computer programs. The first is the ES-LOG program developed as part of a separate GRI research effort and marketed by Walt Whitman Software, Inc. This system performs forward modeling and inversion. The forward modeling generates synthetic logs from a specified Earth model, and the inversion algorithm interprets the logs and builds an Earth model. The program can run on an MS-DOS computer but is CPU intensive and runs better on Unix workstations (such as DEC and IBM RS-6000 series computers). For further information on this software contact

Kent Gestring
Walt Whitman Software, Inc.
12600 West Colfax Ave., Suite A270
Lakewood, Colorado 80215
Phone: (303) 237-2523
Fax: (303) 237-3589

The second technique was the Old Electric Log Advisor (OEA) marketed by The Logic Group. This system uses a knowledge engineering approach to help the user estimate true resistivity in each sand. The knowledge data base was provided by

Dr. George Asquith of Texas Tech University, a petrophysicist with many years of experience using ES logs. Further information on this product can be obtained from

Diane Zbranak

The Logic Group

P.O. Box 50499

Austin, Texas 78763

Phone: (512) 451-5707

Fax: (512) 451-2300

The OEA technique lacks an inversion capability but runs fast on an MS-DOS computer. Generally all the sandstones in the Bend Conglomerate for one well could be computed in 1 or 2 h with OEA, whereas the ES-LOG program would run for 20 to 30 h on an RS-6000 to interpret 200 ft of data.

Because the normal logs are symmetrical and easier to understand, we looked at the long normal to estimate true resistivities. As a first approximation, the long normal reads true resistivity where the sandstones are reasonably homogeneous and at least 6 ft thick.

Modern Log Interpretation

Introduction

Nearly half the wells in the study area had neutron and density tools. The combination of neutron and density tools allows analysts to obtain good estimates of the total porosity. In addition, these curves are useful for estimating the lithology of the formation. The method used was also capable of using the photoelectric effect (PEF) curve when it was available.

The analysis of the wells having at least neutron and density curves was performed first. These wells were then used to calibrate the IES and ES logs as described in the previous section. Interpretation began with the wells that contained core data. The

porosity/permeability data, along with the IR lithology data, were used to calibrate the log-analysis technique and to refine the program and parameters used for the remaining wells.

Log Analysis

The log analysis begins by calculating the volume of shale from the SP and/or the gamma ray using the normal routines

$$VSHG = (GR - GRCL) / (GRSH - GRCL), \text{ and} \quad \text{(C-11)}$$

$$VSHS = (SP - SPCL) / (SPSH - SPCL), \quad \text{(C-12)}$$

where VSHG = shale volume calculated from the gamma ray, GR = gamma-ray value, GRCL = gamma-ray clean value chosen in the cleanest sandstone, GRSH = gamma-ray value chosen in a marine shale, VSHS = shale volume calculated from the SP, SPCL = SP value chosen in a clean sandstone, and SPSH = SP value in the shales.

These values are averaged together and an S curve modifier applied. Two other options available in the program allow the use of spectral gamma-ray data, when available, and the neutron/density curves as shale volume estimators. Neither of these options were used for this study because no spectral gamma-ray data were available and the neutron/density data are confused by the presence of carbonates and bad hole.

The presence of bad hole is determined by looking at the caliper, rugosity, and density curves. The rugosity curve is produced by the environmental correction submodule and determines the rate of change of the caliper. The sidewall tool (density) is more prone to be incorrect when the hole size is changing than when the hole size is large but constant. The density is also used to determine bad-hole conditions because the curve tends to read very high porosities (low bulk densities) when the tool pad cannot make good contact with the side of the hole.

Once bad-hole conditions have been detected, the density is modified on the assumption that the shale volume calculation and the neutron reading are correct (not true

at rare, extreme, bad-hole depths). In shaly sands, the position of the neutron and density points on a crossplot is determined by the amount of shale at a given depth. When bad-hole conditions are encountered, the density moves down in the plot along a line of constant neutron porosity until it reaches the appropriate shale volume line (see Figure C8).

After total porosity is calculated from the neutron–density, a gas-correction algorithm is then applied to account for any gas that is present.

Once the value of the ideal resistivity in the water-filled rock (Ro) is calculated using the dual-water model (see section on Dual-Water Model earlier), this value is compared with the value for Rt, and the water saturation is calculated from the ratio. The effective porosity (porosity of the sand that is capable of giving up fluids) is then calculated as follows:

$$PHIE = PHIT * (1 - VSH), \quad \text{(C-13)}$$

where PHIE = effective porosity (in fractional units), PHIT = total porosity (in fractional units), and VSH = calculated shale volume (in fractional units). Some aesthetics are applied to the water saturation and porosity curves to reduce ridiculous answers in unstable situations.

The lithology is calculated using three algorithms. One algorithm is used when only neutron and density data are available; a second is used when a PEF curve is available. The third algorithm uses the resistivity data to determine the presence of calcite-cemented sandstones and silts when the other techniques fail to find them; this is the same technique used in the IES method described above.

Apparent grain density is calculated from the original bulk density measurement and the total porosity:

$$RHOG = (RHOB - RHOF * PHIT) / (1 - PHIT), \quad \text{(C-14)}$$

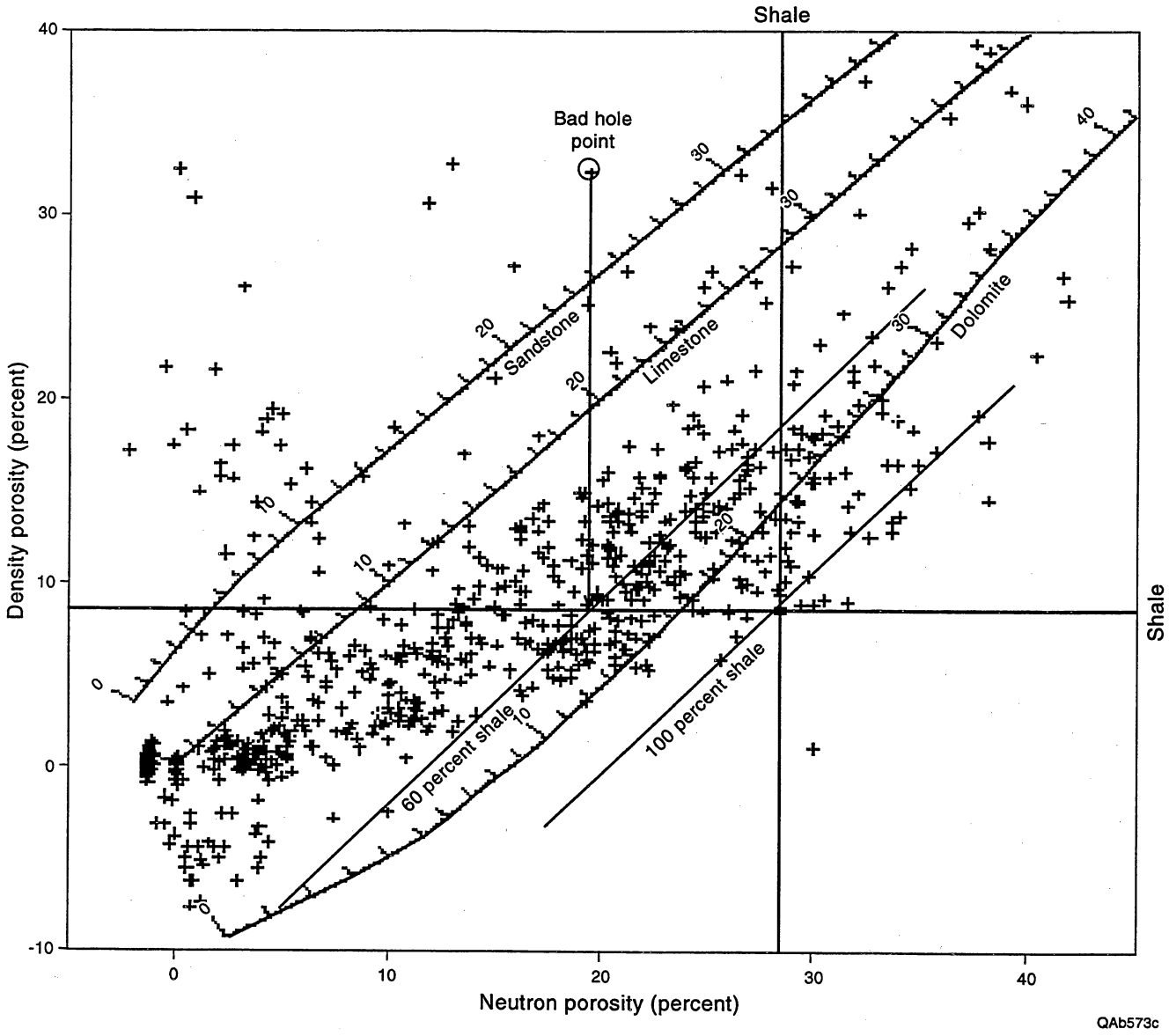

Figure C8. In bad hole, a density point is relocated along the line of the neutron porosity value until it intercepts the appropriate shale volume value. In this example, the shale volume has been calculated from the gamma-ray log to be about 60 percent.

where RHOG = apparent grain density, RHOB = bulk density from the log in g/cc, RHOF = the density of the fluid in g/cc (1.0 g/cc), and PHIT = total porosity in fractional units.

This value is then corrected for shale to give the value of the nonshale matrix. Using logs, we can determine only two or three minerals when only two curves are being used to differentiate them (in this case the neutron and density). Only three minerals are therefore determined: sandstone, calcite, and dolomite. In this case, the dolomite represents all the heavy minerals present in the Bend Conglomerate. The minerals are determined for only two possibilities—either sand/calcite (when the RHOG value is less than 2.71 g/cc) or calcite/ dolomite (when the RHOG value is above 2.71 g/cc).

When a PEF curve exists, an arbitrary variable, U, is calculated from the PEF and RHOB curves using equation C-15. This equation is the definition of U.

$$U = PEF * (RHOB + 0.1883) / 1.0704, \qquad \text{(C-15)}$$

where RHOB = bulk density from the log in g/cc. The apparent U value of the matrix is then calculated from

$$UMA = (U - UF * PHIT) / (1 - PHIT), \qquad \text{(C-16)}$$

where PHIT = total porosity in fractional units, and UF = fluid value of U. The relative proportions of four minerals present are then determined from the UMA/RHOG crossplot (see Figure C9).

Summations

Once the log analysis was completed over the Bend Conglomerate in each of the wells, markers representing the surface boundaries for each of the critical zones were entered into the log-analysis program, and layers were defined on the basis of these markers. Summations were then run for both net reservoir (using a shale volume cutoff and a porosity cutoff) and net pay (using shale volume, porosity, and water saturation cutoffs) for each layer.

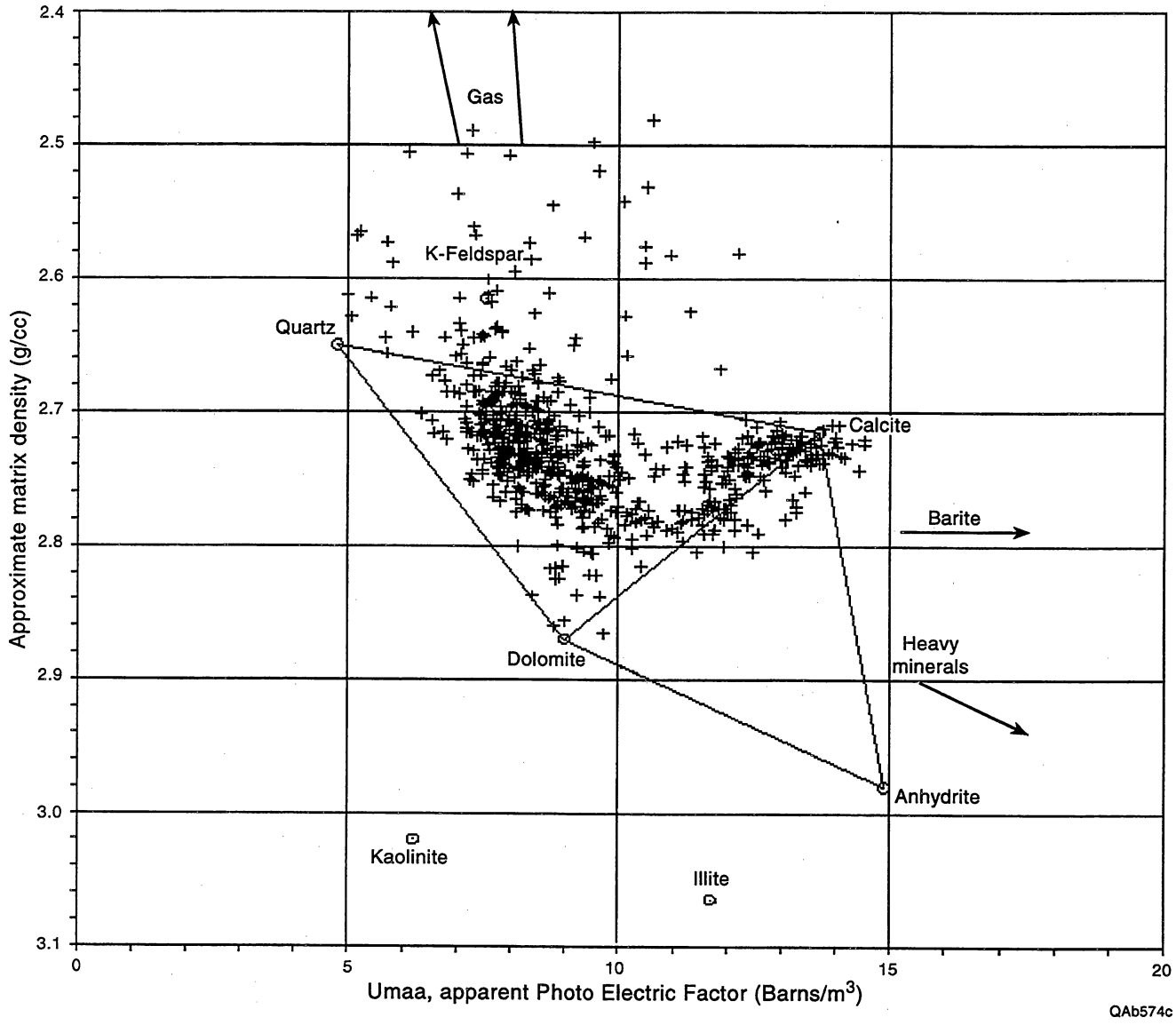

Figure C9. Cross plot of UMA/RHOG used to determine the proportions of up to four minerals in the rock.

Cutoffs

The shale cutoff parameter was chosen to remove any shaly sections that may have too high a porosity calculation due to bad-hole conditions. Bad-hole conditions usually occur in the shalier zones and cause the density logs to read a porosity that is too high. Although the log-analysis program attempted to correct the density reading in these circumstances, the correction was not always successful. A value of 50 percent was chosen for the shale cutoff. For the most part, the porosity cutoff was much more severe and was the parameter that determined whether a data point was selected. Generally the shale cutoff parameter had no effect except to eliminate the occasional bad-hole data.

The porosity cutoff was chosen by examining the porosity versus permeability crossplots made from the core data (see Figures C2, C3, and C20). The permeability cutoff was difficult to determine, but the producible E and E2 sand facies seemed to occur with permeabilities down to about 0.05 md. From the crossplots, this value corresponds to a porosity of 4 percent for both the E and the E2 facies. A value of 4 percent was therefore chosen for the porosity cutoff. A water-saturation cutoff of 60 percent was also used in the net pay summation calculations.

The results of the summation calculations were then used to map the sand characteristics for each of the layers. The net reservoir hydrocarbon pore-volume maps indicate varying hydrocarbon distribution within each layer. These net pay and net reservoir summations were also used extensively in the engineering analysis (see Appendix B).

Facies Determination

Introduction

When facies vary rapidly across a field, defining well-to-well correlations can be difficult. The Bend Conglomerate stratigraphy is complex, and establishing correct correlations is essential to identifying the compartments within the section. Stratigraphic correlations are traditionally done by positioning all, or some, of the wireline curves in a cross-section format and identifying certain curve patterns as belonging to given facies. This type of correlation is easier when all of the logs are of similar types and are presented on similar scales. Nonetheless, identifying various facies from pattern recognition alone is often difficult.

Pattern recognition software designed to identify facies has existed for a number of years. Most of these packages involve sophisticated stochastic techniques and often provide impressive results when applied by skilled users. A principal component analysis technique was used by the analysis team, with the results being good when applied to well logs of similar curve suites but inconsistent when applied to nearby wells that had radically different log suites.

Therefore, a deterministic method for recognizing facies from logs was developed for use in the Bend Conglomerate. Several different approaches were attempted until the final system was chosen. Although the original technique was developed on a Macintosh, it was transferred to the Stacked Curves program to take advantage of its geocolumn display capabilities. Five models were constructed for each of the possible curve suites that we wished to use. Table C3 shows which curves were set up as input data for each of these five models.

Table C3. Log curves used to construct petrophysical models.

MODEL	Res	GR	PEF	NPHI	RHOB
FaciesR	•				
FaciesG	•	•			
FaciesU	•	•	•		
FaciesN	•	•		•	•
FaciesP	•	•	•	•	•

The Res column refers to the suite of resistivity curves: SP, deep resistivity, and shallow resistivity curves. These curves were used in all the models.

Methodology

The facies technique is based on determining the ideal response for each log curve in each facies. The ideal responses were obtained from the cored intervals of the four cored wells. The logs for these cored intervals were shifted to the core by matching the porosity from core to the porosity calculated from the logs. Histograms were then built for each curve in each facies—a total of 84 histograms because only seven curves were used. Many of the histograms provided a well-defined peak, but others were less well defined, and so some judgment had to be used to find the best value. Two examples of well-defined peaks are shown in Figures C10 and C11. An example of a less well defined peak is shown in Figure C12. The poorer quality peaks are associated with the nearness to a bed boundary (most of the logs used have about a 2-ft vertical resolution and therefore do not respond immediately to bed boundaries) or to hole washout as determined by the caliper and/or the rugosity curves. Table C4 shows the values for the curves in each facies that were chosen from the histograms. These values were used in the programs developed to find the facies from the logs.

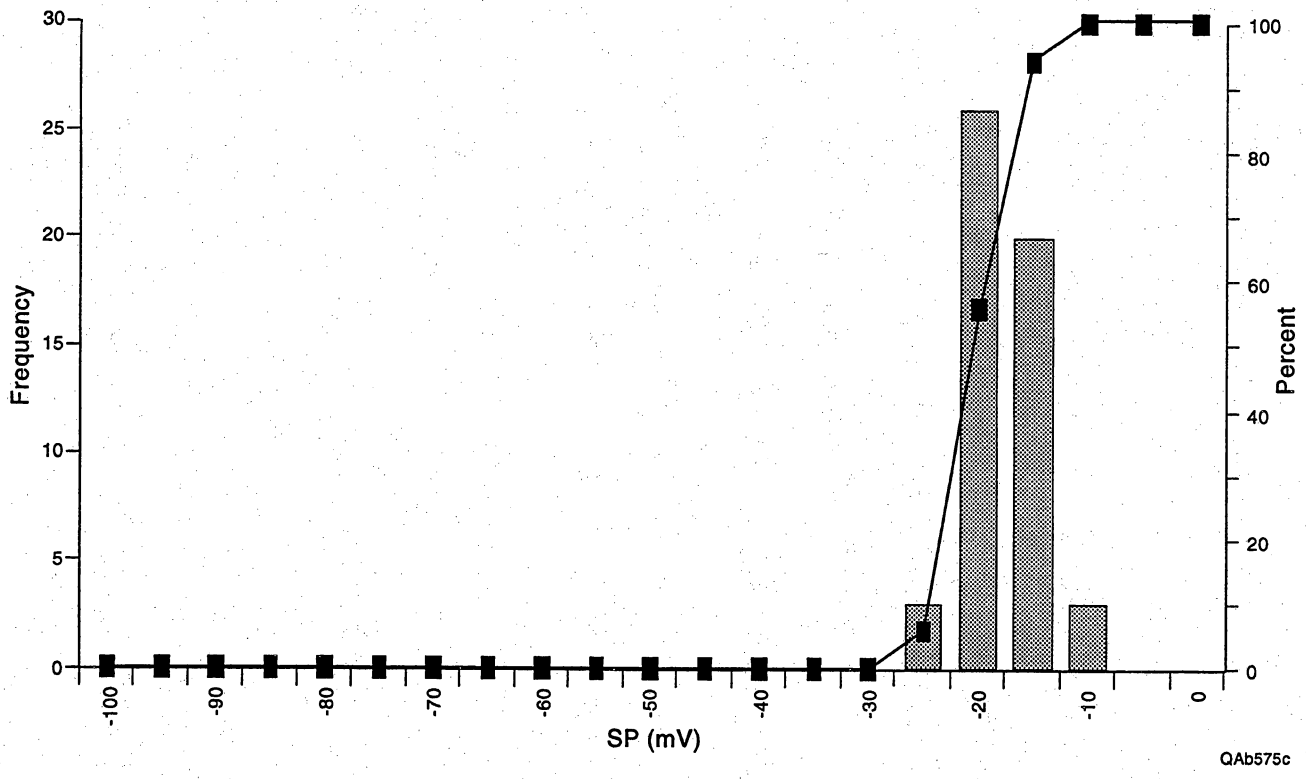

Figure C10. Histogram of the SP curve in the "A" facies.

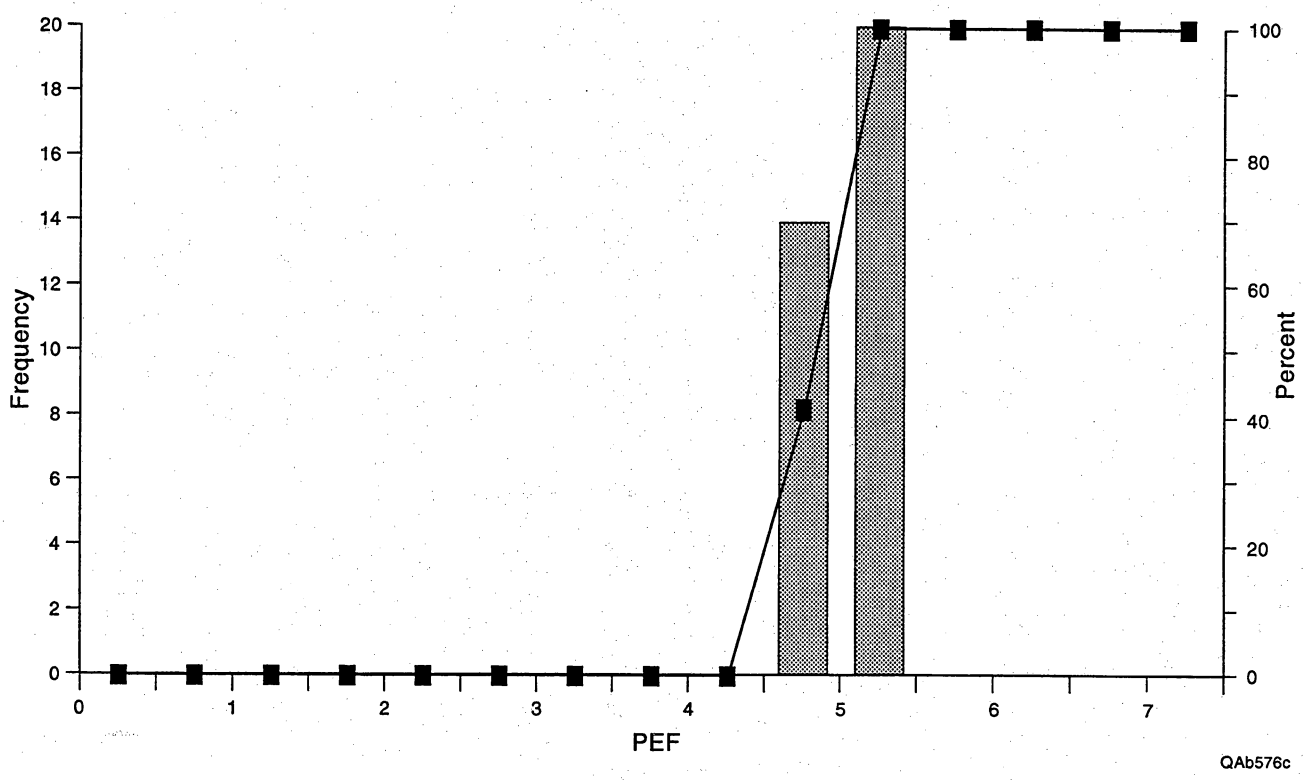

Figure C11. Histogram of the PEF curve in the "K" facies.

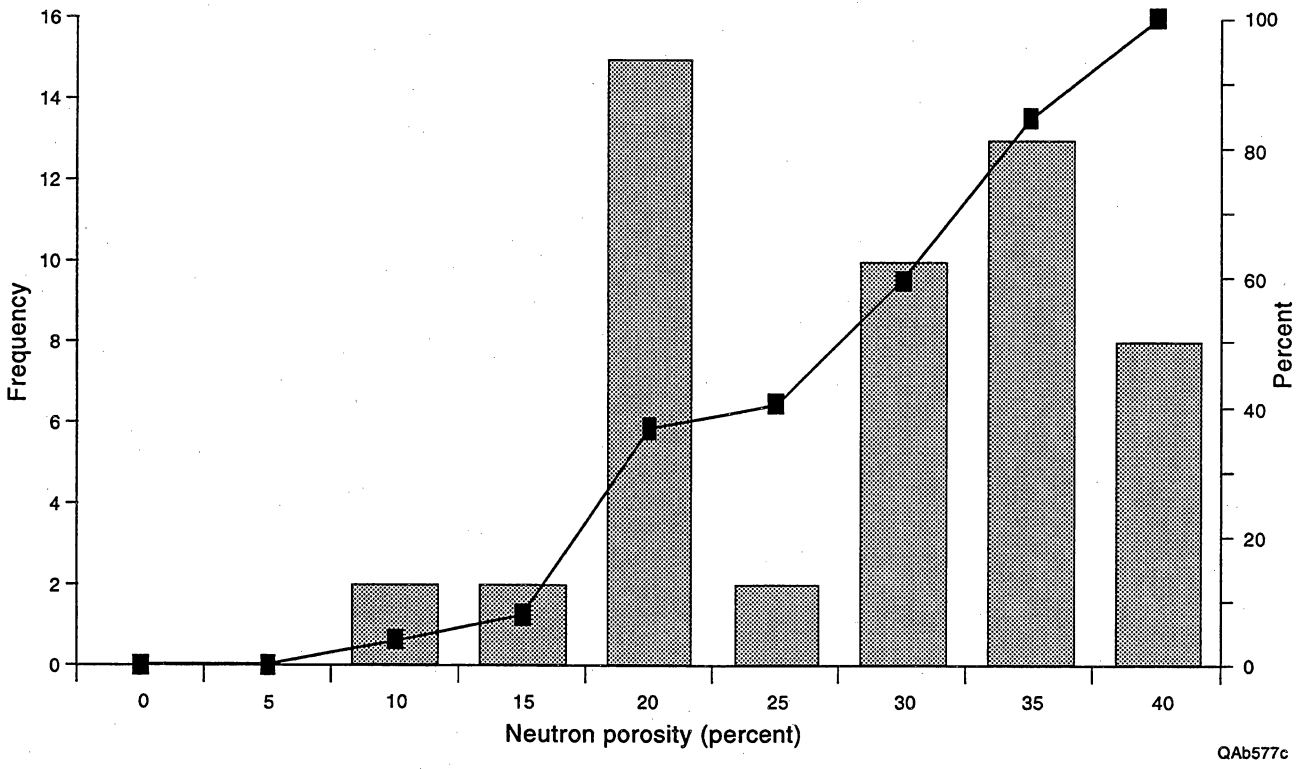

Figure C12. Histogram of the neutron curve in the "A" facies.

Table C4. Ideal values for each curve in each facies, as chosen from histograms of these data sets.

Facies name	Facies no.	NPHI	DPHI	RHOB	PEF	GR	SP	Res deep	Res shal.
A	2	0.36	0.16	2.44	3.9	125	–15	3	7
B	3	0.30	0.08	2.57	3.2	105	–10	7	9
C	8	0.18	0.04	2.64	3.5	90	–10	15	9
D	15	0.05	0.03	2.66	3.5	60	–15	25	25
E	20	0.08	0.15	2.45	2.2	45	–80	60	200
E2	18	0.13	0.12	2.51	2.4	58	–40	20	90
G	6	0.20	0.10	2.54	4.0	115	–20	4	5
G2	9	0.20	0.08	2.58	3.5	102	–18	10	15
H	4	0.28	0.12	2.51	3.5	125	–15	7	10
I	13	0.10	0.05	2.63	3.2	88	–20	9	10
J	10	0.11	0.03	2.66	3.5	90	–15	9	10
K	17	0.02	0.02	2.68	5.0	60	–25	55	300

The programs are set up to determine the difference between the ideal value of a curve for each of the 12 possible facies (see Table C1) and its actual value. The differences for each curve are added up and then divided by the number of curves used by the program. This difference then represents the error function for each facies.

$$errorf = [\ Nc * (\ Logc - Ic\ )\ ], \qquad \text{(C-17)}$$

where errorf = total deviation from the ideal facies f, Nc = normalization for curve c, Logc = the log value of curve c, and Ic = the ideal value of curve c in facies f. The program then finds which of the facies has the smallest error function (errorf) and selects that facies for the depth being calculated. The procedure is continued for each depth.

All versions of the facies program output an error curve that is based on the error function described above—the errorf value divided by the number of input curves used by the program. This curve allows the user to see how well the program is matching the data; large values in the error curve indicate that the program is having some difficulty in choosing an appropriate facies.

A data set was made up of all the core data stacked end to end and the depth-corrected log data for the same interval. Each of the electrofacies programs was run

against this data set, and the calculated electrofacies were compared with the facies from the core descriptions. The results of these calculations are summarized here:

Table C5. Accuracy of electrofacies model predictions.

MODEL	Total Error	Average Error	Hits	% Hits
FaciesR	955	1.41	301	44
FaciesG	1057	1.56	349	51
FaciesU	1121	1.65	340	50
FaciesN	1745	2.57	288	42
FaciesP	1702	2.51	289	43

The average error is the total error for the whole interval divided by the footage of the interval. The hits are the number of times that the core facies agreed with the electrofacies. The number of hits is mostly affected by the bed boundary effects described earlier. The geocolumn displays show the comparisons of the core-described facies with the electrofacies. Some of the facies are found remarkably well by the electrofacies. Others are harder to discriminate because the differences between some of the facies are easy to see when looking at core, but they are not resolved by logs. For example, the logs cannot tell the difference between a calcite-cemented siltstone and a fossiliferous siltstone because the lithological makeup of these two rock types is the same. If we had a log that was sensitive to fossils, this difference could be resolved.

Comparisons of each of the five facies model results with each of the core facies are shown in Figures C13 through C17. These figures are geocolumn displays in which all the core data have been stacked on top of one another (shown on the left of the depth track). The corresponding log data, after being depth-shifted to match the core data and then run through one of the facies calculation models, are shown on the right side of the depth track. The depths displayed in the depth track are in arbitrary values that show the

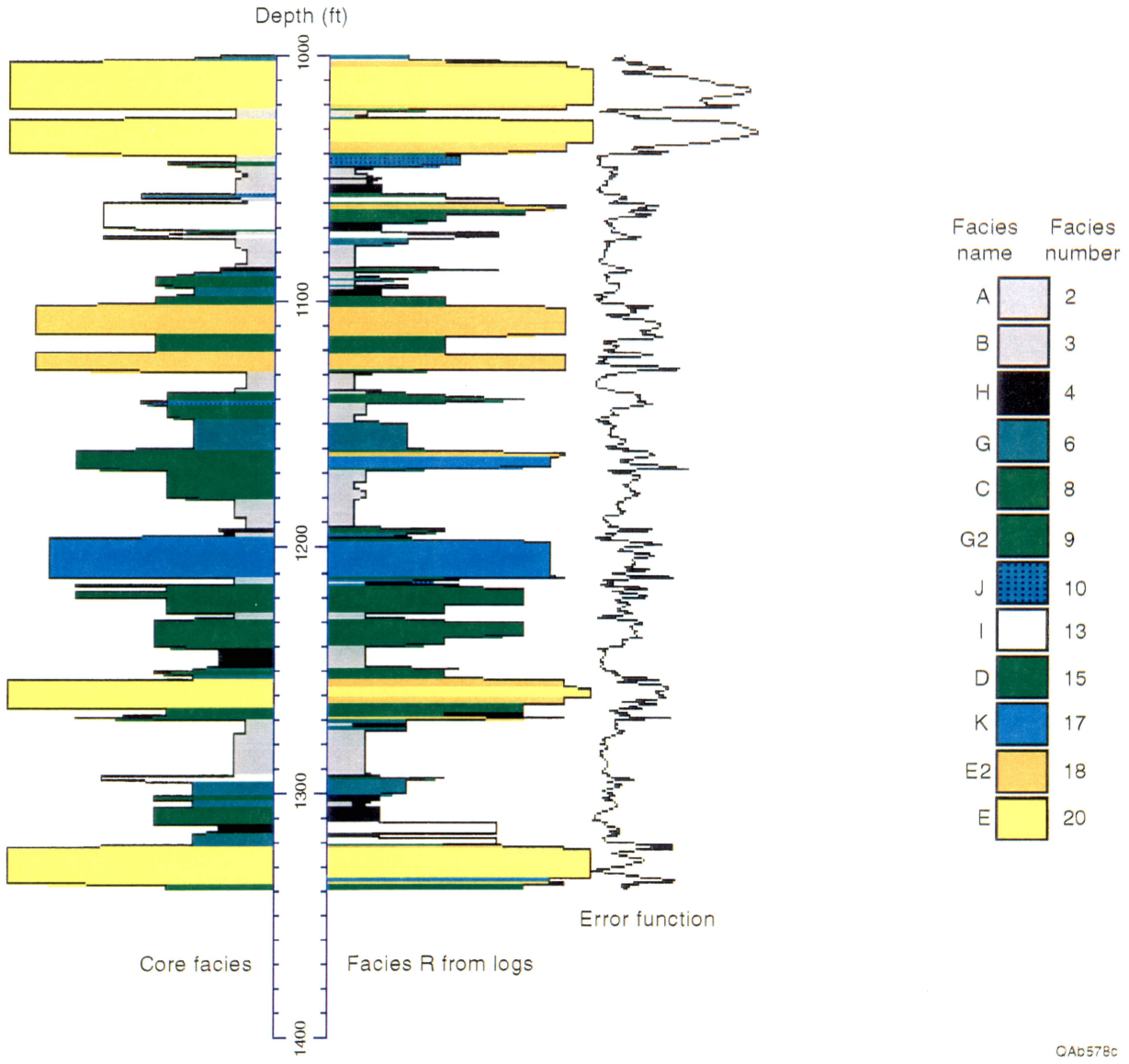

Figure C13. Geocolumn display of all core data stacked on top of one another to the left of the depth track and the corresponding log-derived facies using the FaciesR model to the right of the depth track.

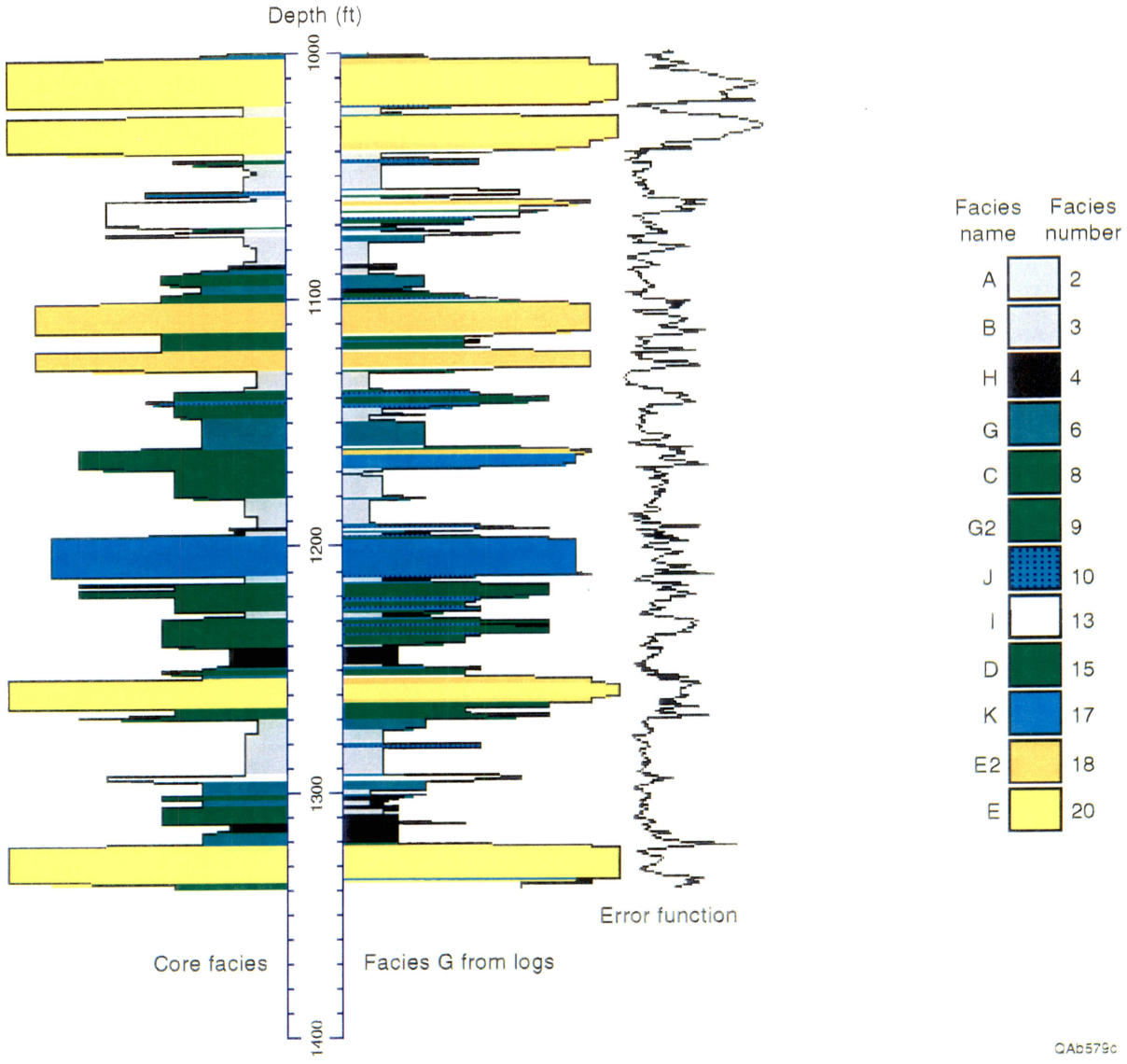

Figure C14. Geocolumn display of all core data stacked on top of one another to the left of the depth track and the corresponding log-derived facies using the FaciesG model to the right of the depth track.

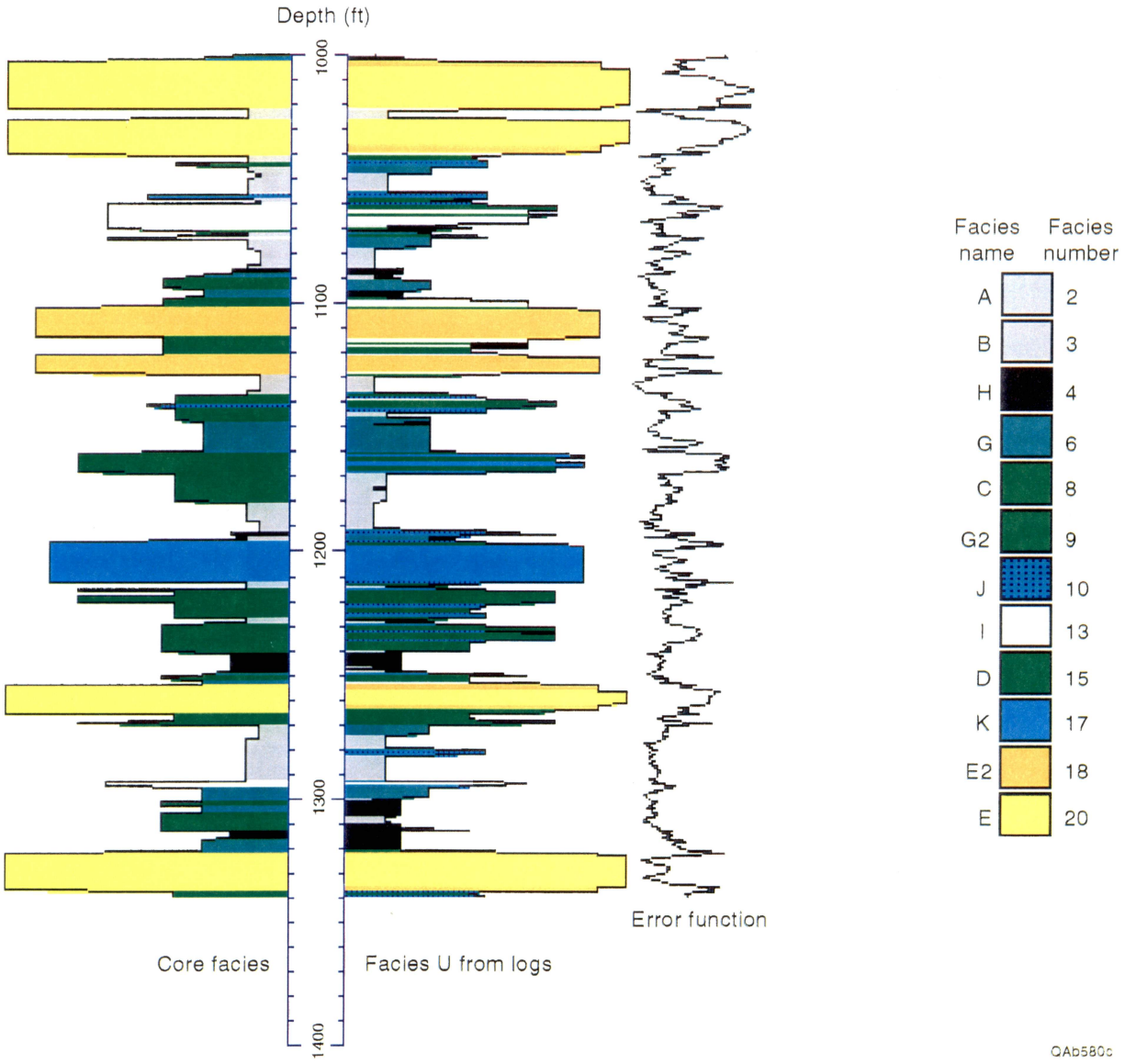

Figure C15. Geocolumn display of all core data stacked on top of one another to the left of the depth track and the corresponding log-derived facies using the FaciesU model to the right of the depth track.

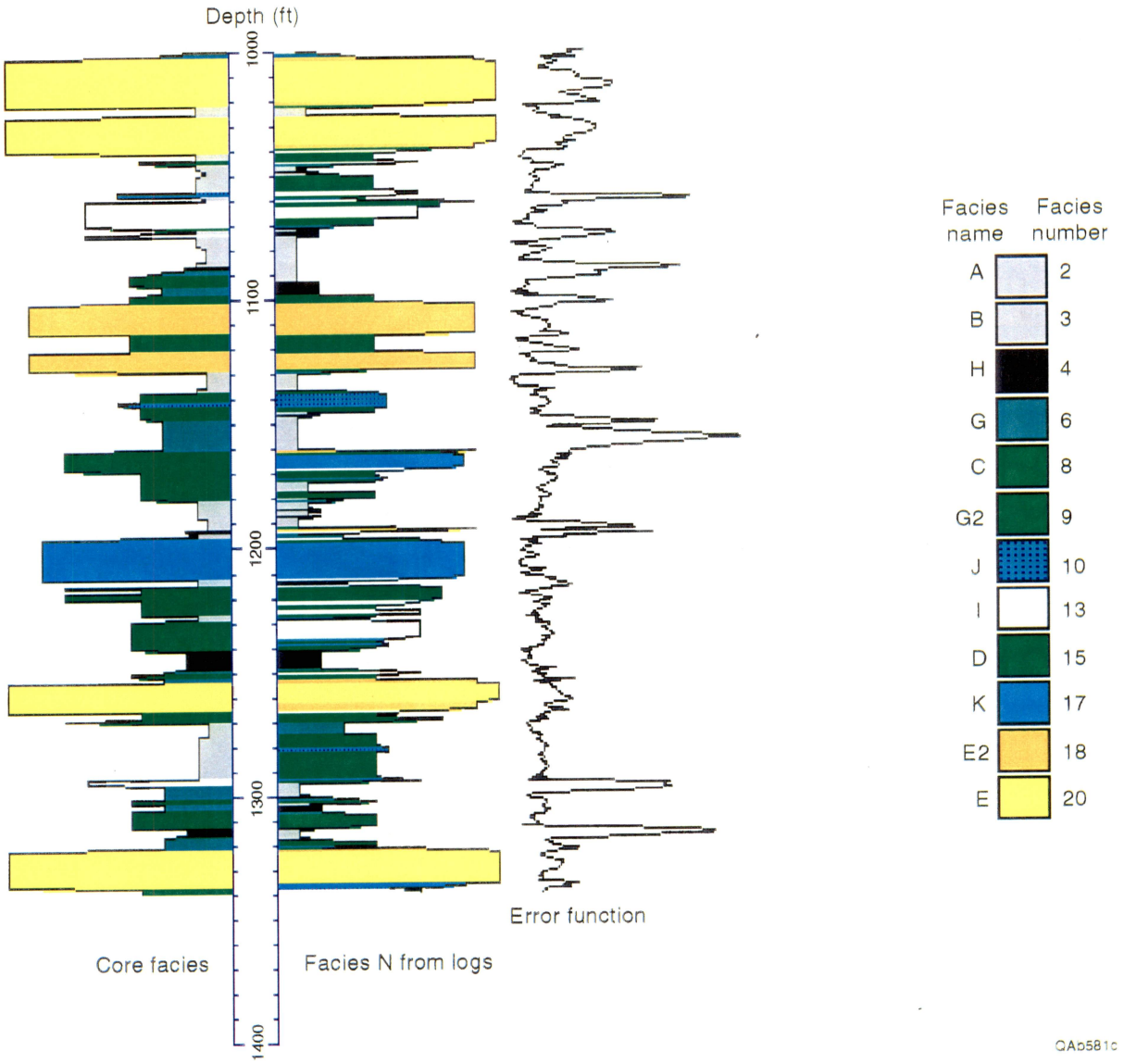

Figure C16. Geocolumn display of all core data stacked on top of one another to the left of the depth track and the corresponding log-derived facies using the FaciesN model to the right of the depth track.

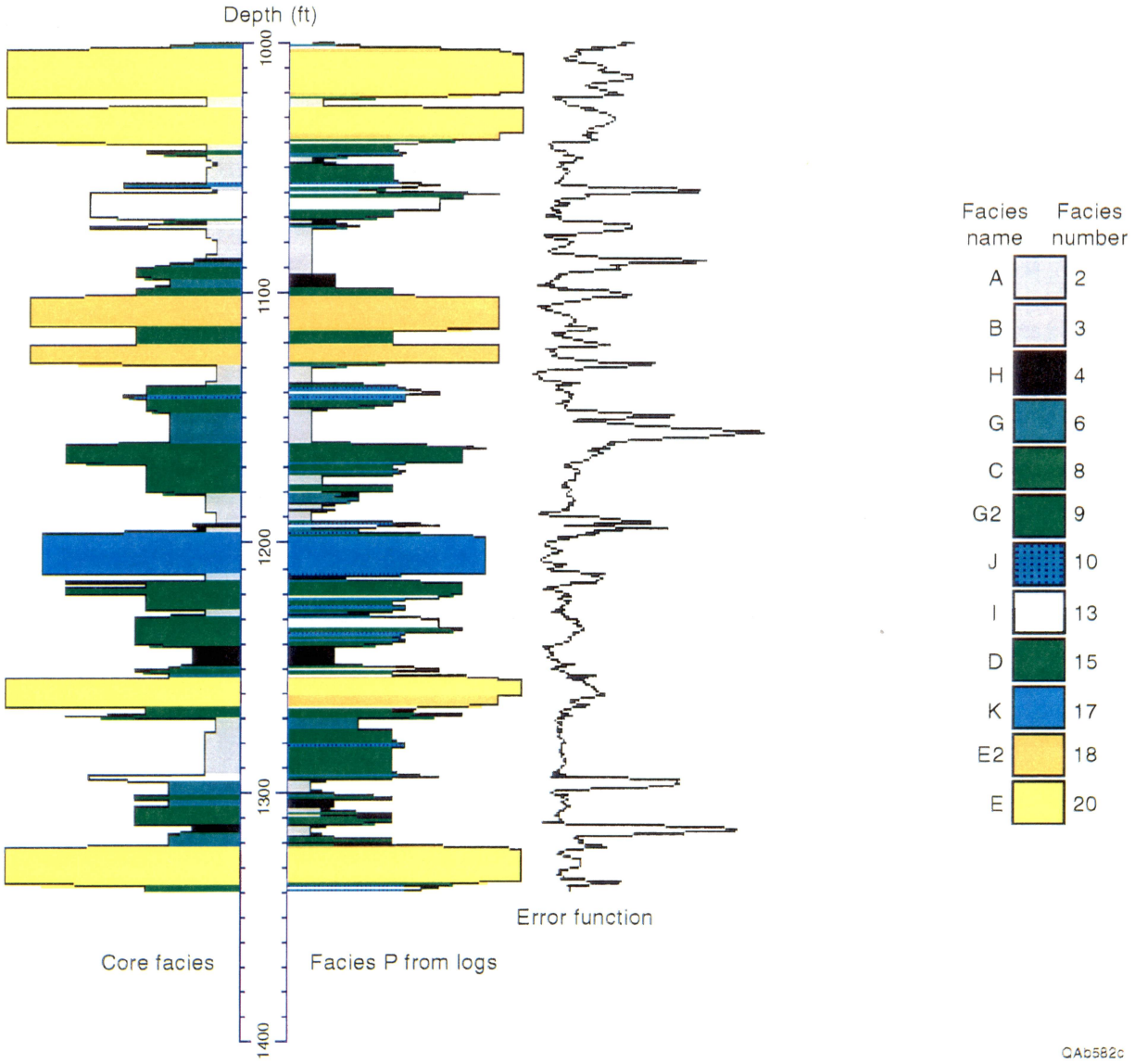

Figure C17. Geocolumn display of all core data stacked on top of one another to the left of the depth track and the corresponding log-derived facies using the FaciesP model to the right of the depth track.

relative depths and are not true depths because these data come from four wells and a number of different sequences.

When applied to the cored data, the error curves indicate that the versions of the program that use the neutron and density curves find higher errors (presumably because of washout). In addition, the versions that include the neutron and density curves find fewer depths of agreement (hits) with the core data than do the other versions.

Before the models were run against the wireline data base, an additional few lines of code were added to the models to force them to predict the E facies when the SP was less than –80 mV and to predict the E2 facies when the SP was less than –40 mV. These facies were found in most cases without this artificial shove, but, in a few instances of poorly calibrated old resistivity logs, the change was required.

Stacked Curves was used to run all the models for each well. Those wells that did not have curves sufficient to run a particular model were automatically bypassed by the Stacked Curves system. Because all the wells had the minimum curves required to run the FaciesR model, this model was run on every well. Cross sections were then made through the study area. The cross sections were made so that the results of only one of the facies models were displayed. The hierarchy of models was set so that the preferred display was in the following order:

1. FaciesU
2. FaciesG
3. FaciesR

Note that the first model (FaciesU) required the greatest number of curves and that the last model (FaciesR) required the minimum set of resistivity curves.

The facies model used on the displays is indicated by the color of the bounding curve on the geocolumn for each well in the cross sections. FaciesU is indicated by a black bounding curve, FaciesG by a blue bounding curve, and FaciesR by a red bounding curve. The bounding curve is set by the values of the facies (facies number) as shown in

column 2 of Table C4. These facies numbers are loosely related to the hardness of each of the facies, so that the geocolumn display resembles an outcrop display. Note also that the color of each facies is also determined by this same number.

Figure C18 shows a typical cross section through the Caddo sequence using the geocolumn display. Note that the marine limestone facies (K) is predominant in the B Yates 12, B Yates 6, and Ashe A5 wells; in the other wells, this facies has been replaced by sandstone facies (E and E2). Figure C19 shows the interpretation of this cross section, indicating that the marine sequence has been eroded by erosional surface ES 95 and replaced by fluvial deposits, with sandstone associated with the greater accommodation space. The marine limestone (K facies) in the B Yates 12 well has a square boundary into the shaly facies above and below it. The sandstones (E facies) in the C Yates 1 and Ashe A1 wells terminate upward through a series of facies into the shaly facies, indicating an upward-fining sequence similar to that represented in the ideal genetic sequence described in the geologic interpretation presented in Appendix A. It is worth noting that even though the actual facies in these upward-fining sequences may be in error at any given depth due to the vertical resolution of the wireline tools, the pattern of the sequence is still maintained.

Figure C20 shows a cross plot of porosity versus the permeability of all the core plugs taken from the four cored wells. The symbols represent the 12 facies described from core. Note that the E facies belongs to the higher permeability sands in the trend from porosity = 6 percent, permeability = 0.1 md to porosity = 15 percent, permeability = 60 md. The E2 facies is associated with the lower trend, indicating sandstones and/or siltstones of a lower permeability. In the cross section shown in Figure C21, the Sealy C-2 well shows a sandstone with a predominant E facies developed above the ES95 erosional surface (the Upper Caddo zone). The Sealy B-3 well has a sandstone above the ES95 surface that is entirely E2 facies according to the facies from wireline logs computation. Figure C22 shows the production histories for these two wells in the Upper

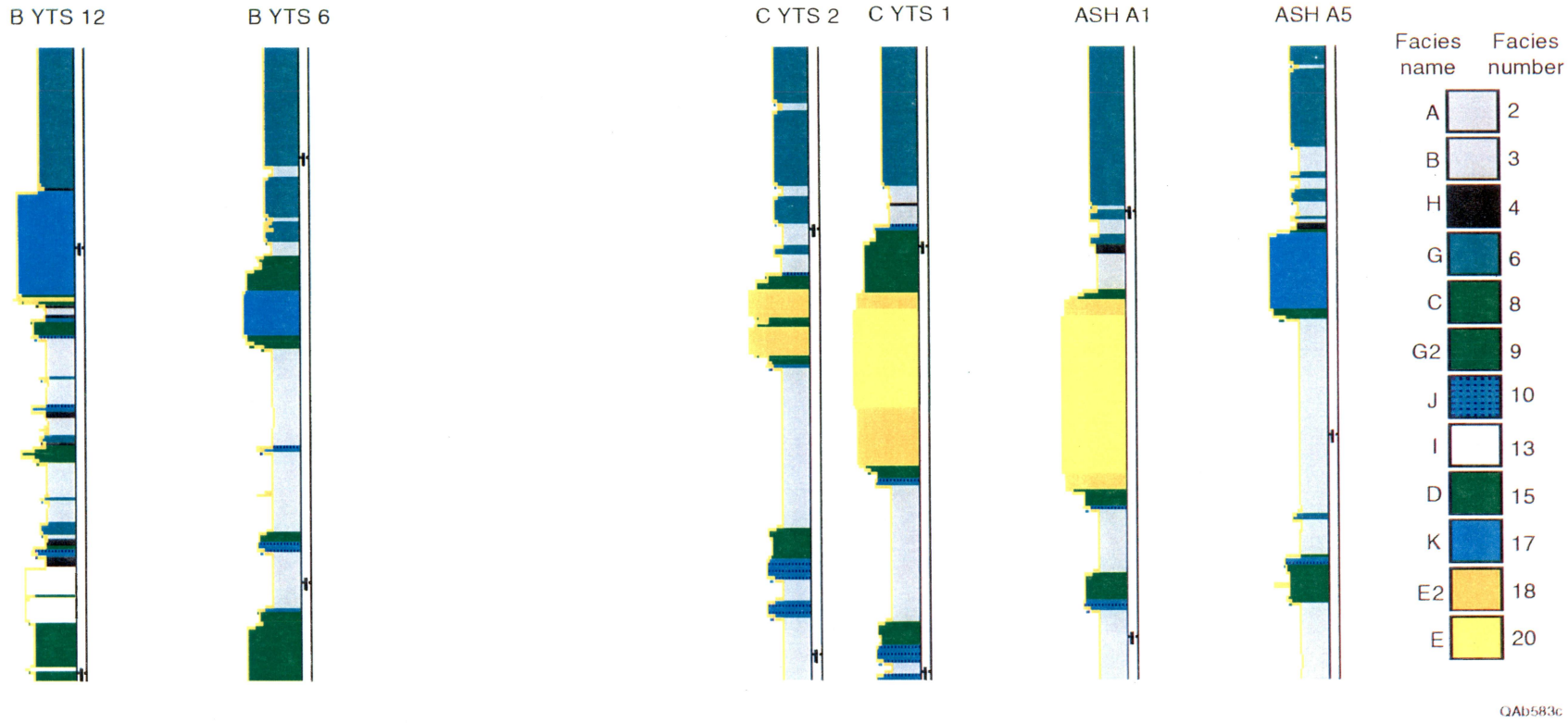

Figure C18. A geocolumn display cross section. This section is through the Caddo sequence.

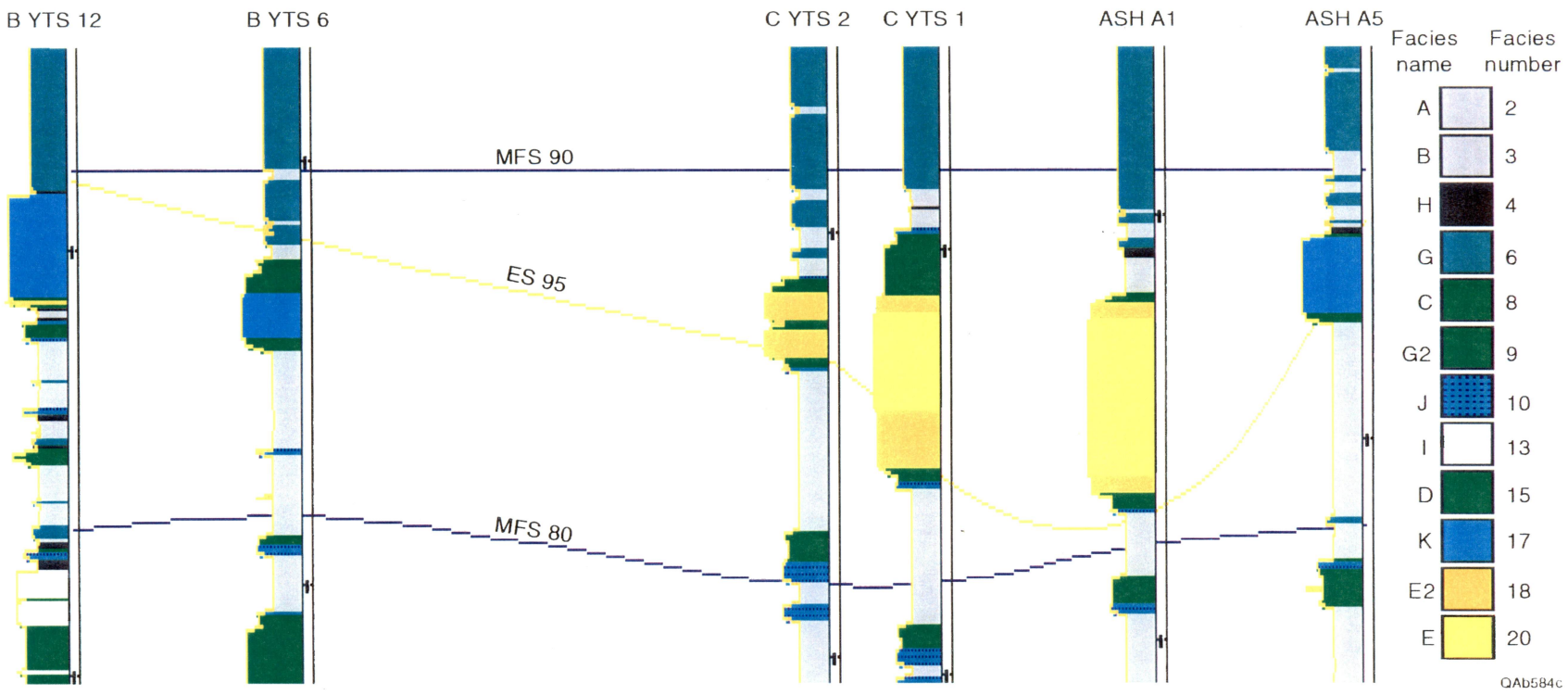

Figure C19. Interpreted version of the cross section shown in Figure C18.

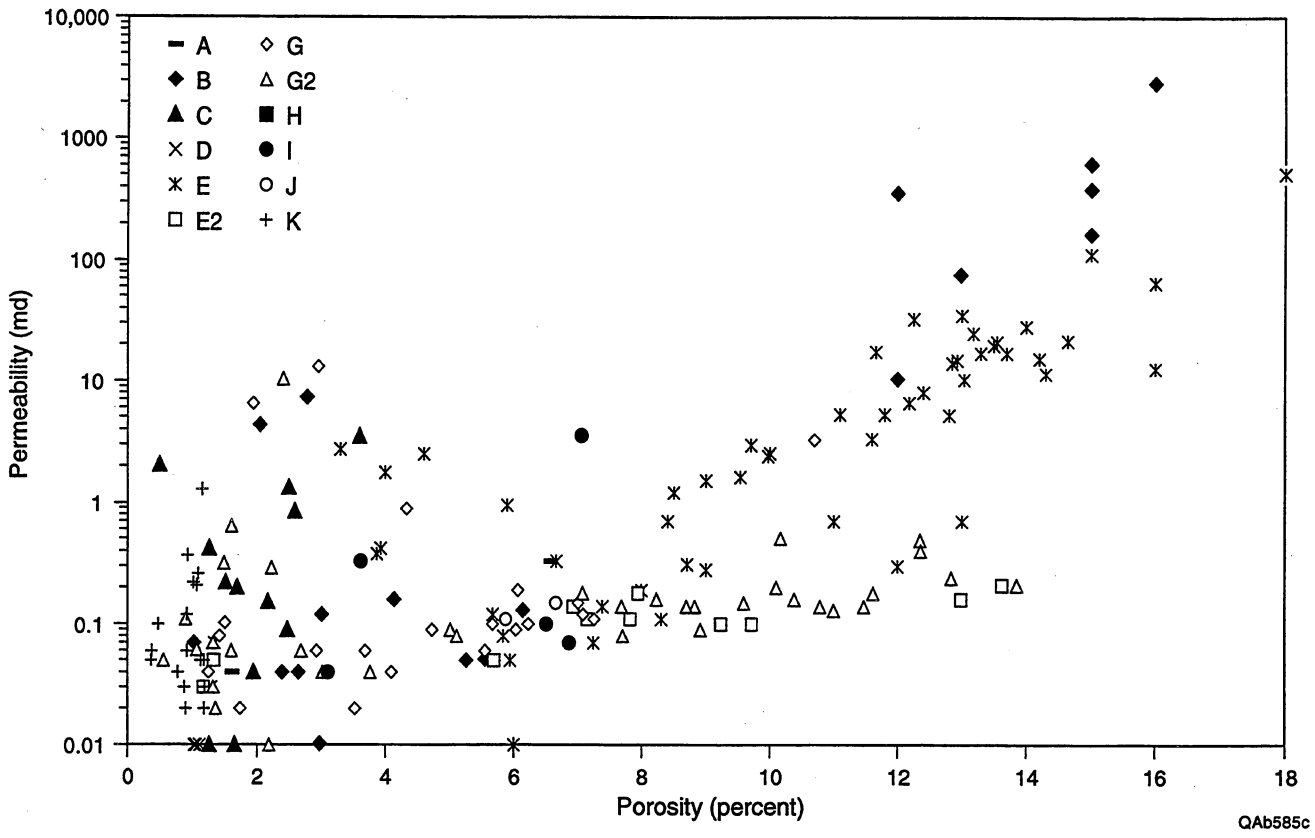

Figure C20. Cross plot of porosity vs. permeability for all core plugs from the four cored wells. The colors represent the 12 facies described using the core data.

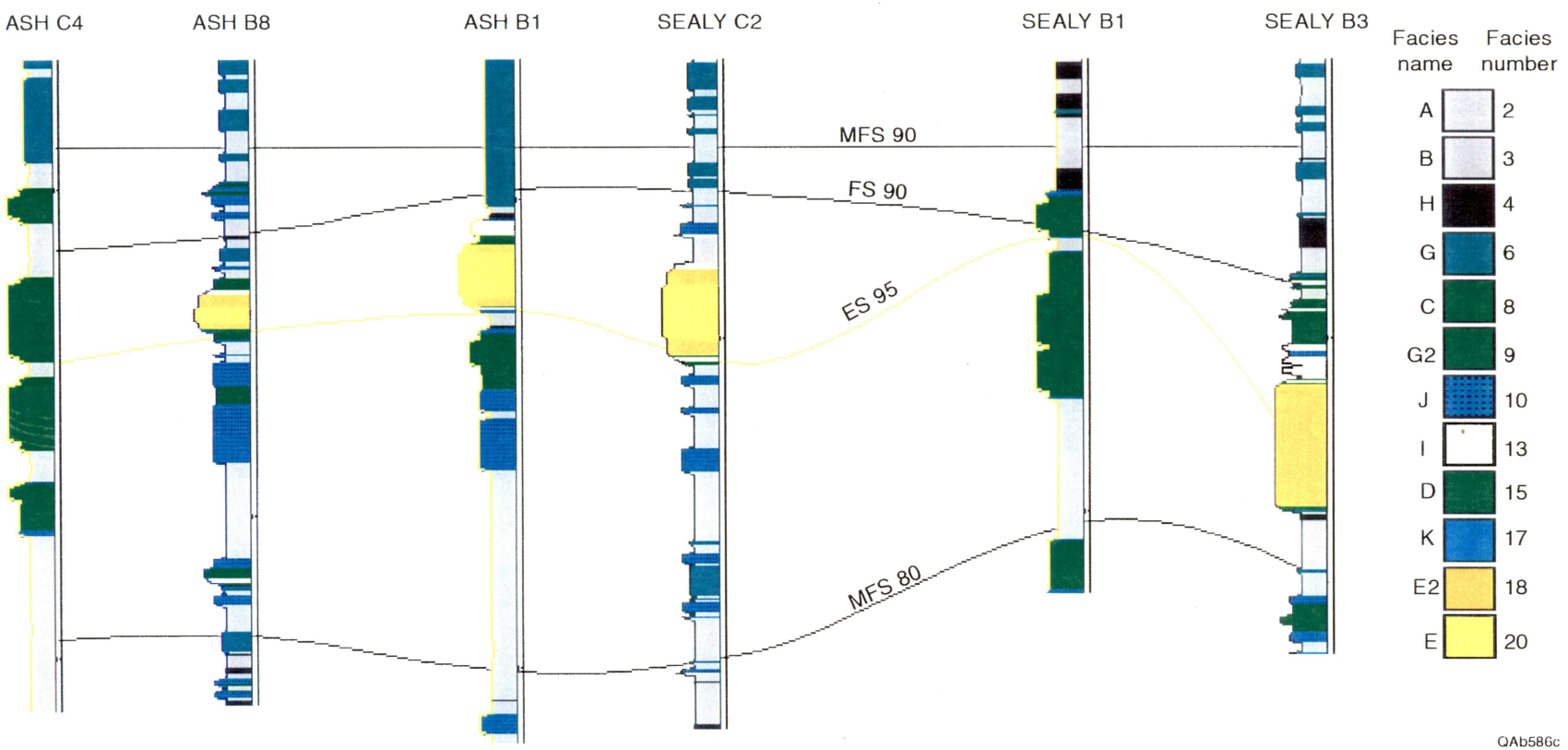

Figure C21. Cross section through the Upper Caddo in the northeast part of the study area.

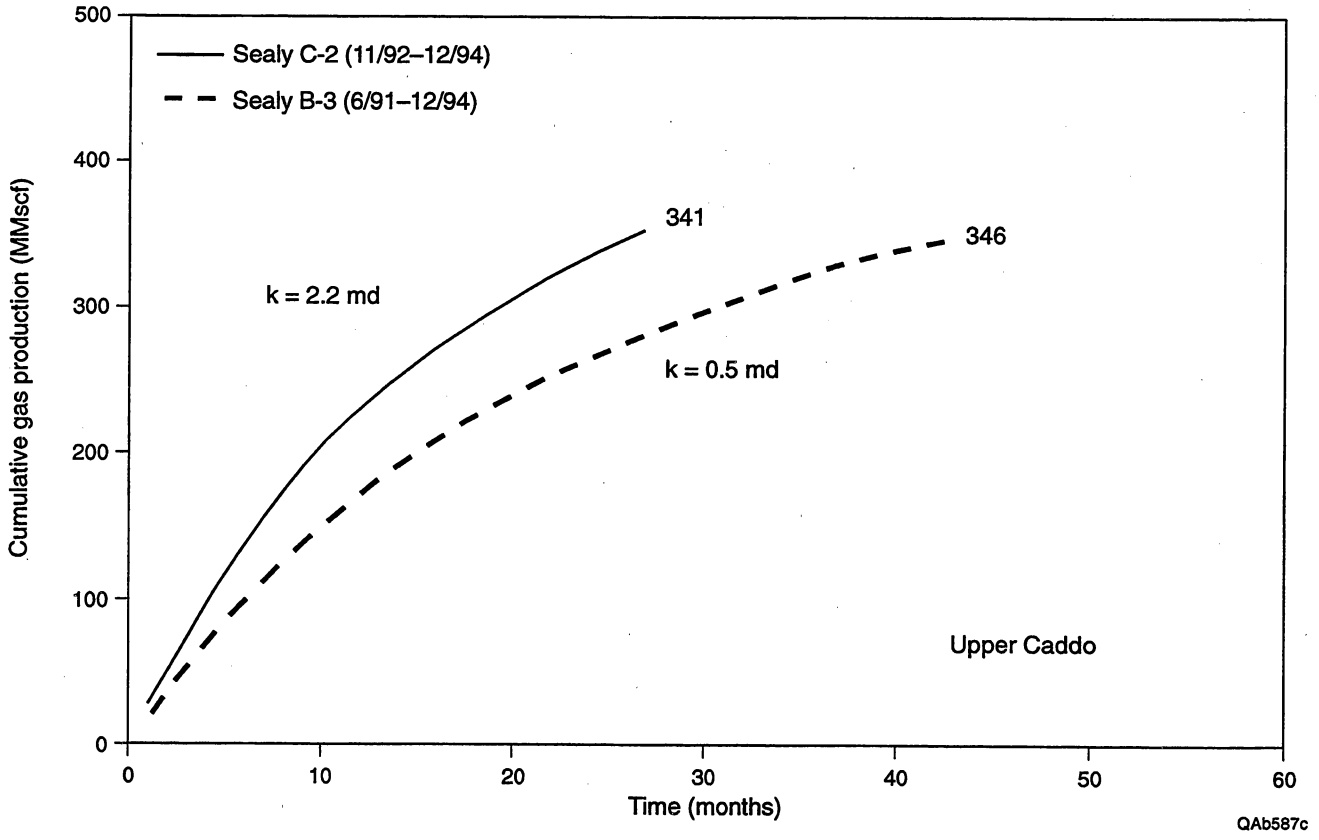

Figure C22. Production histories of the Sealy C-2 and Sealy B-3 wells; both wells are completed in the Upper Caddo.

Caddo zone; the production was isolated (i.e., not commingled) in both of these wells. Production data analysis calculates a lower average permeability (0.5 md) in the Sealy B-3 well and a higher value (2.2 md) in the Sealy C-2 well (see Appendix B). The facies determination from logs appears able to distinguish between the higher and lower permeability sandstones that were detected from the core data (see Figure C20).

Advantages of the Facies Technique

The facies technique developed for this study has several advantages when using log data to interpret the geology of the Bend Conglomerate:

- This deterministic technique is easier to use than are stochastic methods, including principal component analyses that require specialized computer programs and extensive knowledge and experience to run.
- The procedure can be used over a broad range of tool suites, including wells that have only old resistivity logs.
- The calculation generates good pattern recognition (for example, the upward-fining sequence described in Figure C19), even where the vertical resolution of the logging tool is less than the thickness of some of the beds in the sequence.
- The algorithm appears to be able to distinguish between sandstones of different permeability characteristics.
- The results are valuable in sequence stratigraphy interpretation.
- The technique is readily adapted to other fields with similar facies recognition problems.

APPENDIX D

BOONSVILLE 3-D SEISMIC PROGRAM—WAVETESTING, DESIGN, ACQUISITION, AND PROCESSING

Introduction

The 3-D seismic grid at Boonsville field covered approximately 26 mi^2, starting at the west shore of Lake Bridgeport and extending westward across Wise County and into Jack County. The positions of the source and receiver lines within the 26-mi^2 area are shown in Figure D1. Approximately half of the survey was positioned in Wise County and half in Jack County.

Extensive research was done to determine the optimal 3-D seismic field procedures that should be used to image the thin-bed reservoirs deposited in the low-accommodation conditions that existed during Atoka time on this shelf margin of the Fort Worth basin. This seismic field program involved the following research:

1. Establishing vertical wavetesting as a technique for comparing seismic sources and for selecting the optimal source parameters for imaging Midcontinent thin-bed reservoirs.
2. Demonstrating the value of horizontal wavetesting as a technique for determining the optimal receiver geometry to use in a 3-D seismic survey so that the recorded data have a maximum bandwidth.
3. Verifying the interpretational value of a novel, staggered-source-line, staggered-receiver-line recording geometry, which allows 3-D data to be sorted into (a) large bins with high stacking fold or (b) small bins with low stacking fold.
4. Documenting the traveltime differences, if any, exhibited by an explosive seismic source and a swept-frequency source in Midcontinent rocks.

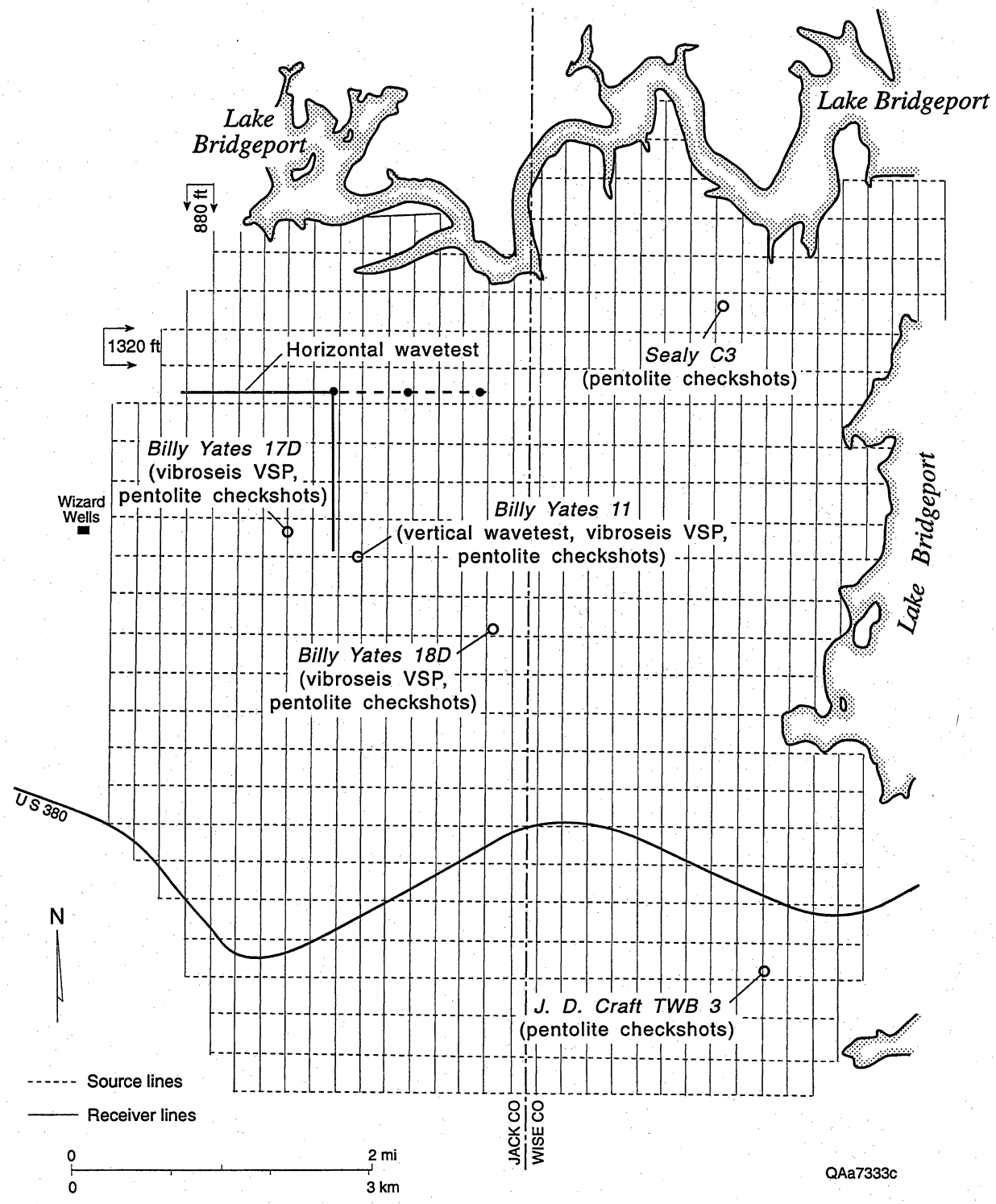

Figure D1. The source-receiver grid used to record the Boonsville 3-D seismic data. The locations of key velocity control wells and wavetest sites are indicated. The north-south receiver lines are spaced at intervals of 880 ft, and the east-west source lines are separated a distance of 1,320 ft. The horizontal wavetest site is further explained in Figure D12.

5. Demonstrating the economic and technical advantages of using small explosive charges in shallow holes, rather than the usual convention of larger charges in deep holes, as a 3-D seismic energy source in Midcontinent prospects.

This section documents the research techniques used in these investigations and the technical conclusions that resulted. These research findings should apply in Midcontinent basins other than the Fort Worth basin.

Wavetesting

Both vertical and conventional horizontal wavetests were done at Boonsville field to determine the type of source that should be used and the type of receiver array geometry that should be deployed to optimize 3-D seismic data quality and to maximize seismic signal bandwidth. The first phase of the 3-D seismic program was to conduct a vertical wavetest and to record a vertical seismic profile (VSP) in the Billie Yates 11 well inside the planned 3-D seismic grid (see Figure D1 for well location).

On-site inspection of the 3-D seismic area showed that about one-third of the 26-mi^2 grid was heavily timbered, particularly in the northern and eastern portions abutted to Lake Bridgeport. Vibroseis sources could not be used in these forested areas because permitting restrictions in some properties prohibited clearing vibroseis driving lanes through the timber, and in other properties, landowners imposed excessive costs for disposing of all felled trees. As a consequence, the most logical sources to use in these timbered areas were explosives in shot holes, although these shot holes had be prepared by drills that were small enough to wend their way through the timber without having to cut any trees.

Thus, the planning for the 3-D seismic wavetesting began with the requirement that explosive sources had to be used in a large part of the survey area. Because vibroseis sources could be used in the lightly timbered southwestern half of the area and would be a more economical source than drilled shot holes, the objectives of the vertical wavetest were to

compare the effective bandwidths of vibroseis and explosives and to determine whether these two sources could (and should) be intermingled in the subsequent 3-D data acquisition effort.

Vertical Wavetesting

In Texas, different legal requirements must be met for shot hole construction, depending on whether the hole depth is less than 20 ft or more than 20 ft (Fig. D2). When a shot hole is 20 ft or more deep, a plug of bentonite at least 13 ft thick must be placed in the hole, and then a special plastic cap must be secured at the top of the hole (Fig. D2b). This shot hole construction design is a legal requirement that has been imposed in an effort to prevent surface contaminants from gaining access to subsurface aquifers. These construction requirements add a cost of about $40 to each shot hole and significantly impact the economics of 3-D seismic data acquisition.

None of these requirements is imposed when the shot hole depth is less than 20 ft (Fig. D2a). Thus, one objective of the Boonsville wavetesting was to verify whether explosives detonated in shallow holes could be an effective 3-D seismic source. Shallow holes were desired, not only for reasons of economy, but because shallow holes would be much easier to prepare by the small drill rigs that would have to be used in the timbered portions of the survey area.

The explosive charge selected for testing was the C-10 design, comprised of 10 ounces of high-velocity pentolite molded into a directional charge that focuses the energy downward (Fig. D3). These charges were planted in holes 10 ft deep with the assumption that this hole depth was adequate for good energy coupling, and yet minimal rifling (i.e., hole blowouts) would occur. This directional charge is also available as C-20 and C-30 options (20 and 30 ounces of pentolite, respectively), but these larger explosives were thought to be too powerful for a 10-ft hole depth and were not tested. C-20 and C-30 charges should be considered for programs in which shot holes are deeper than 10 ft or in which charges can be cemented in place.

During wavetesting, the C-10 charges were shot in a five-hole pattern so that 50 ounces of high-velocity pentolite were detonated as a uniformly distributed source spanning 40 ft centered about the source flag (Fig. D4). This design is a reasonable approximation of a seismic point

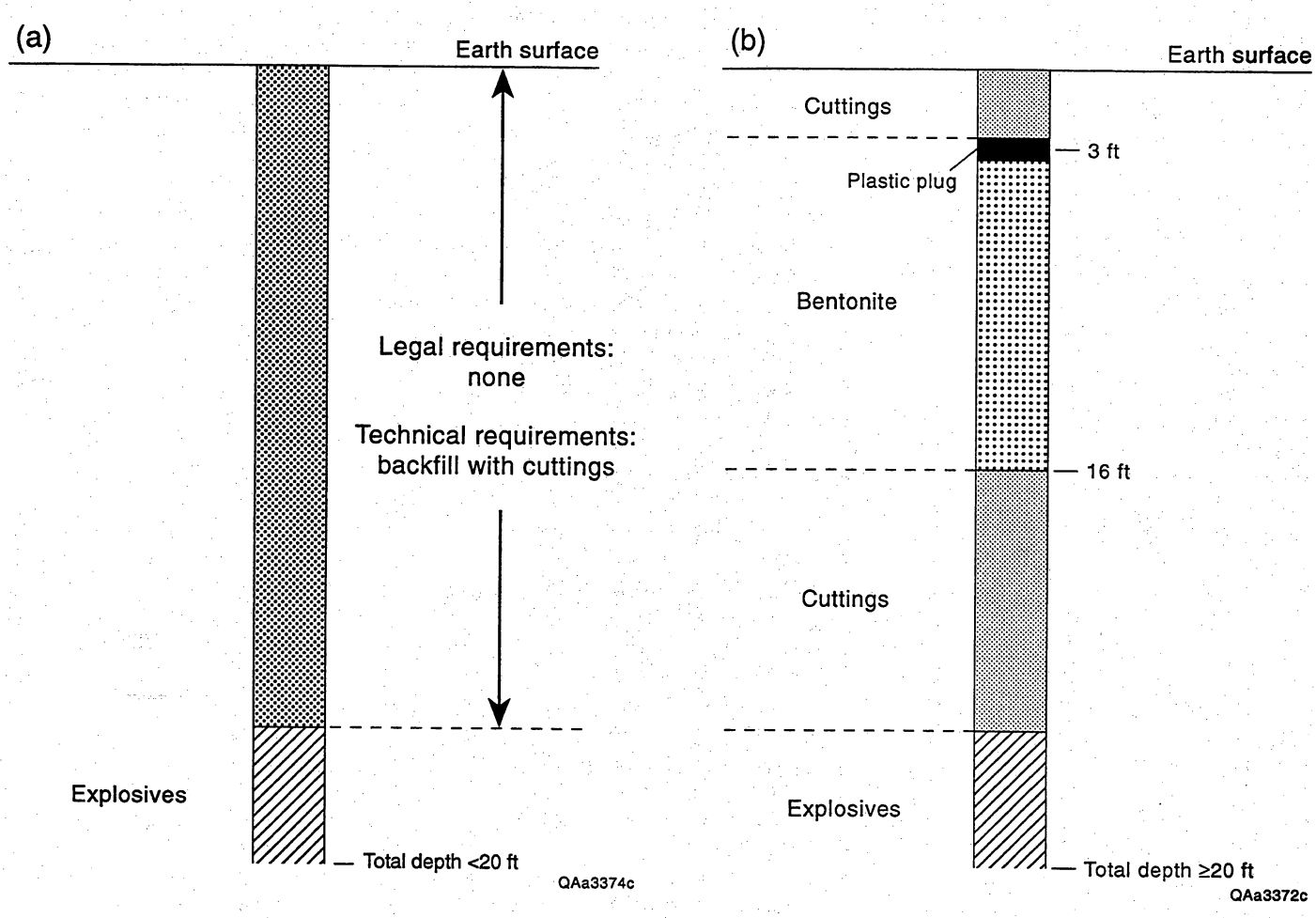

Figure D2. The construction requirements for shot holes in Texas when the hole depth is (a) less than 20 ft and (b) 20 ft or more.

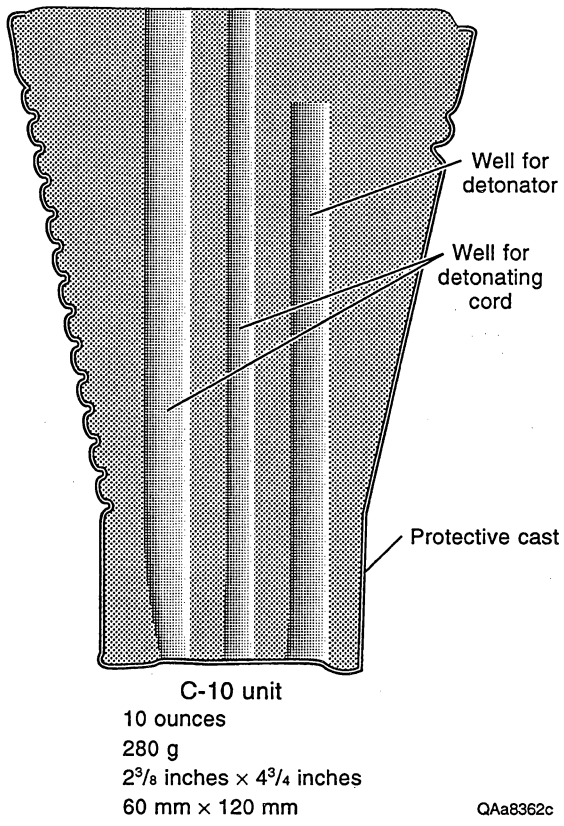

Figure D3. The C-10 directional charge used as the seismic energy source in the Boonsville 3-D survey. The C-10 package contains 10 ounces of high-velocity pentolite, and when the package is buried with the large end downward, the molded shape of the charge creates a large downward force.

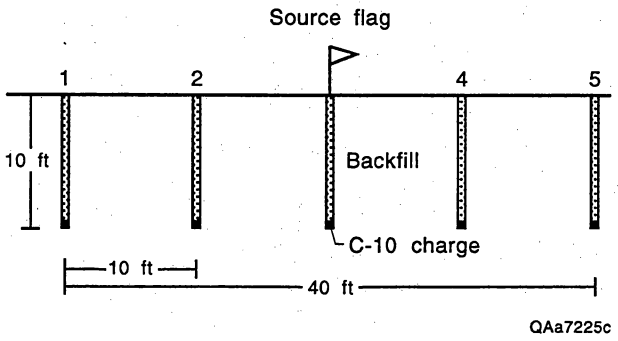

Figure D4. The five-hole source array geometry used at each source station within the Boonsville grid. Five shot holes were drilled inline, centered on the source flag, and spaced 10 ft apart. Each hole was 10 ft deep and loaded with a C-10 directional charge. All five holes were detonated simultaneously.

source. All five holes were wired in series so that if an electrical break occurred in any one of the five detonating caps, none of the charges would fire. This technique ensured that all shots recorded during wavetesting and during the subsequent 3-D recording would be consistent, in that they each involved simultaneous detonation of five 10-oz charges distributed as shown in Figure D4. No shot holes blew out during the vertical wavetesting at the Billie Yates 11 well, so it was decided that 10-ft shot holes would indeed be appropriate for the subsequent 26-mi^2 3-D grid. Later, during the 3-D seismic data acquisition, sometimes one shot hole (and in a few rare occasions, two) blew out in the five-hole arrays, but the overall negative effect of this reduced energy output for a few shotpoints randomly dispersed throughout the 3-D survey area was minimal.

The vertical wavetesting geometry used at Boonsville field is illustrated in Figure D5. Twelve five-hole arrays, each array designed as diagrammed in Figure D4, were prepared at an offset distance of 420 ft (Fig. D5b), and the wavefields generated by these shots were recorded at vertical intervals of 500 ft as the receiver was lowered down the Billie Yates 11 well (Fig. D6). These vertical wavetest data were numerically analyzed on site to determine the energy level and the spectral bandwidth of the pentolite-generated wavelet as it propagated down to, and through, the targeted Atokan-age Bend Conglomerate reservoirs occurring between depths of 4,500 and 6,000 ft (approximately) in the Billie Yates 11 well.

The spectra of the downgoing pentolite wavelets were calculated within minutes of recording each wavelet so that on-site decisions could be made about how to set vibrator parameters to create a vibroseis wavelet that would equal or surpass the energy content and the bandwidth of the pentolite wavelet. These on-site spectral calculations are plotted in Figure D7 and show that these small, shallow, directional charges produce a remarkably broadband signal spectrum exceeding 200 Hz.

Western Geophysical, having been alerted that the Bureau wanted to achieve the widest possible bandwidth in this vertical wavetest, had its chief vibrator engineer, together with Pelton's Vice President of Research, on site to test Pelton's newest vibrator electronics control

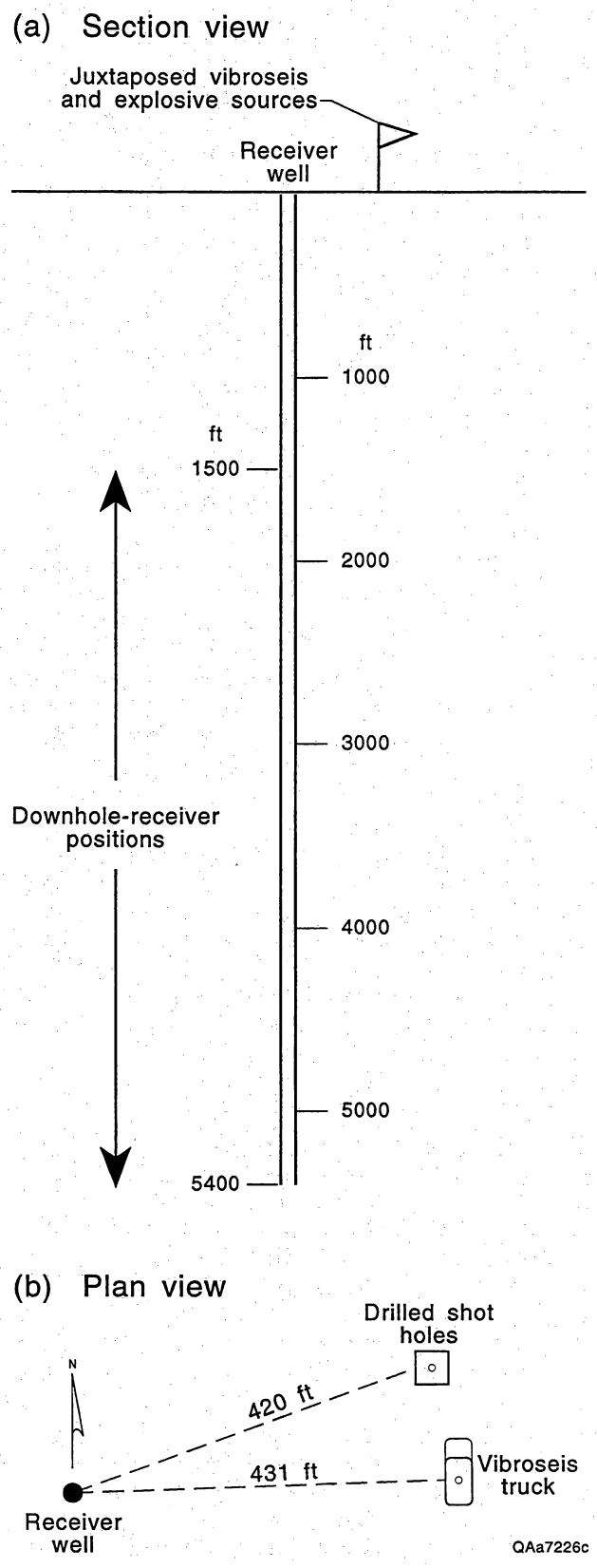

Figure D5. The geometry used to record vertical wavetest data in the Billy Yates 11 well. Well location shown in Figure D1. The objective of the test was to determine the relative bandwidths and vertical traveltimes of vibroseis and pentolite wavelets.

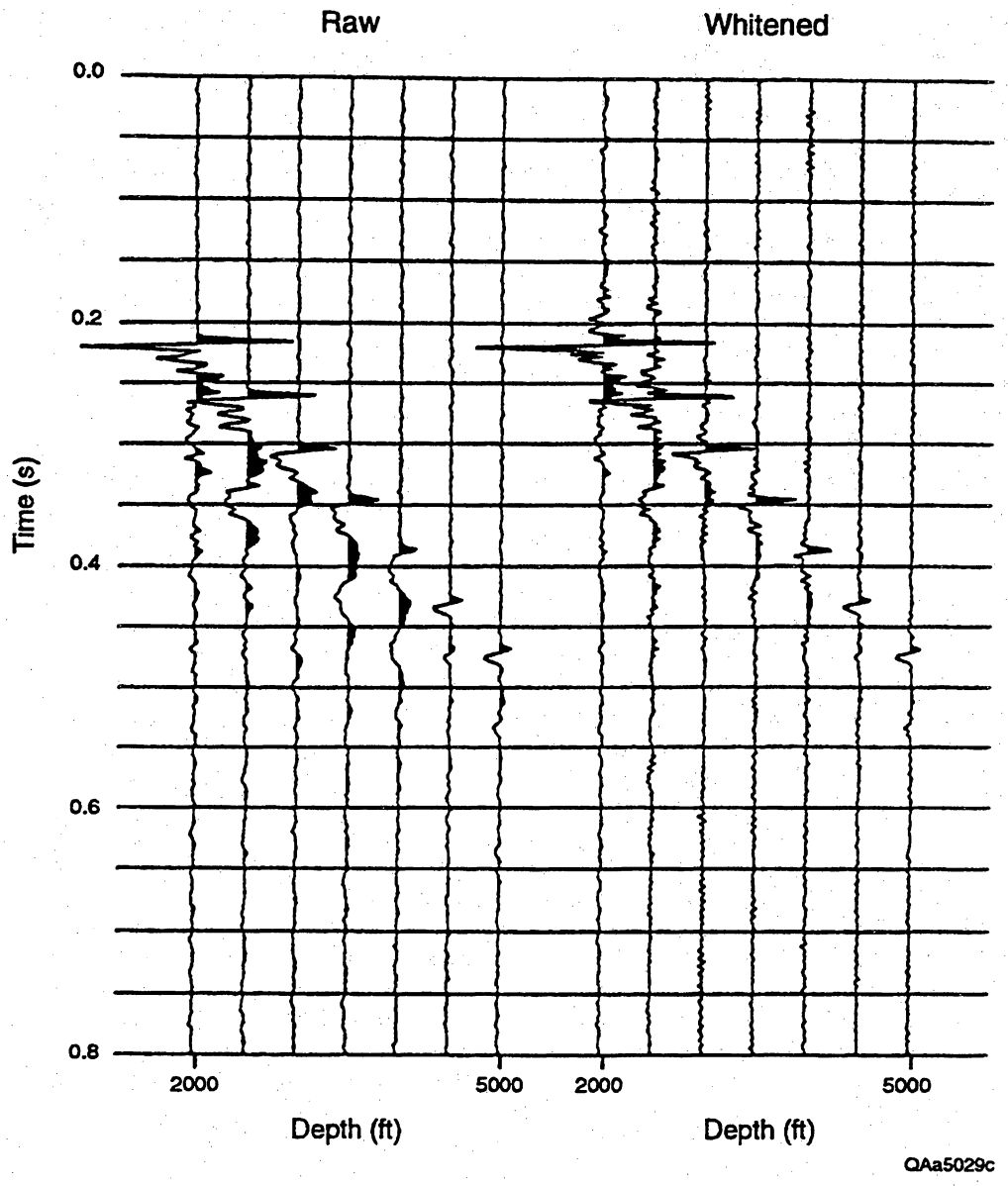

Figure D6. Some of the vertical wavetest data generated by C-10 directional charges detonated in five-hole patterns constructed as shown in Figure D4 and recorded in the Billy Yates 11 well. The source-receiver geometry used to record these data is diagrammed in Figure D5.

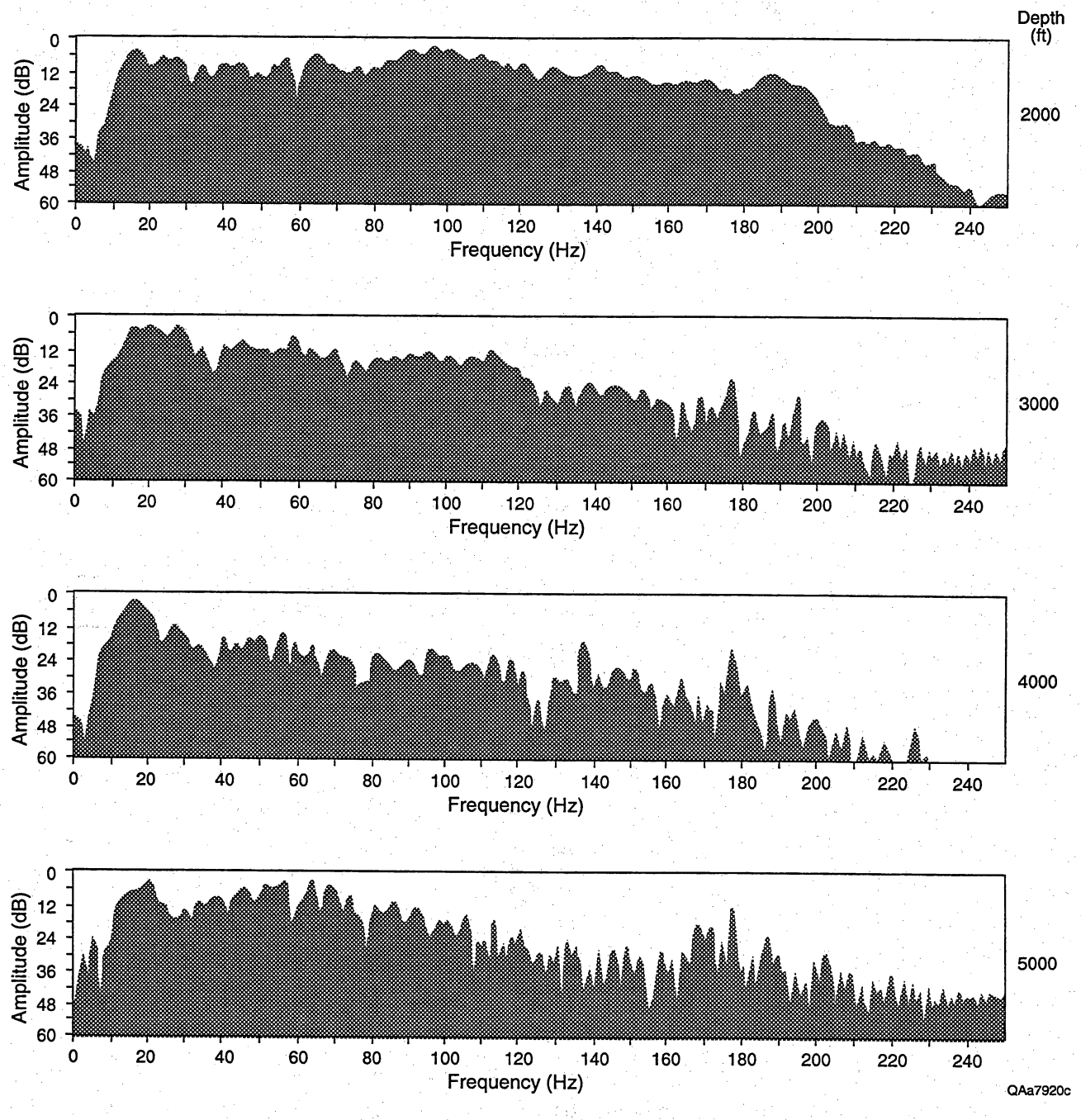

Figure D7. Amplitude spectra of the pentolite-generated vertical wavetest data shown in Figure D6. These spectra document that the pentolite wavelets are extremely broadband and contain frequency components exceeding 200 Hz. The recording system used in this test required that the wavelets be recorded at a sample rate of 2 ms, so the spectral roll-off above 180 Hz is produced by the 2-ms alias filter in the recording system and is not a true reduction of the wavelet energy. The numbers labeled on the right margin indicate the depths where the spectral analyses were done. The Atoka-age reservoirs begin at a depth of about 4,500 ft.

system. On the basis of the pentolite bandwidth evidence (Fig. D7), these engineers were instructed to begin tests to confirm that the vibrator to be used for the vibroseis portion of the vertical wavetesting could demonstrate acceptable ground-force-phase-locking between 10 and 200 Hz. After extensive effort, it was decided that ground-force-phase-locking could not be achieved above 160 Hz, so the vibroseis vertical wavetesting, conducted on the upward trip of the downhole receiver, was done using a 6–160-Hz nonlinear sweep. The resulting wavetest data comprised a zero-offset VSP (Fig. D8) and also allowed the spectra of the downgoing vibroseis wavelets to be calculated at the same receiver depths that pentolite wavelets had been analyzed (Fig. D9).

These vertical wavetest data demonstrated that both pentolite and vibroseis sources would produce exceptional wideband data in the Boonsville survey area. Most important, the vertical wavetests confirmed that the small C-10 directional charges would be an excellent source option when they were detonated in shallow (10-ft) shot holes. On the basis of this vertical wavetest, it was decided that the shot hole array design shown in Figure D4 would be used for the entire 26-mi^2 survey, and that pentolite and vibroseis sources would not be intermingled in the data recording.

Horizontal Wavetesting

The vertical wavetesting program conducted in the Billie Yates 11 well defined the source (C-10 directional charges) that should be used in the Boonsville 3-D seismic program. The next phase of the seismic program was to conduct horizontal wavetesting to determine the receiver array design that should be used. This receiver testing was done approximately 1 mile north of the Billie Yates 11 well (Fig. D1).

The vertical wavetesting had already documented that the C-10 directional charges selected for the Boonsville energy source, when deployed in shallow 10-ft holes, could illuminate the targeted thin-bed, Atokan-age reservoirs with a wavelet having a frequency content as high as

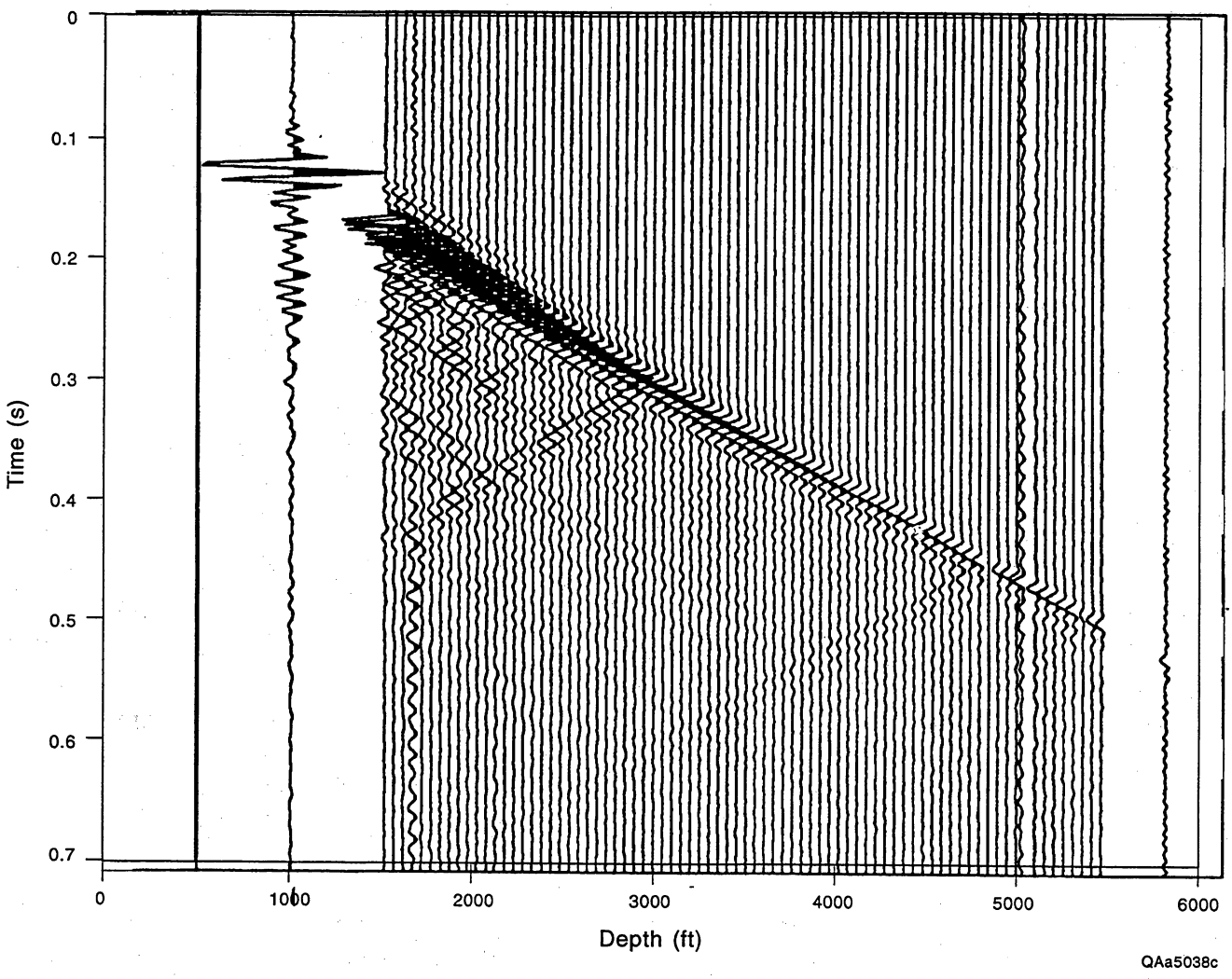

Figure D8. Vibroseis vertical seismic profile recorded in the Billy Yates 11 well. Well location shown in Figure D1. The source-receiver geometry used when recording these data is diagrammed in Figure D5.

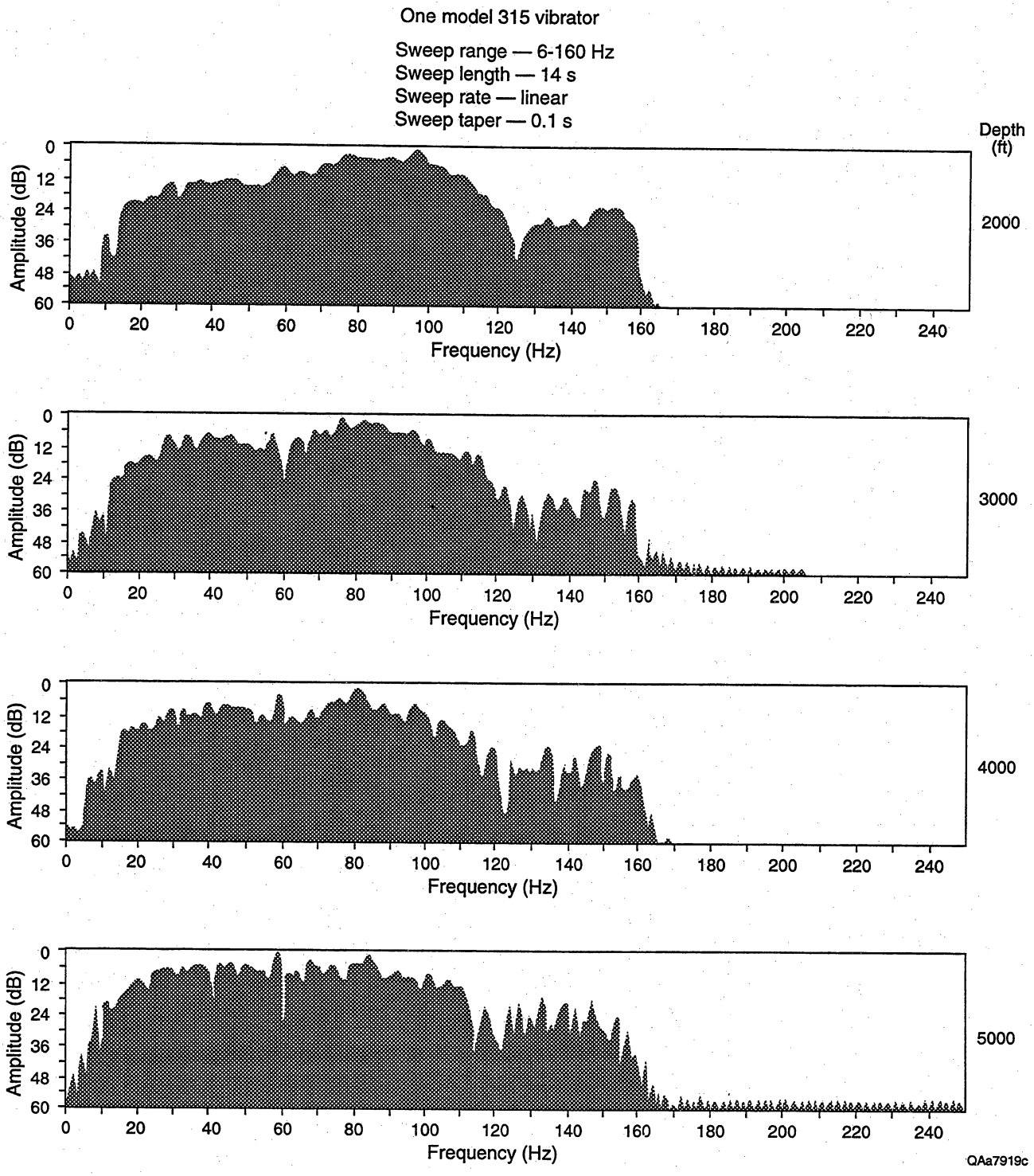

Figure D9. Amplitude spectra of vibroseis vertical wavetest data recorded at the same receiver depths as the pentolite data in Figure D6. After extensive testing, the source vibrator could not demonstrate acceptable ground-force-phase-locking above 160 Hz, so the VSP data were generated using a nonlinear 3-dB/octave sweep, 14 s long, that began at 6 Hz and ended at 160 Hz. A nonlinear sweep was used to maximize the energy content at the higher frequencies.

200 Hz (Fig. D7). The objective of the horizontal wavetesting was to determine what receiver array geometry would best preserve these high frequencies in the reflected wavefield.

The basic concepts of receiver array design are summarized in Figures D10 and D11. Receiver design theory requires that the time-moveout across a receiver array not exceed one-half of the time period associated with the highest frequency component that is to be recorded. If we assume that the maximum recorded frequency is 200 Hz, this requirement means that the array moveout cannot exceed (1/2)(1/200 Hz) = 2.5 ms. According to the array moveout equation in Figure D10, the array length L that satisfies this design criterion is

$$L = (0.0025\, t_o\, V^2)/X, \qquad \text{(D-1)}$$

where t_o is the one-way travel time to the reflector that is to be imaged, V is the average velocity to that reflector depth, and X is the offset distance between the subsurface reflection point and the center of the receiver array. Using the values

t_o = 0.45 s for the Atoka reservoirs,

V = 12,000 ft/s for the average velocity to these reservoirs, and

X = 5,000 ft for the maximum offset

results in L having a value of 32 ft.

Now that theory has specified the desired length L of the surface receiver array that will not attenuate 200-Hz data in the reflected wavefield, the next requirement is to decide how far apart adjacent receiver arrays should be so that this 200-Hz-frequency component is not attenuated by the trace-to-trace normal moveout (NMO) corrections that are done to the recorded data. The NMO requirement that has to be imposed on the receiver spacing is shown in Figure D11. This requirement states that the time moveout DT between adjacent receiver stations N and (N-1), which are a distance DX apart, should not exceed the time moveout dt across the array of length L, or

$$(DT/DX) \leq (dt/L). \qquad \text{(D-2)}$$

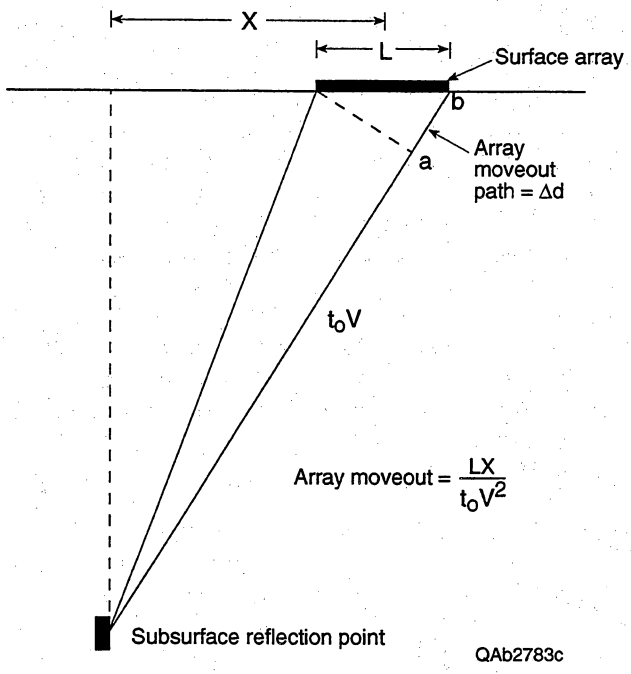

Figure D10. Geometrical theory used to design the dimensions of the surface-positioned seismic receiver arrays at Boonsville field. The magnitude of the array moveout (i.e., the time shift across the array) for an array of length L is the time required for an upgoing reflection to traverse the extra path length Δd between the raypaths to the receivers at opposite ends of the array, Δd being the distance between points a and b. The time smearing of the reflection arrival time resulting from this moveout defines the maximum frequency that can be correctly preserved in the recorded data. If high frequencies are to be preserved, the array length L must be short so that this time shift and wavelet smearing are small. V is the average velocity; t_o is the one-way reflection time.

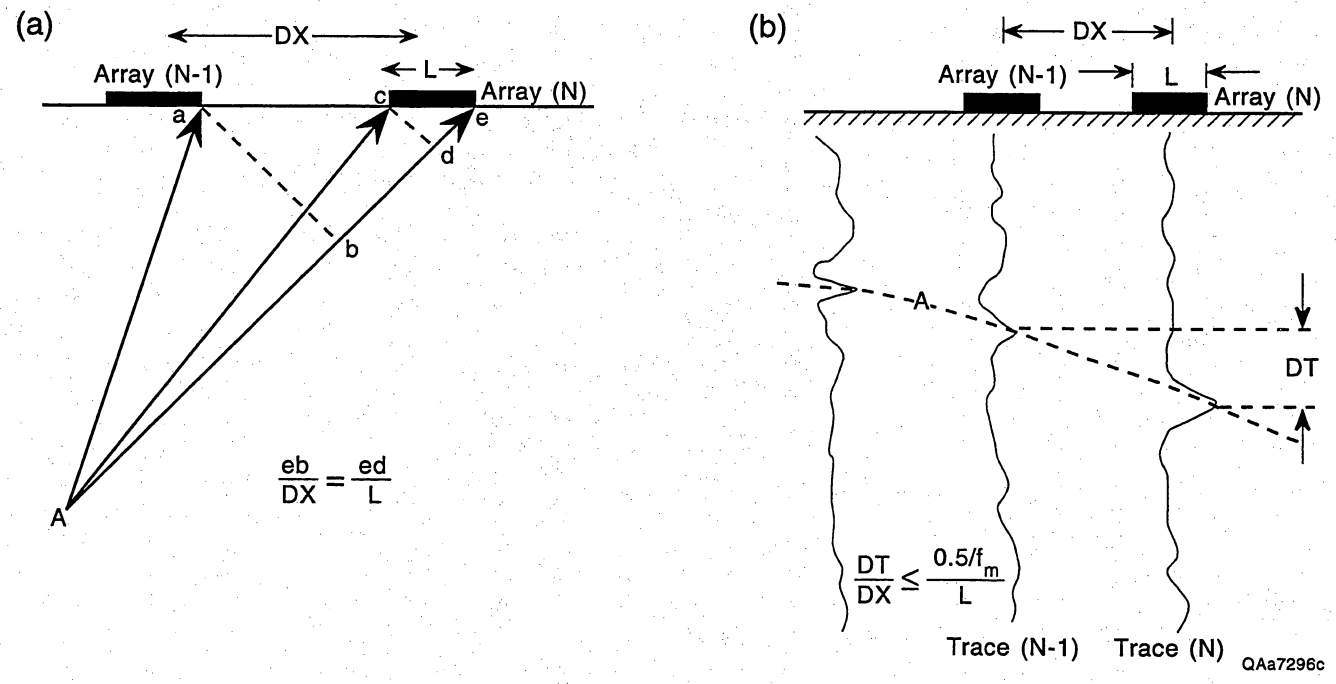

Figure D11. The theory in Figure D10 defines the criteria used to select the proper length L of a single receiver array. The theory shown here expands that design concept to define how far apart adjacent receiver arrays should be. Panel (a) shows the geometrical relationships between the reflected raypaths that arrive at two receiver arrays separated a distance DX. Panel (b) illustrates how this receiver interval DX can be calculated by defining the maximum time moveout DT that should exist for a reflection signal A recorded by these two arrays. The moveout DT should not exceed one-half of the time period associated with the dominant frequency f_d in the reflection signal; i.e., DT should be $\leq 0.5/f_d$. The equation in (b) follows from the equation in (a) by defining the traveltime over distance *eb* in panel (a) to be DT, the traveltime over distance *ed* to be dt, and then setting dt equal to one-half of the time period of the highest frequency component, or 0.5/fm.

The objective is to determine what the receiver spacing DX should be. Reordering equation 2 and ignoring the inequality sign gives

$$DX \sim (DT/dt)L. \tag{D-3}$$

The maximum allowable array moveout dt has already been defined as $(0.5/f_m)$, where $(1/f_m)$ is the time period of the maximum frequency component in the reflected wavefield. Array designers use a similar logic to define the maximum trace-to-trace moveout DT and set DT equal to $(0.5/f_d)$, where $(1/f_d)$ is the time period of the dominant frequency component in the reflection data. This logic is followed because as long as the dominant wavefield frequency is preserved in the trace-to-trace reflection moveouts, the normal moveout corrections for the reflection event can be accurately calculated. Equation 3 can thus be rewritten as

$$DX \sim (f_m/f_d)\, L. \tag{D-4}$$

If $f_m = 200$ Hz and we assume $f_d \sim 40$ Hz, then

$$DX \sim 5\, L, \tag{D-5}$$

or DX ~ 160 ft. On the basis of this theory and the attendant assumptions, receiver groups should not be separated much more than 200 ft, and preferably less than 200 ft.

Using this array design theory, the horizontal wavetest program was laid out as illustrated in Figure D12. Three source stations, spaced at intervals of 2,640 ft, were prepared in an east-west direction. Three five-hole arrays were drilled and loaded at each of these source stations, following the design shown in Figure D4. To measure reflection wavefields in both the inline and crossline directions relative to each shot, receiver lines were laid out in both east-west and north-south directions. Each line had 24 receiver stations with a spacing of 220 ft between adjacent receiver flags, which is a spacing roughly equivalent to that determined by the logic leading to equation 5. This geometry allowed reflection wavefields to be recorded for source-to-receiver offsets ranging from 220 ft to 10,560 ft, an offset range greater than what would be

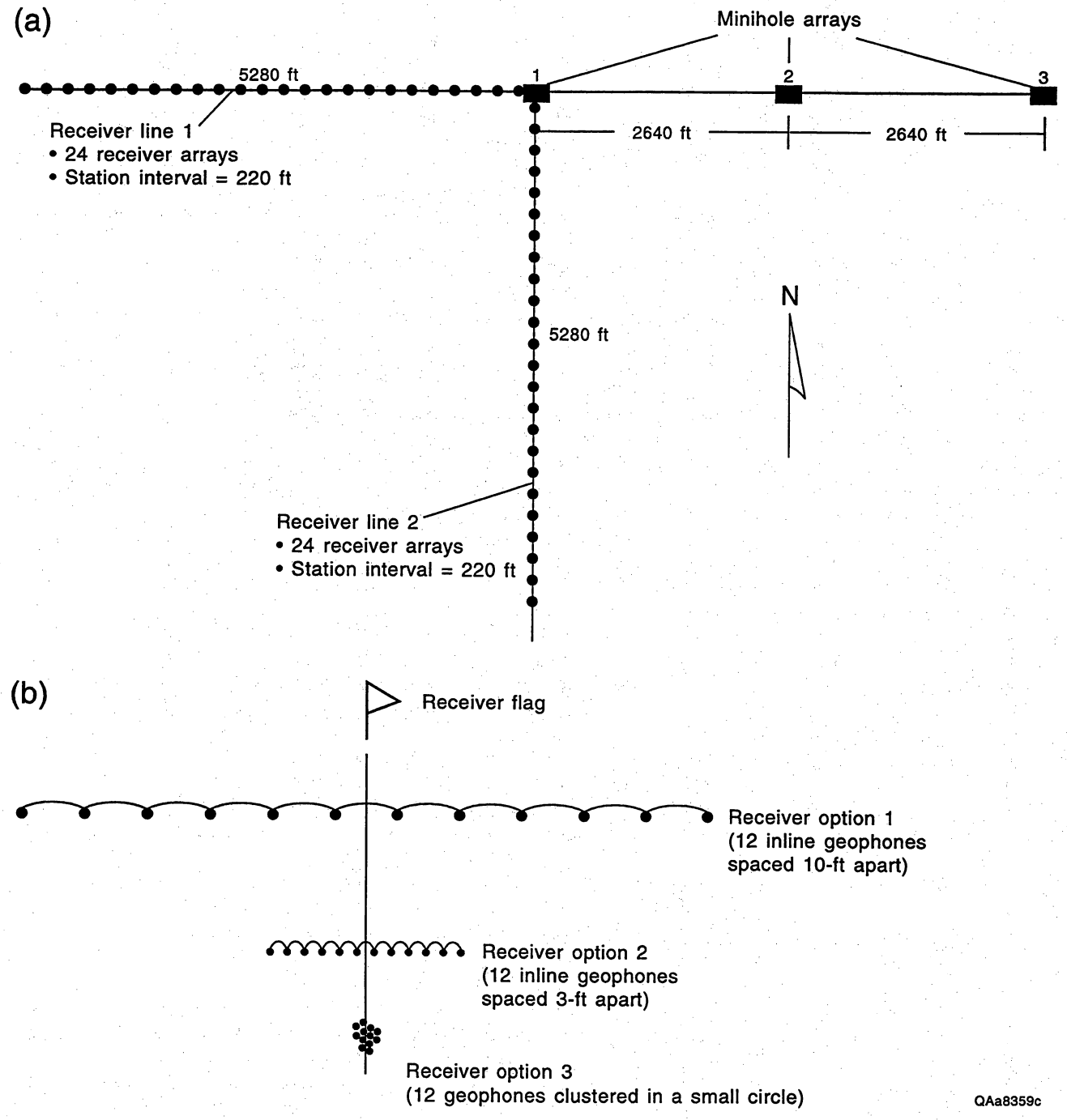

Figure D12. Horizontal wavetesting concepts implemented at Boonsville field. The test site is indicated in Figure D1. In (a), five-hole arrays were constructed at each of the three east-west source stations (solid rectangles) following the design concept shown in Figure D4. Receiver flags were surveyed at the locations indicated by the solid circles to create two receiver lines, one oriented east-west and one oriented north-south. The three receiver array options shown in (b) were constructed at each of these receiver flags.

required to image the targeted Atokan-age reservoirs occurring at depths between 4,500 and 6,000 ft.

Three receiver array designs were deployed at each receiver flag (Fig. D12b). In design 1, 12 inline geophones were spaced 10 ft apart to form a linear array 110 ft long; in design 2, 12 geophones were spaced 3 ft apart to form a linear array 33 ft long; and in design 3, 12 geophones were clustered inside a circle having a diameter of approximately 5 ft. In concept, the two smaller arrays should preserve the high-frequency components of the reflected wavefield (see comments related to equation 1) but should not cancel low-frequency ground roll, whereas the larger 110-ft array should attenuate some of the ground roll but perhaps also attenuate some of the high frequencies in the reflected signal. The purpose of the horizontal wavetesting was to determine which array design recorded a wavefield that had the desired wide reflection bandwidth but still reduced the ground roll noise to an acceptable level.

Some of the wavetest data recorded with these receiver design options are shown in Figures D13 and D14. In each array geometry, the data are dominated by ground roll noise, and no reflection events are obvious in any of the receiver responses. To determine whether reflections were present underneath the high-amplitude noise, the data were transformed into the frequency-wavenumber (f-k) domain. The value of these transforms (Figs. D15 and D16) is that they reveal energy alignments over a much wider range of amplitudes (typically 60 dB or more) than can be determined by a visual inspection of wiggle trace data (typically a range of only 20 dB or less).

Even in this high-resolution f-k domain, there was little evidence of reflection events, and the obvious implications were that the minihole shots created a strong ground roll and that there was probably a considerable amount of near-surface scattered noise also. On the basis of these horizontal wavetests, a 3-D receiver array length of 110 ft was selected over the shorter length of ~30 ft, which was anticipated would be supported by the test results. This longer array length was chosen because, due to the obvious generation of strong ground roll at this test site, it seemed wiser to have a reasonably long array that would partially attenuate ground roll than to

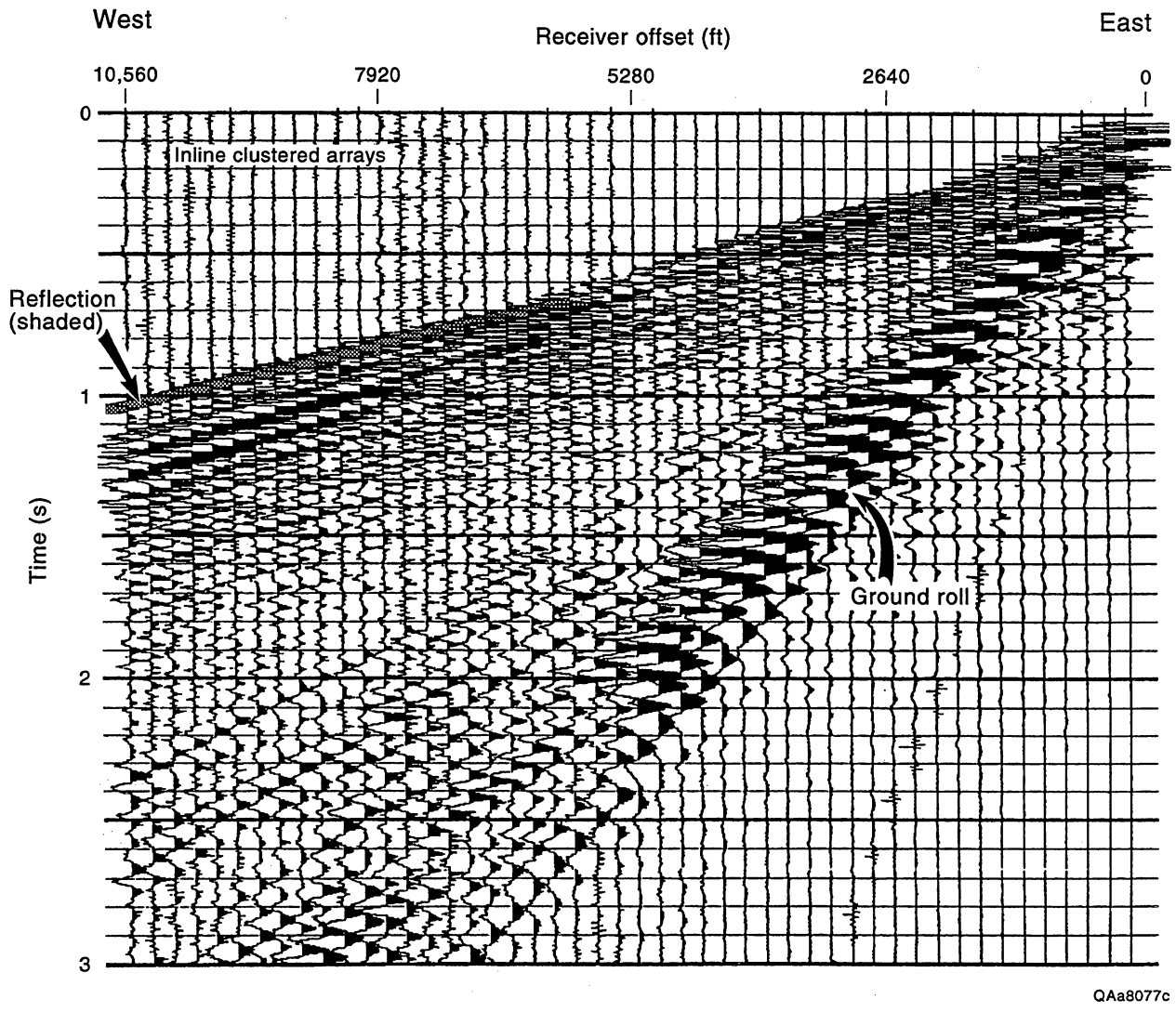

Figure D13. An example of the horizontal wavetest data recorded using the point receiver option (12 geophones clustered inside a circle having a diameter of approximately 5 ft). The receivers were deployed along receiver line 1, the east-west arm of the wavetest array (Fig. D12). This display combines the responses of two different explosive shots. The traces between offset distances of 0 and 5,280 ft are the response of the 24 east-west clustered receiver stations to a shot from minihole array 1 (Fig. D12), and the traces between receiver offsets of 5,280 and 10,560 ft are the response of these same 24 receiver stations to a shot from minihole array 3. Ground roll noise is strong; some reflection energy can be seen at the longer offsets. The linear events between the ground roll noise and the shaded reflection are refractions.

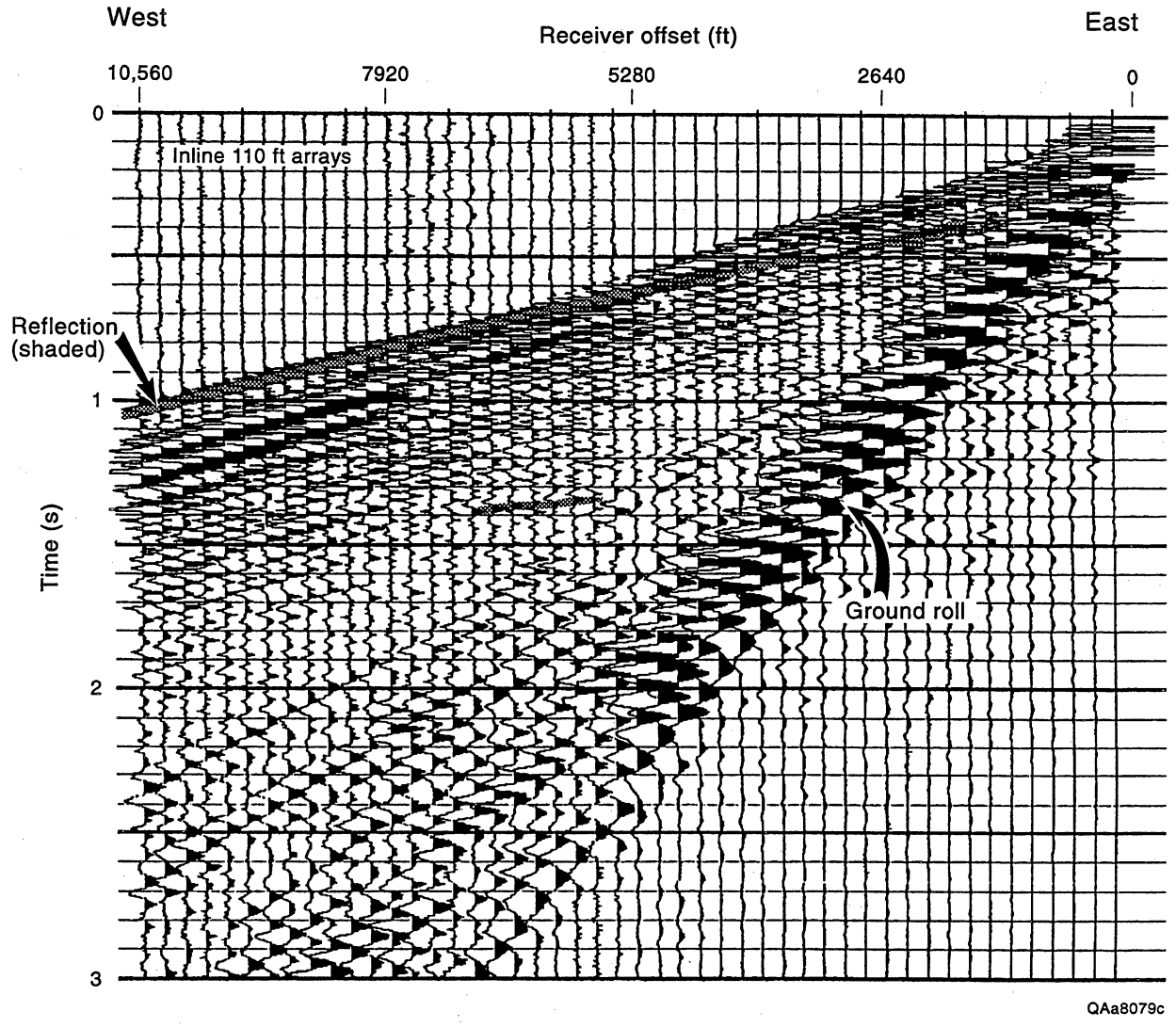

Figure D14. Horizontal wavetest data recorded using a moderately long receiver array (12 geophones spaced 10 ft apart to form a 110-ft array). The receivers were deployed along receiver line 1, the east-west arm of the wavetest array (Fig. D12). This display combines the responses of two different explosive shots. The traces between offset distances of 0 and 5,280 ft are the response of the 24 east-west, long (110-ft) receiver stations to a shot from minihole array 1 (Fig. D12), and the traces between receiver offsets of 5,280 and 10,560 ft are the response of these same 24 receiver stations to a shot from minihole array 3. Ground roll noise is strong; some reflection energy can be seen at the longer offsets, and a modest reflection is shaded just above 1.4 s between offset distances 5,720 and 7.040 ft. The linear events between the ground roll noise and the upper shaded reflection are refractions.

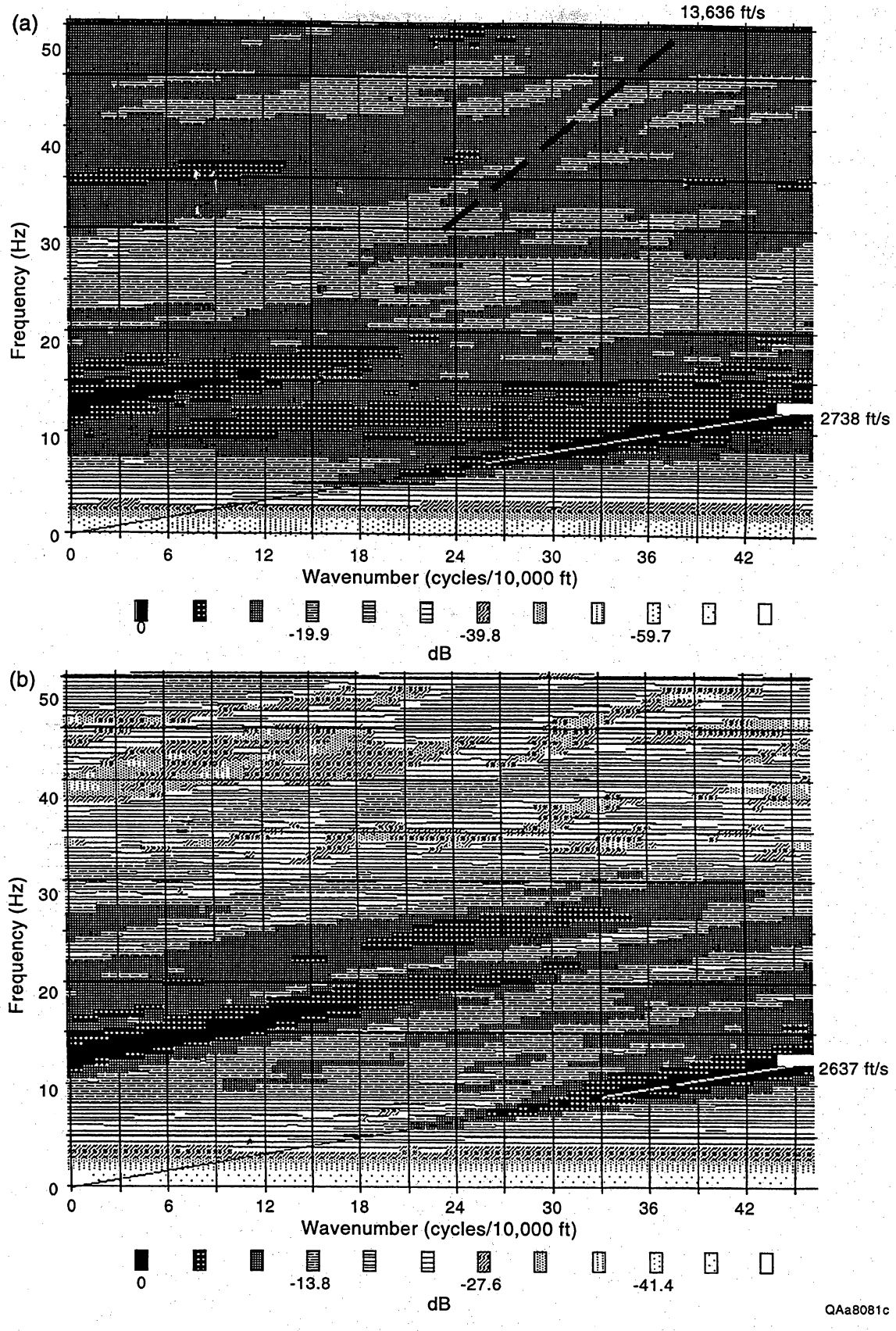

Figure D15. The horizontal wavetest data recorded on east-west receiver line 1 after transforming to the f-k domain. (a) The f-k spectrum of the 110-ft long receiver arrays. The f-k energy alignment exhibiting a velocity of 2,738 ft/s is the ground roll event labeled in Figures D13 and D14. Only hints of reflection signal exist, such as the modest energy alignment with a velocity of 13,636 ft/s. (b) The f-k spectrum of the clustered receiver array responses. Ground roll energy (velocity 2,637 ft/s) dominates the data, and it is difficult to find any evidence of reflected signal.

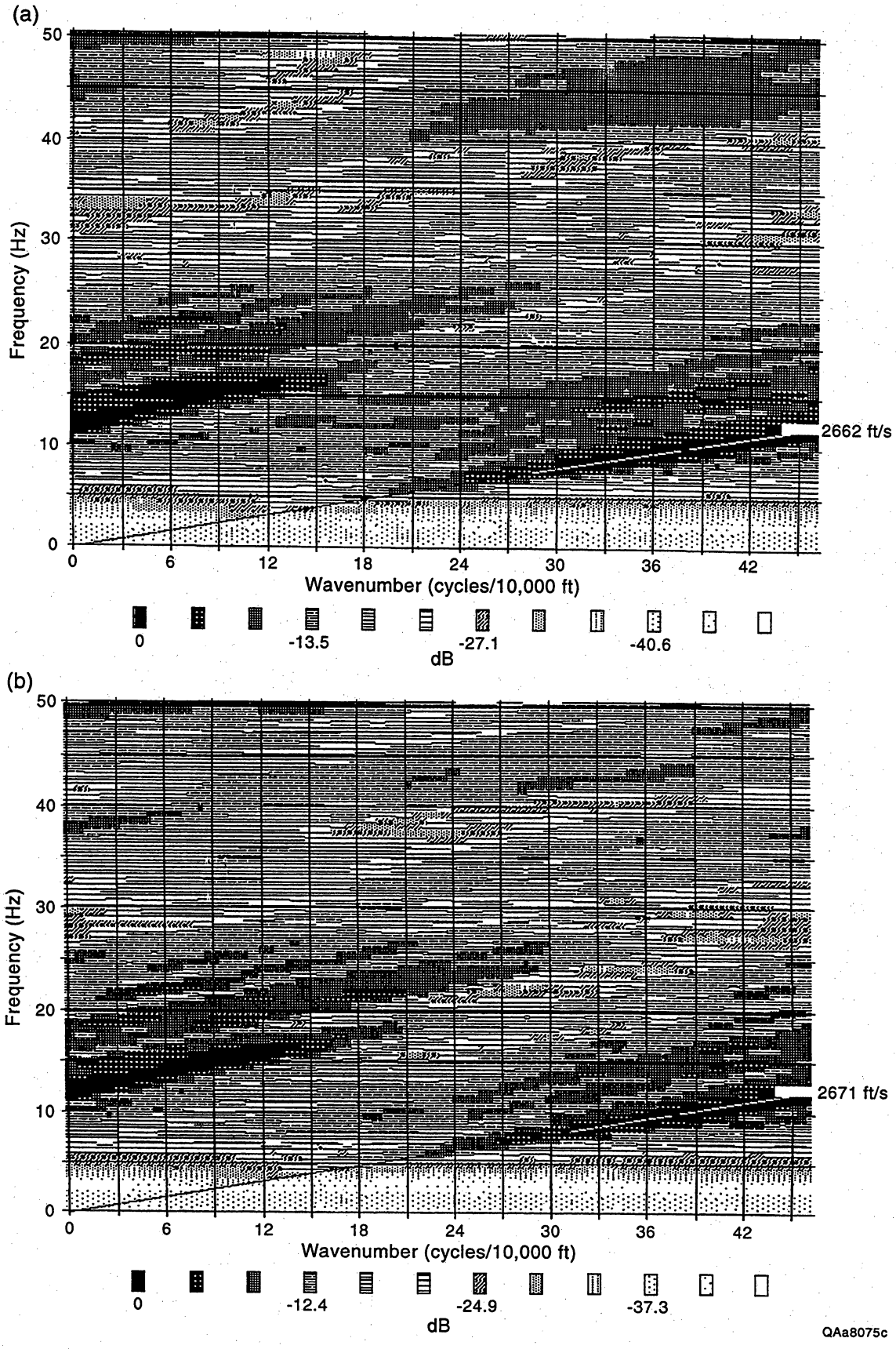

Figure D16. The horizontal wavetest data recorded on north-south receiver line 2 (Fig. D12) after transforming to the f-k domain. (a) The f-k spectrum of the 110-ft long receiver arrays. (b) The f-k spectrum of the clustered receiver arrays. Both spectra are dominated by ground roll and there is little evidence of reflected signal. Ground roll was expected to be strong on this test line because the receiver arrays were broadside to the shot.

have a short array that would ensure that frequencies greater than 150 Hz were not severely attenuated.

Design

Staggered-Line Geometry

A unique 3-D source-receiver geometry, referred to as a staggered-line grid, was implemented at Boonsville field. The geometrical pattern that was used is illustrated in Figure D17. In this geometry, adjacent source lines were shifted by one-half of the source interval, and, likewise, adjacent receiver lines were shifted by one-half of the receiver interval. This recording technique allowed the data to be sorted into large, higher fold bins [measuring (0.5 × source interval) × (0.5 × receiver interval)] or into small, lower fold bins [measuring (0.25 × source interval) × (0.25 × receiver interval)]. At Boonsville, the receiver and source intervals were both 220 ft, so the sizes of the two stacking-bin options provided by this staggered-line geometry were 110 × 110 ft and 55 × 55 ft, as shown in Figure D17.

This recording geometry allowed higher fold, large-bin data to be used as the primary data set for determining accurate residual statics and precise stacking velocities and for a first-pass interpretation, and lower fold, small-bin data to be used when greater lateral resolution was needed in the interpretation process. The technical advantage of this staggered-line technique is that the increased lateral resolution it provides is accomplished by directly sorting the data into small bins during the stacking process and not by doing some type of poststack trace interpolation that converts a large trace spacing to a smaller trace spacing. The economic advantage is that small-bin data are acquired at the lower cost of large-bin-data acquisition.

Line Spacing and Stacking Fold

As shown in Figure D17, the basic field design plan was to space receiver lines 880 ft apart and to separate source lines a distance of 1,320 ft. This source-receiver line geometry was

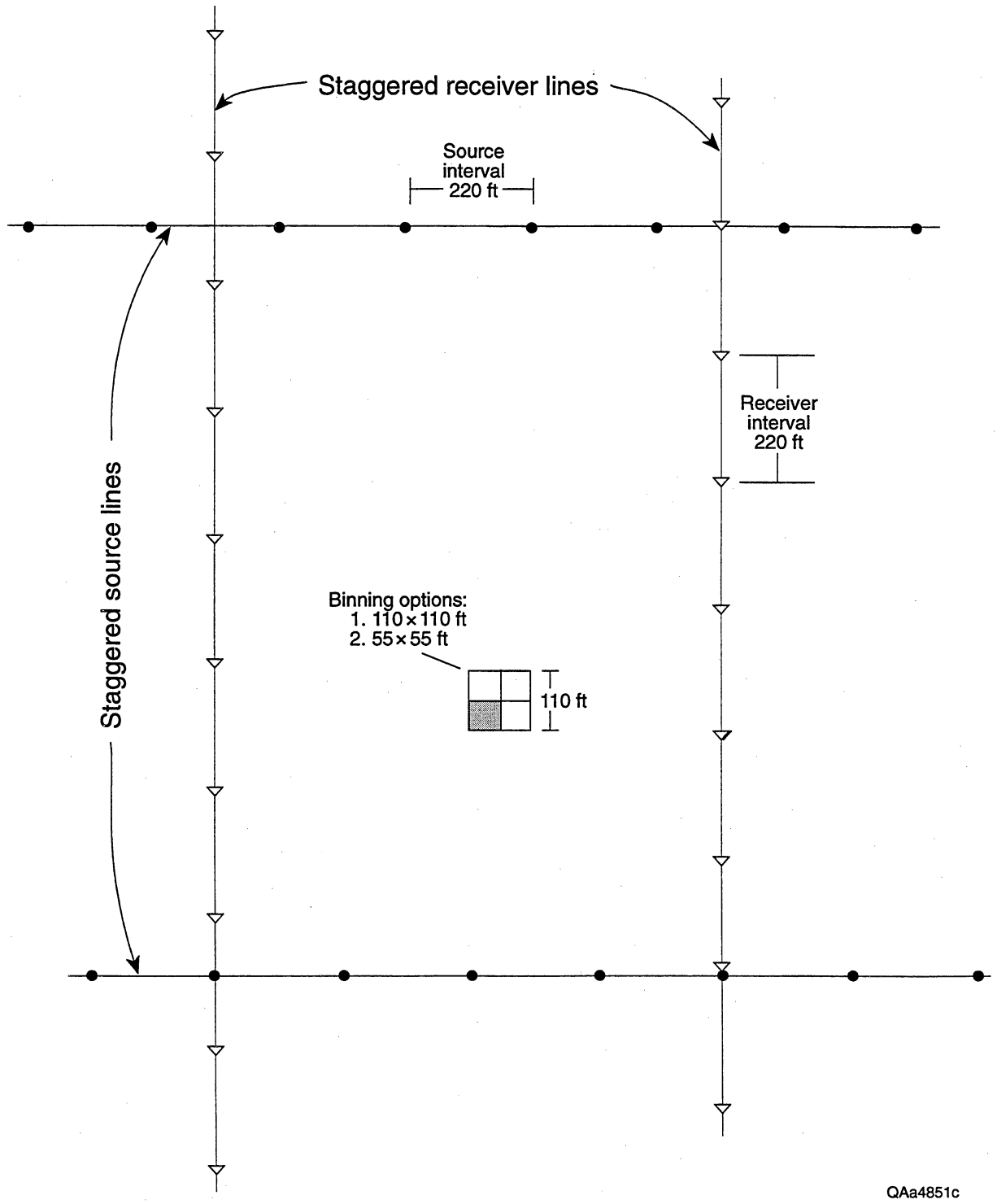

Figure D17. The staggered-line geometry used at Boonsville field. Source flags and receiver flags were stationed 220 ft apart so that the size of the conventionally defined stacking bin was 110 × 110 ft. In the staggered-line technique, adjacent receiver lines were shifted north or south by one-half of the receiver interval (a shift of 110 ft), and adjacent source lines were shifted east-west by one-half of the source interval (a shift of 110 ft). This geometry allows the data to be sorted into stacking bins measuring 110 × 110 ft or into smaller bins measuring 55 × 55 ft.

surveyed over the 26-mi^2 3-D seismic area, except that in some locations, the line spacings were varied to avoid production facilities and to minimize cultural problems. The stacking folds that resulted from this geometry when the data were sorted into 110- × 110-ft bins and then into 55- × 55-ft bins are shown in Figures D18 and D19, respectively. The increased stacking fold shown along the east and south margins of the grid resulted because extra source stations were drilled in these areas to cause the stacking fold to build to a high level rapidly. The two stacking-fold distributions in Figures D18 and D19 differed by a factor of 4, as expected, because the respective stacking bin areas differed by a factor of 4.

Acquisition

Recording System

Northern Geophysical used an I/O System Two to record the Boonsville 3-D data. This modern seismic recording system was important in the project because it generated 24-bit data words to increase dynamic resolution and to allow lower amplitude reflection signals to be extracted from noisy field records than could have been if the data had been recorded with a system that generated 16- or 18-bit data words. Horizontal wavetesting had already shown that noisy field records and weak reflection amplitudes would be common inside the Boonsville grid (Figs. D13–D16).

Recording Aperture

The Atokan-age reservoirs at Boonsville field occur at depths from 4,500 to 6,000 ft, so the 3-D receiver aperture was designed as eight adjacent receiver lines, each 2.5 mi long, as shown in Figure D20. This aperture created a maximum source-receiver offset of 6,600 ft in the north-south direction and 3,520 ft in the east-west direction (Fig. D20). Ideally, the east-west offset should also have been ~6,000 ft (the depth of the deepest reservoir to image), but an aperture of this size was not possible because the data were recorded at a sample rate of 1 ms. The eight-line

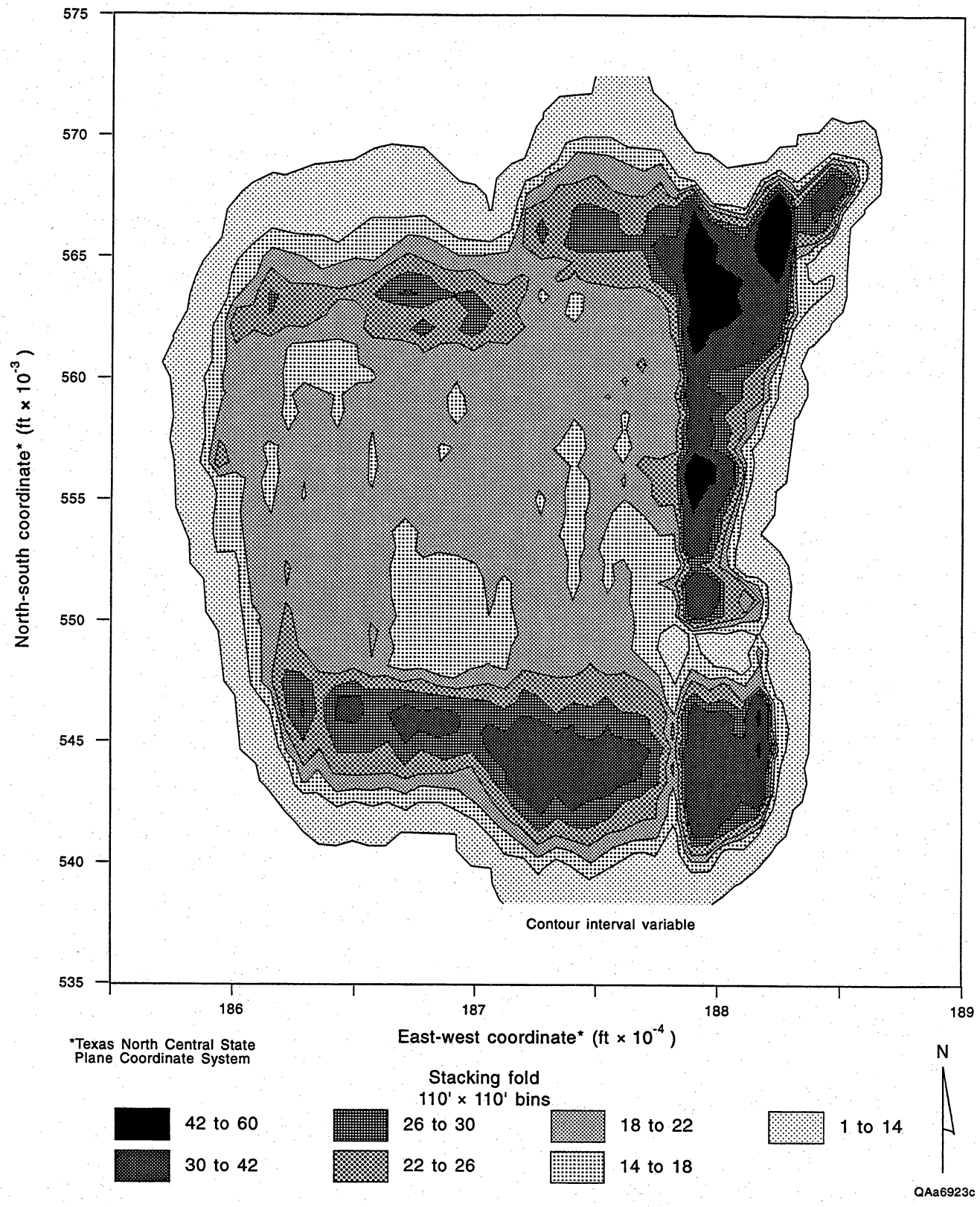

Figure D18. Stacking fold for the 110- × 110-ft bins as determined by trace sorting during data processing.

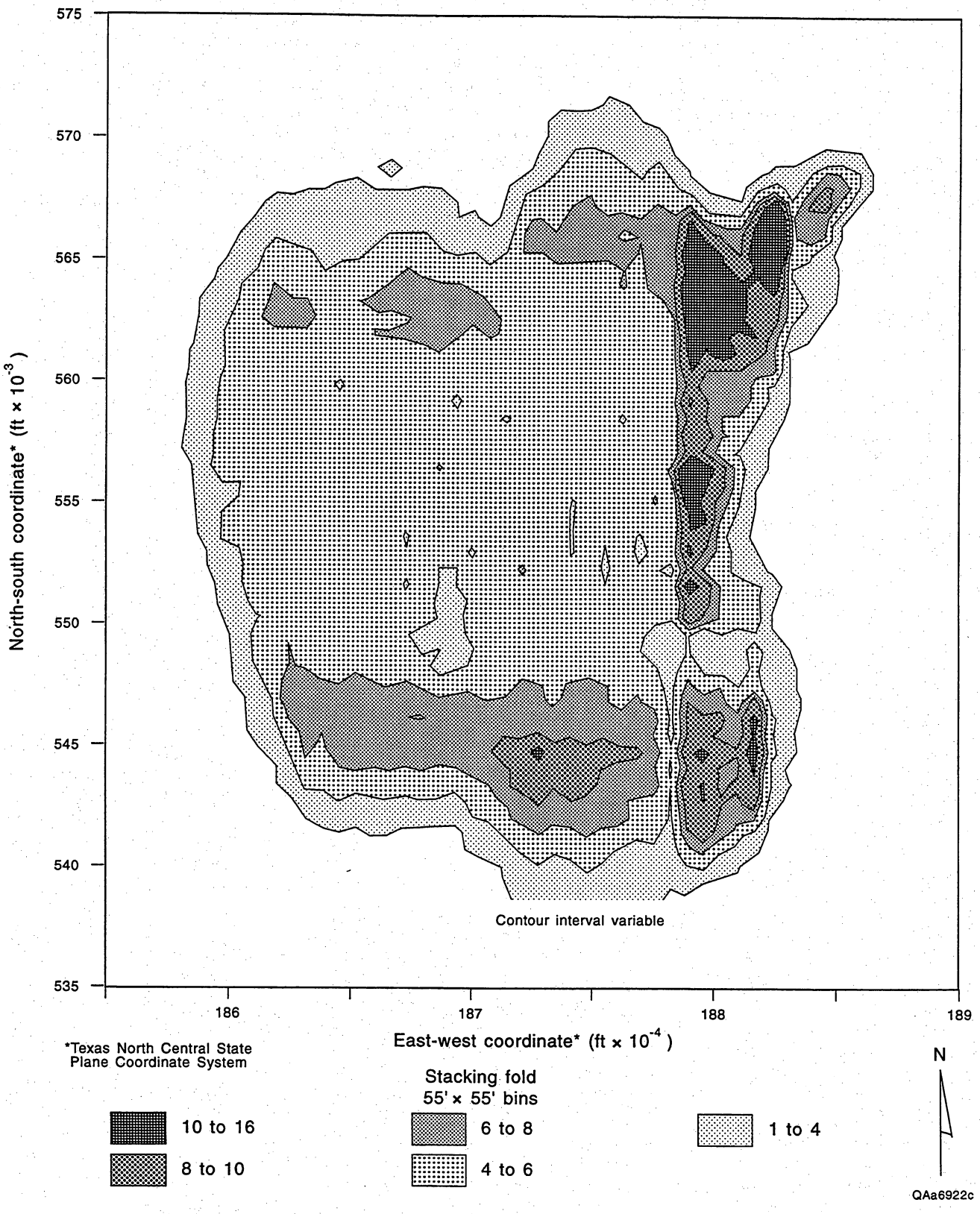

Figure D19. Stacking fold for the 55- × 55-ft bins as determined by trace sorting during data processing.

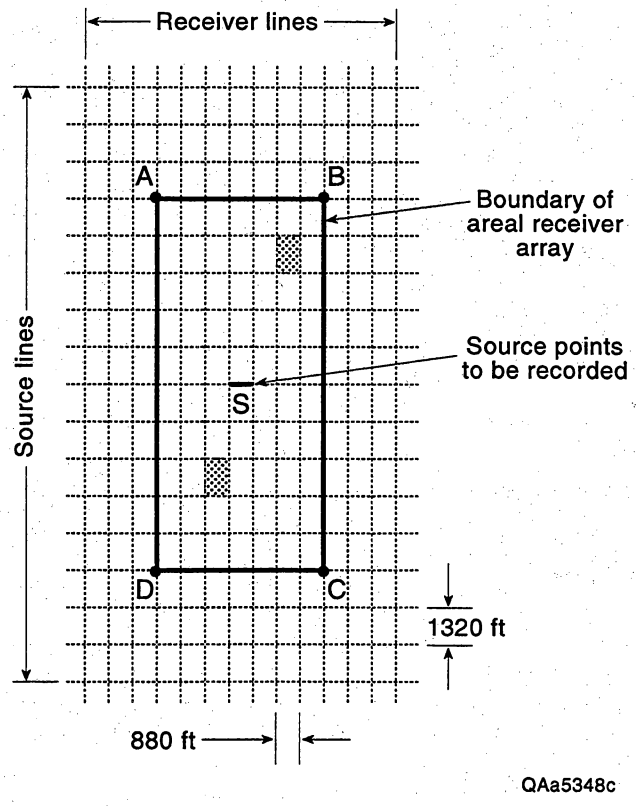

Figure D20. The receiver aperture ABCD used at Boonsville field. The aperture involved eight north-south receiver lines, each 2.5 mi long and spanning 10 source line intervals. The east-west width of the aperture was 1 1/6 mi (i.e., seven receiver line intervals of 880 ft). The shotpoint was always at S, the center of the aperture. The local source-receiver geometry within each cell of this aperture (such as either of the two shaded cells) is defined in Figure D17.

aperture in Figure D20 contains 468 receiver stations (61 stations/line × 8 lines), and the I/O System Two could not record significantly more data channels without resorting to a data sample rate of 2 ms. A sample rate of 1 ms was preferred over 2 ms so that the high-frequency components of the wavefield (>150 Hz) would not be attenuated by the alias filter in the recording system. Subsequent data analysis showed that this aliasing concern was not justified, and a sample rate of 2 ms and a wider east-west recording aperture could have been used.

Data Recording in Nonoverlapping Apertures

Typically, 3-D seismic data are recorded using continuously overlapping receiver apertures. In this standard industry technique, energy sources are activated at successive source stations that are juxtaposed immediately next to each other to form a continuous, unbroken movement of the seismic source across the survey area. Each source wavefield is recorded by an appropriate receiver aperture that also moves uniformly and continuously in space to stay centered about the moving source point; i.e., the receiver apertures continuously overlap from source point to source point.

The I/O System Two seismic recording system used in the Boonsville study allowed a much greater flexibility for defining which source points and what receiver apertures could be recorded. Specifically, the system removed the requirement of a continuous overlapping receiver aperture and allowed data to be recorded in widely separated, nonoverlapping receiver apertures whenever that procedure expedited the data collection activity.

All of the shot hole arrays inside the 26-mi^2 Boonsville survey were drilled and loaded before any receivers were deployed. Once an appropriate number of receiver lines (12 to 15) were laid out across the entire north-south extent of the grid (typically 5 mi of cable per line, Fig. D1), the flexible I/O software allowed the receiver aperture diagrammed in Figure D20 to be activated about any source point falling inside a north-south-oriented strip roughly 1 mi wide (east-west) passing through the center of this grid of 12 to 15 north-south receiver lines.

This ability to *turn on* a receiver aperture anywhere within this large recording strip introduced considerable efficiency into the field recording process. Specifically, with this capability the speed of data recording was controlled more by how many shooters were in the field than by any other factor. To illustrate the concept, a hypothetical recording scenario using this flexible positioning of a receiver aperture is depicted in Figure D21. In this example, 22 receiver lines are assumed to be laid out, and three shooters are positioned across the receiver grid at locations S_1, S_2, and S_3. The recording truck can be positioned anywhere in this 22-line grid and still be electrically connected to the entire grid. At Boonsville, each source line segment S_1, S_2, and S_3 spanned four shotpoints because the receiver line spacing was 880 ft and the shotpoint interval was 220 ft (Fig. D17). Receiver aperture $A_1B_1C_1D_1$ is turned on first, and shooter S_1 connects a shooting box to one of the four minihole arrays spanned by distance S_1. Once the data from this shot are recorded, receiver aperture $A_2B_2C_2D_2$ is activated, and shooter number 2 electrically connects a minihole array inside source segment S_2 to the recording truck. As soon as this shot is recorded, receiver aperture $A_3B_3C_3D_3$ is turned on, and shooter number 3 electrically connects a shotpoint inside segment S_3 to the recording truck. The shooting sequence then returns to shooter 1, who has moved to a new shotpoint inside segment S_1.

This technique of recording arbitrarily positioned receiver apertures allows shooters to be widely separated over a 3-D grid for optimal field flexibility, and modern recording systems, like the I/O System Two or its equivalent, allow the appropriate receiver aperture to be quickly centered (in an electrical sense) about the X-Y coordinates of the selected shotpoint. This technique cannot be used easily with most older recording systems, so when it is desired to implement this procedure of recording nonoverlapping receiver apertures, a modern recording system with the proper acquisition software should be contracted.

Although this technique of using nonoverlapping receiver apertures is attractive for dynamite shooting when a large area of shot holes has been drilled and preloaded, it does not have as much appeal for vibroseis recording unless a large number of vibrators are mobilized so

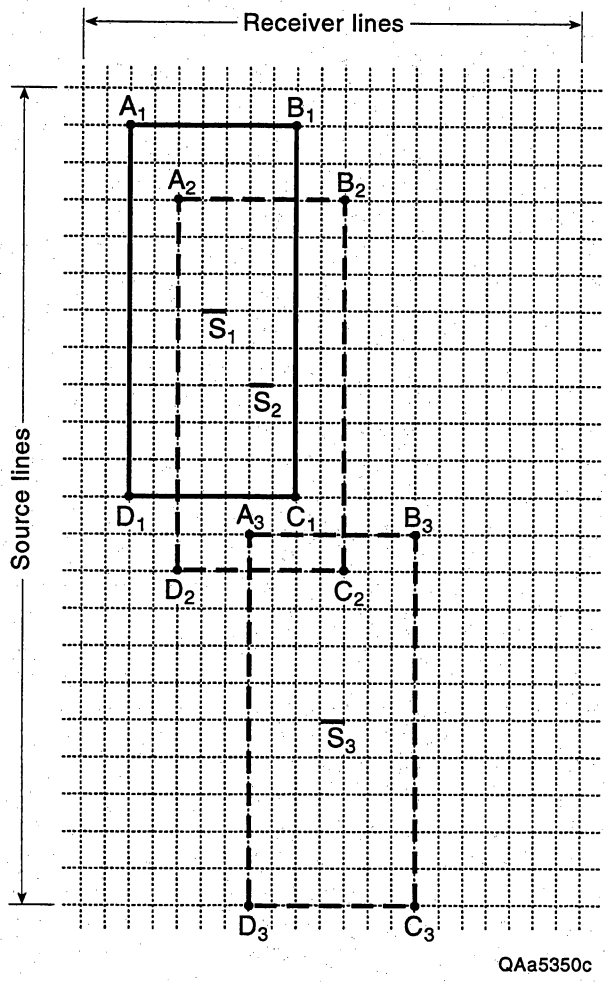

Figure D21. To increase the number of shots recorded per day, the Boonsville data were recorded using multiple shooters positioned at preplanned locations S_1, S_2, and S_3. A state-of-the-art recording system (I/O System Two) was used, which allowed receiver apertures $A_1B_1C_1D_1$, $A_2B_2C_2D_2$, and $A_3B_3C_3D_3$ to be quickly activated about S_1, S_2, and S_3 as soon as the shooters at these locations were ready to power their shooting boxes. This shooting technique differs from the usual industry practice of moving successive receiver apertures no farther than one receiver line spacing or one receiver interval.

that two or more vibrator source arrays can be created and positioned at different locations inside the 3-D grid.

Data Quality

An example of the Boonsville data recorded using the source-receiver concepts and the recording geometry described in the preceding sections is shown in Figure D22. Data from only five of the eight receiver lines involved in this particular recording aperture (see Fig. D20) are shown. Each displayed line contains 61 traces representing the responses recorded at the 61 receiver stations distributed over the north-south extent of the receiver line.

These records are typical of most data recorded across the Boonsville grid in that they contain a considerable amount of ground roll noise, and only a few reflection events can be seen. The strong ground roll noise was not unexpected, on the basis of the horizontal wavetesting results (Figs. D13–D16). Vertical seismic profiling had already confirmed that numerous reflection events would be created (Fig. D8), so the extraction of these relatively weak, wideband reflection signals from field records of this quality presented a challenging data-processing problem. The data-processing techniques used to create 3-D seismic images from these Boonsville records are discussed in the following sections.

Processing

The Boonsville 3-D data were processed by Trend Technology, Inc., Midland, Texas. Trend imposed stringent processing requirements to preserve the high frequencies that were known, from vertical wavetesting, to exist in the reflection signals generated by the C-10 directional charges used as the energy source at Boonsville field. Because many field records had a high level of noise contamination (Fig. D22), the processing procedures that Trend used produced remarkably good 3-D images of the targeted Atokan thin-bed stratigraphy. The data-processing technology used to image the thin-bed reservoirs distributed throughout Boonsville field are

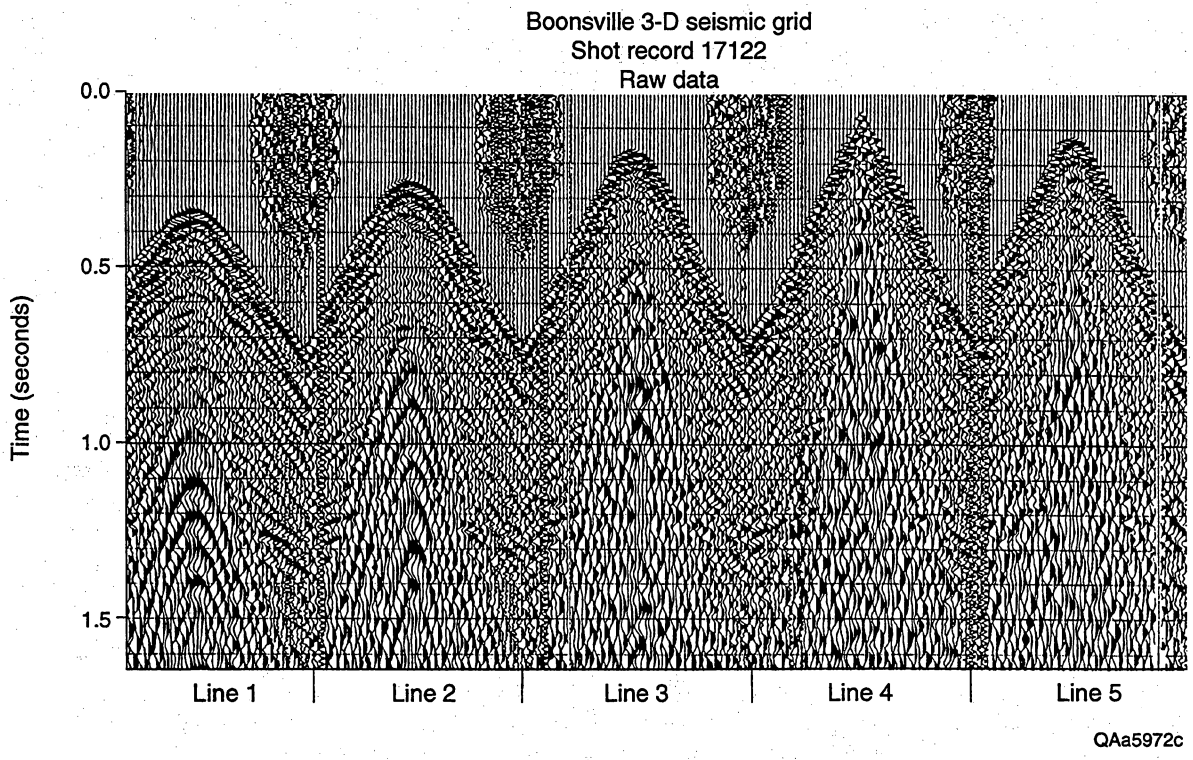

Figure D22. Typical field data recorded across the Boonsville 3-D grid. Each "line" represents the response of a single north-south receiver line inside the recording aperture (Fig. D20). Only five of the eight receiver lines involved in the receiver aperture are shown. Each line has 61 receiver stations within its 2.5-mi length; hence, there are 61 data traces in each line display. The data exhibit strong ground roll noise that camouflages most of the reflection events.

summarized in Table D1, and the more critical components of this processing procedure are described in the following sections.

Table D1. Boonsville 3-D data-processing sequence.

(1)	Surface and Subsurface Maps
(2)	Geometry Definition and Application
(3)	Prefilter 17-250 Hz
(4)	Surface-Consistent Deconvolution
(5)	Refraction Statics: Datum = 900 ft, Velocity = 8000 ft/s
(6)	Velocity Analysis
(7)	Refraction Statics: Datum = 900 ft, Velocity = 8000 ft/s
(8)	CDP Stack
(9)	Automatic Residual Statics: Iterate 6 Times
(10)	Velocity Analysis
(11)	Normal Moveout
(12)	Spectral Balance
(13)	CDP Residual Statics
(14)	CDP Stack (55- and 110-ft bins)
(15)	Interpolate Missing CDP's at edges of data volume (55-ft bins only)
(16)	3-D Migration

Deconvolution Tests

Vertical wavetesting demonstrated that the small C-10 directional charges used as the seismic source at Boonsville field produced a seismic wavelet having frequencies of up to 200 Hz (Fig. D7). However, horizontal wavetesting showed that reflection signals having this wide bandwidth would be masked by strong, low-frequency ground roll and surface-related noise (Figs. D13–D16). Consequently, one of the early processing tests was to determine what usable signal bandwidth actually existed in the 3-D field records because the dynamic range of the data was significantly enhanced by the availability of the 24-bit data words created by the I/O System Two data acquisition hardware.

Some of these bandwidth investigation results are shown in Figures D23 and D24. In each example, the raw field record and its associated frequency analysis are displayed on the left. The right-hand display shows the same field record after the noise has been attenuated by a low-cut filter, and the higher frequency components have been emphasized by an appropriate deconvolution operator. These tests demonstrated that wideband reflections did indeed exist throughout the Atokan interval (approximately 0.8 to 1.0 s) and that the reflection signals contained robust energy spanning a frequency range from about 10 Hz up to approximately 150 Hz. Although the initial goal of preserving frequencies up to 200 Hz in the raw field records appears not to have been realized, the spectra resulting from these tests still had impressive bandwidths that spanned almost four octaves.

Static Corrections

Because the Boonsville data contained reflection signals with frequencies as high as 150 Hz, precise static corrections were essential to preserve the high-frequency components of these signals in the final 3-D images. In addition to correcting the shot and receiver elevations to a uniform depth datum, both refraction statics and residual statics were calculated and applied as iterative processes until the time shifts that had to be applied to the traces that were summed in each stacking bin converged to an acceptably small value.

The refraction statics calculated for the Boonsville survey are shown in Figure D25. Two iterations of refraction statics were done (Table D1), with each iteration improving the accuracy of the velocity analysis and the resulting stacked image. The large corrections shown at the edges of the maps in Figure D25 (a and b) should be ignored because these values are extrapolations of the real static corrections beyond the boundaries of the actual seismic grid. However, valid static corrections as large as 30 ms were required at some source and/or receiver coordinates, which are significant time shifts for frequencies exceeding 100 Hz. For example, the 100- and 150-Hz components of the reflected wavefield have time periods of 10 and 6.7 ms, respectively. Thus, a static correction of 20 ms is equivalent to a time misalignment of two full wavelengths of the

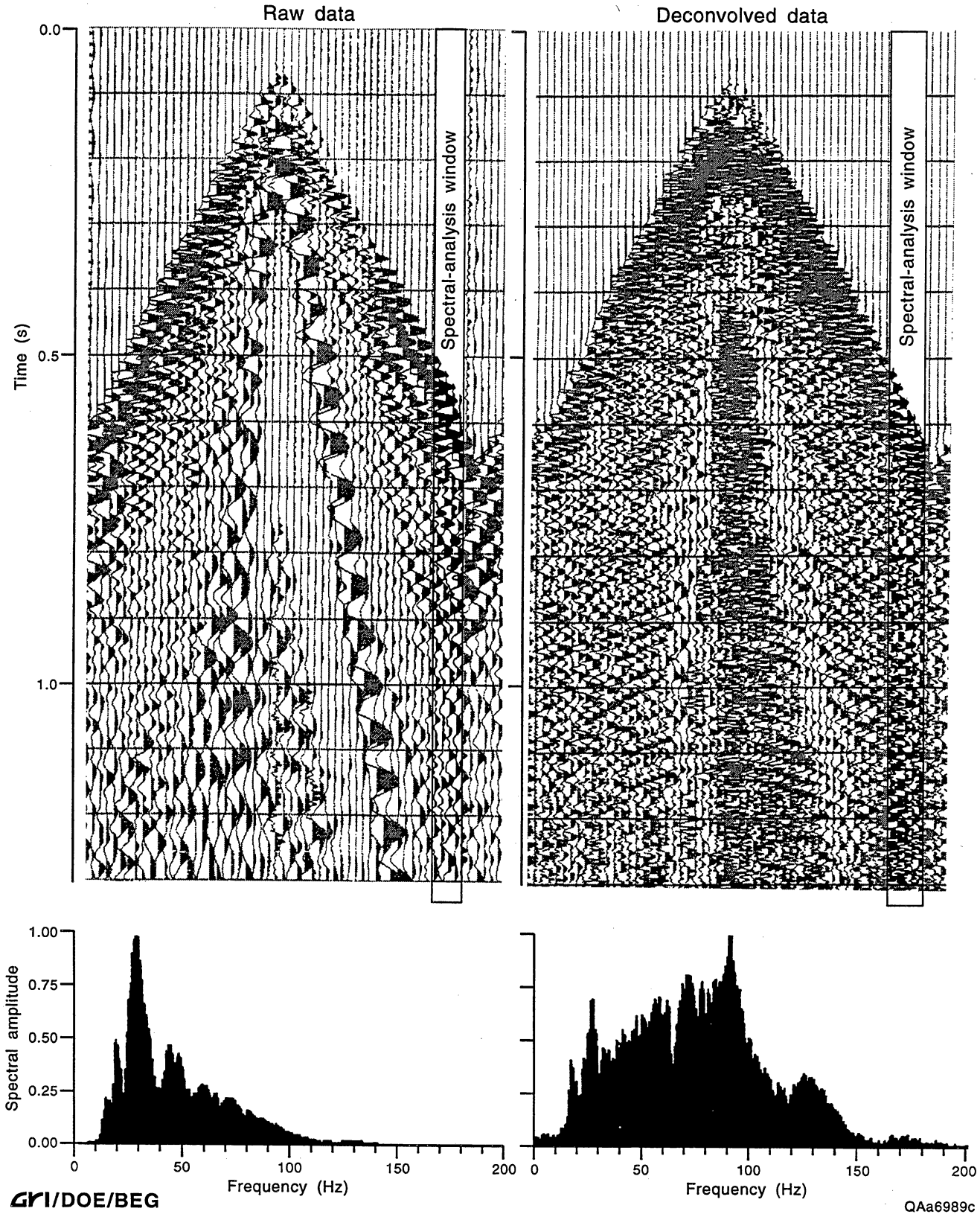

Figure D23. Deconvolution test of the far-offset traces of a Boonsville field record to determine the usable bandwidth of the reflection signals. A low-cut filter removed most of the low-frequency ground roll and other surface-related noises that are evident in the raw field record (Fig. D22) before the deconvolution operator was applied to the data. After deconvolution, the reflection signal spectrum for the far-offset traces extends from 10 to 150 Hz, which is a spectral width of almost four octaves.

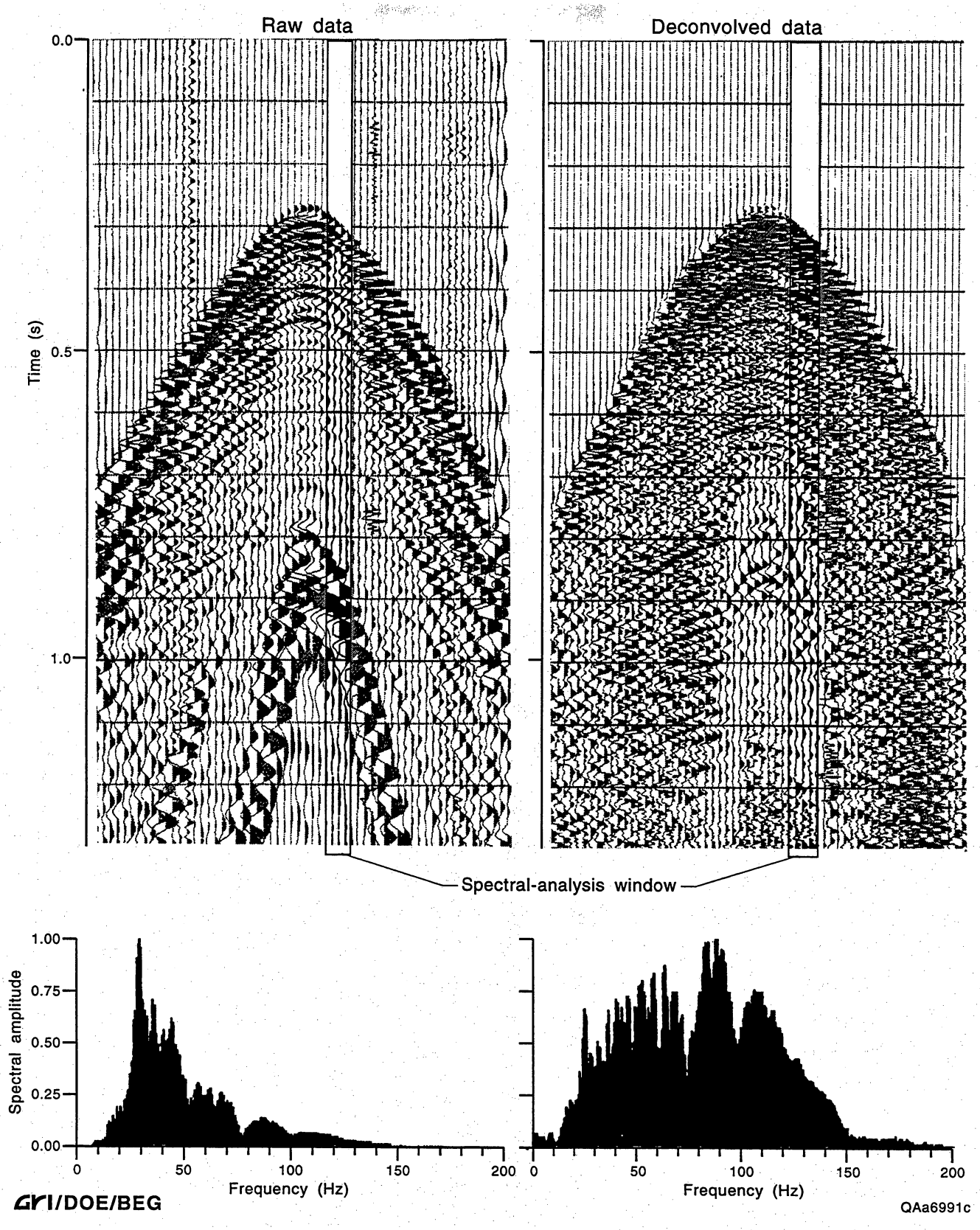

Figure D24. Deconvolution test of the near-offset traces of a Boonsville field record to determine the usable bandwidth of the reflection signals. A low-cut filter removed most of the low-frequency ground roll and other surface-related noises that are evident in the raw field record (Fig. D22) before the deconvolution operator was applied to the data. After deconvolution, the reflection signal spectrum for the near-offset traces extends from 10 to 150 Hz, which is a spectral width of almost four octaves.

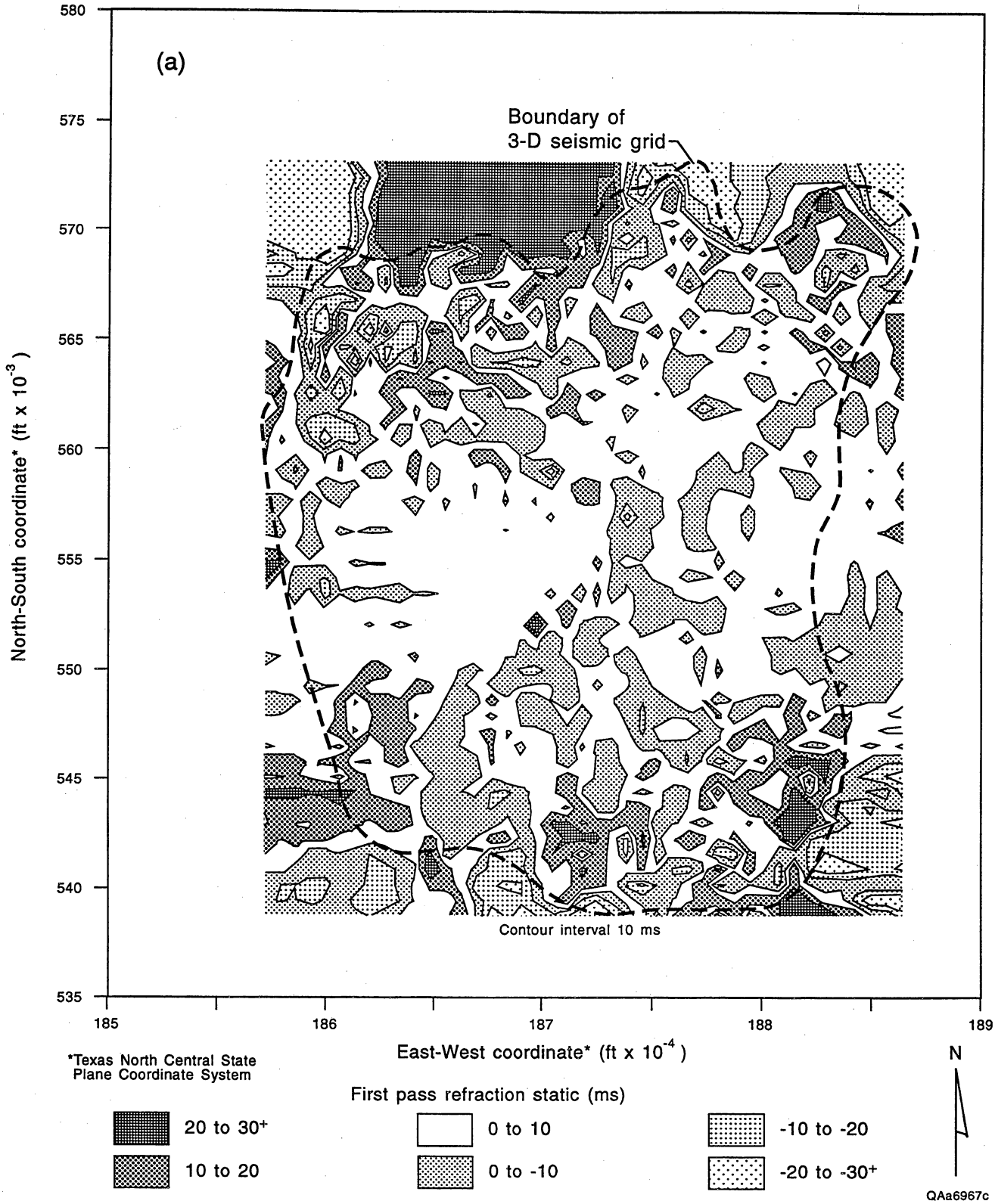

Figure D25. Refraction statics, (a) first pass and (b) second pass, applied to the Boonsville 3-D data. The boundary of the 3-D grid is superimposed on the statics map to separate valid static values inside the grid from invalid values around the edges of the map, which exist only because the mapping software extrapolates data all the way to the edges of the map coordinates.

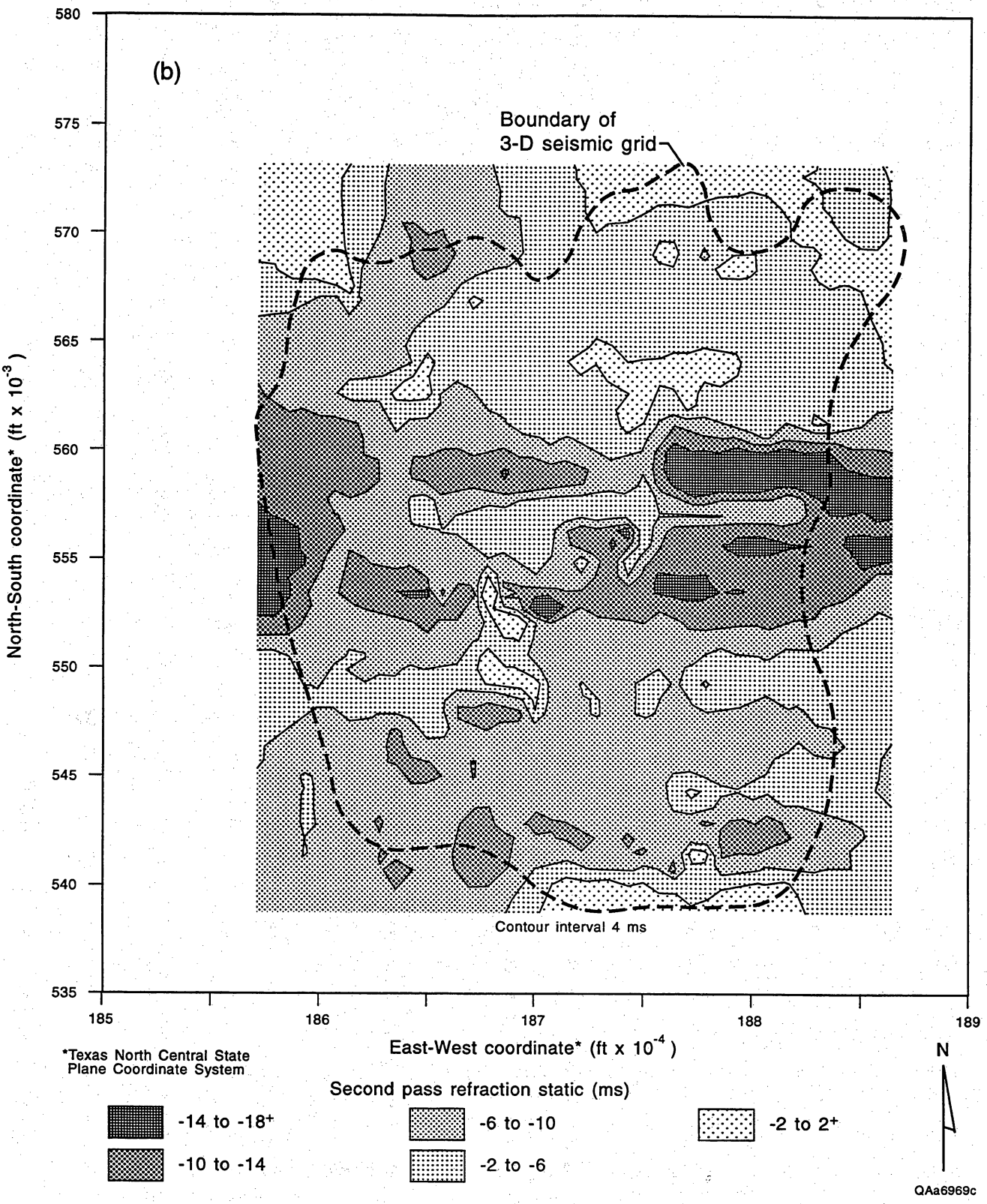
(b)
Boundary of
3-D seismic grid
Contour interval 4 ms
580
575
570
565
560
555
550
545
540
535
185
186
187
188
189
North-South coordinate* (ft x 10-3)
East-West coordinate* (ft x 10-4)
*Texas North Central State
Plane Coordinate System
Second pass refraction static (ms)
-14 to -18+
-10 to -14
-6 to -10
-2 to -6
-2 to 2+
N
QAa6969c

100-Hz component of the reflection signal and three full wavelengths of the 150-Hz component, which is the upper bound of usable signal frequency at Boonsville.

Normally, refraction statics are calculated only once. A second refraction statics analysis was done with the Boonsville data to confirm that the time picks used in the first analysis were correct. A two-pass refraction statics effort is a good procedure to use when the processing objective is to ensure that high-frequency stacked data are to be created.

The residual static calculation procedure in Table D1 was a six-stage iteration process, and the static corrections determined in the first and fourth iterations are displayed in Figure D26. (The fifth and sixth iterations were localized to small areas where there appeared to be cycle skips in the static calculations.) The first residual static calculation showed that, although the preceding refraction static corrections (Fig. D25) had significantly improved the trace alignments needed for optimum stacking, major static errors of 6 to 8 ms (approximately one wavelength of the higher frequency components) still existed in much of the 3-D grid. As shown in Figure D26 (a and b), the residual static corrections converged with each iteration, finally reaching the desired objective where no static correction exceeded one time sample (± 1 ms) anywhere inside the 3-D grid. (During the 3-D data interpretation, two locations were found where the migrated data appeared still to have a static-induced cycle skip.)

Velocity Analysis

Often velocity analyses are performed at intervals of approximately .5 mi across a 3-D seismic grid, and the optimal stacking velocities at these analysis sites are then used to construct an areal velocity map that can be used to stack data at every common depth point (CDP) in the grid. A much more detailed velocity analysis was done at Boonsville field so that the high-frequency portion of the reflection wavefield would be properly time shifted by the velocity moveout corrections before traces were summed at any of the CDP locations.

Specifically, velocity analyses were done along east-west lines separated by only 440 ft; i.e., along every fourth row of the 110- × 110-ft stacking bins inside the 3-D grid. Within each of

these east-west lines, a velocity analysis was done at every CDP, not at CDP's spaced .25 or .5 mi apart, using 50 different velocity functions. As a consequence, approximately 850,000 velocity panels were created across the Boonsville survey area, which is about two orders of magnitude more velocity information than is usually used to determine stacking velocities.

The reason for doing such detailed velocity analyses can be demonstrated by considering a simple mathematical approximation of the normal moveout experienced by a reflection event from the Atoka interval at Boonsville field. Mathematically, the normal moveout of a reflection event (i.e., the difference between the reflection arrival times at a zero-offset receiver and at a far-offset receiver) can be approximated by the equation,

$$\Delta t = \frac{X^2}{2V^2 t_o}, \tag{6}$$

where Δt is the normal moveout in seconds, X is the offset distance to the receiver in feet, V is the average velocity in ft/s down to the reflector depth, and t_o is the reflection arrival time in seconds at the zero-offset receiver position (i.e., at X=0). If we assign the values,

X = 6,000 ft (approximately the largest receiver offset) and

t_o = 0.8 s (approximately the top of the Bend interval),

and allow the average velocity V to have first a value of 12,000 ft/s and then a value of 12,200 ft/s, then the moveout corrections applied to a trace at an offset of 6,000 ft for each of these velocity possibilities are 156 and 151 ms, respectively. The time difference of 5 ms between these two time adjustments is approximately the same as the 6.7-ms time period of the 150-Hz component of the reflection signal. Thus, the objective that frequencies as high as 150 Hz be preserved during the Boonsville data processing required that the stacking velocities be determined over the complete 3-D grid to an accuracy of approximately ± 50 ft/s, which is a demanding requirement.

This type of detailed velocity study was done twice during the data processing (Table D1). Examples of the final stacking velocities determined at Boonsville are given in Figures D27 through D29. Figure 27 shows the north-south velocity behavior along inlines 100 and 200,

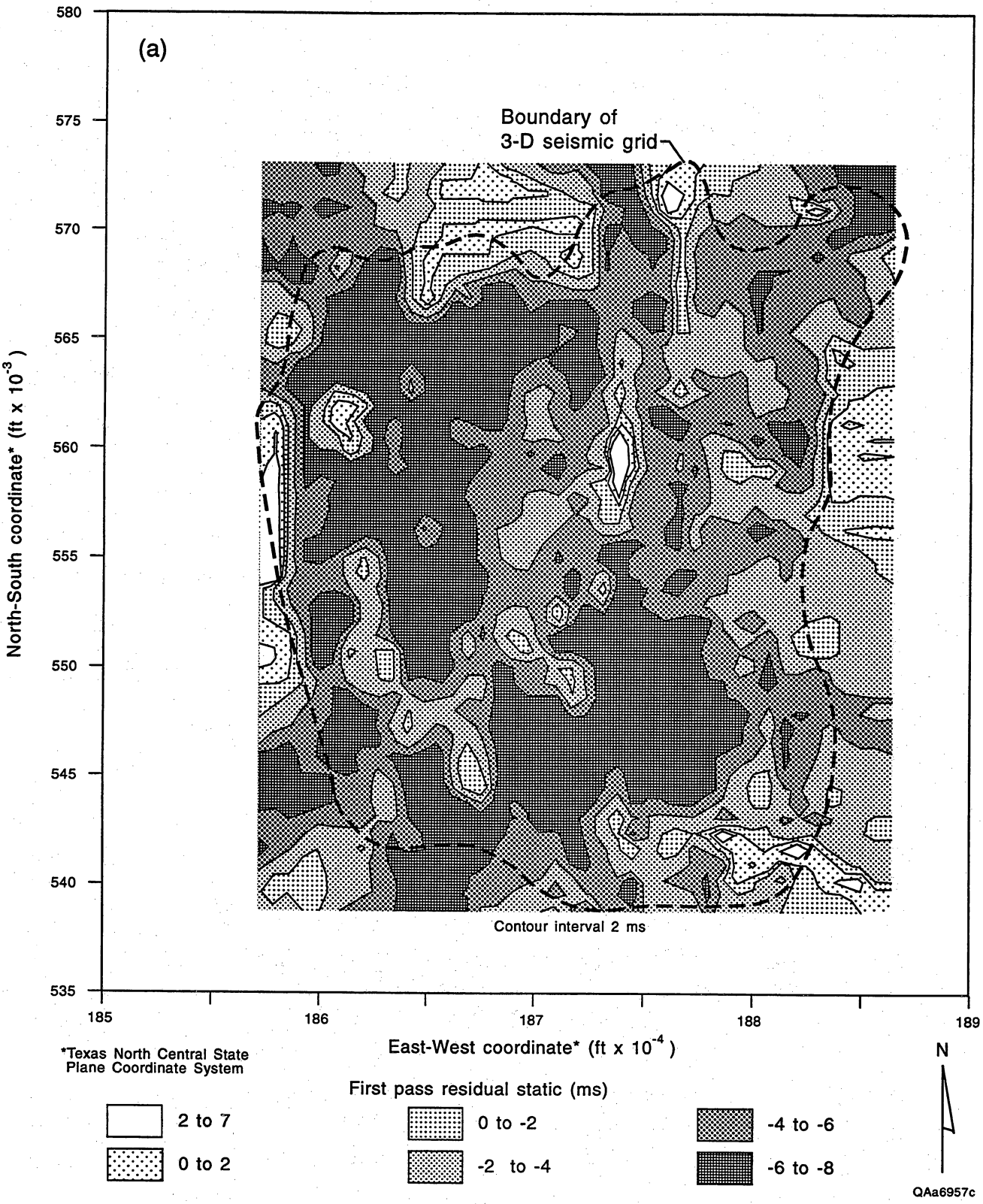

Figure D26. Residual statics, (a) first pass and (b) fourth pass, applied to the Boonsville 3-D data. The boundary of the 3-D grid is shown to isolate the valid static calculations inside the 3-D area from the invalid values outside the boundary that are simply the result of the mapping software extrapolating values to fill all of the mapping space.

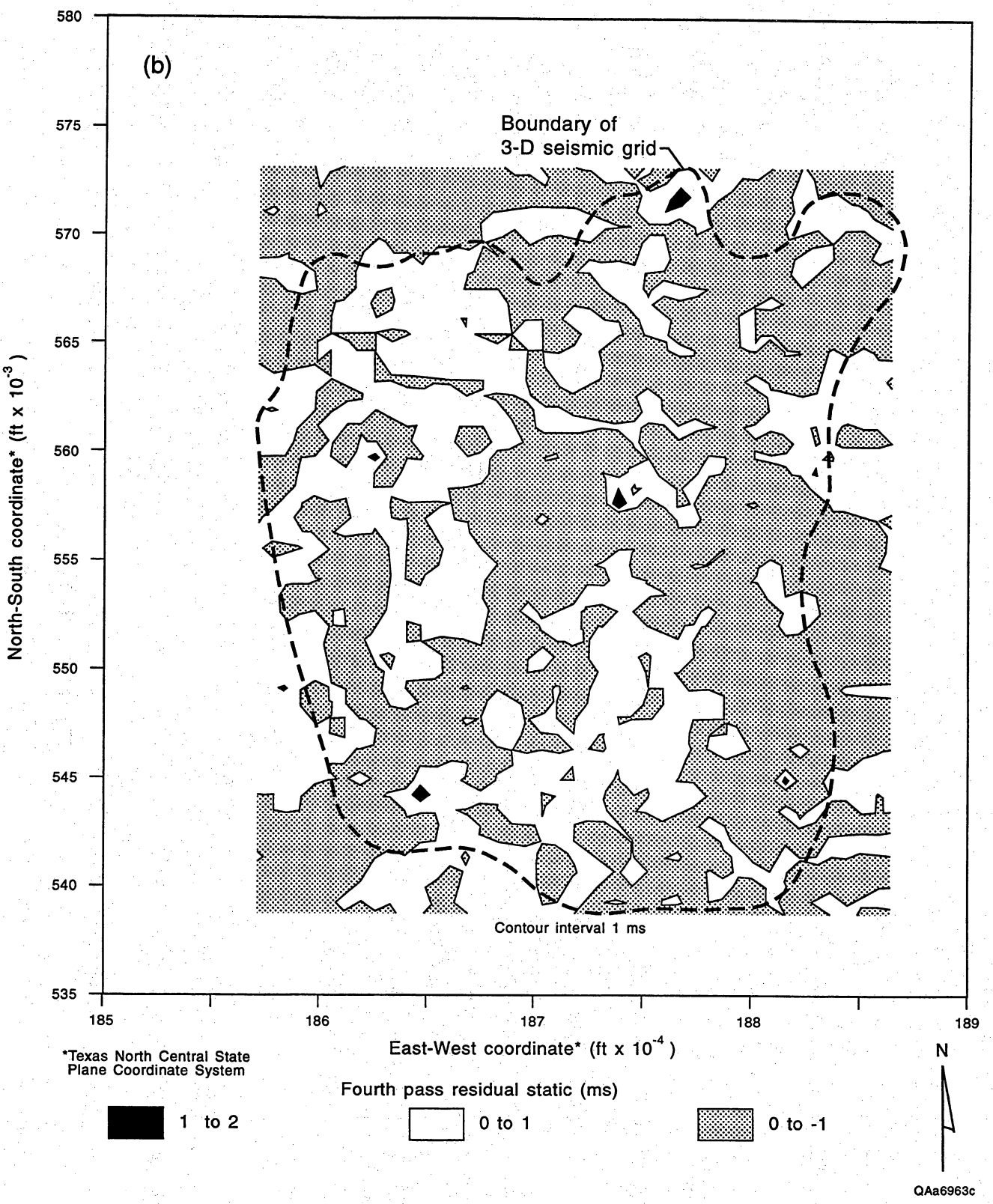
(b)
Boundary of
3-D seismic grid
Contour interval 1 ms
North-South coordinate* (ft x 10-3)
East-West coordinate* (ft x 10-4)
580
575
570
565
560
555
550
545
540
535
185
186
187
188
189
*Texas North Central State
Plane Coordinate System
Fourth pass residual static (ms)
1 to 2
0 to 1
0 to -1
N
QAa6963c

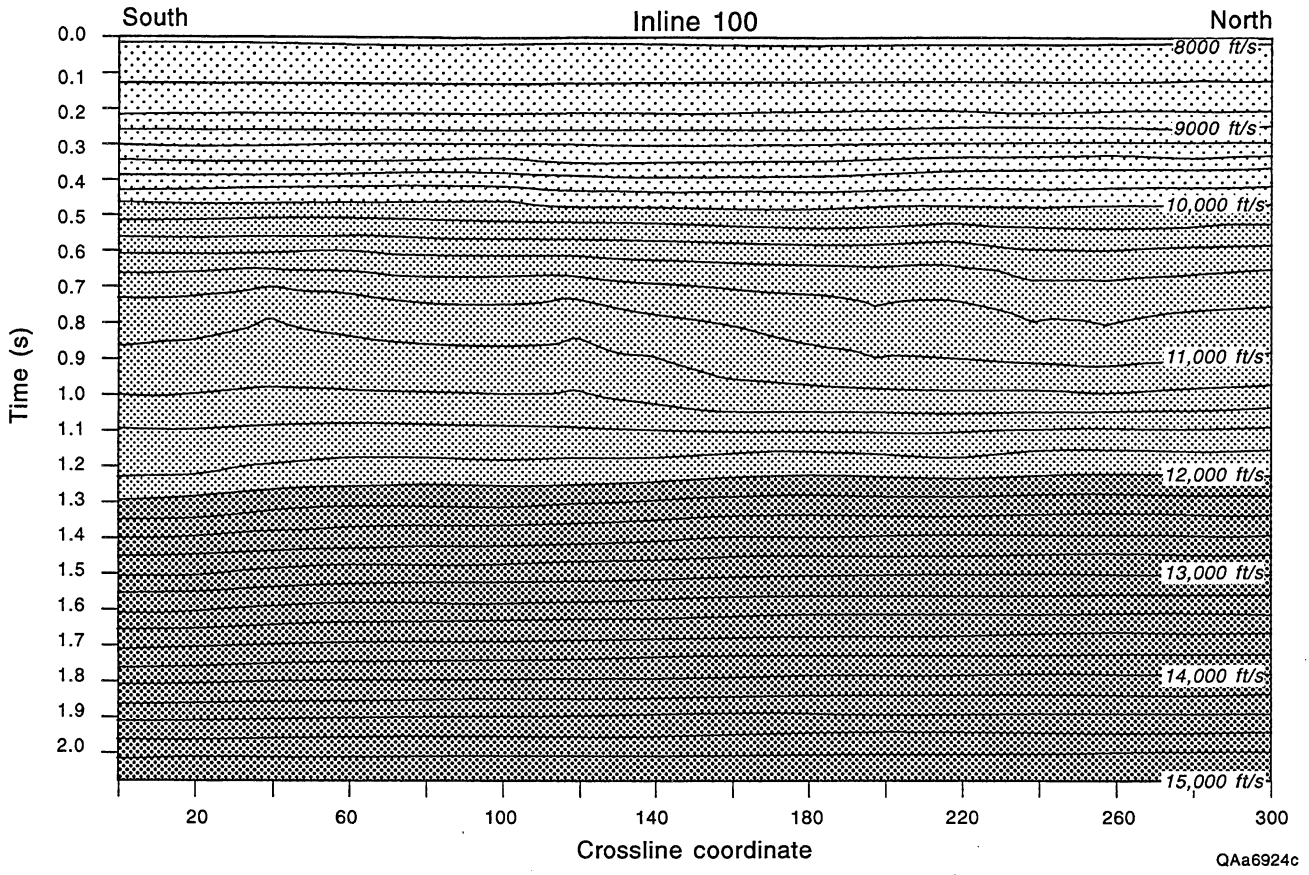

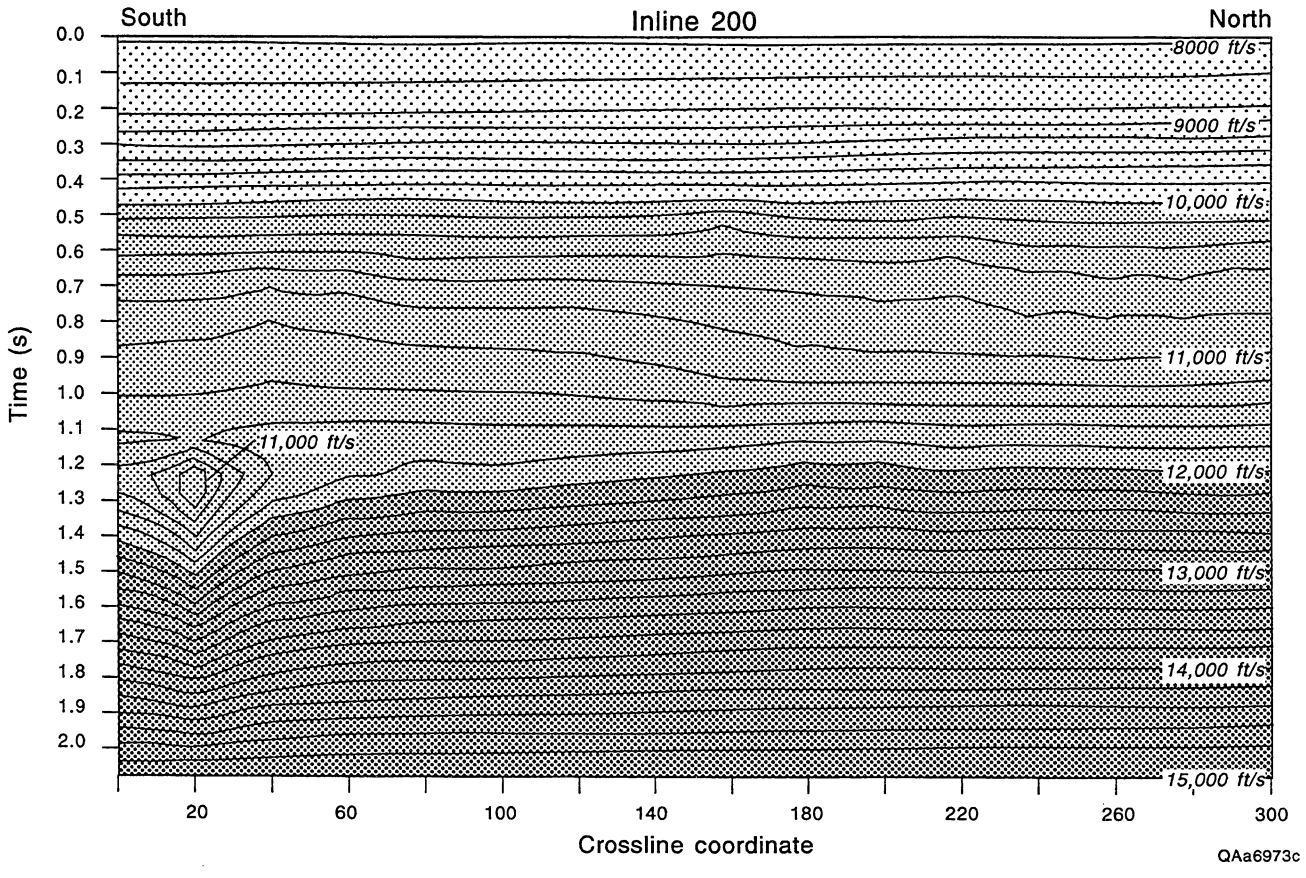

Figure D27. South-north profiles of the final stacking velocities along inlines 100 and 200. See Figure D29 to locate these inline coordinates. The deep velocity disruption occurring near crossline coordinate 20 results from a deep karsted zone, a geologic phenomenon discussed in chapter 2.

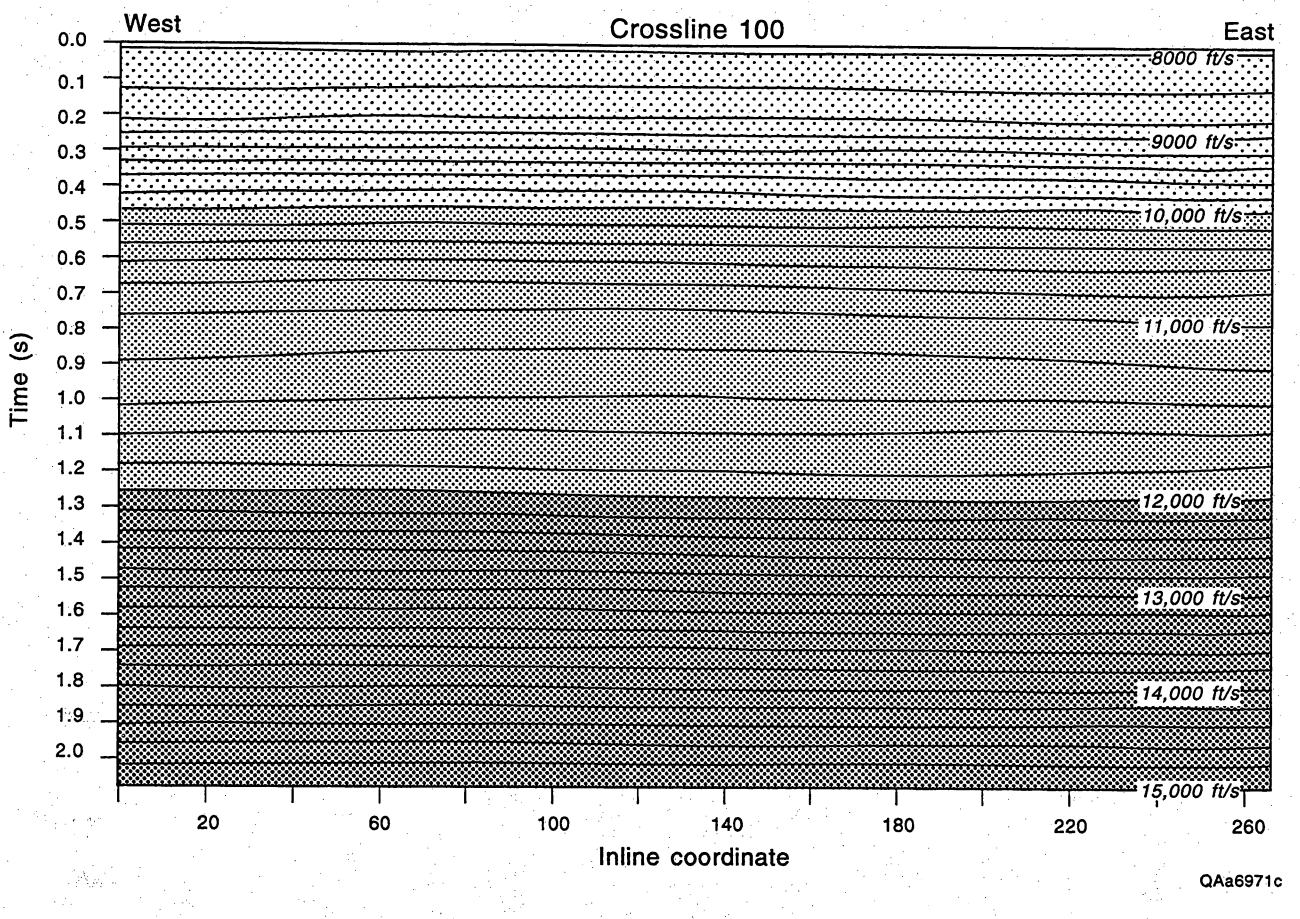

Figure D28. West-east profile of the final stacking velocities along crossline 100. See Figure D29 to locate this crossline coordinate. The velocity behavior is relatively smooth along this profile.

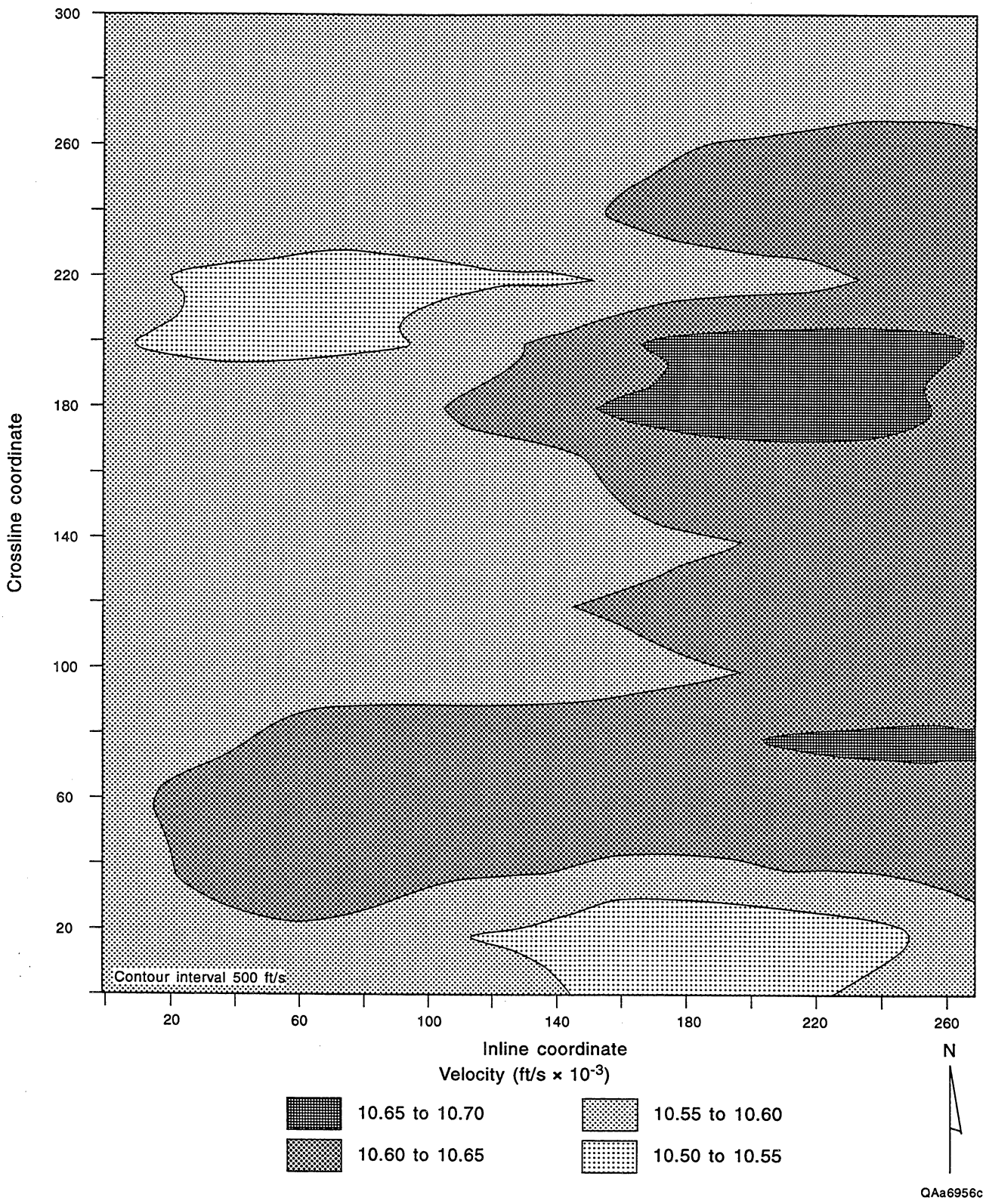

Figure D29. A time slice cutting the 3-D stacking velocity volume at 1.1 s. This map shows the areal variation in stacking velocity immediately below the Atokan-age reservoirs that are to be imaged.

whereas Figure D28 shows how the stacking velocity varies in an east-west direction along crossline 200. Figure D29 is a time slice through the 3-D velocity volume at 1.1 s, showing how the velocity varies in an areal sense just below the lowest Atokan-age reservoir.

Spectral Balancing

Of all the numerical procedures used during the processing of the Boonsville 3-D data, spectral balancing probably had the greatest positive impact on data quality. Because spectral balancing is a lengthy numerical calculation, as will be explained, the Boonsville data were stacked first without using spectral balancing to determine whether acceptable reservoir images could be produced by conventional processing. In this preliminary stacking effort, the application of standard deconvolution algorithms comprised the principal procedures used to preserve the widest possible data bandwidth. The resulting stacked data were judged not to have the bandwidth nor the signal-to-noise character that were needed for imaging the thin-bed Atokan-age reservoirs in Boonsville field. Consequently, the processing was redone by first spectrally balancing all field records, then calculating new statics and stacking velocities, and restacking the data. Comparisons of stacked lines created with and without spectral balancing during these two tests are shown in Figures D30 and D31. The spectrally balanced data have a wider bandwidth, superior resolution, and better signal-to-noise character, demonstrating the importance of the spectral balancing procedure for imaging thin-bed midcontinent reservoirs.

Spectral balancing is a demanding computational procedure. The lengthy computation time results because the process is not a poststack procedure, but a prestack calculation that is applied to every trace of every field record on a trace-by-trace basis. In the case of the Boonsville 3-D data, the spectral balancing computation required 6 days (144 hours) of continuous runtime on a Sun SPARC 10, which is a significant demand on computer resources. The objectives of spectral balancing are to cause all traces of all field records to have equivalent frequency spectra and for these spectra to exhibit a flat response over the widest possible bandwidth. A hypothetical example of the concept is shown in Figure D32 where the frequency content of a wideband

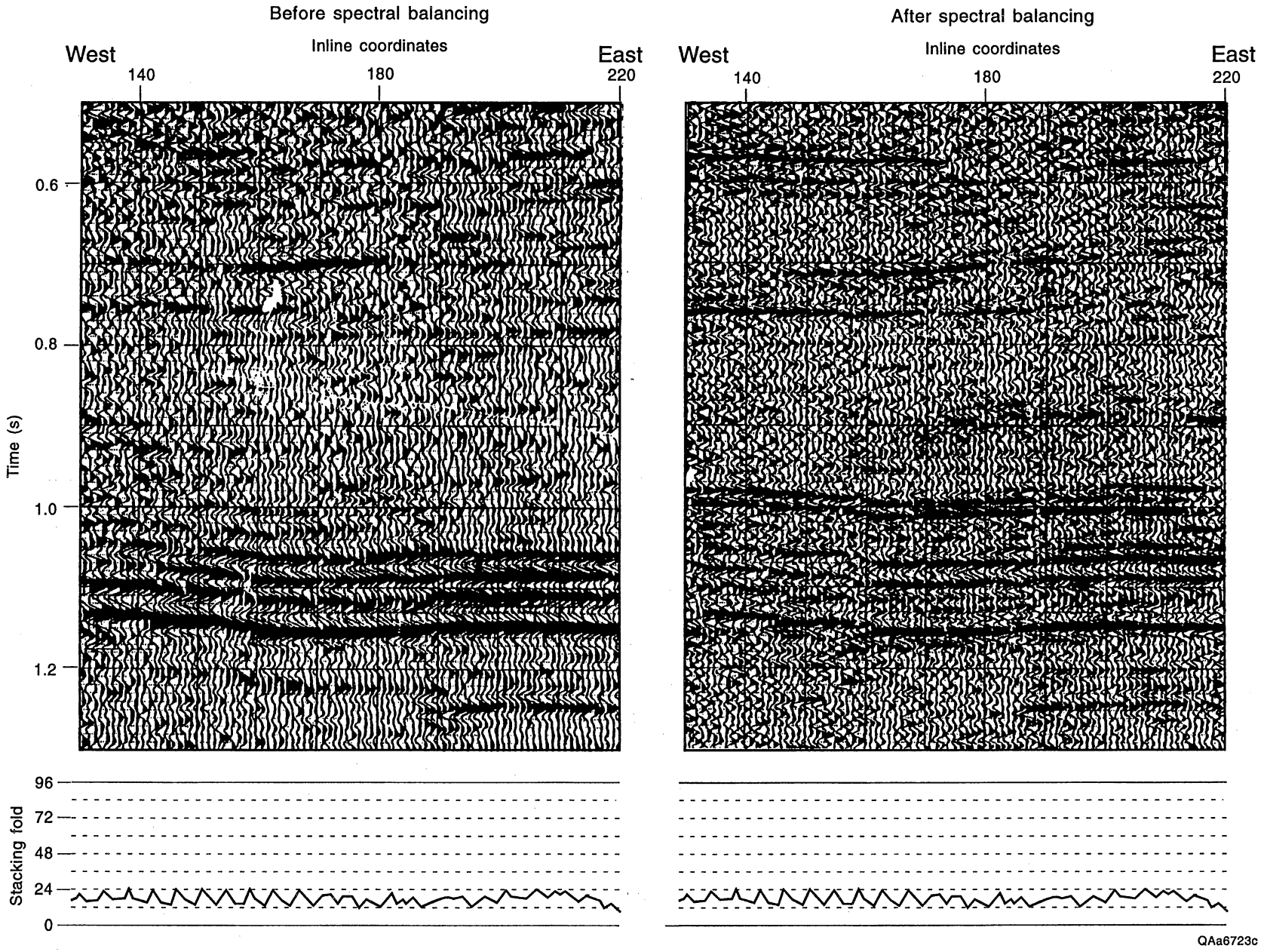

Figure D30. A comparison between Boonsville data stacked without spectral balancing (left) and with spectral balancing (right). The spectrally balanced data have better resolution and exhibit dramatic improvements in signal-to-noise in some critical time intervals. See, for example, the strong reflection signal near 1.0 s in the spectrally balanced data. This reflection event is critical for interpreting the Atoka interval, which extends from 0.8 to 1.1 s (approximately).

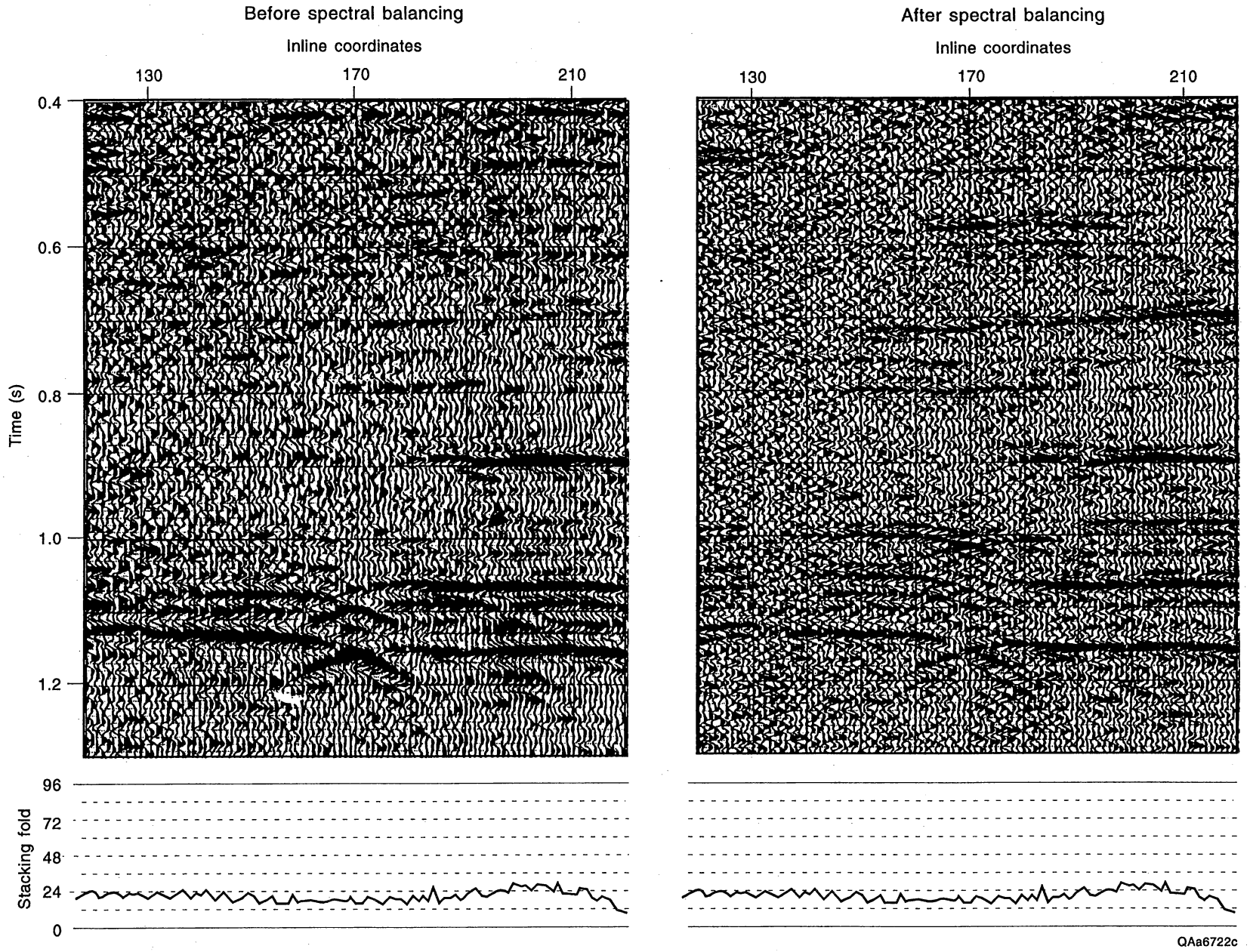

Figure D31. A second comparison between Boonsville data stacked without spectral balancing (left) and with spectral balancing (right). Again, the spectrally balanced data have a superior resolution and reveal reflection events in the Atoka interval (~0.8 to 1.1 s), which cannot be easily interpreted in the image on the left.

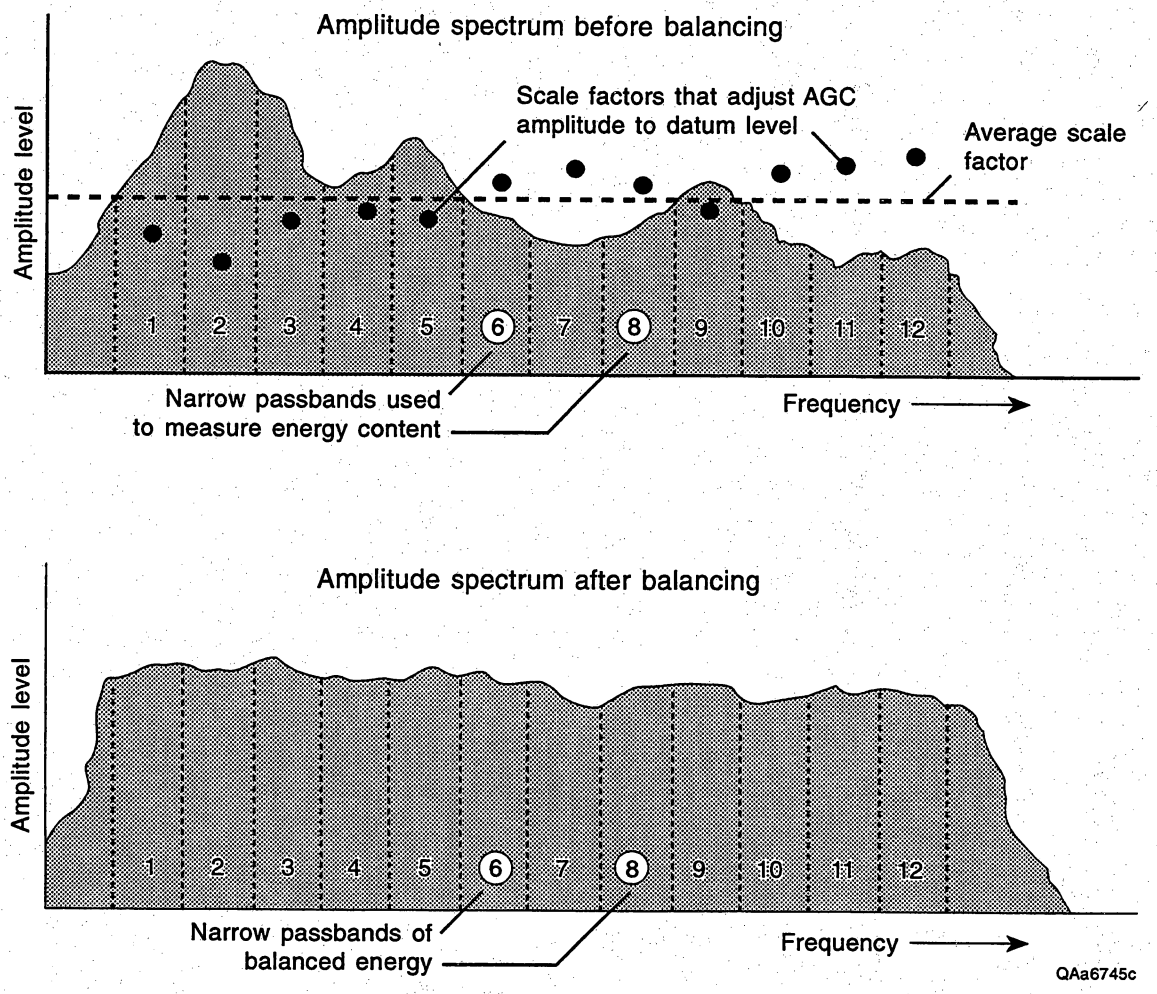

Figure D32. (Top) The shaded curve shows the frequency content of a hypothetical seismic trace. Lower frequencies dominate this spectrum, which means the spatial resolution of the seismic trace is not optimal. (Bottom) The numerical process of spectral balancing adjusts the amplitudes of the frequency components inside successive spectral passbands so that the spectrum is altered to have a flat response across the complete signal bandwidth. When a seismic trace is modified so that its spectrum is equivalent to this balanced spectrum, the spatial resolution of the trace is increased because the influence of low frequencies is reduced while the influence of high frequencies is increased. The solid circles in the top panel show the scale factors that could be used to adjust the amplitudes of the frequency components in each passband to a more uniform level. The actual amplitude scaling factors are calculated in the time domain as illustrated in Figure D33.

spectrum (top) is altered so that the energy content is uniformly distributed across the complete frequency range of the data (bottom); i.e., the bottom spectrum is balanced across the complete signal bandwidth.

Spectral balancing is done in successive, narrow passbands such as those indicated by the twelve frequency intervals in Figure D32. In practice, the computation is not done in the frequency domain as one might assume from this figure but is implemented in the time domain following the procedural path(s) diagrammed in Figure D33.

Analysis of the Boonsville seismic field records showed that the signal bandwidth diminished significantly above 150 Hz, so spectral balancing was not attempted for frequencies that greatly exceeded this signal cutoff. The specific filters used to spectrally balance the Boonsville data are shown in Figure D34. Each filter had a passband width of 10 Hz and rolloff widths of 5 Hz at the low end and 20 Hz at the high end. The first full-pass frequency was set at 15 Hz, and the low-end rolloff for this filter (filter 1 in Fig. D34) eliminated most of the low-frequency ground roll noise as well as much of the cultural noise created by gas compressors and other surface-based mechanical equipment operating throughout the 3-D grid. The full-pass portion of each filter overlapped the full-pass portion of the preceding filter by 25 percent (i.e., by 2.5 Hz). The full-pass portion of the eighteenth, and last, bandpass filter in the sequence ended at 152.5 Hz, where the signal frequency effectively ended in the field records. This filter suite resulted in computation loop A (Fig. D33) being exercised 18 times for each data trace of every Boonsville field record. Because the Boonsville data were sampled at 1 ms and the record length was 2 s, computation loop B (Fig. D33) generated 2,000 trace amplitude scaling factors, one for each data sample of the trace being processed, during each execution of loop A. The result of this extensive trace-by-trace spectral balancing was the improvement in the stacked 3-D image documented in Figures D30 and D31.

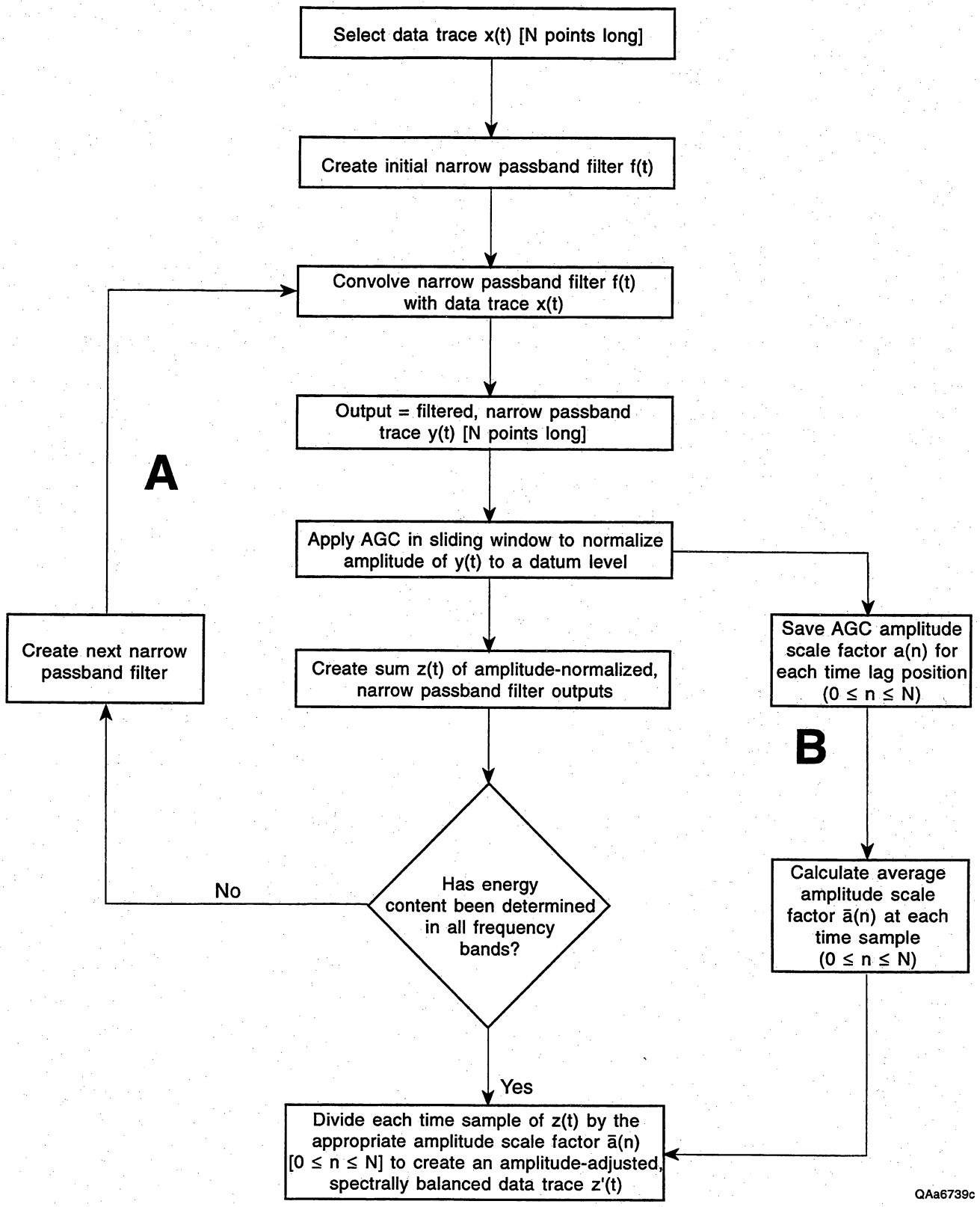

Figure D33. Flow chart showing the numerical steps involved in spectral balancing. Computation loop A creates the overlapping narrow passband filters and applies them in the time domain. Computation loop B creates the scale factors used to adjust each data sample of the output trace, a different scale factor being used for each data sample.

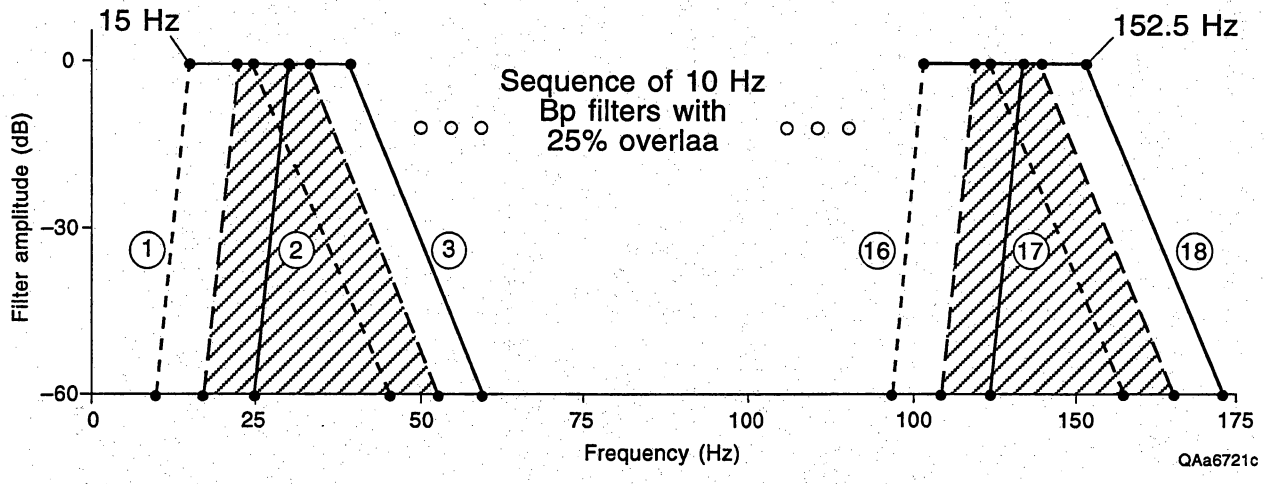

Figure D34. The specific bandpass (BP) filters created in computation loop A (Fig. D33) for the Boonsville data. A total of 18 filters were used to span the signal bandwidth extending from 15 to 152.5 Hz. Each filter had a full-pass interval that was 10 Hz wide, and the width of the rolloffs at the lower and upper ends of each filter was 5 and 20 Hz, respectively. The full-pass interval of each filter overlapped the full-pass interval of the preceding filter by 25 percent (i.e., by 2.5 Hz).

APPENDIX E
SEISMIC ATTRIBUTES

The numerical attributes that are traditionally extracted from seismic data are instantaneous amplitude, instantaneous phase, and instantaneous frequency. Taner and Sheriff (1977) and Taner et al. (1979) introduced seismic interpreters to these attributes, and since that introduction almost 20 years ago, numerous algorithms have been implemented to calculate these seismic properties (for example, Hardage, 1987, p. 199–206). All of these attributes are based on using the Hilbert transform to convert a real seismic trace into a complex seismic trace having an imaginary and a real component, the real component being an exact replication of the original seismic trace. The mathematical details of these computational algorithms will not be described; the calculation procedure will instead be described graphically.

Fundamental Principles

The concept of a complex seismic trace is illustrated in Figure E1. In this illustration, **x**(t) represents the real seismic trace, which in this study would be a single trace from the Boonsville 3-D migrated data volume, and **y**(t) is the Hilbert transform of **x**(t). Present algorithms calculate **y**(t) quite rapidly. These two data vectors are displayed in a 3-dimensional (x,y,t) space, where t is seismic traveltime, x is the real data plane, and y is the imaginary plane. The actual seismic trace **x**(t) is confined to the real x-plane, and **y**(t), the Hilbert transform of **x**(t), is confined to the imaginary y-plane. When **x**(t) and **y**(t) are added vectorally, the result is a complex seismic trace **z**(t) (that is, the trace comprises a real and an imaginary part), which has the shape of a helical spiral extending along, and centered about, the time axis, t. The projection of this complex function **z**(t) onto the real plane is the real seismic trace **x**(t), and the projection of **z**(t) onto the imaginary plane is **y**(t), the calculated Hilbert transform of **x**(t).

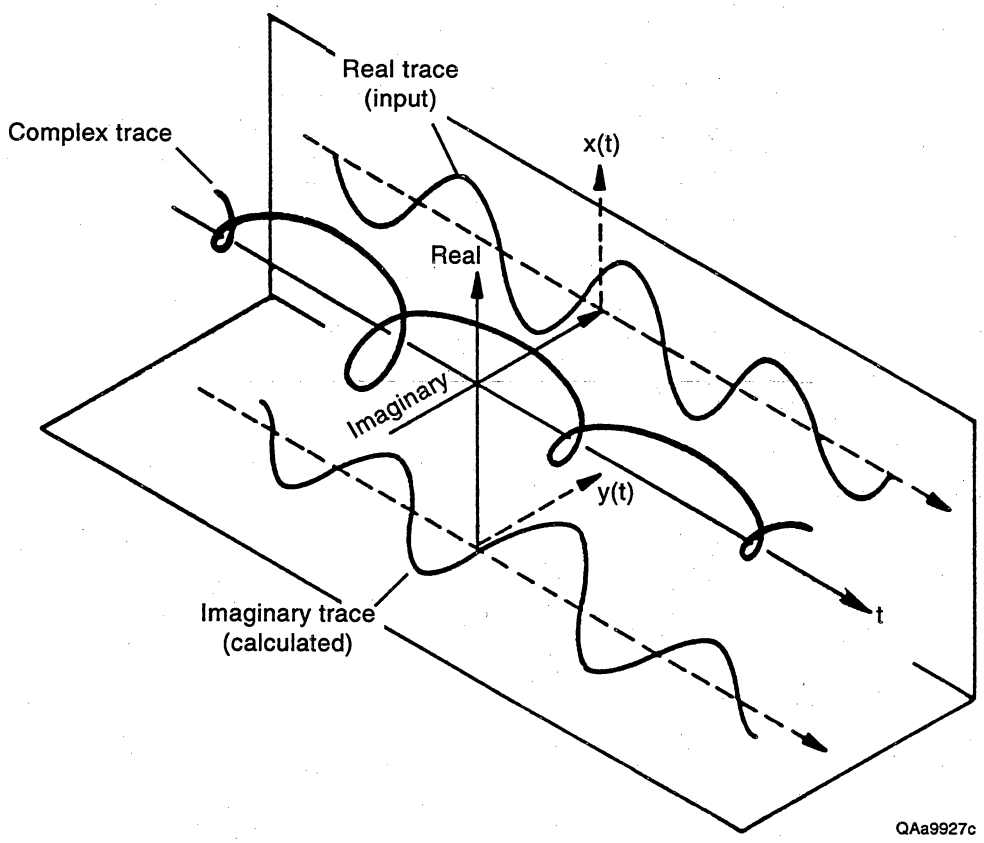

Figure E1. Graphical illustration of a complex seismic trace. The real part of the complex trace is an actual seismic trace, which in this study would be a single trace from the final migrated 3-D seismic data volume. The imaginary part is a mathematical function calculated from the real trace by a Hilbert transform process. When the real and imaginary traces are added in a vector sense, the result is a helical spiral centered about the seismic time axis. This helical trace is the complex seismic trace.

The reason for converting the real seismic trace **x**(t) into a seemingly more mysterious complex seismic trace **z**(t) is illustrated in Figure E2, where the concepts of instantaneous seismic amplitude, phase, and frequency are introduced. At any point on the time axis, a vector a(t) can be calculated that extends away from the t axis in a perpendicular plane to intersect the helically shaped complex seismic trace **z**(t). The length of this vector is the amplitude of the complex trace at that particular instant of time, hence the term *instantaneous amplitude*. Mathematically, this amplitude value a(t) can be calculated as

$$a(t) = \sqrt{x^2(t) + y^2(t)}\ , \tag{1}$$

because both x(t) and y(t) are known quantities, **x**(t) being the actual seismic trace and y(t) being the calculated Hilbert transform of **x**(t).

The orientation angle $\phi(t)$ of this vector a(t), which is usually measured relative to the positive axis of the real x-plane, is defined as the phase of **z**(t) at that instant in time, hence the term *instantaneous phase*. Numerically, the phase angle is calculated as

$$\phi(t) = \tan^{-1} \frac{y(t)}{x(t)}\ . \tag{2}$$

As seismic time progresses, the vector a(t) not only moves along the t axis, but it also continually rotates about the time axis to maintain contact with the spiraling complex trace **z**(t). Each full rotation of the vector about the time axis increases the phase value by 360°.

In any oscillating system, and specifically for a seismic trace, frequency can be defined as the time rate of change of the phase angle. This fundamental definition is used to describe the frequency behavior of the complex seismic trace, so that the *instantaneous frequency* $\omega(t)$ at any seismic time sample is given by

$$\omega(t) = \frac{d}{dt}\,\phi(t)\ . \tag{3}$$

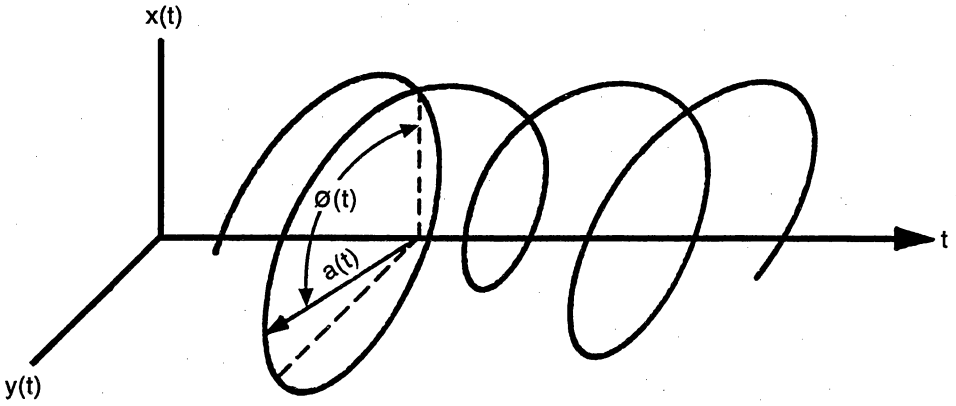

$a(t) = \sqrt{x^2(t) + y^2(t)}$ – instantaneous amplitude

$\phi(t) = \tan^{-1}\left(\frac{y(t)}{x(t)}\right)$ – instantaneous phase

$\omega(t) = \frac{d\phi(t)}{d(t)}$ – instantaneous frequency

QAa9926c

Figure E2. Graphical illustration of seismic attributes—instantaneous amplitude a(t), instantaneous phase $\phi(t)$, and instantaneous frequency $\omega(t)$—which can be calculated once a complex seismic trace is created. The formulae used in the calculations are listed in the figure.

Graphical Example of Instantaneous Amplitude

Equations 1, 2, and 3 will now be applied to a single seismic trace to illustrate some of the characteristics of the instantaneous amplitude, phase, and frequency functions that are used in seismic interpretation. An example of an instantaneous amplitude calculation is illustrated in Figure E3. The data trace in the bottom panel is the actual seismic trace; the real and imaginary components of the associated complex seismic trace $\mathbf{z}(t)$ are identified in the top panel. As in all Hilbert transform processes, the real part of this complex trace is identical to the actual seismic trace in the bottom panel. The instantaneous amplitude function a(t) that results when equation 1 is applied to the complex trace components $\mathbf{x}(t)$ and $\mathbf{y}(t)$ is shown in the top panel. Because this a(t) function is a smooth curve passing through the apices of all the peaks and troughs of the real seismic trace, it is sometimes referred to as an *envelope function.*

Importantly, the extrema of the instantaneous amplitude function do not occur at the same seismic times as do the extrema of the real seismic trace $\mathbf{x}(t)$. Thus, when doing an amplitude interpretation of seismic data within a specific time window, two different answers can be obtained, depending on whether the interpreter analyzes the amplitudes of the actual data or the magnitudes of the instantaneous amplitude functions.

Graphical Example of Instantaneous Phase

A calculation of the instantaneous phase associated with a typical seismic trace is illustrated in Figure E4. The bottom panel in the figure is the actual seismic trace, and the real and imaginary components of the associated complex trace are shown in the center panel. Applying equation 2 to the real and imaginary components of the complex seismic trace (center panel) produces the instantaneous phase function at the top of the figure. Although phase is a positive function that monotonically increases in magnitude with seismic time, it is customarily plotted as a repetitive, wraparound function with plot limits of 0 to 360° (or –180° to +180°), as is done in this display. Each wraparound of

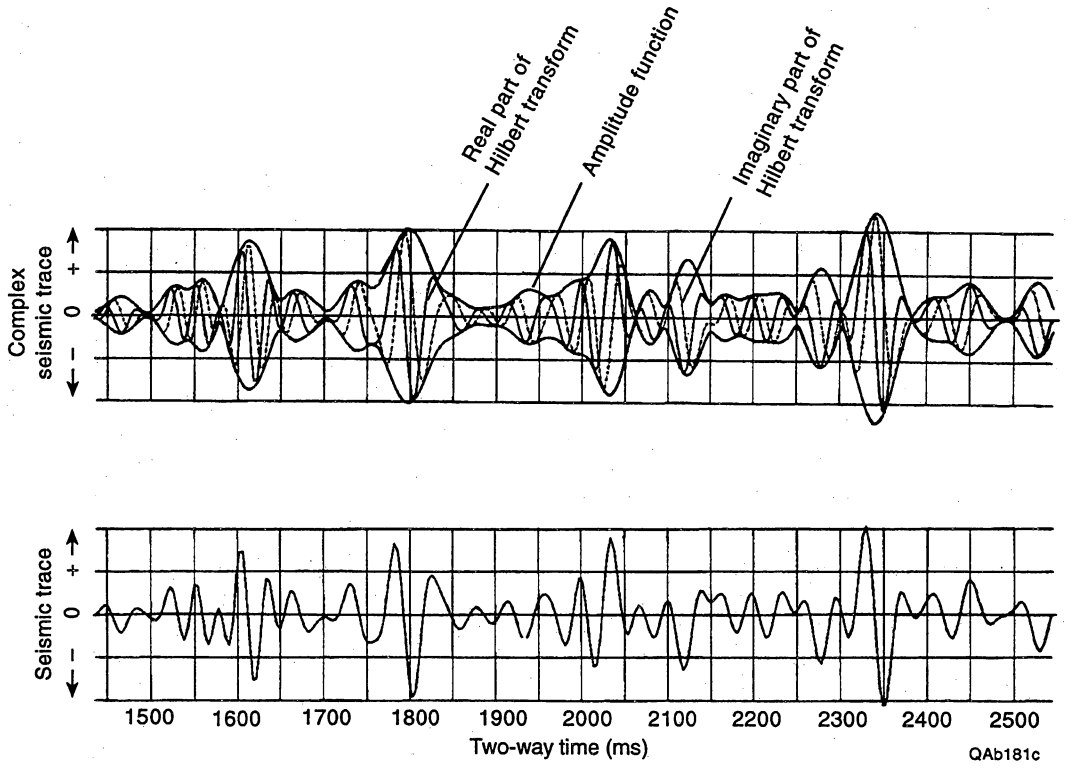

Figure E3. Illustration of the instantaneous amplitude seismic attribute calculated for an actual seismic trace. The actual trace is shown in the bottom panel. The real and imaginary components of the associated complex seismic trace are shown in the top panel, with the real component being an exact replica of the actual seismic trace, as required. The instantaneous amplitude function is the smooth, gently oscillating envelope curve that passes through the apex of each peak and trough of both the real and imaginary components.

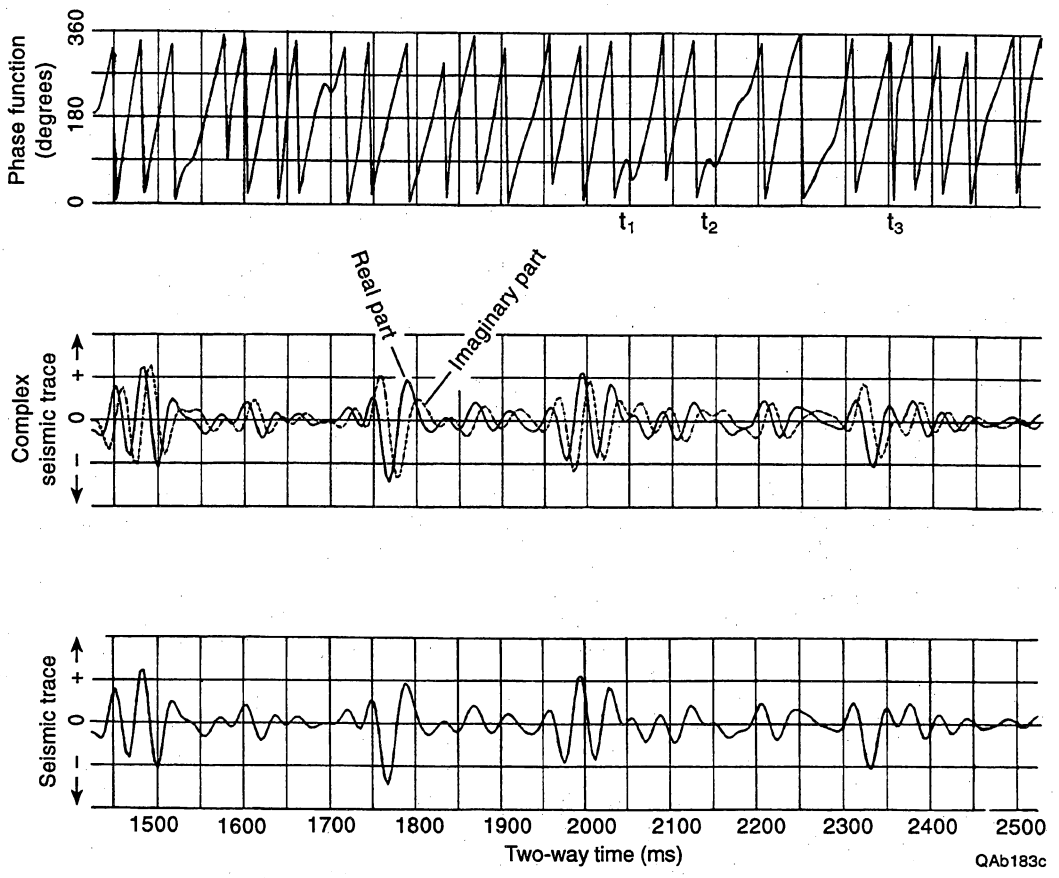

Figure E4. The instantaneous phase seismic attribute function. The real seismic trace is shown in the bottom panel, the real and imaginary components of the associated complex seismic trace are shown in the center panel, and the calculated instantaneous phase is shown in the top panel. The phase behavior at times t_1, t_2, and t_3 (top panel) is discussed in the text of this appendix.

360° corresponds to a full rotation of the a(t) vector about the time axis as that vector stays in contact with the spiraling complex seismic trace **z**(t) (refer to Fig. E2).

Instantaneous phase can be calculated with the same ease and the same accuracy in the low-amplitude zones of a seismic trace as it can in the high-amplitude regions. Thus, a chronostratigraphic surface in a low-amplitude region of a 3-D seismic data volume can usually be constructed quicker and more accurately by interpreting the surface in a 3-D volume of instantaneous phase than by trying to track a constant phase value across the low-amplitude seismic wiggle traces.

Graphical Example of Instantaneous Frequency

The instantaneous frequencies calculated for this same seismic trace are shown in the top panel of Figure E5. The bottom two panels in this display are identical to those described in Figure E4. Although negative frequencies cannot exist physically, this instantaneous frequency function exhibits negative values at time positions t_1 and t_2. Comparing the time coordinates of these anomalous frequency values with the time coordinates of the instantaneous phase function in Figure E4 shows that the phase does not exhibit its usual, monotonically increasing behavior in these time intervals, causing the time rate of change of phase (or the slope of the phase function), which is the instantaneous frequency, to be negative at time samples t_1 and t_2.

We will show later (Figs. E6 through E11) that these anomalous negative frequency values are often the most important information provided by any of the seismic attributes. It is thus essential that the software that calculates instantaneous frequencies not camouflage these physically unrealizable negative frequency values, which is what some algorithms have done, and some still do. For example, negative frequencies can be camouflaged to unsuspecting interpreters when the software simply changes the algebraic sign of any negative value to a positive sign, which is a quality check that some software programmers have mistakenly implemented. At times t_1 and t_2 in Figure E5, such

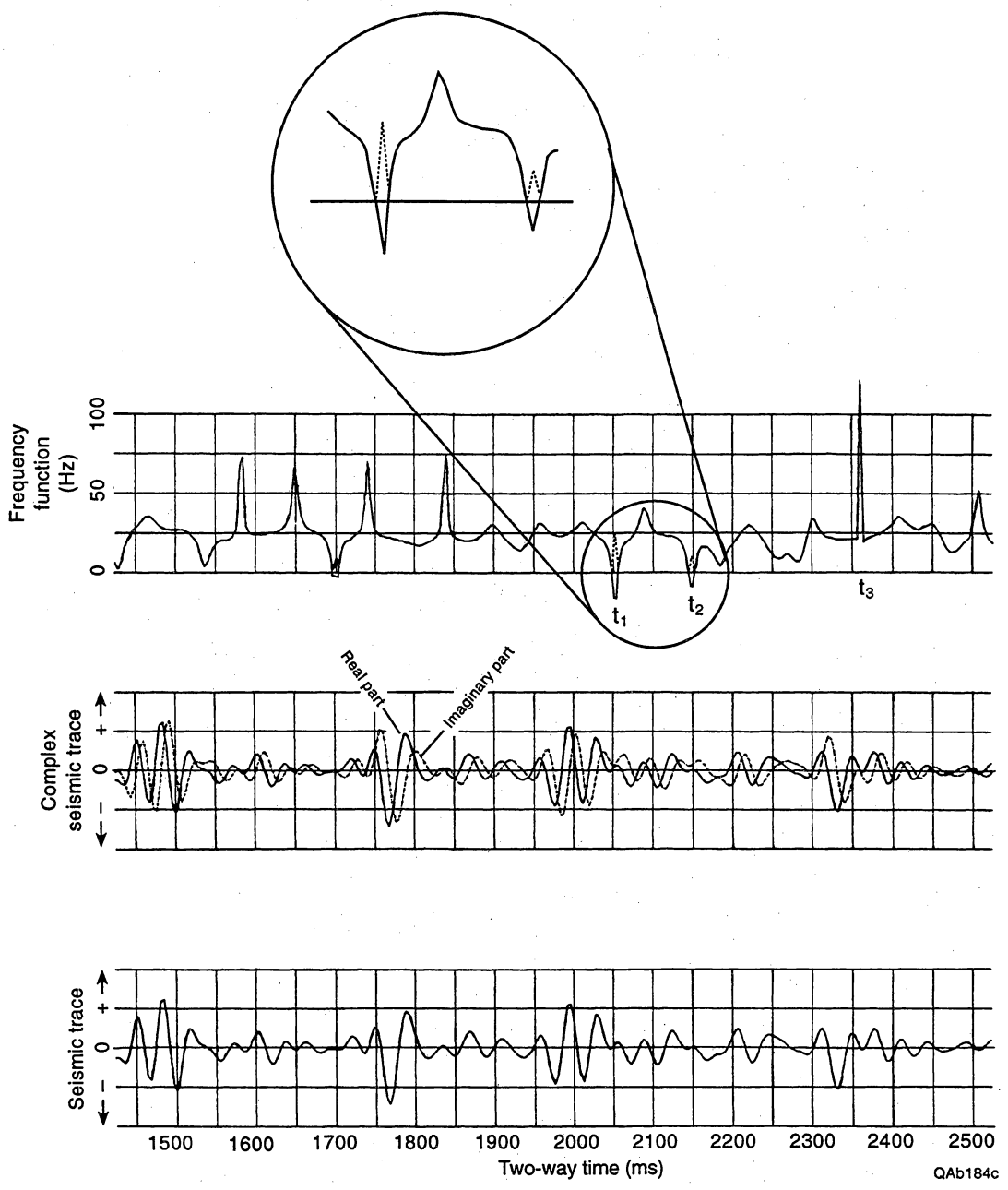

Figure E5. The instantaneous frequency seismic attribute function calculated for the same seismic trace discussed in Figure E4. The bottom two panels are identical to the two bottom data panels in Figure E4. The calculated instantaneous frequency function is shown in the top panel. The frequency behavior at times t_1, t_2, and t_3 is discussed in the text of this appendix.

software would create frequency values that follow the dashed curves shown in the enlarged view (always positive numbers), rather than the correct solid-line curve (negative numbers). The Boonsville 3-D seismic interpretation was done with Landmark software, which preserves anomalous negative instantaneous frequencies, as a robust interpretation system should.

It should also be emphasized that a digitally sampled time function such as a seismic trace cannot contain positive frequencies that exceed the Nyquist frequency limit f_n, which is given by

$$f_n = \frac{1}{2\Delta t}, \tag{4}$$

where Δt is the time sampling interval of the seismic data. Because the seismic trace example used in Figure E5 was sampled at 4 ms, the highest positive frequency that can exist in this data trace is 125 Hz (equation 4). Yet at time position t_3, the instantaneous frequency exceeds the allowed Nyquist bound (125 Hz). According to Figure E4, the instantaneous phase exhibits an extremely steep slope in the vicinity of this time value, causing the instantaneous frequency to achieve anomalous positive values that exceed the Nyquist limit.

It will be shown in the case history interpretations that these anomalous positive frequencies, like the anomalous negative frequencies previously discussed, are invaluable in seismic interpretation. Thus, it is essential that the interpretation software not camouflage these anomalous positive values either, which some algorithms have done by simply clipping the anomalous high positive magnitudes to a value equal to or slightly less than the Nyquist limit f_n. The Landmark software used to interpret the Boonsville data preserved the anomalous positive frequencies created by the Hilbert transform, which was a great benefit when interpreting subtle stratigraphic boundaries in the Bend Conglomerate interval, as will be emphasized in the remainder of this appendix and also in the case histories described in the main text of this report.

Using Anomalous Frequency Values to Define Stratigraphic and Structural Discontinuities

A fundamental objective of the Boonsville research was to determine what seismic attributes, if any, could reveal potential compartment boundaries in the Bend Conglomerate interval. Historically some seismic stratigraphers who have used Hilbert transform attributes as interpretational aids have found that the anomalous frequency values just described (i.e., any positive values that exceed the Nyquist limit or any negative values) are extremely valuable because these anomalous values pinpoint where stratigraphic and/or structural discontinuities occur, even when these discontinuities are subtle, semi-invisible features in the seismic wiggle trace data. Unfortunately, these stratigraphic interpretations have been largely confined to proprietary reports, and essentially none have entered the public domain. The remainder of this appendix will provide a public documentation of the interpretive value of these anomalous instantaneous frequencies.

Anomalous Frequency Behavior at Stratigraphic Pinch-Outs

The Boonsville 3-D seismic data volume was converted to a 3-D volume of instantaneous frequencies so that time slices could be made to show the areal mathematical behavior of instantaneous frequencies associated with interesting geologic features. One of these time slices is shown in Figure E6. The color bar used in this display shades all negative frequency values as a contrasting bright red and all excessively large positive frequencies as a bright green, and an inspection of the time slice shows that numerous narrow trends of negative frequencies are distributed over this constant-time surface. Random spatial patterns of anomalous frequencies, such as the pattern in the southwest corner of this time slice between crossline coordinates 40 and 80 and inline coordinates 80 and 120, rarely have a significant geological meaning, but patterns that align in narrow continuous trends, whether linear or sinuous, are highly

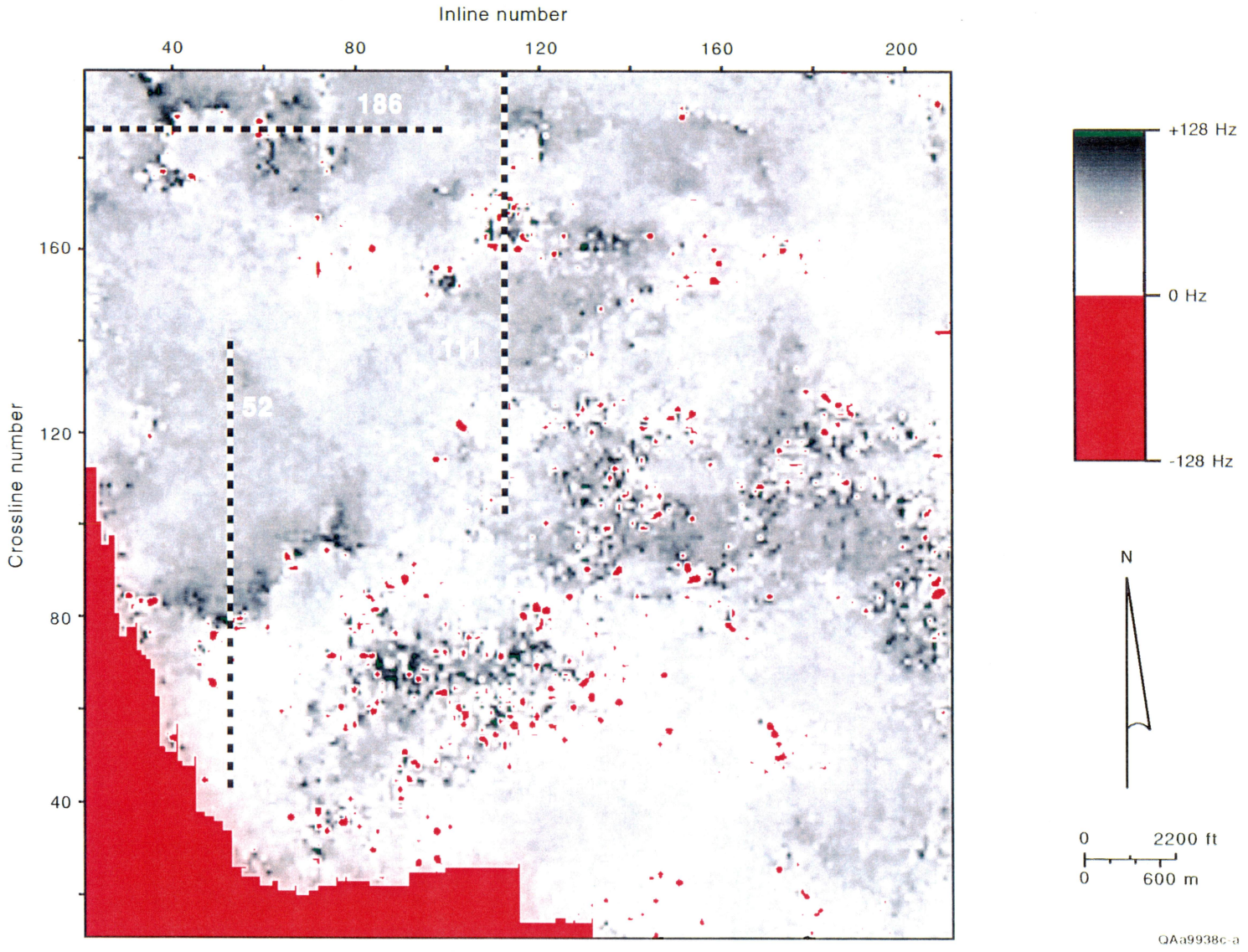

Figure E6. A time slice cutting through the Boonsville 3-D instantaneous frequency volume at a two-way time of 900 ms. The color bar is chosen so that anomalous frequency values (any negative value or any extreme positive value) are emphasized. Seismic profiles 52, 111, and 186 will be used to illustrate how these anomalous instantaneous frequency values define structural and stratigraphic discontinuities.

significant. Three examples where anomalous frequencies develop such trends will be examined.

The first pattern is the east-west-meandering trend occurring along crossline coordinate 80 (approximately) between inline coordinates 40 to 80. Inline profile 52 crosses this anomaly and is shown as Figure E7. Note the stratigraphic pinch-out occurring at a two-way time of 900 ms (the position of the time slice in Figure E6) at crossline coordinate 80 (the position of the anomalous frequency trend). Similar anomalous frequencies occur at pinch-outs that are considerably more subtle than the one shown here. Examples of instantaneous frequency being used to image subtle pinch-outs will be emphasized in the main body of the text because such pinch-outs are important indicators of compartment boundaries.

Anomalous Frequency Behavior at Reef Buildups

Referring again to the time slice in Figure E6, there is an interesting circular pattern of anomalous frequencies near the intersection of crossline coordinate 160 and inline coordinate 110. Inline 111, which crosses this anomaly, is shown as Figure E8. At a two-way time of 900 ms (the position of the time slice), there is a mounded feature at crossline coordinate 160. Although no well penetrates this feature, nearby log control from the B Yates 18D well shows that limestone units exist at this stratigraphic level, suggesting that the feature is a small reef. The boundary of this mounded buildup, be it reef or whatever, is precisely imaged by anomalous frequency values.

Anomalous Frequency Behavior at Collapsed Zones

A second circular pattern of anomalous frequencies exists near crossline coordinate 180 and inline coordinate 45 in Figure E6. Crossline profile 186 is chosen to illustrate this feature and is shown in Figure E9. In this instance, the circular feature is one of the numerous karst collapsed zones discussed in chapter 2 that exist throughout the

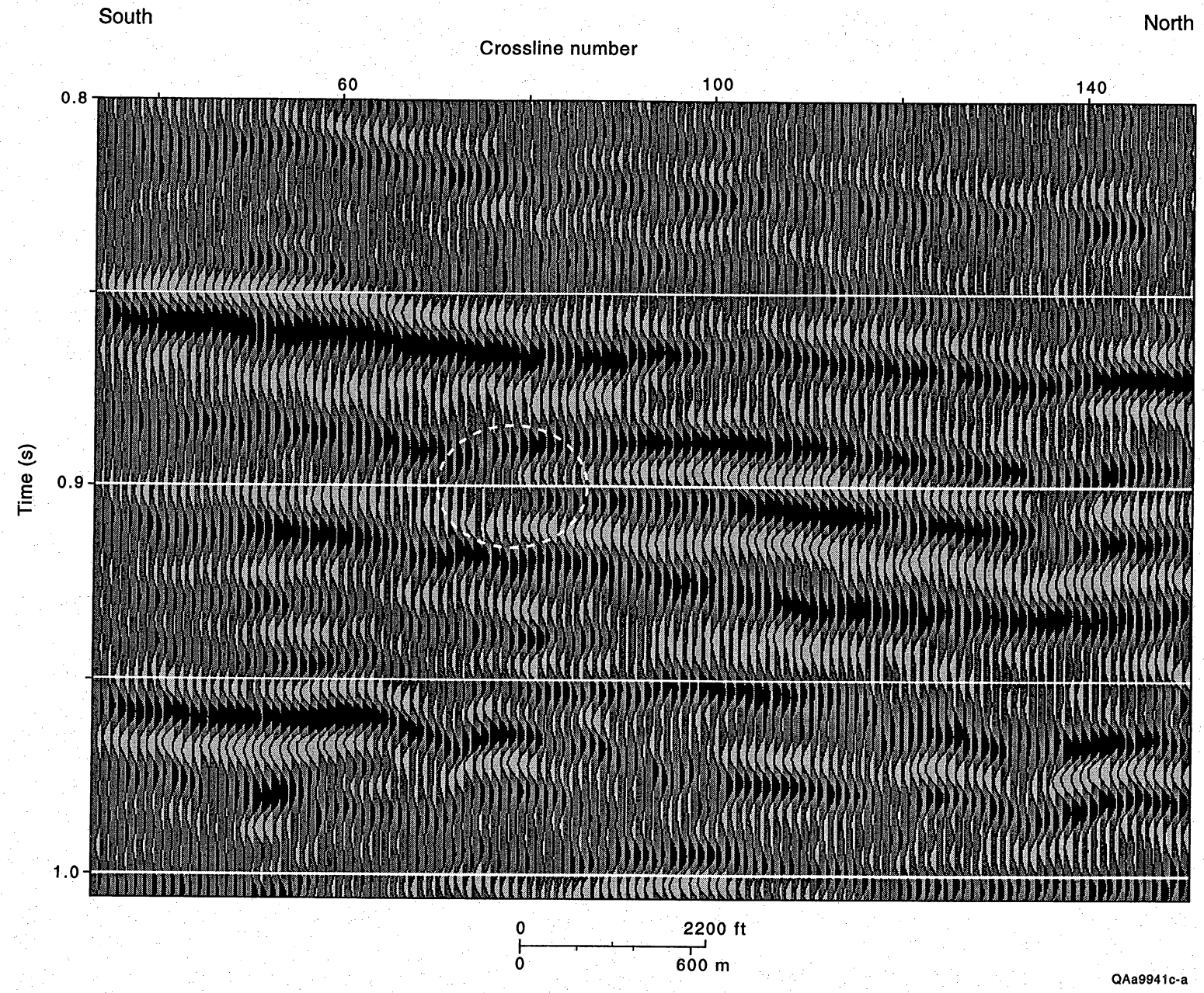

Figure E7. Inline profile 52 showing that the anomalous instantaneous frequency values in the vicinity of crossline coordinate 80, which form part of the east-west trend shown in the 900-ms time slice in Figure E6, are associated with a stratigraphic pinch-out. These anomalous frequencies occur at 900 ms near the center of the circled area.

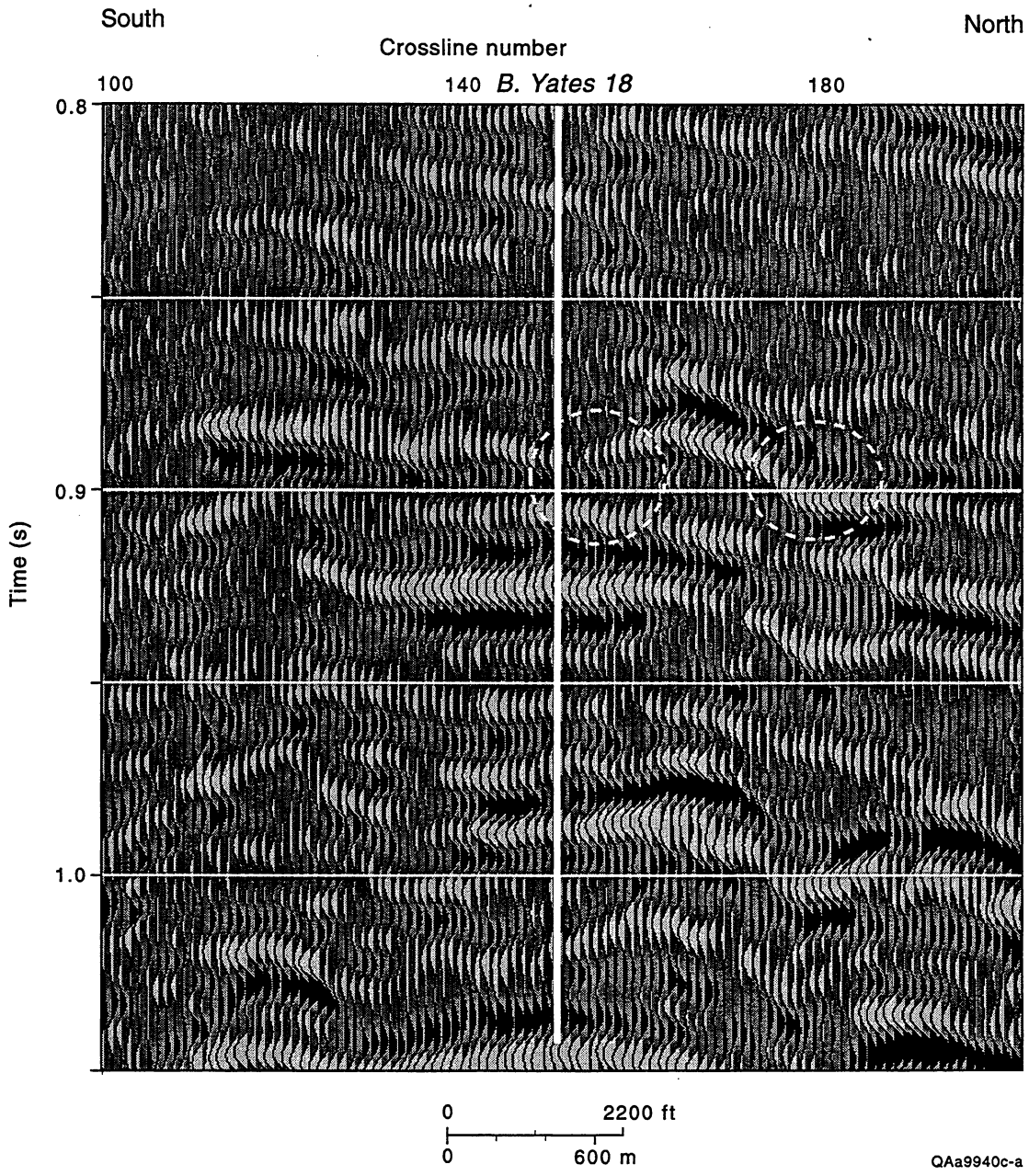

Figure E8. Inline profile 111 showing that the anomalous instantaneous frequency values in the vicinity of crossline coordinate 165, which form a ring in the 900-ms time slice in Figure E6, are associated with a stratigraphic mound (reef?). These anomalous frequencies occur at 900 ms near the centers of the two circled areas.

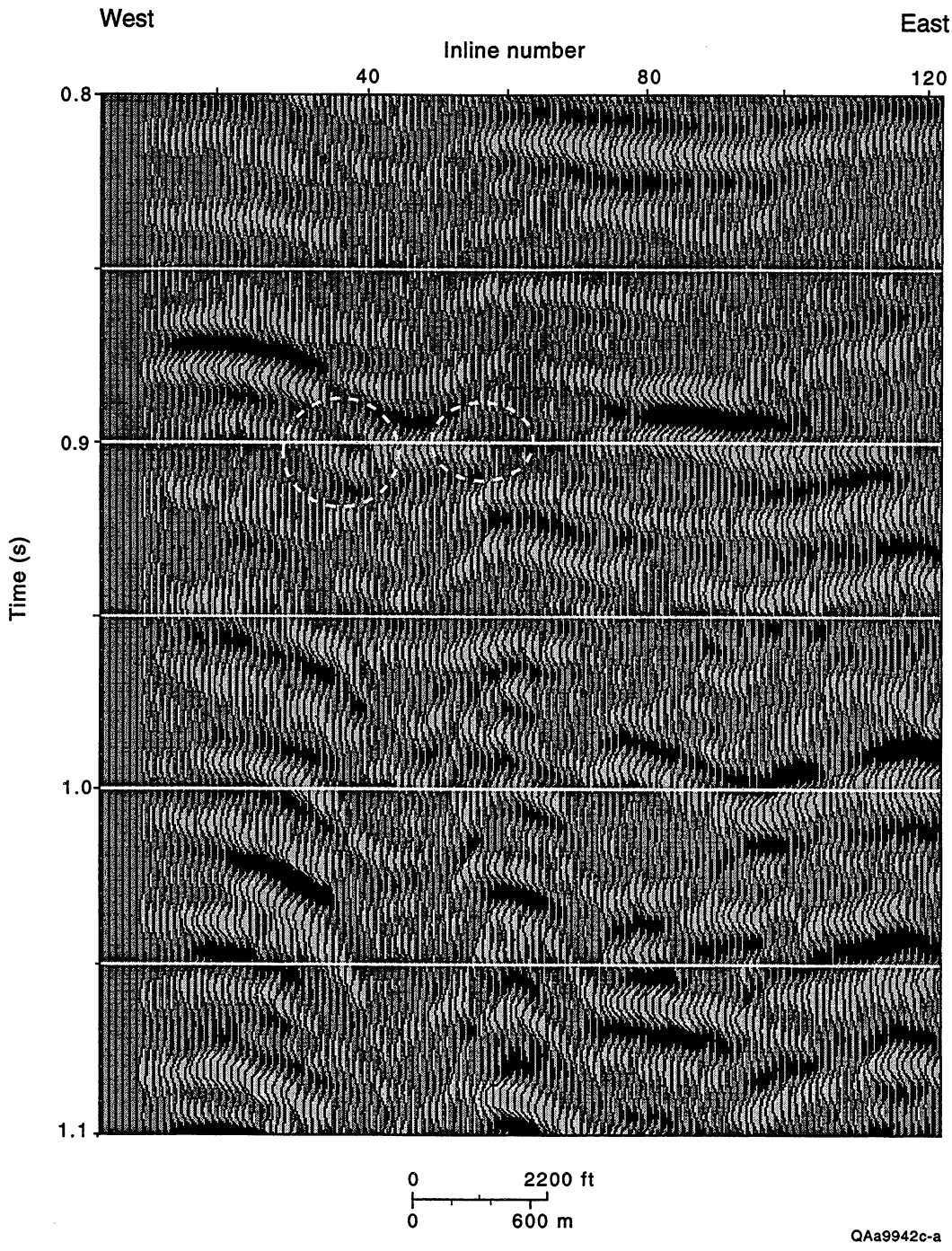

Figure E9. Crossline 186 showing that the anomalous instantaneous frequency values in the vicinity of inline coordinate 45, which form a circular pattern in the 900-ms time slice in Figure E6, are associated with a structural, karst-generated collapsed zone. These anomalous frequencies occur at 900 ms near the centers of the two circled areas.

Boonsville study area. Again, anomalous frequency values align along the circumference of this stratigraphic disruption of the Bend Conglomerate section.

Anomalous Frequency Behavior at Faults

A deeper time slice through the 3-D volume of instantaneous frequencies at 980 ms is shown in Figure E10. In this image, there is a linear east-west trend of anomalous frequencies along crossline 170 (approximately) between inline coordinates 130 and 180. Inline profile 147 (Figure E11) crosses this frequency anomaly and shows that at 980 ms, there is a fault break at crossline coordinate 170. Investigation of the Boonsville 3-D data shows that anomalous frequencies consistently pinpoint faults that are much more subtle than the one shown in this example.

Interpretational Applications

The principle shown by these examples is that most anomalous instantaneous frequency values indicate some type of distortion in the seismic reflection waveform. Because waveform distortions are often associated with pinch-outs, faults, and lateral facies changes, these anomalous frequencies tend to be direct indicators of lateral structural or stratigraphic discontinuities. These frequency attributes are thus valuable indicators of reservoir compartment boundaries, and examples of instantaneous frequency being used to analyze reservoir compartment size and shape are distributed throughout this report.

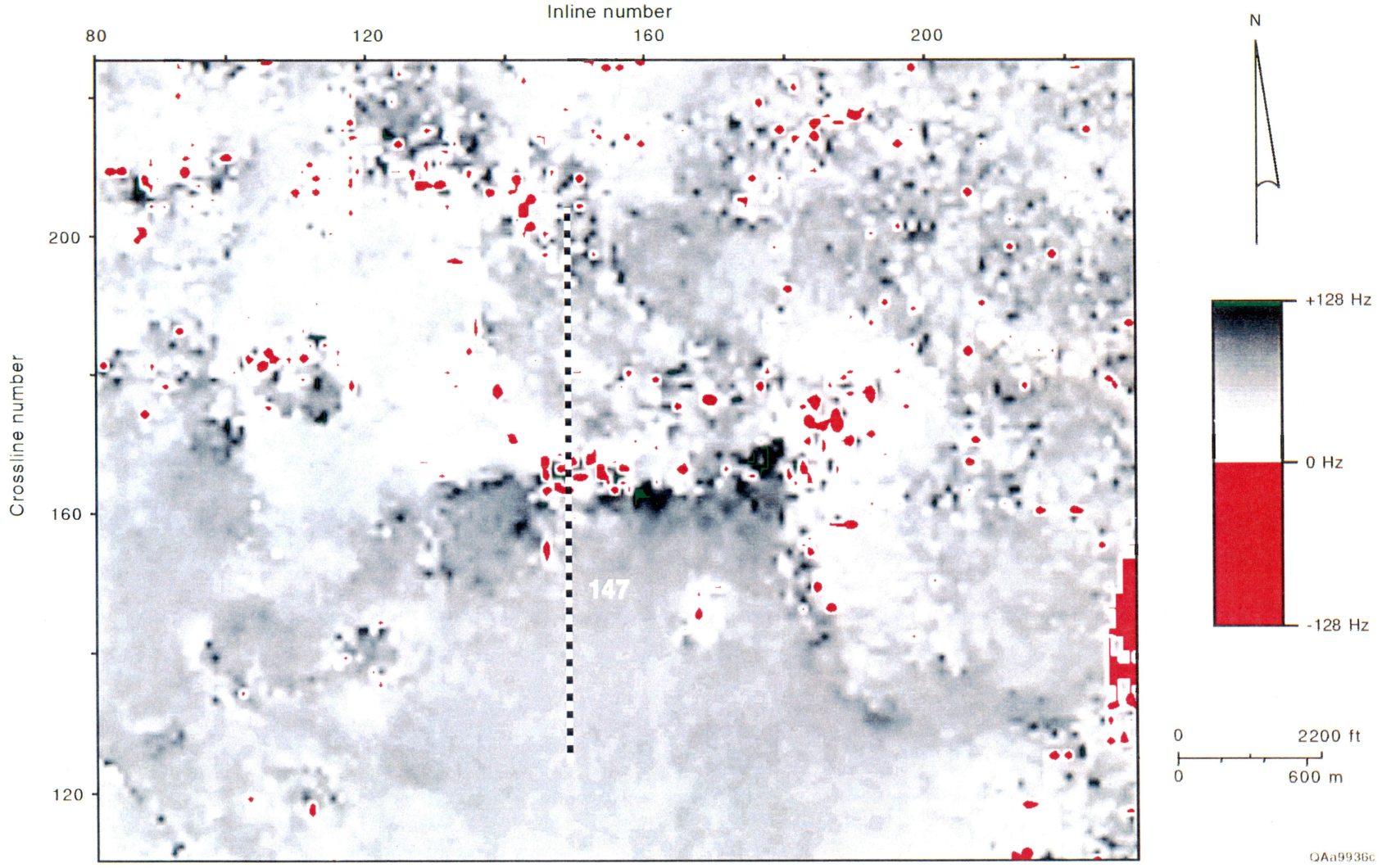

Figure E10. A time slice cutting through the Boonsville 3-D instantaneous frequency volume at a two-way time of 980 ms. The color bar is chosen so that anomalous frequency values (any negative value or any extreme positive value) are emphasized. Seismic profile 147 will be used to illustrate how the east-west linear trend of anomalous frequencies near crossline coordinate 170 maps a fault.

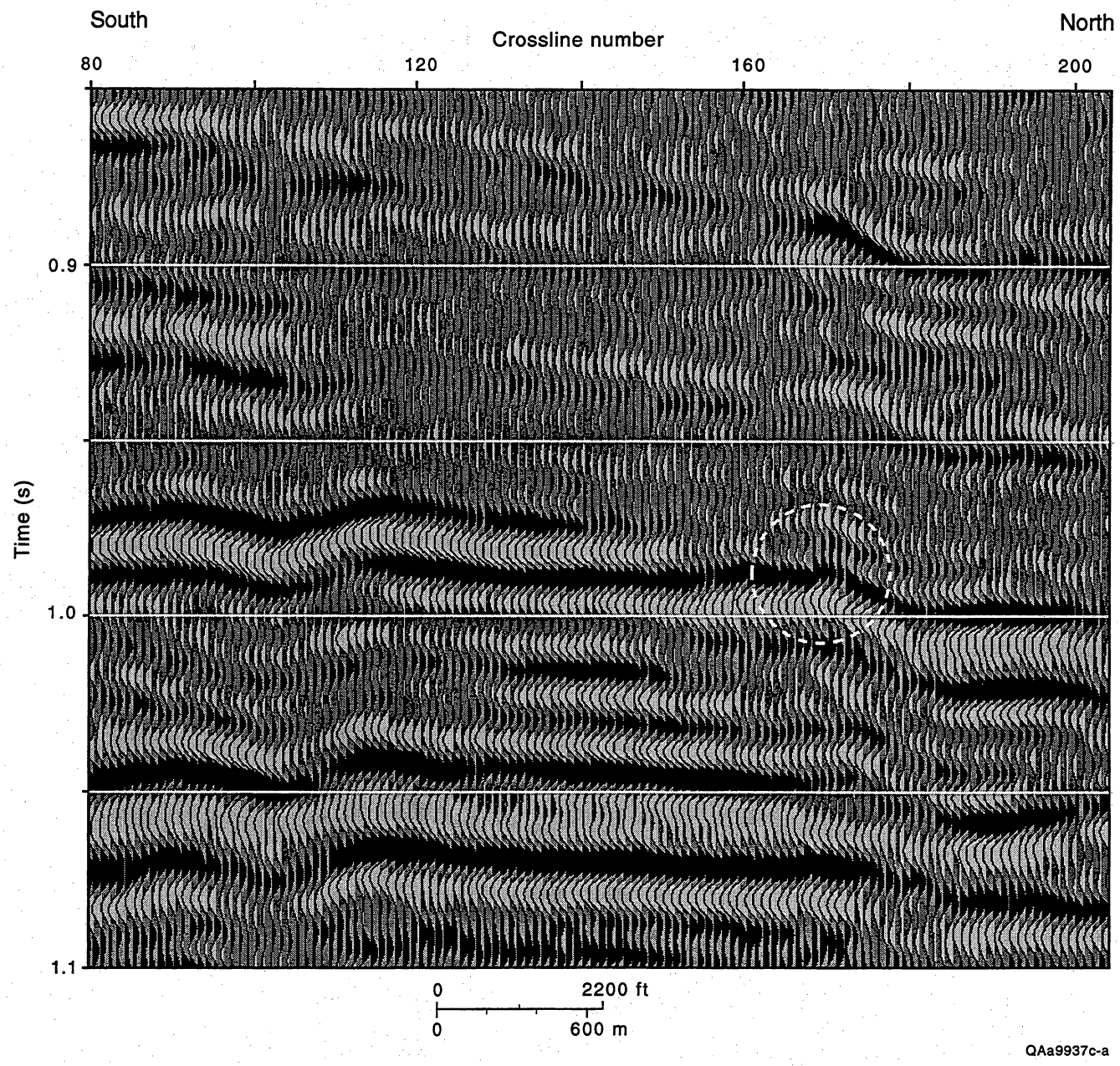

Figure E11. Inline profile 147 showing that the anomalous instantaneous frequency values in the vicinity of crossline coordinate 170, which form an east-west linear trend in the 980-ms time slice in Figure E10, are associated with a fault. These anomalous frequencies occur at 980 ms near the center of the circled area.

References

Hardage, B. A., 1987, Seismic stratigraphy: Geophysical Press, London, 432 p. (Now available from Elsevier Science Ltd., Oxford, England.)

Taner, M. T., Koehler, F., and Sheriff, R. E., 1979, Complex seismic trace analysis: Geophysics, 44, p. 1041–1063.

Taner, M. T., and Sheriff, R. E., 1977, Application of amplitude, frequency, and other attributes to stratigraphic and hydrocarbon determination: American Association of Petroleum Geologists Memoir 26, p. 301–327.

APPENDIX F

INTERPRETING THIN-BED STRATIGRAPHY IN 3-D SEISMIC DATA VOLUMES

Probably the most challenging problem in constructing seismic images of thin-bed reservoirs is to define precisely where the stratal surface representing a specific targeted thin bed is located in the seismic reflection response. This appendix describes a methodology that can be used to position thin-bed stratigraphy accurately in 3-D seismic data volumes. This methodology was particularly important in the Boonsville project because many of the depositional sequences that had to be seismically imaged were thin beds that could not be seismically *resolved*; that is, there were no distinct peaks and troughs at the top and bottom boundaries of the bed. Even though the time thickness of these thin beds could not be resolved, the beds could usually be *detected* because they were positioned within a specific, laterally continuous reflection peak or trough whose time coordinate could be defined by an appropriate depth-to-time calibration function. The challenge faced by a seismic interpreter is to select the correct peak or trough that contains the targeted thin bed.

Correcting for Velocity Anisotropy and for Time Shifts Produced by Data Processing, Variable Source Wavelets, and Variation in Depth Datum

The critical measurement needed for calibrating seismic traveltime with stratigraphic depth is a zero-offset, or a moderate-offset, vertical seismic profile (VSP) because VSP data provide the following information, which is most important when positioning thin-bed images in a 3-D seismic data volume:

(1) a precise relationship between vertical traveltime and stratigraphic depth and

(2) an image, based on vertical seismic velocities and vertical seismic traveltimes, of the stratigraphic thin beds penetrated by the VSP well.

These interpretational benefits of VSP-derived data are emphasized in Figure F1.

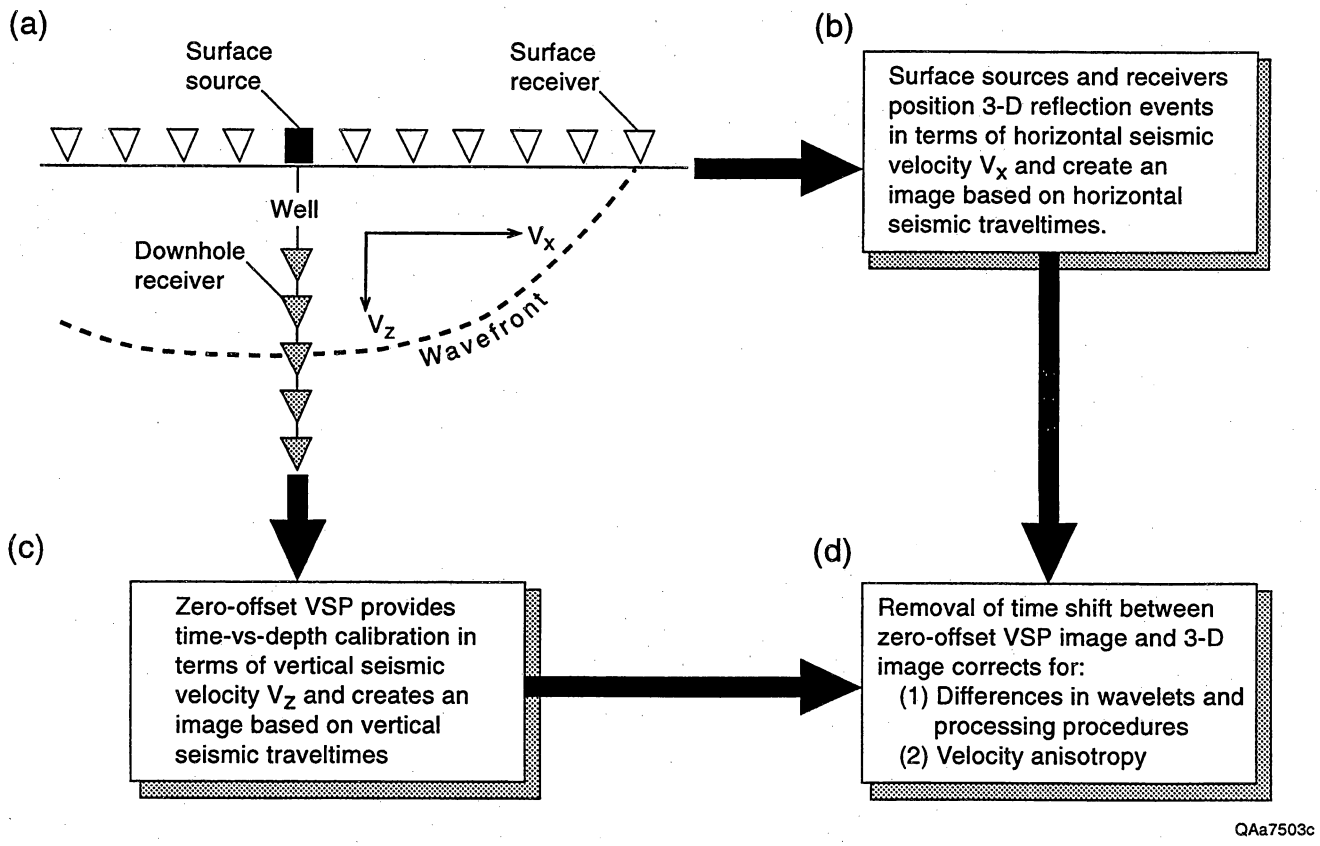

Figure F1. The concept of positioning thin beds in 3-D seismic images. (a) Source-receiver geometry involved in zero-offset VSP acquisition and 3-D data acquisition. The dashed wavefront is elliptical, not spherical, because of velocity anisotropy caused by the horizontal seismic velocity Vx in the Earth being faster than the vertical seismic velocity Vz. (b) Statement emphasizing that the time positions of surface-recorded 3-D reflection events are controlled by horizontal seismic velocity Vx. (c) Statement that the time positions of reflection events in a zero-offset VSP are controlled by vertical seismic velocity Vz. VSP data provide a rigorous linkage between the stratigraphic depth of a thin bed and the vertical traveltime to that depth. (d) The final step in calibrating the correct time position of a thin bed in a 3-D image is to determine the time shift between the VSP image (where the time positions of thin beds are known) and the 3-D image.

The key phrases used here to describe the information provided by a zero-offset VSP (and a moderate-offset VSP also) are *vertical seismic velocities* and *vertical seismic traveltimes*. The word *vertical* is stressed because vertical ray paths and a vertical source-receiver geometry are involved in VSP data recording (Fig. F1a). In contrast, it is *horizontal* velocity that controls the time positions of reflection events that are generated by surface sources and then recorded by offset surface-based receivers, which is the geometry used in a 3-D seismic grid (Fig. F1a and F1b). This observation results because velocity V in the normal moveout equation (equation 6 of App. D) that time-shifts reflections before stacking is the velocity in the horizontal direction. In general, seismic velocities measured in the Earth are anisotropic, with velocity V_x in the horizontal direction usually being faster than velocity V_z in the vertical direction. This anisotropic behavior is the reason the wavefront in Figure F1a is drawn as an ellipse in which the wavefront has traveled farther in the horizontal direction than in the vertical direction. This velocity anisotropy ($V_z<V_x$) exists because the Earth is more layered, and therefore more heterogeneous, in the vertical direction than it is in the horizontal direction.

Recording zero-offset and moderate-offset VSP data at depth increments of 50 ft or so through a stratigraphic interval provides a detailed and precise relationship between *vertical* traveltime and stratigraphic depth. This depth-versus-time calibration allows any geologic or engineering measurement that is known as a function of depth to be accurately positioned as a function of time in zero-offset and moderate-offset VSP images. The next (and last) critical step of seismic thin-bed interpretation is to determine how these VSP images (which are images in which reflections are positioned in terms of vertical traveltime and where vertical traveltime can be directly associated with depth) should be shifted in time to correlate with a 3-D image (which is an image in which reflection events are positioned in terms of horizontal traveltime, not vertical traveltime, and where there is no defined relationship between horizontal traveltime and depth).

This last step of the thin-bed calibration procedure is done by time-shifting the VSP image relative to the 3-D image at the VSP control well until the VSP reflection events and the 3-D reflection events align in an optimal manner. Often a VSP reflection event occurs at a time that is slightly greater than where it occurs in 3-D data because the vertical velocity V_Z is usually less than the horizontal velocity V_X. The amount of time shift required for optimal alignment of the VSP and 3-D images may not be the same for shallow reflection events as for deep reflection events if the magnitude of the velocity anisotropy changes with depth.

In addition to accounting for the traveltime differences caused by velocity anisotropy, this time shifting of VSP and 3-D images to determine optimal image alignment also removes any timing differences that exist in the two images due to (1) different wavelets being involved in the VSP and 3-D data, (2) different data-processing procedures being used to create the two images, and (3) a different depth datum being used to define when $t = 0$ in each image. These observations are emphasized in Figure F1d. This time shifting and alignment of VSP and 3-D images to adjust for any phase differences that exist between the 3-D and VSP data due to (1) different wavelets being involved in the respective data recordings and (2) different data-processing procedures being used to make the images is the major reason VSP data, rather than velocity checkshots, are preferred for depth-to-time calibration. Velocity checkshots do not provide an independent image of the subsurface that can be correlated with the 3-D image to confirm whether wavelet phase differences, and therefore timing differences, exist between the 3-D data and the data used to define the depth-to-time calibration function. Both checkshot and VSP data were used for depth-to-time calibration in the Boonsville study.

Equivalent Source Requirement

It is not unusual to observe slightly different traveltimes between seismic wavefields generated by impulsive sources and wavefields produced by vibratory sources. Sometimes small traveltime differences are noted even between wavefields generated by different impulsive sources—for example, when air-gun wavefields are compared with explosive wavefields or with weight-drop wavefields. These traveltime differences can sometimes be removed by numerical equalization procedures during data processing, but when confronted with the problem of interpreting thin sequences in a 3-D seismic data volume, one should use the same energy source for recording the depth-to-time calibrating data (velocity checkshot and VSP data) as the source that is used to produce the 3-D seismic wavefields. If a vibroseis source is used for the 3-D survey, a vibroseis source should be used to acquire the checkshot and/or VSP data. If explosives were used to generate the 3-D data, explosives should be used as the checkshot source and as the VSP source.

To calibrate the Boonsville sequence stratigraphy of the Boonsville 3-D seismic data, velocity checkshots were recorded in five wells across the study area. Because small directional charges deployed in 10-ft shot holes were used to generate the 3-D data, these same directional charges were detonated in 10-ft holes to produce the checkshot data. The checkshots were typically recorded at vertical intervals of 500 ft.

It is quite expensive to prepare the large number (approximately 300) of loaded shot holes needed for an explosive-source vertical seismic profile because VSP data are typically recorded at vertical intervals of 50 ft over a vertical aperture of approximately 3,000 ft. For reasons of economy, therefore, when VSP data were recorded in three of these four Boonsville velocity control wells, the energy source that was used was vibroseis rather than loaded shot holes. Numerical wavelet equalization techniques were then used to adjust the vibroseis VSP images to a vertical traveltime coordinate frame

equivalent to that which would have resulted if loaded shot holes had been used. An explosive-source VSP image was thus created in each well from a less costly vibroseis VSP image.

Measuring Vertical Traveltime-versus-Depth inside the Boonsville 3-D Grid

The relationship between stratigraphic depth and vertical seismic traveltime was determined at five locations inside the 26-mi^2 Boonsville 3-D grid: the B Yates 11, B Yates 17D, B Yates 18D, Sealy C3, and J. D. Craft TWB 3 wells (Fig. F2). Two measurements were made in the B Yates 11, 17D, and 18D wells—(1) VSP data were recorded using a surface vibrator as the energy source and (2) a checkshot survey was done in which C-10 directional charges deployed in 10-ft holes were used as the energy source. These directional charges are described in Appendix D.

The depth-versus-time curves observed in the B Yates 11 and 18D wells are shown in Figure F3. A comparison of these curves is essential for two reasons:

1. It is important to know whether vibroseis and pentolite wavelets exhibit significantly different traveltimes. If there are major differences in the traveltimes of the wavelets emitted by these two sources, then special steps must be taken if the Boonsville VSP data (which are generated by vibroseis sources) are used to calibrate the 3-D seismic data (which are generated by pentolite sources).
2. It is important to know whether anisotropy causes significant traveltime differences to exist between vertical travel paths (the pentolite checkshot curves) and slant travel paths (the offset VSP curves). If the traveltime differences are minor, then the pentolite checkshot data can be used as depth-to-time calibration data for the 3-D seismic data without our having to apply dynamic adjustments to the checkshot times.

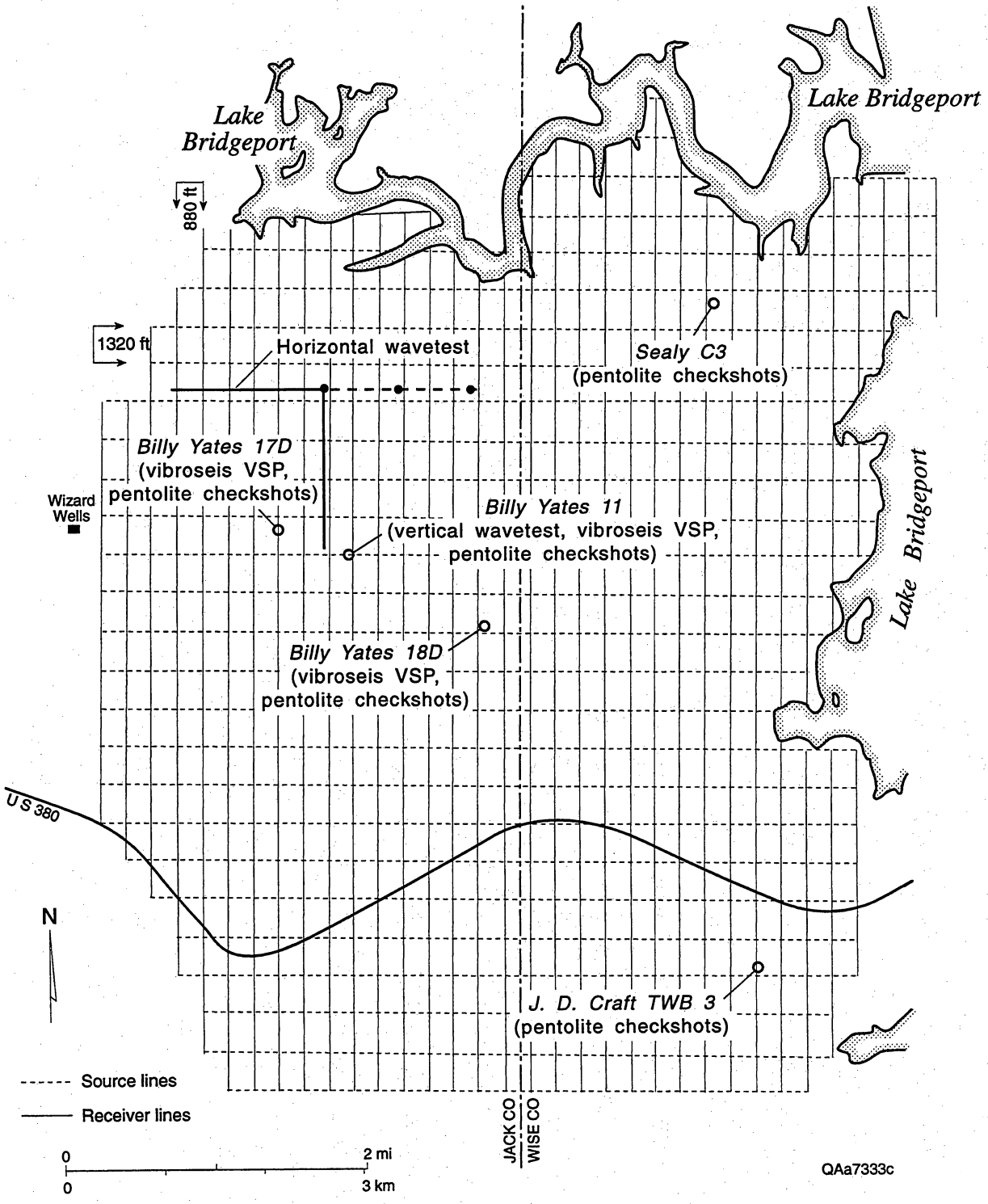

Figure F2. Location of wells where velocity checkshots and VSP data were recorded.

Visual inspection of Figure F3 shows that the two traveltime curves measured for vertically traveling pentolite checkshot wavelets and the two traveltime curves measured for vibroseis VSP wavelets (one [B Yates 11] based on vertical travel paths and one [B Yates 18D] based on slant paths) follow a similar, but not identical, trend. To determine the potential impact of the traveltime variations manifested by these pentolite and vibroseis wavelets, and by their vertical and slant travel-path geometries, we show the same data in a different format in Figure F4. Here we plot the difference between the depth predicted by each traveltime curve and the depth predicted by the average of all four traveltime curves. This plot allows these important conclusions to be made:

1. Pentolite and vibroseis wavelets do not exhibit significant traveltime differences in our study area. This conclusion is supported by the pentolite and vibroseis traveltime curves measured in the B Yates 11 well, which compare traveltimes along the same vertical travel paths. The depths predicted by these two traveltime curves differ by no more than 50 ft within the Bend Conglomerate, which is not a significant difference because slight errors in picking first-arrival times in these high-velocity rocks can create depth differences of 20 to 30 ft.
2. Velocity anisotropy may indeed be a problem that has to be dealt with when calibrating stratigraphic depth to the Boonsville 3-D seismic data. This concern is supported by the depth difference of approximately 100 ft occurring between the two traveltime curves that were recorded in the B Yates 18D well (one a measurement using vertical travel paths and one a measurement using slant travel paths). A depth difference of this magnitude within the Bend Conglomerate concerns us because (1) it cannot be attributed to imprecise picking of first arrivals and (2) some of the Bend Conglomerate sequences are thinner than 100 ft.

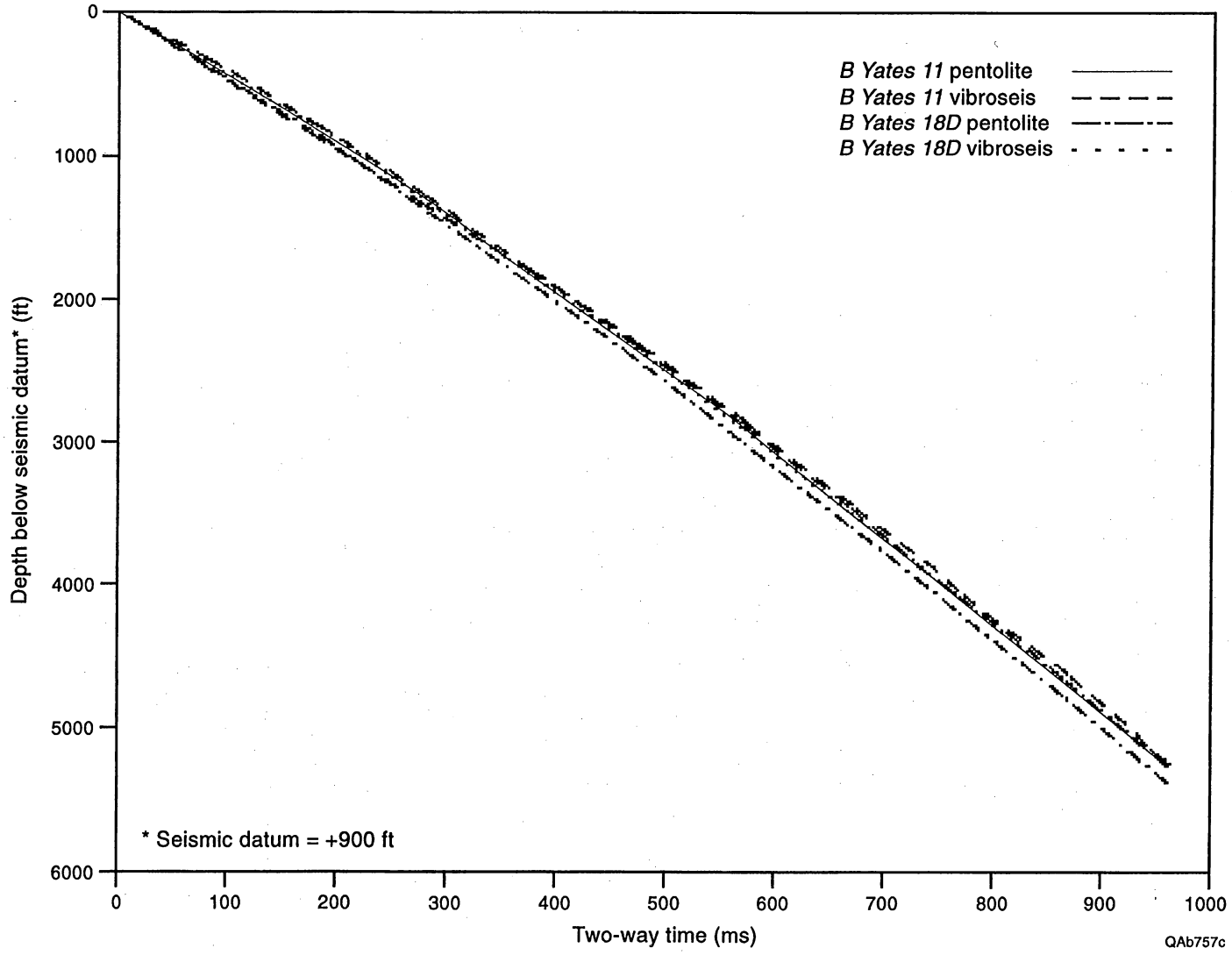

Figure F3. Time-vs-depth functions measured for vibroseis and pentolite (C-10 directional charges) wavelets inside the Boonsville 3-D seismic grid. Well locations are shown in Figure F2.

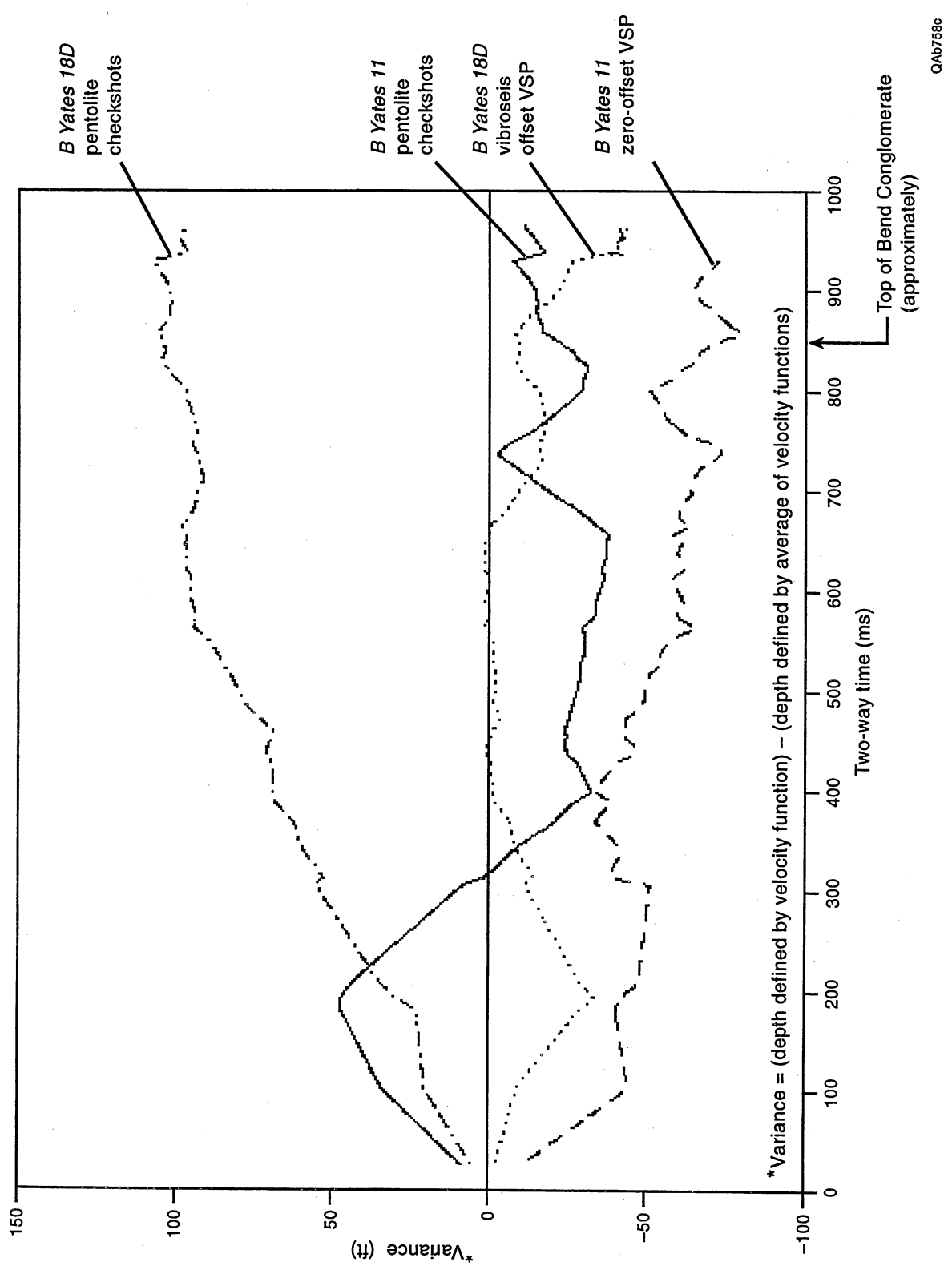

Figure F4. Variance in depth predictions associated with the traveltime functions shown in Figure F3.

On the basis of this concern, we decided to investigate the problem of velocity anisotropy across the project area. A part of this investigation was to determine whether the variation of vertical traveltimes, measured at different sites across the 3-D seismic grid, was approximately the same magnitude as the variation seen between vertical and slant travel paths at the B Yates 18D well (Fig. F4). Vertical traveltimes for pentolite wavelets were measured at four wells, the B Yates 11, 17D, 18D, and Craft TWB No. 3 (see Fig. F2). These traveltime curves are displayed in Figure F5, and the variances in the depth predictions provided by these traveltime curves are shown in Figure F6.

We analyzed velocity anisotropy by concentrating on the data display in Figure F6. Because the Craft TWB No. 3 curve had an erratic behavior compared with those of the other traveltime curves, we reviewed the Craft TWB No. 3 data but could not find any significant errors in our first break picks. These Craft TWB No. 3 data may simply have inherent time-zero errors introduced by the recording systems and/or the shooting box; as a precaution, we put less weight on these data, than on the other traveltime data, when doing depth-to-time conversions.

The traveltime data recorded in the B Yates 11, 17D, and 18D wells are quite reliable, and the curves in Figure F6 show that vertical traveltimes vary in a way that causes depth differences of 100 ft to occur over distances of less than 1 mi (the distance between the B Yates 11 and 18D wells). These depth differences are the same order of magnitude as the depth differences observed for vertical and slant path traveltimes at the B Yates 18D well, so we concluded that we could ignore velocity anisotropy as a potential source of depth-to-time error because we had vertical traveltime control wells distributed across the 3-D seismic grid. In other words, we established enough vertical traveltime control wells across the project area so that regardless of where we did a depth-to-time conversion inside the 3-D seismic grid, one of these velocity control wells was close enough to that site to allow a local depth-to-time calibration function to be used. This interpretational approach ensures that a correct vertical velocity function is

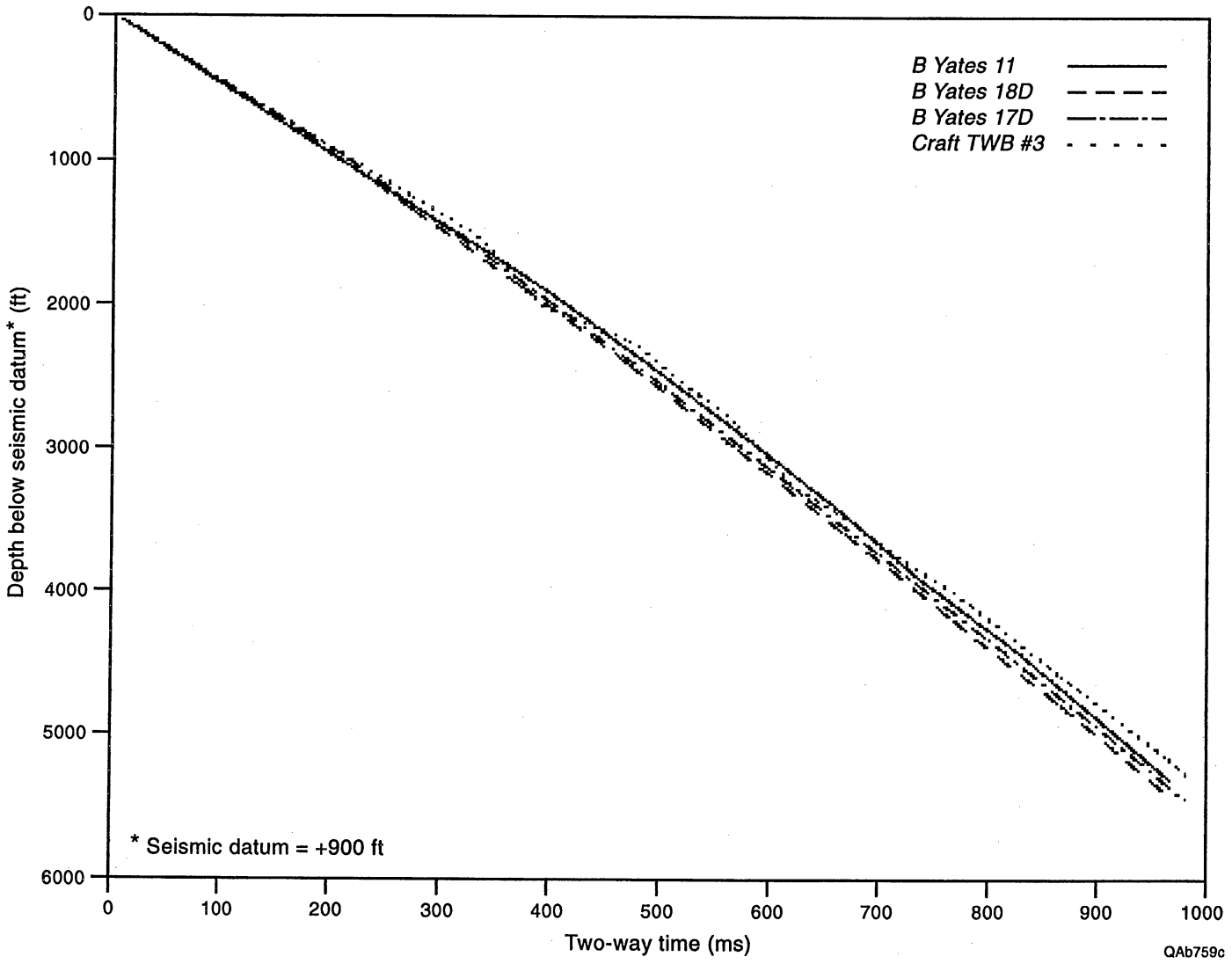

Figure F5. Time-vs-depth functions derived from pentolite-wavelet checkshot data recorded in different wells within the Boonsville 3-D seismic grid. Well locations shown in Figure F2.

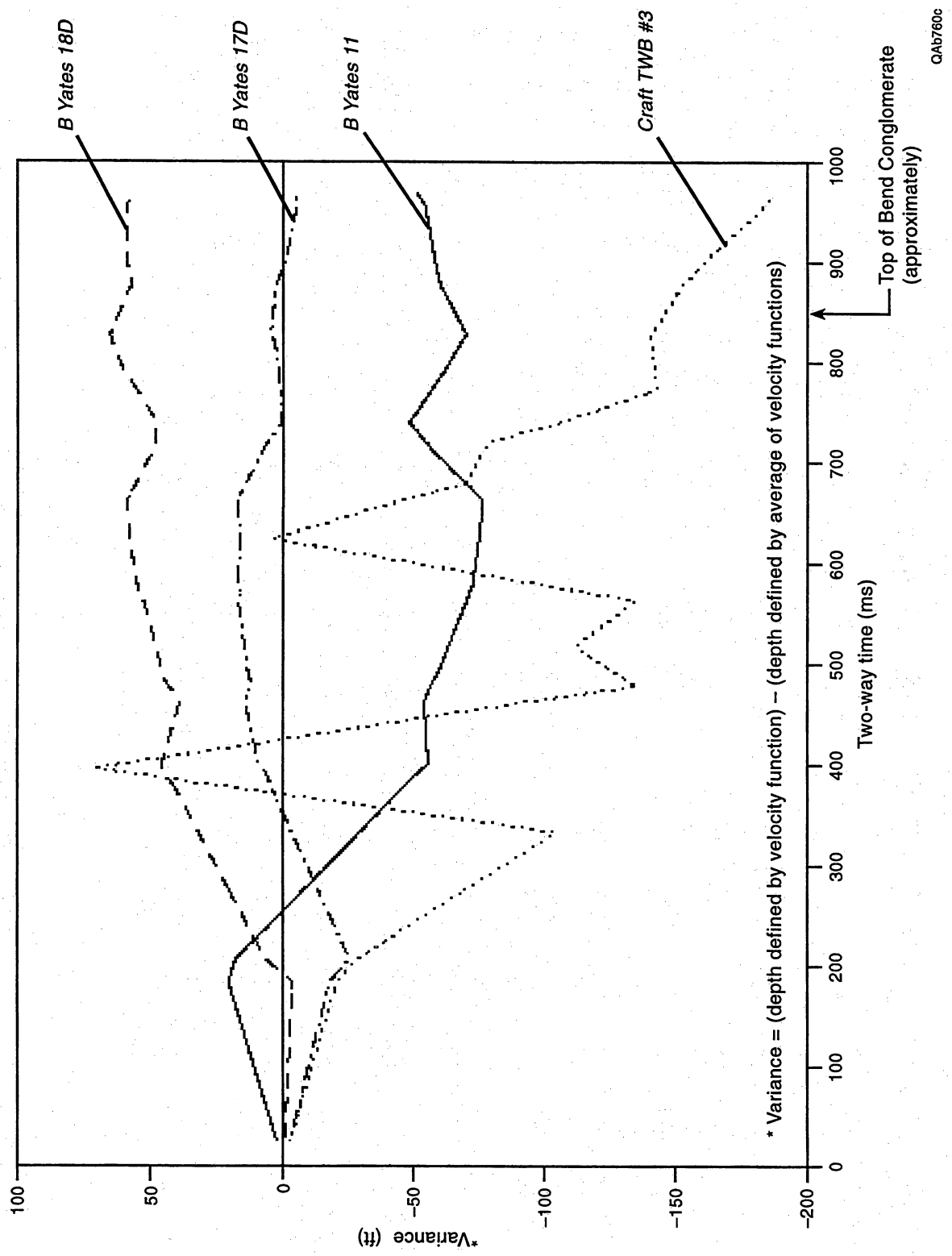

Figure F6. Variation in depth predictions associated with the traveltime functions shown in Figure F5.

used for the calibration, even if the rocks do exhibit anisotropic velocity behavior. Our experience leads us to make the following recommendation:

> *For precise depth-to-time conversion across a sizable 3-D seismic grid, vertical traveltime calibration functions should be established at intervals of approximately 2 mi across the grid.*

Comparison of VSP and 3-D Seismic Images

Regardless of how much care is used in 3-D seismic data recording and processing, interpreters often have lingering doubts about the accuracy of the 3-D images once they begin to use the data for thin-bed interpretation. It is, therefore, important to obtain one or more independent seismic images of the thin-bed stratigraphy and compare these images with the 3-D seismic images. At Boonsville, we acquired these independent images by recording offset VSP's at two wells, the B Yates 17D and 18D.

A comparison between the VSP and 3-D images at the B Yates 18D well is given in Figure F7. These two images are quite similar and indicate that the 3-D seismic data are reliable for thin-bed interpretation. Most of the differences between VSP and 3-D seismic images, and specifically between these shown here for the 18D well, are due to three factors:

1. Different source wavelets are involved in the two images—a vibroseis wavelet in the VSP data and a pentolite wavelet in the 3-D data.
2. Different wavelet processing procedures are used in the two image constructions.
3. A VSP image is a 2-D stack of VSP traces, but a 3-D image is a 3-D migration of 3-D traces. By definition, 2-D stacking and 3-D migration produce different images.

Considering these factors, it is remarkable that the VSP and 3-D images are as similar as they are. The wavelet differences resulting from factors 1 and 2 can be

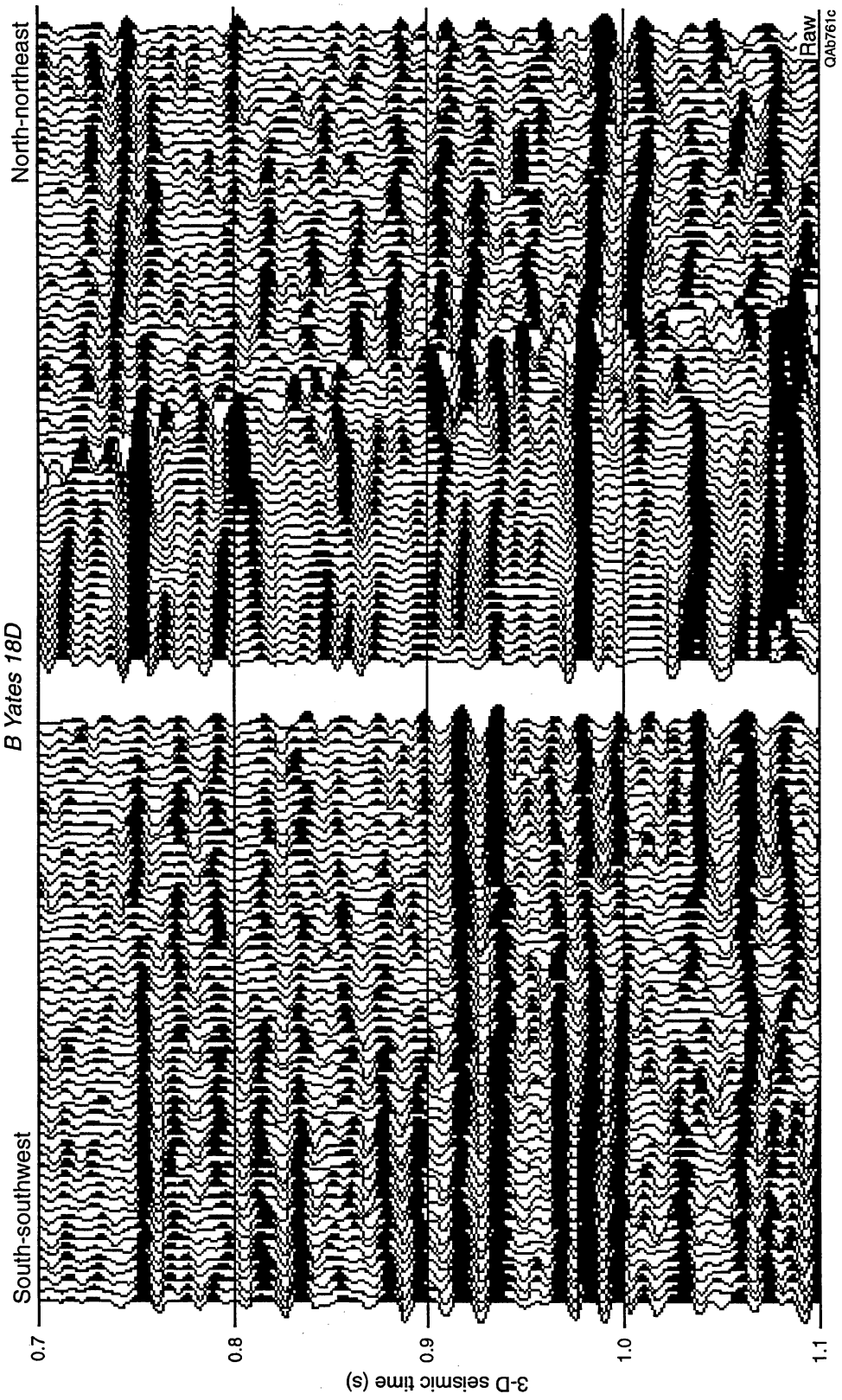

Figure F7. Comparison between contractor-delivered VSP images and 3-D seismic images at the B Yates 18D well.

minimized by applying a numerical equalization operator to the VSP image that causes its basic wavelet to have the same phase and amplitude spectra as does the basic wavelet in the 3-D data. Figure F8 shows the image comparison after such an equalization procedure and demonstrates that the images are even more alike once they contain basic wavelets that are numerically equivalent. Note particularly the improved image match that occurs between 0.8 and 1.0 s.

At the B Yates 17D well, we recorded two offset VSP's to further confirm whether the 3-D seismic images accurately portrayed the Bend Conglomerate stratigraphy. The comparison between the contractor-delivered VSP images and the 3-D seismic images at the B Yates 17D well are shown in Figures F9 and F11; the comparison between our numerically equalized VSP images and the 3-D image are shown in Figures F10 and F12. Like the situation at the B Yates 18D well (Fig. F8), these image comparisons confirm that the Boonsville 3-D seismic data are quite accurate and can be used for interpreting thin Bend Conglomerate sequences with high confidence. We recommend that all 3-D seismic interpreters follow our procedure if possible:

> *To confirm that a 3-D seismic image is sufficiently accurate for thin-bed interpretation, one or more VSP images should be recorded inside the 3-D grid and compared with the 3-D image.*

SEISMIC INTERPRETATION PROCEDURE USED TO IMAGE BEND CONGLOMERATE THIN BEDS

An important assumption was invoked when interpreting the thin-bed images in the Boonsville 3-D seismic data volume, namely,

> *A seismic reflection event (i.e., a reflection peak or trough) follows a chronostratigraphic surface, which is a depositional surface that existed at a fixed geologic time. Because different lithological facies occur across a depositional surface, a seismic reflection may image different*

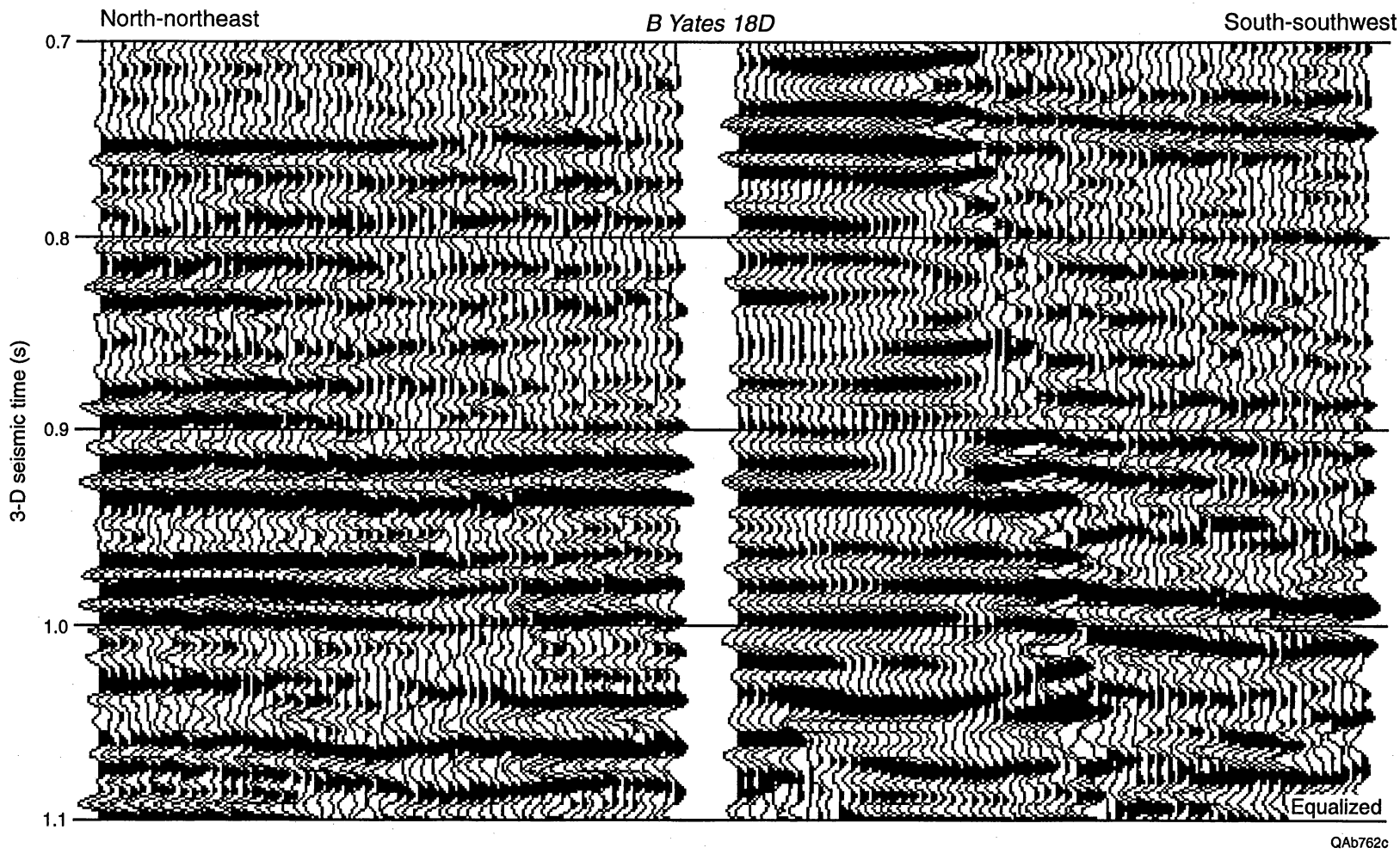

Figure F8. Comparison between wavelet-equalized VSP and 3-D images at the B Yates 18D well.

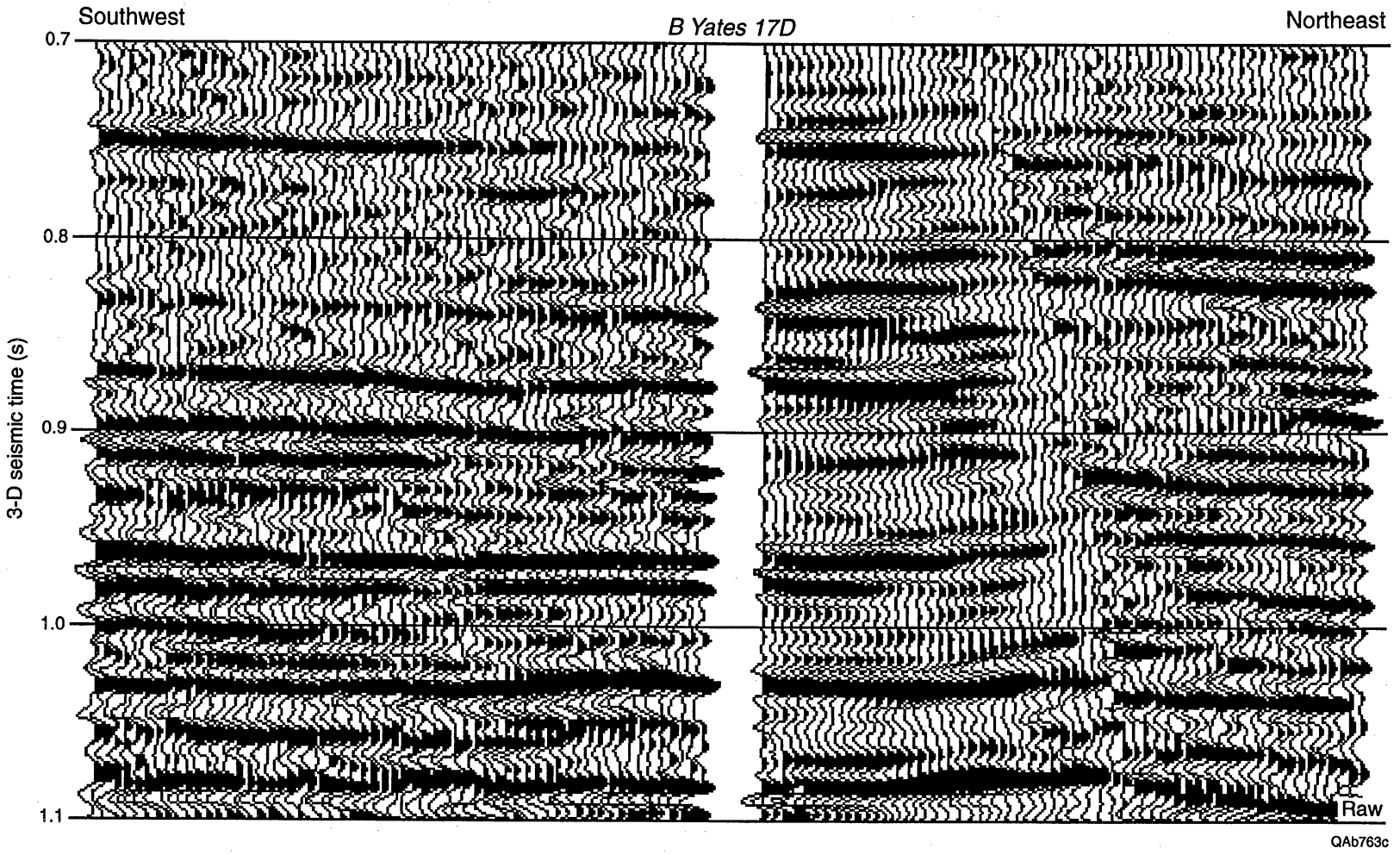

Figure F9. Comparison between contractor-delivered VSP image (northeast source offset location) and 3-D seismic image at the B Yates 17D well. VSP images are usually not accurate near the outer curved edge of the image, and interpretation should concentrate on comparing 3-D and VSP reflection waveshapes close to the VSP well.

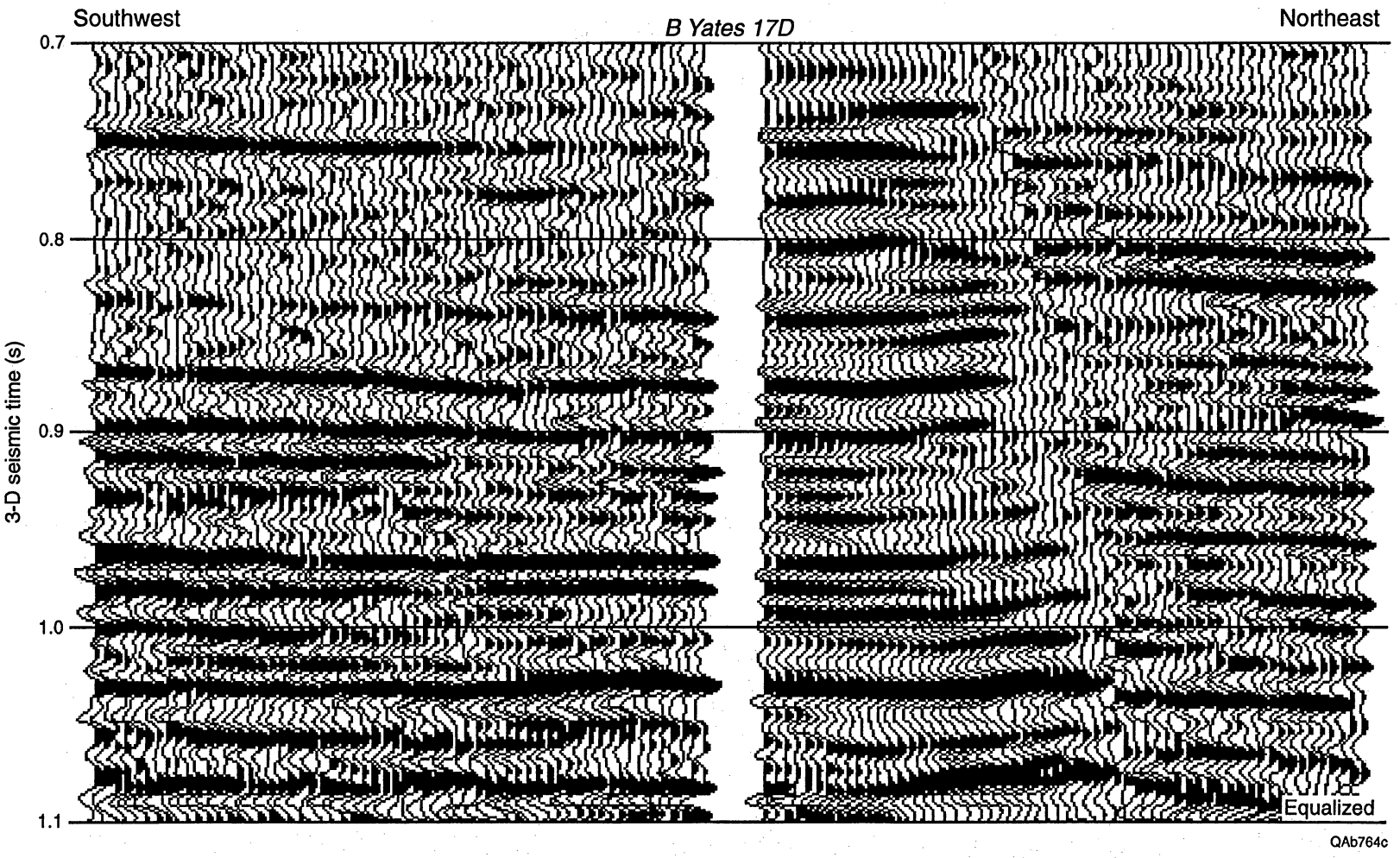

Figure F10. Comparison between wavelet-equalized VSP image (northeast source offset location) and 3-D seismic image at the B Yates 17D well. VSP images are usually not accurate near the outer curved edge of the image, and interpretation should concentrate on comparing 3-D and VSP reflection waveshapes close to the VSP well.

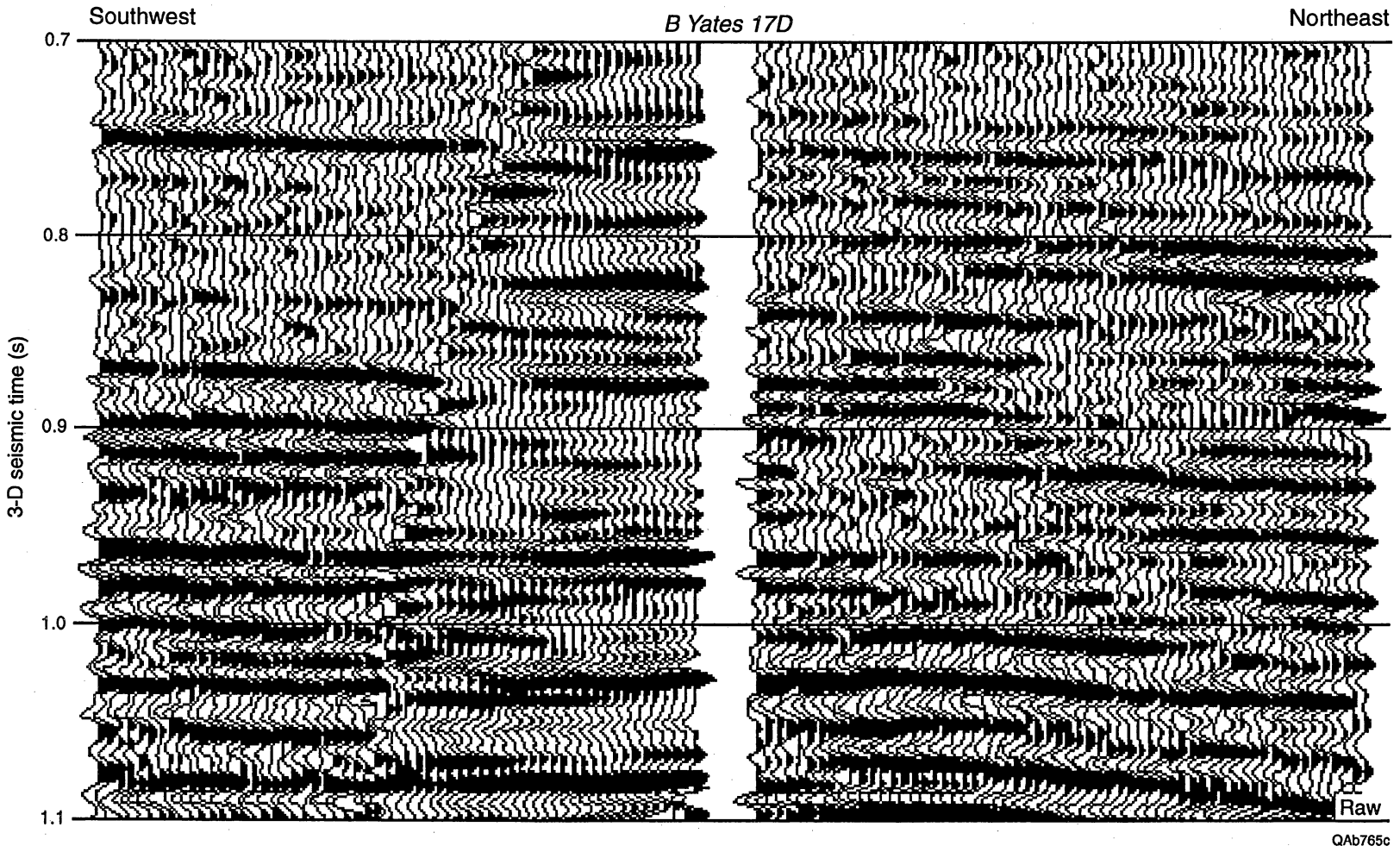

Figure F11. Comparison between contractor-delivered VSP image (southwest source offset location) and 3-D seismic image at the B Yates 17D well. VSP images are usually not accurate near the outer curved edge of the image, and interpretation should concentrate on comparing 3-D and VSP reflection waveshapes close to the VSP well.

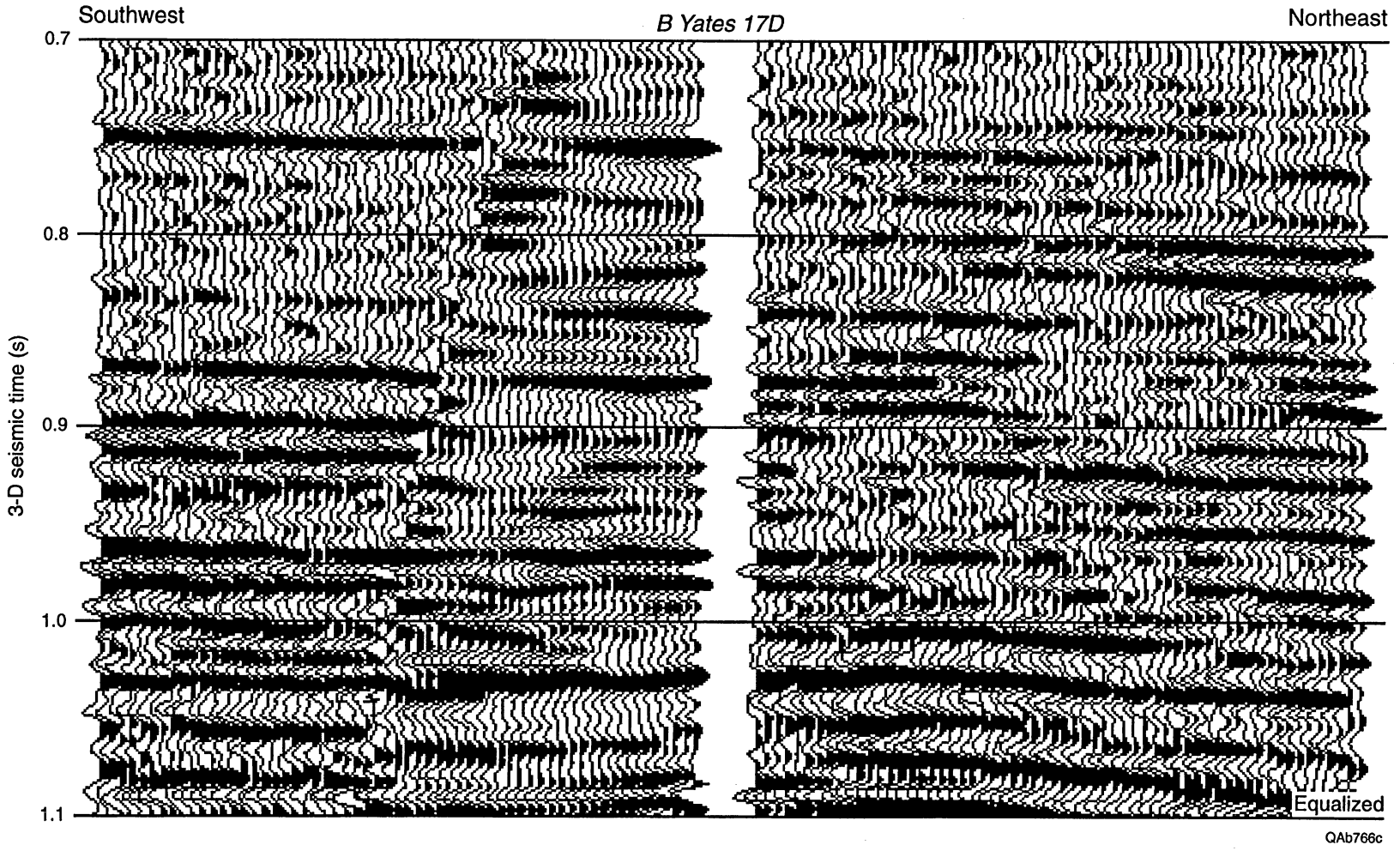

Figure F12. Comparison between wavelet-equalized VSP image (southwest source offset location) and 3-D seismic image at the B Yates 17D well. VSP images are usually not accurate near the outer curved edge of the image, and interpretation should concentrate on comparing 3-D and VSP reflection waveshapes close to the VSP well.

lithological contrasts at different reflection points along the stratal surface that it defines.

This assumption is not accepted by all seismic interpreters, but it is a basic premise of seismic stratigraphy and was used in the Boonsville interpretation.

To create a 3-D seismic image of a thin bed, it is essential that a chronostratigraphic surface be constructed that is seismically conformable to the thin bed in the local area where the thin-bed interpretation is being done. Once such a surface is created, all of the traces in the 3-D volume can then be time shifted so that this chronostratigraphic interface is flat everywhere in the data volume, and then time slicing can be done in this time-shifted 3-D data volume. There are two reasons for doing such a time shift:

(1) At the time of deposition, most depositional surfaces are reasonably flat in a local sense. Thus, this time shifting approximately restores the ancient topographic surface that existed locally at the time the targeted thin-bed sedimentation occurred, and this time-shifted image often allows seismic interpreters to more easily see the stratigraphic relationships that immediately preceded and followed the local thin-bed deposition.

(2) It is easier to write software that rapidly extracts and exhibits seismic attributes across a surface when all the data points on that surface are forced to occur at the same seismic traveltime rather than allowing the data points to remain on a time-varying seismic surface.

Any constant-time slice made within a reasonably narrow time window immediately above or below a flattened chronostratigraphic surface is assumed to be a single depositional surface that is conformable to the flattened reference surface. That is, each such time slice is assumed to also be a chronostratigraphic surface. When one of these horizon slices is made at the seismic traveltime where VSP (or checkshot) control defines a particular thin bed is positioned, that horizon slice is assumed to be an image that is dominated by the sedimentation pattern and the stratigraphy of the targeted thin bed, but

which also contains some less-dominating, but observable, phasing effects created by stratigraphy extending a few tens of feet above and below the target thin bed.

Present interpretation software defines one of the three following features of a reflection wavelet as the phase point that can be represented as an interpreted seismic surface: (1) the extremum of the wavelet peak, (2) the extremum of the wavelet trough, or (3) the zero-crossing between the peak and trough. In the Boonsville 3-D interpretation, either peaks or troughs, not zero-crossings, were used to construct chronostratigraphic surfaces.

Any reflection event that is chosen to be a reference chronostratigraphic surface and that will then be used to flatten a 3-D data volume for time slicing purposes should exhibit the following properties:

1. The event should have a signal-to-noise character that is of sufficient quality to allow a reliable interpretation.
2. The event should be continuous and extend across all, or a large portion of, the area spanned by the 3-D data volume.
3. The event should be reasonably close to the time position of the thin bed that is to be interpreted so that the assumption of conformability between the chronostratigraphic surface and the thin bed is more likely to be correct.

Sometimes all three of these conditions cannot be satisfied and compromises have to be made. Common compromises are to allow a deviation in condition 3 by selecting a good-quality, areally pervasive reflection event that is slightly unconformable to the targeted thin bed, or to alter requirement 2 by choosing a flattening event that does not extend over a large area but is conformable to the targeted thin bed in a critical portion of the study area. The implementation of the preceding assumptions and procedures during the Boonsville data interpretation is described in the following sections.

Defining Areally Pervasive Chronostratigraphic Surfaces

Inspection of the Boonsville 3-D data volume led to the conclusion that many of the thin-bed reservoirs in the Atokan interval could be assumed to be conformable, at least in a local sense, to one of four seismic chronostratigraphic surfaces that extended across the complete 3-D survey area, and which divided the Bend Conglomerate interval into three intervals of almost equal thickness. These four sequence boundaries are defined in Figure F13 as:

1—Caddo (MFS90),
2—Davis (MFS70),
3—Runaway (MFS50), and
4—Vineyard (MFS20 for the top and MFS10 for the base),

where MFS is an abbreviation for *maximum flooding surface.*

The areally consistent reflection event defining each of these chronostratigraphic surfaces was selected in the following way:

1. Several wells (typically 25 to 30) were chosen that were distributed in an approximately uniform manner over the complete 26-mi^2 3-D grid and in which the stratigraphic depths of the Vineyard, Runaway, Davis, and Caddo boundaries were known.
2. A series of meandering seismic lines, each line connecting 4 to 6 of these calibration wells, were extracted from the 3-D data volume. An example showing the paths taken by two of these well-tie lines is shown in Figure F14.
3. The vertical traveltime required for a pentolite-generated wavelet to travel to the depth of each of the four sequence boundaries in each of the calibration wells was determined using the average of the B Yates 11, 17D, and 18D pentolite traveltime functions specified in Figure F5.

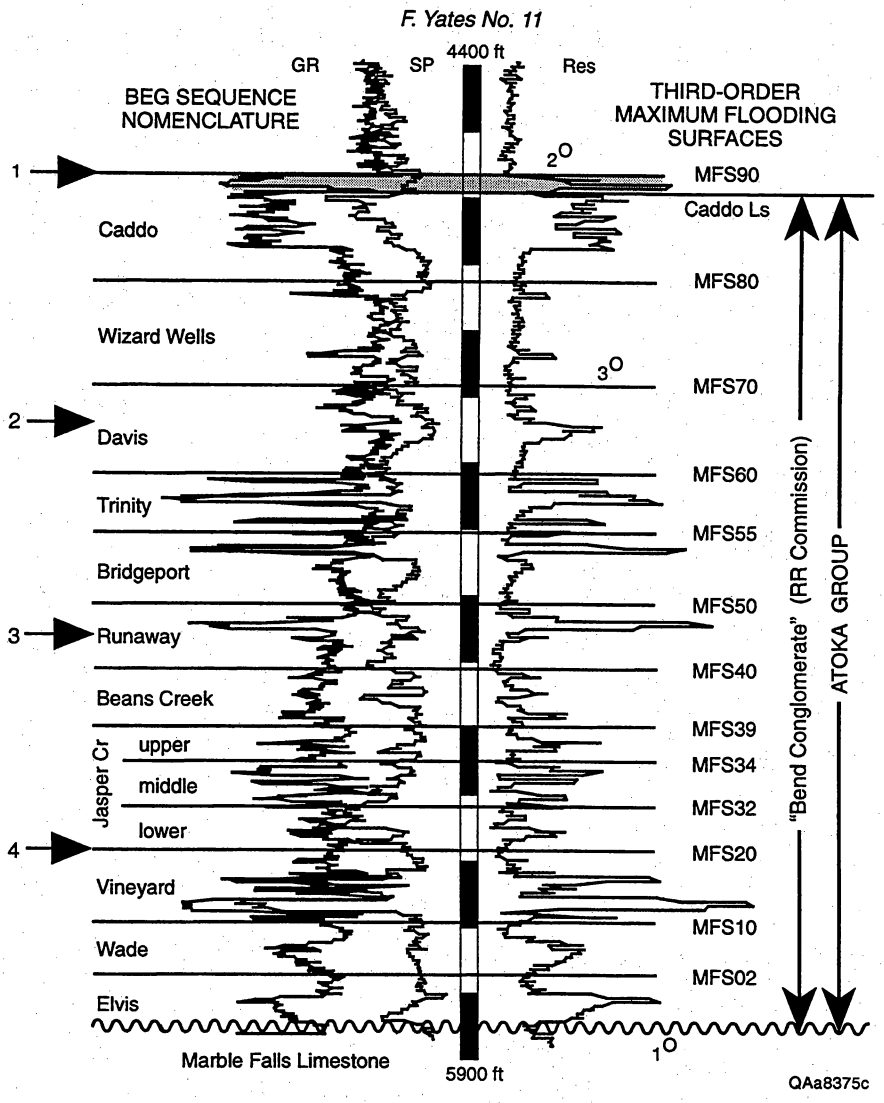

Figure F13. Stratigraphic nomenclature used to define depositional units and sequence boundaries in Boonsville field. The numbers 1, 2, 3, 4 in the left margin define the stratigraphic positions of four seismic chronostratigraphic surfaces that were interpreted across the complete 26-mi^2 3-D survey.

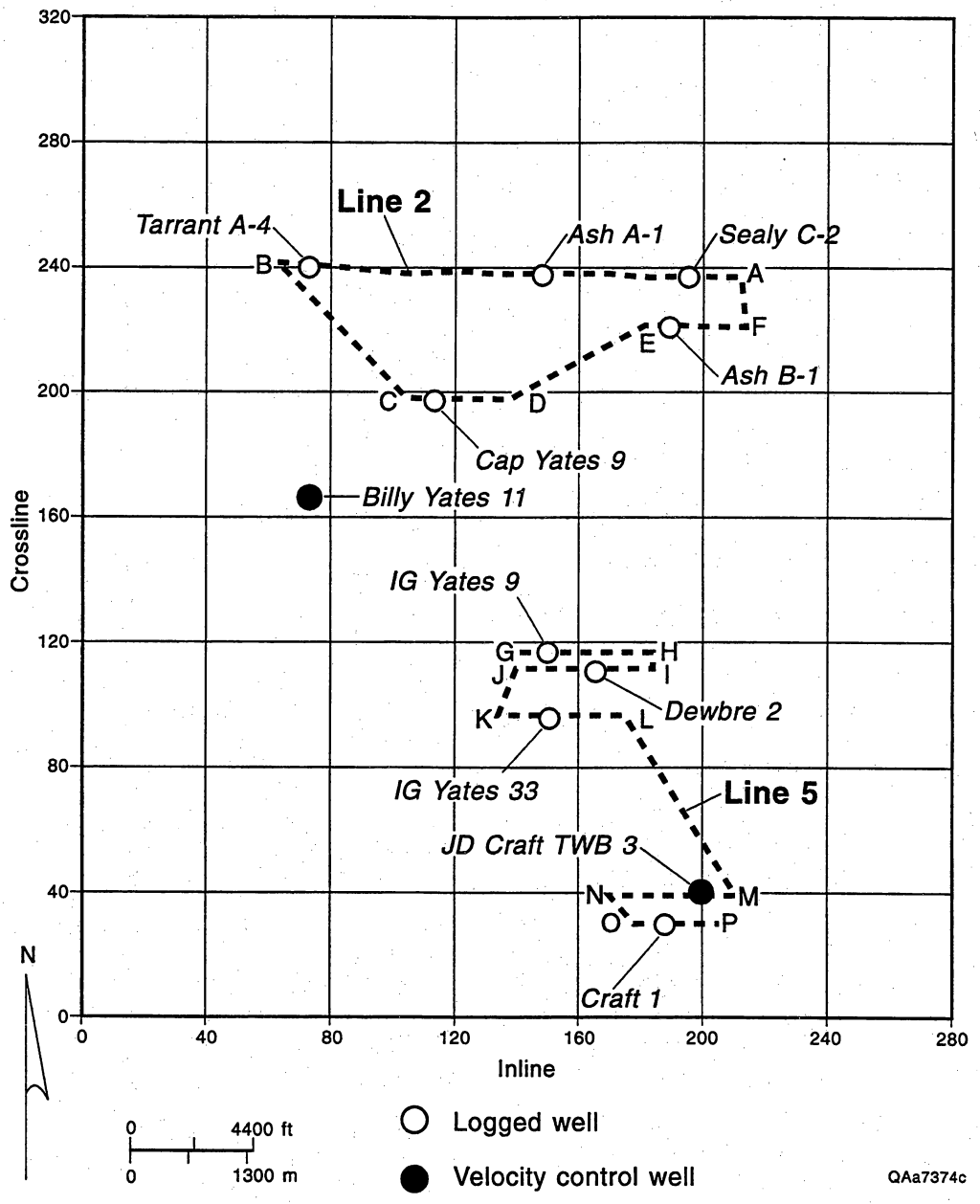

Figure F14. A map showing some of the wells used to identify the time positions of chronostratigraphic surfaces inside the Boonsville 3-D grid. Meandering lines, such as Line 2 and Line 5, were extracted from the 3-D data volume to define the two-way traveltime positions of key sequence boundaries among small subsets of the wells, with each line establishing a seismic stratigraphic tie among 4 to 6 wells. Wells were chosen so that these tie lines could be created over the entire 26-mi^2 area spanned by the 3-D survey.

4. At each well coordinate on each of these tie lines, tic marks were superimposed on the 3-D reflection data at the vertical traveltimes determined in step 3 to show where each of the four chosen chronostratigraphic surfaces should be positioned in the 3-D image at that particular well site.
5. A judgment was then made as to which seismic reflection event (i.e., which reflection peak or which reflection trough) was reasonably conformable to all of the tic marks made for each of the four sequence boundaries and which also met the other criteria required for a chronostratigraphic surface (i.e., good signal-to-noise and lateral continuity over an acceptable portion of the 3-D area). Two examples of the tic-mark positions and the seismic chronostratigraphic surfaces that were judged to best fit each set of tic marks are illustrated as Figures F15 and F16. These well-tie lines are the arbitrary profiles labeled Line 2 and Line 5 in Figure F14.

In the two examples illustrated in Figures F15 and F16, the time picks for the top and base of the Vineyard were positioned on a reasonably consistent reflection phase, and there was little doubt where to position the chronostratigraphic reference surface (surface No. 4) that would be used to flatten and extract images of thin-bed units deposited in the deep Atoka interval. Similarly the time picks for the top of the Runaway sequence fell on a consistent reflection waveform feature, and the final interpreted Runaway horizon surface No. 3 (Figs. F15 and F16) was chosen to be a good-quality reflection trough below and conformable with these calibration tic marks.

The time picks for the top of the Davis sequence occurred on a consistent reflection trough in Figure F16, but these picks are slightly above this same trough in Figure F15. Some judgment had to be used to decide which reflection event near these Davis picks was the best choice for a Davis-age chronostratigraphic surface. After inspecting well-tie lines over the complete 26-mi^2 area, the best-quality, areally pervasive reflection that

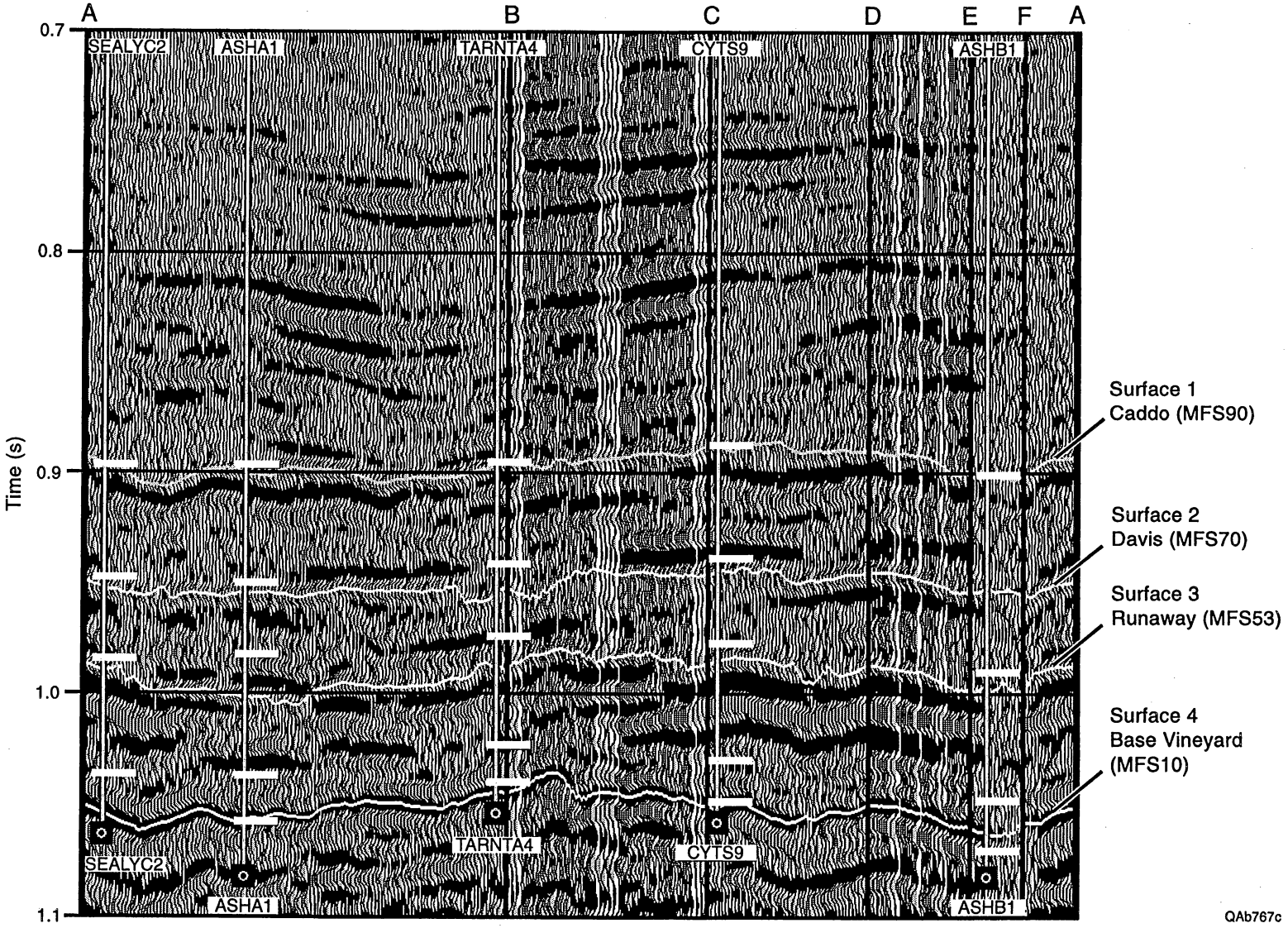

Figure F15. Arbitrary seismic line following the path labeled Line 2 in Figure F14. The positions of the labels ABCDEF correspond to the coordinates labeled ABCDEF on the map (Fig. F14). At each well location, heavy white tic marks are drawn so that they pass through the pentolite-based vertical traveltime corresponding to the depth of the Caddo, Davis, Runaway, and Vineyard sequence boundaries penetrated by the well. The time-versus-depth calibration curves in Figure F5 were used to define these time coordinates. The horizons labeled 1, 2, 3, 4 are the seismic events that were selected as the best choices for the chronostratigraphic surfaces that are closest to, and conformable with, the traveltime tic marks for the top of the Caddo, Davis, and Runaway, and the base of Vineyard sequences, respectively.

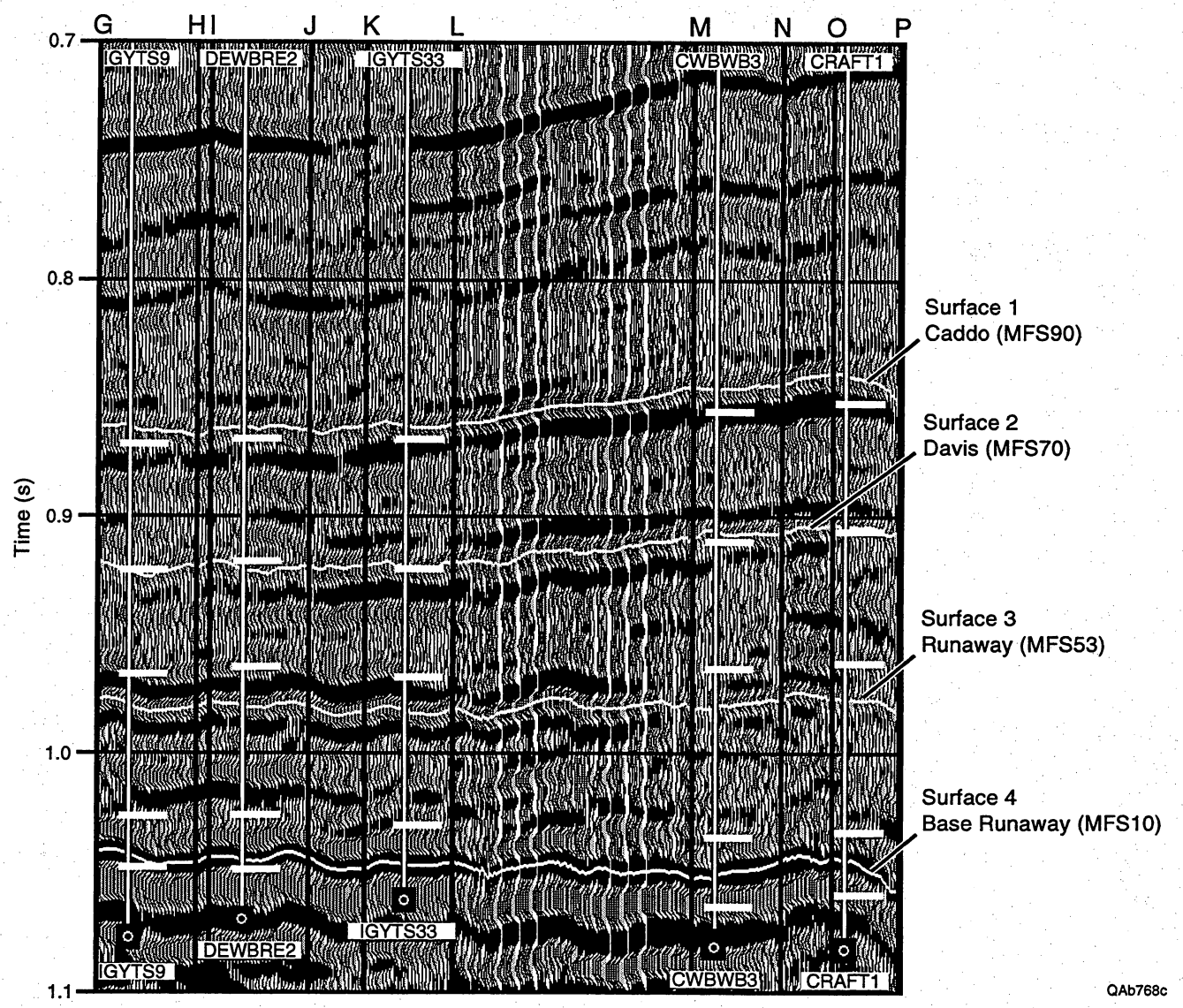

Figure F16. Arbitrary seismic line following the path labeled Line 5 in Figure F14. The positions of the labels GHIJKLMNOP correspond to the coordinates labeled GHIJKLMNOP in the map (Fig. F14). At each well location, heavy white tic marks are drawn so that they pass through the pentolite-based vertical traveltime corresponding to the depth of the Caddo, Davis, Runaway, and Vineyard sequence boundaries penetrated by that well. The time-versus-depth calibration curves shown in Figure F5 were used to define these time coordinates. The horizons labeled 1, 2, 3, 4 are the seismic events that were selected as the best choices for the chronostratigraphic surfaces that are closest to, and conformable with, the traveltime tic marks for the top of the Caddo, Davis, and Runaway, and the base of the Vineyard sequences, respectively.

could serve as a Davis-age chronostratigraphic surface was judged to be the event labeled Surface 2 in Figures F15 and F16.

In the northern part of the 3-D grid, the well picks for the Caddo fell on a consistently robust reflection event (Fig. F15), but in the southern part of the grid, the Caddo picks fell slightly below this same reflective event (Fig. F16). Surface 1 shown in Figures F15 and F16 was judged to be the best choice for a continuous seismic event that was conformable to all of the Caddo picks.

Building Areally Continuous Chronostratigraphic Surfaces

Once the four chronostratigraphic surfaces shown in Figures F15 and F16 were defined on a number of arbitrary well-tie lines across the Boonsville 3-D grid, the surfaces were then manually transferred onto a regularly spaced grid of inlines and crosslines that intersected these meandering, randomly spaced well-tie lines. This regularly spaced line grid is referred to as a *seeding grid* because it served as the seed information to drive the automatic event-picker software that converted the interpreted horizons on each individual line of the grid into an areally continuous surface. The seeding grid used for the Caddo chronostratigraphic surface is shown in Figure F17. The line spacing was smaller along the northern edge of the survey and in a narrow east-west strip just south of crossline 200 because the lateral continuity of reflections deteriorated in these areas, making it more difficult for the automatic interpolation software to construct a continuous chronostratigraphic surface in these regions. The seeding grids for the other three Atokan-age seismic chronostratigraphic surfaces were similar to this Caddo grid. This interpretational procedure was used to generate all seismic structure and attribute maps shown in this report.

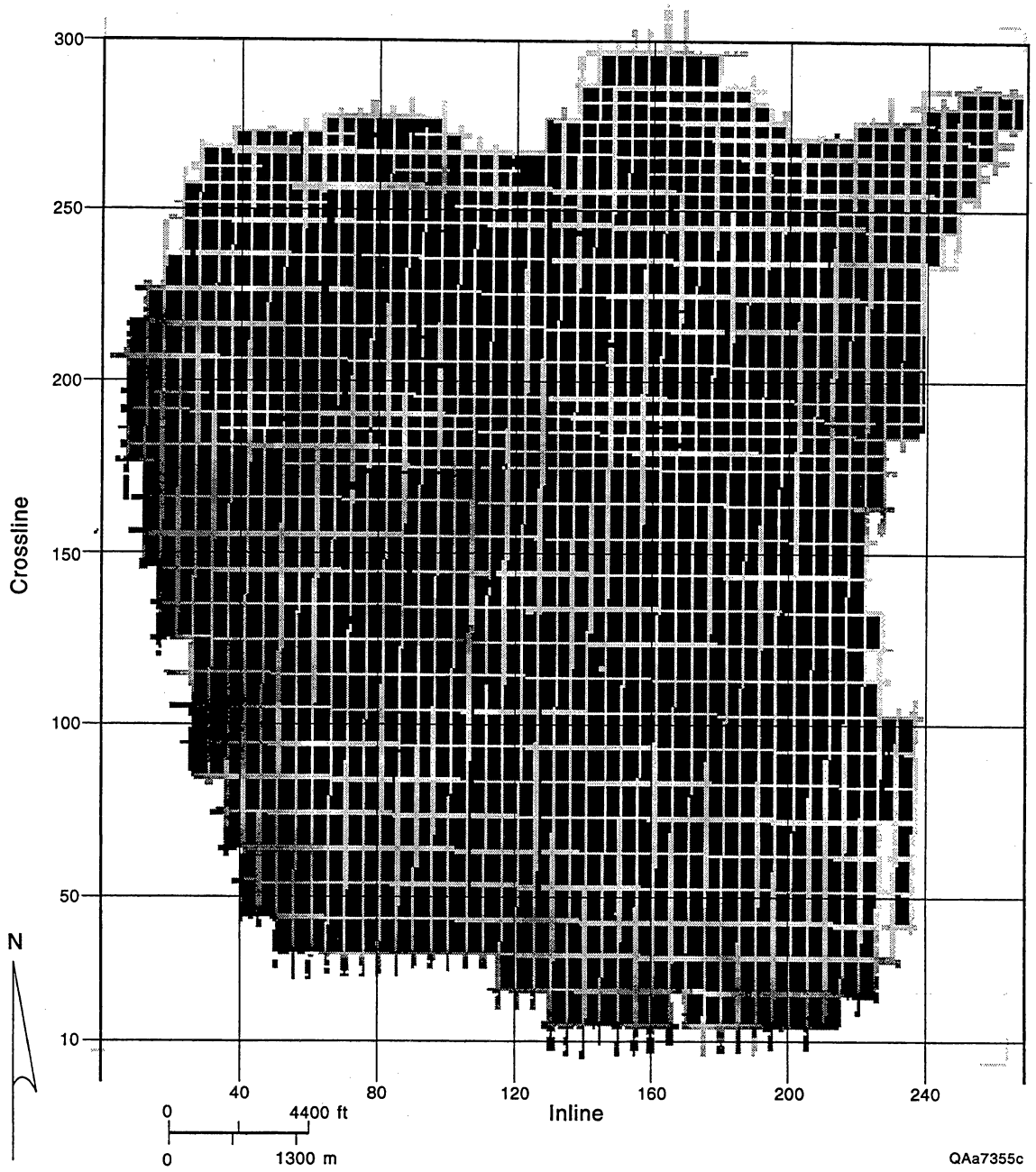

Figure F17. The seeding grid for the Caddo chronostratigraphic surface. The Caddo chronostratigraphic horizon was first defined on a series of arbitrary well-tie lines, such as those shown in Figures F15 and F16, and this horizon was then transferred to each of the lines in this seeding grid. In areas of difficult interpretation, such as the northern edge of the survey and the region south of crossline 200, the line spacing of the seeding grid was reduced. Once the horizon interpretation was satisfactorily tied across the grid, the Landmark software used by Bureau interpreters then created a continuous, smooth chronostratigraphic surface that connected the manually interpreted horizons defined across this seeding grid.

G. GLOSSARY

All italicized words appearing in a definition are defined elsewhere in the glossary.

accommodation space — that volume below *base level* within a depositional basin that is available for the accumulation of sediments.

acoustic impedance — the product of *seismic velocity* and *rock* density.

aggradation — the vertical accumulation of sediment within a *depositional system* (cf. *progradation, regression*).

allocyclic — of or relating to changes in *cyclothemic* deposition within a depositional basin that result from processes external to the basin (cf. *autocyclic*).

amplitude — the maximum numerical value expressed by a regularly and periodically varying quantity as measured from its equilibrium value (which, by definition, equals zero).

API units — one of two different measures of radioactivity on well logs as designated by the American Petroleum Institute. One unit is for the calibration of gamma-ray counters, the other for neutron detectors.

asthenosphere — the semimolten, plastic layer of the upper *mantle* immediately below the *lithosphere*, upon which the *tectonic plates* move.

Atoka Group — a *sequence* of *rock*s that overlies the *Marble Falls Formation* and underlies the *Strawn Group*. Within the *Fort Worth Basin*, it corresponds to the *Bend Conglomerate* (as designated by the Texas Railroad Commission) plus the *Caddo Limestone* and, as such, is nearly equivalent to the *Atokan Series*.

Atokan — the second *epoch* of the *Pennsylvanian Period*, extending from 308 to 310 million years ago; the *series* of stratigraphic *rock* units deposited during this time; of or relating to this *epoch* of time or its *series* of *rocks*.

autocyclic — of or relating to changes in *cyclothemic* deposition within a depositional basin that result from processes within the basin itself (cf. *allocyclic*).

bandpass filter — a digital filter that is applied to *seismic* data to limit the frequency content of the data to a specific range. The range so designated is the pass band.

base level — the level below which a river cannot erode its channel. Base level is an equilibrium surface with erosion occurring above it and deposition occurring below it. In most situations, base level is equivalent to sea level.

base level cycle — a cycle of rise and fall in relative sea level resulting from periodic changes in *eustatic sea level*, sediment supply, *tectonic* subsidence, or *physiography* of the depositional substrate.

basement — the crystalline igneous and metamorphic rocks that underlie the younger sedimentary deposits of the *crust*; the *rock* units below those with which a study is concerned, usually implying *rock* units below the hydrocarbon-productive interval.

bedding plane — a planar or nearly planar surface of a stratified sedimentary unit that separates it from the next stratified unit; a plane of deposition.

Bend Arch — the *peripheral bulge* west of the *Fort Worth Basin* produced by incremental loading along the *Ouachita Thrust Belt*.

Bend Conglomerate — an informal grouping of Atokan *rocks* used by operators in the *Fort Worth Basin* and designated by the Texas Railroad Commission as extending from the top of the *Marble Falls Formation* to the base of the *Caddo Limestone*. In this report, we treat the Bend Conglomerate as equivalent to the formally designated *Atoka Group*, which extends from the top of the *Marble Falls Limestone* to the base of the *Strawn Group* (top of the *Caddo Limestone*).

bin — a small, discrete area, usually square or rectangular, inside a *3-D seismic* image that encompasses a single *seismic trace* of the final, processed 3-D data volume. The number of *bins* required to span the entire 3-D image space is the same as the number of data *traces* in the final processed 3-D data volume, one *trace* passing vertically through the center of each *bin*.

biostratigraphy — the correlation of *rock* units on the basis of their fossil content.

bottom-hole pressure — the fluid or gas pressure produced in a well bore at the depth of the *reservoir* formation, which, in many cases, is near the bottom of the well bore.

bridge plug — a volume of concrete or a mechanical device placed in a well bore at a specified depth to seal off the hole below it.

Caddo Limestone — a *carbonate* unit of *Atokan* age occurring within the *Fort Worth Basin*. The Texas Railroad Commission designated the top of the *Bend Conglomerate* as being the base of the *Caddo Limestone*, but the faunal and age relationships of the latter unit indicate that it should be included within the *Bend Conglomerate*, as is done in this report (cf. *Bend Conglomerate*).

calcite — a relatively soft *mineral* composed of calcium carbonate ($CaCO_3$) that may occur as a pore-filling cement in *reservoir* sandstones or may comprise a limestone.

Cambrian — the first *period* of the *Paleozoic Era*, extending from 530 to 510 million years ago; the *system* of stratigraphic rock units deposited during this time; of or relating to this *period* of time or its *system* of rocks.

carbonate — of or relating to a *mineral* containing the carbonate ion (CO_3^{-2}); of or relating to a *rock* consisting primarily of *minerals* containing the *carbonate* ion.

carbonates — *rocks* consisting primarily of *minerals* containing the carbonate ion (CO_3^{-2}), i.e., limestone.

casing — the metal pipe placed within a borehole and cemented into place to prevent fluids from flowing into or out of the borehole.

cement — *mineral* crystals precipitated within the pore spaces of a sediment that bind the individual *mineral* grains together, thereby creating a solid, coherent mass.

Cenozoic — the *era* of geologic time extending from 66 million years ago to the present and including the *Tertiary* and *Quaternary Periods*.

centipoise — a measure of viscosity defined as $1/100^{th}$ of a *poise*.

channel fill — *fluvial* sediments filling a channel.

checkshot — a seismic measurement that establishes a rigorous relationship between stratigraphic depth and vertical *seismic* traveltime. The measurement is done by lowering a geophone by wireline to a specified depth in a well and then recording the *seismic* response generated by a surface energy source positioned near the wellhead.

chert — a hard, cryptocrystalline or microcrystalline silica *mineral* (SiO_2) exhibiting conchoidal fracture and commonly occurring as nodules in a *carbonate rock*.

chronostratigraphic horizon — widespread physical boundary, surface, or interval, the same age everywhere it occurs, therefore separating overlying younger strata from underlying older strata (cf. *time line*).

clastic — of or relating to *detrital* grains or a *rock* composed of them; the texture of such a *rock*.

clastics — *rock* composed of *detrital* grains.

clean sand — sandstone or sandy sediment that has been well sorted by natural processes so that it is almost entirely composed of *quartz* grains (>95%).

clinoform — the steeply dipping sediments deposited on the advancing frontal slope of a delta; of or relating to such sediments or the sloping delta front.

compartment — a space within a larger *reservoir* that, in terms of fluid flow, is totally or partially isolated from the rest of the *reservoir*.

condensed section — a thin, sedimentary succession or unit continuously deposited during times of very slow sedimentation. Condensed sections, often organic rich, correlate to much thicker sections elsewhere within the depositional basin.

convergent plate boundary — a boundary between two colliding *tectonic plates*, characterized by extensive geological activity and deformation.

craton — the geologically stable region of a continent that has not undergone significant *tectonic* deformation for several hundred million years. The craton includes both the *shield* and the surrounding *platform*.

Cretaceous — the third and last *period* of the *Mesozoic Era*, extending from 144 to 66 million years ago; the *system* of stratigraphic *rock* units deposited during this time; of or relating to this *period* of time or its *system* of *rocks*.

crossbedding — sedimentary layers more than 1 cm in thickness that are inclined relative to the main *bedding planes* because they were originally deposited on a sloping surface.

crossline — that direction in an onshore 3-D *seismic* survey that is perpendicular to the direction that the geophone cables are deployed (cf. *inline*).

crust — the outermost layer of the Earth, averaging in thickness from 30 to 45 km (18 to 27 mi) under the continents and 6 to 10 km (4 to 6 mi) under the oceans.

current-ripple mark — asymmetric ripple marks produced by unidirectional currents of air or water moving over a sandy surface.

cyclothem — very regular *facies* succession resulting from one cycle of periodic changes in relative sea level.

darcy — a standard measure of *permeability* defined as the passage of 1 cm^3 of fluid of one *centipoise* viscosity flowing in 1 sec under a pressure differential of one atmosphere through a porous medium having a cross-sectional area of 1 cm^2 and a length of 1 cm.

deltaic — of or relating to river deltas or *depositional systems*.

depositional system — a depositional environment and its characteristic *facies*.

depth-to-time conversion function — a mathematical function used to convert *seismic* traveltimes to stratigraphic depths.

Desmoinesian — the third *epoch* of the *Pennsylvanian Period*, extending from 303 to 308 million years ago; the *series* of stratigraphic *rock* units deposited during this time; of or relating to this *epoch* of time or its *series* of *rocks*.

detrital — of or relating to the broken fragments derived by weathering and erosion of preexisting *rock*s.

Devonian — the fourth *period* of the *Paleozoic Era*, extending from 362 to 408 million years ago; the *system* of stratigraphic *rock* units deposited during this time; of or relating to this *period* of time or its *system* of *rocks*.

diachronous — being of different ages in different areas.

diagenesis — those changes that occur within a sediment or sedimentary *rock* between burial and *metamorphism*, exclusive of weathering and erosion. Diagenesis is defined as occurring at temperatures under 100° C., in contrast to metamorphosis, which occurs at temperatures over 100° C. (cf. *metamorphism*).

dip — the slope of a *rock* unit as measured perpendicular to *strike*, i.e., the angle a *rock* unit makes to the horizontal.

distributary — one of the small, diverging streams into which a larger river will split as it reaches its *base level*.

divergent plate boundary — a boundary between two *tectonic plate*s that are separating.

dolomite — a *mineral* composed of calcium magnesium carbonate ($CaMg(CO_3)_2$) that may occur as a pore-filling cement in sandstones or may comprise a dolostone.

downcutting — the downward erosion within a stream channel (cf. *incisement*).

downdip — the direction in which a bed is *dipping*.

drainage area (of a well) — the region over which a given well is able to draw fluid or gas from the *reservoir rock*.

dyne — the force necessary to give 1 gm an acceleration of 1 cm/sec.

Ellenburger Group — a *sequence* of rocks, widespread across Texas, deposited during the *Ibexian Epoch* of the *Ordovician Period*. *Karstification* of the Ellenburger Limestone is responsible for much of the structural control on *facies* within Boonsville field.

epoch — a unit of geologic time into which *periods* are subdivided for more precise correlations.

era — a unit of geologic time consisting of one or more *periods*.

erosion surface (ES) — surface, boundary, or interval showing evidence of erosion associated with an abrupt decrease in water depth; e.g., coarse *channel-fill* sandstone overlying a sharp boundary with underlying marine shale. Because they indicate some interval of time not represented by strata, erosional surfaces are *unconformities*.

Euramerica — the *Paleozoic* continent consisting of what is now North America and Europe.

eustatic sea level — global sea level.

"Exxon" sequence — relatively conformable succession of genetically related strata bounded by *unconformities* or their correlative conformities.

facies — areally and stratigraphically restricted sedimentary unit that differs in appearance, *lithology*, or fossil content from adjacent sedimentary units, thereby allowing inferences to be made about its depositional environment; any group of *rocks* having a similar overall character.

facies dislocation — an interruption of a normal *Walther's Law* succession of depositional *facies* (cf. *facies offset*).

facies offset — an interruption of a normal *Walther's Law* succession of depositional *facies* (cf. *facies dislocation*).

fault block — a *crustal* unit, bounded by faults, that results from extensive *normal faulting* in a region such that the *crust* is broken into separate blocks with different orientations and elevations.

ferroan calcite — a variety of *calcite* having a significant amount of iron impurities.

field trace — a seismic response measured in the field by a single receiver group. Multiple field traces are typically processed to produce a final, summed *seismic trace* (cf. *seismic trace, fold*).

flexural moat — a deep, asymmetric *crustal* depression adjacent to an *overthrust belt* caused by incremental loading due to the emplacement of successive *thrust sheets* within the belt. The *flexural moat* shallows away from the belt, grading into a slightly upwarped *peripheral bulge* (cf. *foreland basin, peripheral bulge*).

flooding surface (FS) — a *chronostratigraphic horizon*, boundary, or interval showing evidence of an abrupt increase in water depth.

fluvial — of or relating to a river or its *depositional system.*

fold (stacking fold) — the number of discrete *seismic field traces* that reflect from the same subsurface area or *bin.* If N field *traces* reflect from a *bin,* these *traces* are processed and summed to create a single *trace* positioned at the center of that *bin.* This summed *trace* is is said to have a stacking fold of N.

footwall — in describing a fault, the body of *rock* below an inclined fault plane.

foraminiferan — a protozoan belonging to the Class Sarcodina, Order Foraminifera, characterized by having a shell of one or more chambers composed of calcium *carbonate* or agglutinated particles.

foreland basin — a depositional basin created by subsidence immediately adjacent to an *overthrust belt* (cf. *flexural moat*).

formation — the fundamental *lithostratigraphic unit* and one whose thickness is sufficiently great to allow it to be adequately mapped. *Formations* are combined together into *groups* and subdivided into *members*.

Fort Worth Basin — a triangular-shaped depositional basin in North-Central Texas created during the Late *Paleozoic* by a *flexural moat* adjacent to the *Ouachita Thrust Belt.*

frequency — the number of cycles of a periodic motion in a unit of time, usually 1 sec.

fusulinid — an extinct, large foraminifer belonging to the Suborder Fusulinina characterized by a long, ellipsoidal shell with complex internal chambering.

gas gravity — the density or mass per unit volume of a gas.

genetic sequence — regressive, generally upward-coarsening succession of *facies* bounded by marine *flooding surfaces*. A *genetic sequence* records one complete cycle of changes in relative sea level (deep–shallow–deep).

Gondwanaland (Gondwana) — the *Paleozoic* continent consisting of modern South America, Africa, Antarctica, India, Australia, Arabia, and parts of southern Europe and the southeastern United States.

graben — the downthrown *crustal* block between two *normal faults*.

group — a *lithostratigraphic unit* consisting of one or more *formations*.

hanging wall — in describing a fault, the body of *rock* above an inclined fault plane.

high-fold bin — a *bin* containing a relatively large number of reflected *seismic field traces* (cf. *bin, fold*).

highstand — time during which *base level* elevation is at a maximum and therefore above the local *shelf* edge; of or relating to such a period.

highstand depositional systems tract (HST) — an upward-coarsening *facies* succession representing *progradational, offlapping facies* that filled *accomodation space* during a *base level* maximum and subsequent fall. The tract is usually capped by an *erosional surface*.

Hilbert transform — a mathematical calculation that extracts amplitude, frequency, and phase information from a *seismic trace*.

humus — macerated plant material derived from the land or present in a soil.

Ibexian — the first *epoch* of the *Ordovician Period*, extending from 476 to 505 million years ago; the *series* of stratigraphic *rock* units deposited during this time; of or relating to this *epoch* of time or its *series* of *rocks*.

impermeable— having no significant *permeability*.

index fossil — an easily recognized, widespread fossil having a short geologic range used to readily date the *rocks* within which it occurs.

incisement — the *downcutting* of a stream channel into the underlying *rock* so as to form a narrow, steep-walled valley.

infield reserve growth — increase of *reserves* within an oil or gas field that has typically been considered fully developed.

inline — the direction in which receiver cables are deployed when recording 3-D *seismic* data (cf. *crossline*).

inner core — that portion of the Earth's interior below the *outer core*. It extends from about 5,200 km in depth (3300 mi) to the center of the Earth and is about 1,200 km (725 mi) in radius. The inner core has a nickel–iron composition but is solid because of the incredible pressure.

instantaneous amplitude — the amplitude behavior of a *seismic trace* calculated at each time sample of the *trace* (cf. *Hilbert transform, seismic attribute*).

instantaneous frequency — a frequency property of a *seismic trace* calculated at each time sample of the *trace* (cf. *Hilbert transform, seismic attribute*).

instantaneous phase — the phase values of a *seismic trace* (limited, by definition, to the range of 0° to 360°) calculated at each time sample of the *trace* (cf. *Hilbert transform, seismic attribute*).

isopach — line on a map connecting points of equal true thickness of a *rock* or stratigraphic unit.

Jurassic — the second *period* of the *Mesozoic Era*, extending from 208 to 144 million years ago; the *system* of stratigraphic *rock* units deposited during this time; of or relating to this *period* of time or its *system* of *rocks*.

karst — a terrain, typically composed of limestone, dominated by erosion through dissolution. Areas that have *karst* topography are characterized by *sinkholes*, caverns, disappearing streams, etc.

karstification — the process by which an area acquires a *karst* terrain.

lamination — a very thin (<1 cm) layer within a sedimentary unit that is nevertheless recognizable because of its differing color, composition, and/or texture relative to the adjacent layers.

lithology — the physical characteristics of a *rock*, such as color, texture, and composition.

lithosphere — the uppermost, rigid part of the *mantle*, immediately beneath the *crust*. The *lithosphere* is about 100 to 150 km (60 to 90 mi) thick under the continents and 70 km (45 mi) thick under the oceans and constitutes the bulk of the *tectonic plates*.

lithostratigraphic unit — a stratified *rock* unit whose components are grouped together on the basis of shared or similar *lithology*, generally having recognizable contacts with adjacent rock units.

low-fold bin — a *bin* containing a relatively small number of reflected *seismic field traces (*cf. *bin, fold).*

lowstand — time during which *base level* elevation is at a minimum and therefore below the local *shelf* edge; of or relating to such a period.

lowstand depositional systems tract (LST) — terrestrial and transitional *facies* that filled *accommodation space* during a *lowstand.*

mantle — that portion of the Earth's interior between the *crust* and the *outer core*, extending from about 10 to 45 km (6 to 27 mi) in depth to 2,900 km (1,800 mi) in depth. The mantle is largely composed of semimolten *silicate minerals* under great pressure.

Marble Falls Formation (Limestone) — the predominantly limestone unit underlying the *Atoka Group* within the *Fort Worth Basin* and Llano area.

maximum flooding surface (MFS) — a *chronostratigraphic* interval associated with *facies* representing the deepest water depth encountered in a succession of strata; commonly represented by a thin, *condensed section* of black or dark-gray marine shales deposited in an oxygen-poor, sediment-starved environment.

member — a *lithostratigraphic unit* into which *formations* are subdivided for more precise correlations.

Mesozoic — the *era* of geologic time extending from 245 million years ago to 66 million years ago and including the *Triassic*, *Jurassic*, and *Cretaceous Periods*.

metamorphism — those changes that occur within a *rock* between *diagenesis* and melting. Metamorphism is defined as occurring at temperatures of over 100° C. (cf. *diagenesis*).

mineral — a naturally occurring, inorganic solid having an ordered internal atomic arrangement and a chemical composition that varies within known limits.

Mississippian — the fifth *period* of the *Paleozoic Era*, extending from 323 to 362 million years ago; the *system* of stratigraphic *rock* units deposited during this time; of or relating to this *period* of time or its *system* of *rocks*.

Missourian — the fourth *epoch* of the *Pennsylvanian Period*, extending from 295 to 303 million years ago; the *series* of stratigraphic *rock* units deposited during this time; of or relating to this *epoch* of time or its *series* of *rocks*.

Morrowan — the first *epoch* of the *Pennsylvanian Period*, extending from 310 to 323 million years ago; the *series* of stratigraphic *rock* units deposited during this time; of or relating to this *epoch* of time or its *series* of *rocks*.

net pay — the sum of the thicknesses of *reservoir rock* in a given locality.

normal fault — a fault in which the *footwall* has moved up relative to the *hanging wall*.

offlap — a *sequence* of sediments in which each overlying unit represents a more nearshore or terrestrial depositional environment and pinches out progressively closer to the center of the depositional basin. *Offlap* occurs as a result of *regression* produced by falling sea level or a rising landmass.

onlap — a *sequence* of sediments in which each overlying unit represents a more offshore depositional environment and pinches out progressively closer to the margins of the depositional basin. Onlap occurs as a result of *transgression* produced by rising sea level or a subsiding landmass.

Ordovician — the second *period* of the *Paleozoic Era*, extending from 439 to 505 million years ago; the *system* of stratigraphic *rock* units deposited during this time; of or relating to this *period* of time or its *system* of *rocks*.

Ouachita Thrust Belt — the linear trend of deformation and thrusting produced by the collison of *Gondwanaland* and *Euramerica* during the Late *Paleozoic*.

outer core — that portion of the Earth's interior between the *mantle* and the *inner core*, extending from about 2,900 km (1,800 mi) to 5,200 km (3,300 mi) in depth. The outer core has a nickel–iron composition and is molten because of the intense heat at this depth.

overthrust belt — a linear trend of deformation and thrust faulting produced along a *convergent plate boundary*.

paleomagnetism — the remnant magnetism left within a *rock* or *mineral* caused by its having crystallized with respect to the Earth's magnetic field; the study of paleomagnetism to determine the orientation and strength of the Earth's magnetic field during the geologic past.

Paleozoic — the *era* of geologic time extending from 530 million years ago to 245 million years ago and including the *Cambrian*, *Ordovician*, *Silurian*, *Devonian*, *Mississippian*, *Pennsylvanian*, and *Permian Periods*.

pay zone — the vertical interval in a stratigraphic section from which extraction of oil or gas is economically profitable.

Pennsylvanian — the sixth *period* of the *Paleozoic Era*, extending from 323 to 290 million years ago; the *system* of stratigraphic *rock* units deposited during this time; of or relating to this *period* of time or its *system* of *rocks*.

pentolite — an explosive used as a *seismic* energy source.

perforation — a deliberate puncture made in a well *casing* to allow fluids or gas to flow into the borehole from the *rock*.

period — the fundamental unit of geologic time originally recognized on the basis of its unique fossil assemblage. *Periods* are grouped together into *eras*, and subdivided into *epochs*.

peripheral bulge — a slightly upwarped area of *crust* distal to an *overthrust belt*. The subsidence produced by loading within the belt creates a *flexural moat*, which in turn induces a slight bulge around its distal margin (cf. *flexural moat*).

permeability — a measure of how well connected pore spaces are within a *rock*, i.e., how well fluids can be transmitted through the *rock*.

Permian — the seventh and last *period* of the *Paleozoic Era*, extending from 290 to 245 million years ago; the *system* of stratigraphic *rock* units deposited during this time; of or relating to this *period* of time or its *system* of *rocks*.

petrophysics — that branch of geology studying the physical properties of *rocks*.

phase — a point in a cycle of regular, periodic motion as measured with respect to the instant at which the motion started. The phase is expressed as a value from 0 to 360°, one cycle of the periodic motion beginning at 0° and returning to the starting point at 360°.

physiography — the surface features of the Earth or a descriptive study thereof.

platform — the geologically stable region of a continent covered by nearly horizontal, undeformed sedimentary units and underlain by crystalline *basement rocks*.

poise — a standard measure of viscosity defined as 1 *dyne*/sec/cm^2.

porosity — that percentage of the total volume of a *rock* not occupied by *mineral* grains or intergranular cements.

potassium feldspar (K-spar) — a hard aluminosilicate *mineral* containing potassium ($KAlSi_3O_8$) and having two cleavage planes that intersect at approximately 90°.

Precambrian — the interval of time extending from the formation of the Earth until the formation of the base of the Cambrian (530 million years ago); of or relating to this interval of time or the *rocks* formed during it.

progradation — the seaward or basinward building, nearshore accumulation of sediment in a depositional setting (cf. *aggradation*, *regression*).

pyrite — a golden or bronze-colored metallic *mineral* composed of iron sulfide (FeS_2), which exhibits cubic crystal structure and a conchoidal fracture.

quartz — a common, hard, crystalline silica *mineral* (SiO_2) exhibiting conchoidal fracture and hexagonal symmetry.

Quaternary — the second *period* of the *Cenozoic Era*, extending from 2 million years ago to the present; the *system* of stratigraphic *rock* units deposited during this time; of or relating to this *period* of time or its *system* of *rocks*.

ravinement surface — a *flooding surface* in which the transgressive movement of the surf zone slightly erodes the underlying sediment.

reflection amplitude — the magnitude of the *seismic* waves that reflect from an interface between *rock* layers.

reflection peak — that part of a *seismic* wiggle trace that swings in the positive direction when plotted or displayed graphically.

reflection trough — that part of a *seismic* wiggle trace that swings in the negative direction when plotted or displayed graphically.

reflector — a boundary within the Earth between materials that have different elastic properties that therefore strongly reflects *seismic* waves and generates *seismic traces* for analysis.

regression — a situation in which relative sea level is falling, moving the shoreline seaward toward the center of the basin. As a result, nearshore and deeper water *facies* are overlain by progressively terrestrial and shallower water deposits.

reserves — identified resources of *mineral*-bearing or *reservoir rock* from which the *mineral* or fuel can be extracted profitably by means of existing technology and under current economic conditions.

reservoir — a *rock* unit with sufficient *porosity*, *permeability*, and *saturation* to yield oil or natural gas.

reverse fault — a fault in which the *footwall* has moved down relative to the *hanging wall*.

rock — an aggregate of one or more *minerals* and/or noncrystalline inorganic solids, or a mass consisting largely of solid organic material that has undergone burial and alteration in the form of *diagenesis* or *metamorphism*.

saturation — the percentage of pore space within a *rock* filled by fluid or gas.

secondary porosity — *porosity* resulting from fracturing or dissolution during *diagenesis*.

secondary recovery — artificially increasing the pressure within a *reservoir* or the mobility of *reservoir* fluids to enhance the retrieval of petroleum or natural gas; incremental recovery in the sense of additional recovery beyond that achieved in early phases of oil or gas field development.

seismic — of or relating to earthquakes or other vibrations within the Earth, including those produced artificially.

seismic attribute — any numerical parameter, such as amplitude, phase, or frequency, that can be extracted from a *seismic trace*.

seismic trace — a generic term used to refer to the data recorded by any receiver(s) detecting Earth movement.

seismic velocity — the speed with which *seismic* waves travel within the Earth.

sequence stratigraphy — conceptual framework for defining *reservoir* architecture. Its main premise is that *seismic* reflections represent *chronostratigraphic horizons* and that these surfaces bound genetically related, time-equivalent rock volumes. Familiar methods of *depositional systems* analysis and *facies* modeling are considered valid only within *rock* volumes (i.e., stratigraphic units) bounded by key *chronostratigraphic horizons.*

sequence — genetically related group of *rock* strata bounded by time-significant surfaces.

series — a *time-rock stratigraphic unit* consisting of those *rocks* deposited during a geologic *epoch.*

shelf — the continental shelf; i.e., that portion of the continental *crust* covered by the ocean. Although mostly limited to the continental margins today, this depositional environment was widespread in the past when large portions of the *craton* were flooded by shallow marine waters and became covered by extensive, nearly horizontal layers of sediments.

shield — the area of a continent in which the *Precambrian* crystalline *basement rocks* are widely exposed.

shoal — an uncemented buildup of coarse *clastic* sediment or shell debris over which the water depth is substantially less than in the area immediately around it.

shoreface — the narrow, inclined zone just seaward of the low-water line along the shore. The *shoreface*, always under water, grades into a lower-angle depositional surface farther offshore.

shut-in period — the time during which the well bore is closed to allow the *bottom-hole pressure* to build up to equilibrium with the fluid or gas pressure in the *reservoir.*

shut-in pressure — the *bottom-hole pressure* measured at the wellhead when the well bore is totally sealed.

silicate — of or relating to a *mineral* with the silicate tetrahedron (SiO_4) forming its basic structure; of or relating to a *rock* consisting primarily of *minerals* containing the silicate tetrahedron.

Silurian — the third *period* of the *Paleozoic Era*, extending from 408 to 439 million years ago; the *system* of stratigraphic *rock* units deposited during this time; of or relating to this *period* of time or its *system* of *rocks*.

sinkhole — a large, deep, roughly circular depression occurring in *karst* terrain formed by the collapse of a cavern roof or by relatively continuous dissolution of soluble rocks such as limestone.

stratal-dominated package — a sedimentary *sequence* deposited more or less continuously and therefore containing few *erosional surfaces* or *unconformities*. As a result, the *rock* units themselves represent much greater amounts of time than do the surfaces between them.

Strawn Group — a *sequence* of *rocks* that overlies the *Atoka Group* (*Bend Conglomerate*). Within the *Fort Worth Basin*, this sequence ranges in age from uppermost *Atokan* to lower *Missourian* and is therefore mostly equivalent to the *Desmoinesian Series*.

strike — the horizontal component of the trend or direction of a *rock* unit.

subaerial — exposed to the open air.

subaqueous — under water.

surface-dominated package — a sedimentary *sequence* containing numerous *erosional surfaces* and *unconformities*, the surfaces between the units representing much greater amounts of time than do the *rock* units themselves.

syntectonic — of or relating to the processes or events occuring during *tectonic* activity.

system — a *time-rock stratigraphic unit* consisting of those *rocks* deposited during a geologic *period*.

systems tract — linkage of contemporaneous *depositional systems*.

tectonic — of or relating to the large *crustal* plates that comprise the outer surface of the Earth or to the deformation resulting from their movement.

tectonic plate — the fundamental unit of the Earth's surface, idealized as a thin, rigid segment consisting of the *crust* and the underlying *lithosphere*. The Earth's surface is broken into about a dozen major and many minor *tectonic plates*, which move slowly upon the underlying *asthenosphere*.

terrigenous — derived or eroded from the land or continents.

Tertiary — the first *period* of the *Cenozoic Era*, extending from 66 to 2 million years ago; the *system* of stratigraphic *rock* units deposited during this time; of or relating to this *period* of time or its *system* of *rocks*.

3-D seismic survey — a data-recording technique in which the reflected *seismic* wavefield generated by a source at a specific coordinate point is recorded by a large number of receivers areally deployed about that source point. This technique differs significantly from 2-D *seismic* surveying, where receivers are deployed in a single straight line about the source point.

thrust fault — a low-angle (<45°) *reverse fault*. Although the movement along the fault is technically vertical, the very low angle of most thrust faults causes the effective movement to be horizontal and typically results in displacements of tens to hundreds of miles.

thrust sheet — a body of *rock* displaced by a *thrust fault* whose surface is nearly horizontal.

tight — having a low *permeability*.

time line — a line drawn through a geologic cross section or correlation diagram that indicates contemporaneous units, separating overlying younger strata from underlying older strata. Ideally, a time line can be equated with an observable surface, boundary, or interval (cf. *chronostratigraphic horizon*).

time-rock stratigraphic unit — a rock unit deposited during a formally named interval of geologic time. The rocks within a time-rock stratigraphic unit are grouped together on the basis of their age, not their *lithology*.

transgression — a situation in which relative sea level is rising and slowly floods the land, moving the shoreline landward away from the center of the basin. As a result, shallow-water and terrestrial *facies* are overlain by progressively deeper water deposits.

transgressive systems tract (TST) — a sedimentary succession representing *onlapping transgressive facies* that filled *accommodation space* during a *base level* rise. The tract usually overlies a *ravinement surface*.

Triassic — the first *period* of the *Mesozoic Era*, extending from 245 to 208 million years ago; the *system* of stratigraphic *rock* units deposited during this time; of or relating to this *period* of time or its *system* of *rocks*.

unconformable — referring to strata or units that immediately overlie an *unconformity*.

unconformity — a contact between two *rock* units that represents some gap in geologic time between the formation of the underlying unit and the deposition of the

overlying sedimentary unit. The *unconformity* corresponds to a period of nondeposition or erosion, often as a result of continental uplift or a fall in sea level.

updip — in a direction opposite but parallel to that in which a bed is *dipping*.

Walther's Law — the stratigraphic principle that states that, in a conformable stratigraphic *sequence*, laterally adjacent *facies* will vertically overlie each other.

wavetest — a *seismic* measurement that determines the signal and noise characteristics of a *seismic* wavefield generated by a specific source and recorded by a specific receiver geometry. Source type and receiver geometry are varied to determine which source and receiver parameters produce wavefields that have desirable signal-to-noise properties.